Catalizadores híbridos bifuncionales para la valorización química de biomasa

Bifunctional hybrid catalysts for the chemical valorization of biomass

Memoria presentada por la licenciada **CRISTINA MEGÍAS SAYAGO** para optar al grado de Doctor con Mención Internacional en Ciencia y Tecnología de Nuevos Materiales por la Universidad de Sevilla.

Fdo. Cristina Megías Sayago

DIRECTORES

Fdo. José Antonio Odriozola **Fdo. Svetlana Ivanova**

Table of contents

Chapter One: General introduction 3

1.1. The biorefinery concept: strategies of biomass conversion 3

1.2. Lignocellulosic biomass 5

1.3. Glucose as chemical precursor 8

1.4. Biomass conversion via polyoxometalate-catalized reactions: new opportunities thought its combination with ionic liquids 11

1.4.1. Polyoxometalates 11

1.4.1.1. General aspects 11

1.4.1.2. Catalytic potential in biomass conversion 14

1.4.2. Ionic Liquids 15

1.4.2.1. General aspects 15

1.4.2.2. Catalytic potential in biomass conversion 16

1.4.3. Polyoxometalate/Ionic Liquids (POM-ILs) hybrid materials 17

1.5. Objectives and Thesis organization 19

Chapter Two: Experimental techniques 29

2.1. Introduction 31

2.2. Characterization techniques 31

2.2.1 X-Ray diffraction based methods 31

2.2.1.1. X-Ray diffraction (XRD) 31

2.2.1.2. Single Crystal X-Ray Diffraction (SCXRD) 34

2.2.1.3. X-Ray Fluorescence (XRF) 35

2.2.1.4. X-Ray Photoelectron Spectroscopy (XPS) 35

2.2.2. Chemical composition analysis (ICP-AES) 37

2.2.3. Transmission Electron Microscopy (TEM) 38

2.2.4. Z potential measurement: isoelectric point (IEP) 39

2.2.5. N_2 physisorption: specific surface area (BET surface area) 39

2.2.6. Temperature programmed reduction (TPR-H_2) 40
2.2.7. Vibrational spectroscopies: Raman and Diffuse Reflectance Infrared Fourier Transform (DRIFT) 41
2.2.8. Ultraviolet-Visible (UV-Vis) spectroscopy 42
2.2.9. Nuclear magnetic resonance (NMR) 43
2.2.10. Oxygen storage complete capacity (OSSC) and oxygen storage capacity (OSC) 44
2.3. Catalytic activity studies 44
2.3.1. Experimental device 44
2.3.2. Catalytic activity tests 46
2.3.3. Analytical methods 47

Chapter Three: Synthesis and characterization of polyoxometalate-ionic liquid based catalysts 51

3.1. Introduction 53
3.2. Catalysts synthesis 54
3.2.1. Synthesis of heteropolyacids 54
3.2.2. Synthesis of the hybrid structures (POM-IL) 56
3.3. Structural characterizations of POM-IL catalysts 57
3.3.1. XRD study 57
3.3.2. Thermogravimetric (TGA) analysis 60
3.3.3. XRD as function of temperature (TXRD) 61
3.3.4. Raman spectroscopy 69
3.3.5. SAXRD analysis of Mo based hybrids 71
3.3.6. Solid state $^{13}C\{^1H\}$ and ^{31}P NMR analysis of Mo based hybrids 73
3.3.7. Single crystal X-ray diffraction of Mo based hybrids 75
3.4. Partial conclusions 79

Chapter Four: Catalytic viability of POM-IL hybrids in biomass valorization 85

4.1. Glucose epimerization 88

4.1.1. Introduction 88

4.1.2. Experimental 92

4.1.3. Catalytic activity: results and discussion 92

4.1.4. Partial conclusions 104

4.2. Glucose oxidation 105

4.2.1. Introduction 105

4.2.2. Experimental 107

4.2.3. Catalytic activity: results and discussion 108

4.2.4. Partial conclusions 115

4.3. Glucose/Fructose dehydration 116

4.3.1. Introduction 116

4.3.2. Experimental 120

4.3.3. Catalytic activity: results and discussion 122

4.3.4. Partial conclusions 139

Chapter Five: Introduction of gold catalysts for biomass-involved oxidation reactions: synthesis and characterization 147

5.1. Introduction 149

5.2. Gold supported on different metal oxides 151

5.2.1. Why metal oxides? 151

5.2.2. Synthesis of catalysts 152

5.2.3. Physicochemical characterization 153

5.2.3.1. XRD of the prepared solids 153

5.2.3.2. Textural properties and gold loadings 154

5.2.3.3. TEM microscopy 155

5.2.3.4. Isoelectric point analysis (IEP) 159

5.2.3.5. TPR-H_2 159

5.3. Gold supported on active carbon 163

5.3.1. Why active carbon? 163
5.3.2. Synthesis of catalysts 164
5.3.3. Characterization 165
5.3.3.1. Colloids characterization: UV-Vis spectroscopy and TEM microscopy. 165
5.3.3.2. AuC characterization 171
5.3.3.2.1. ICP and UV-Vis spectroscopy 171
5.3.3.2.2. XRD and TEM microscopy 172
5.4. Partial conclusions 176

Chapter Six: Aerobic oxidation of glucose and HMF: catalytic screening 182

6.1. Base-Free oxidation of glucose 184
6.1.1. Introduction 184
6.1.2. Gold supported on metal oxides: influence of support 187
6.1.2.1. Experimental 187
6.1.2.2. Catalytic activity: results and discussion 188
6.1.2.3. Partial conclusions 199
6.1.3. Gold supported on carbon: influence of particle size 200
6.1.3.1. Experimental 200
6.1.3.2. Catalytic activity: results and discussion 200
6.1.3.3. Recycling study: results and discussion 205
6.1.3.4. Partial conclusions 215
6.1.4. General conclusion in the base-free oxidation of glucose 216
6.2. HMF oxidation to FDCA 217
6.2.1. Introduction 217
6.2.2. Experimental 220
6.2.3. Gold supported on metal oxides: influence of support 223
6.2.3.1. Catalytic activity: results and discussion 223
6.2.3.2. Synthesis and characterization of homemade supports 243
6.2.3.3. Catalytic activity of homemade series: results and discussion 252
6.2.3.4. Partial conclusions 255

6.2.4. Gold supported on carbon: influence of particle size 256
6.2.4.1. Catalytic activity: results and discussion 256
6.2.4.2. Partial conclusions 259
6.2.5. General conclusion in the HMF oxidation to FDCA 260

General conclusions 268

Conclusiones generales 275

Resumen 283

Anexos 307

Chapter One

GENERAL INTRODUCTION

1.1. The biorefinery concept: strategies of biomass conversion

The biorefinery concept dating from the end of the last century [1,2] is a subject of several definitions during the last decade [3]. For the International Energy Agency, Bioenergy-Task 42, biorefining is the sustainable processing of biomass into a spectrum of marketable biobased products (chemicals, materials, human food and animal feed) and bioenergy (fuels, power and/or heat) [4]. An abundant part of the scientific literature is dedicated to biofuel production, though the biorefineries focusing on bioproducts are also documented [5–8]. In fact, biorefineries involving starch, sucrose or vegetable oils processing to bioproducts have been in operation before the establishment of the biorefinery concept [9,10]. Currently, a multitude of start-ups and SME companies are emerging and exploiting new resources, such as microalgae or sea weeds and developing optimized fermentation processes to produce platform molecules used as building blocks for chemistry [11]. New biorefineries are currently established to process lignocellulosic materials from forestry products, various types of grasses (miscanthus, switchgrass) and agricultural residues [12–16].

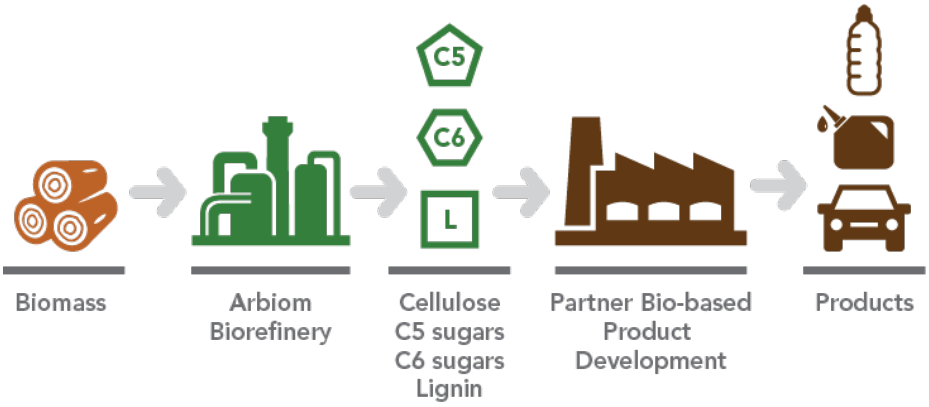

Figure 1.1. The biorefinery concept. Biomass processing into biobased products.

Nevertheless, cost effective processes adapted to the highly functionalized biomass molecular structure have to be developed to make the quality and the price of biobased chemicals competitive with respect to the products obtained by traditional routes from fossil fuels [17–19]. The biomass usually contains impurities, which can affect the catalytic activity and selectivity, obstructing both catalyst recycling and continuous processes [20]. That is why, the design of an efficient and durable catalysts aroused great interest both in academia and industry. Rinaldi and Schüth [21] summarized the challenges that faces the design of an heterogeneous catalyst for biomass processing. The main issue is to develop multifunctional catalyst, having different active sites to be used in cascade-type reactions. The later would imply the reduction of several reactions to one-pot process allowing process intensification [22]. Nevertheless, the effective combination of homogeneous and heterogeneous catalysts in multi-step biomass conversion reactions is also desirable [23].

According to Bozell and Petersen [6,7] two different approaches can be selected to achieve biomass conversion to chemicals:

i) A **target-driven approach**, employing process analysis methodology designed to find the most efficient synthetic route to produce a chemical starting from well-identified platform molecules. This approach may result in an uneconomical production of chemicals with respect to the well-optimized, conventional synthetic routes from hydrocarbons.

ii) A **process-driven approach** whereby the biomass is converted by one or more catalytic processes (hydrogenation, hydrogenolysis, oxidation, etc.) to yield a family of valuable products. This approach does not intent to duplicate chemicals produced from fossil resources and could be more effective to find rapidly new valuable bioproducts.

Despite that, the **target-driven approach** may result uneconomical in comparison with the well-established routes from fossil fuels, it allows the

deep knowing and understanding of the processes, the parameters influencing them and the most efficient catalyst to valorize the biomass in the most efficient way. The efficiency is probably THE base, which drive the current society to a future biobased society.

1.2. Lignocellulosic biomass

Lignocellulosic biomass is the most abundant and available plant material on our planet [24], containing up to 60–70 wt% of sugars/carbohydrates. It is not used for food production, very desirable from ethic point of view, since avoids chemicals to food competition. Lignocellulose is composite material constituted by three biopolymers, cellulose, hemicellulose and lignin, in addiction to small percentage of other compounds such as pectins, proteins and lipids (Figure 1.2.)

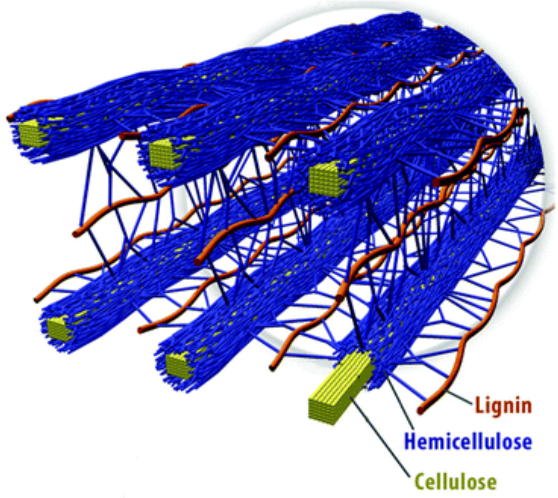

Figure 1.2. Spatial arrangement of cellulose, hemicellulose and lignin in the cell walls of lignocellulosic biomass. Reprinted from ref. [24]

Although the exact composition depends on the species, the plant tissue and growth conditions, a general compositional percentage range could be established, as presented below:

Cellulose is the main component, ranging 35-50 wt% of the total lignocellulosic biomass. It is a linear polymer constituted only by glucose units, which are linked by 1-4-β glycosidic bonds (Figure 1.3.). The β configuration of glucose is the responsible of its linear chain structure, with hydrogen bonds linking these chains into flat sheets. The later enables the packing of numerous cellulose strands into crystalline fibres [25]. Cellulose has the highest degree of polymerization among the three biopolymers, being the number of glucosyl units in one polymer 10 000 or higher [26]. That means that from only one cellulose strand, 10 000 or more glucose units could be obtained.

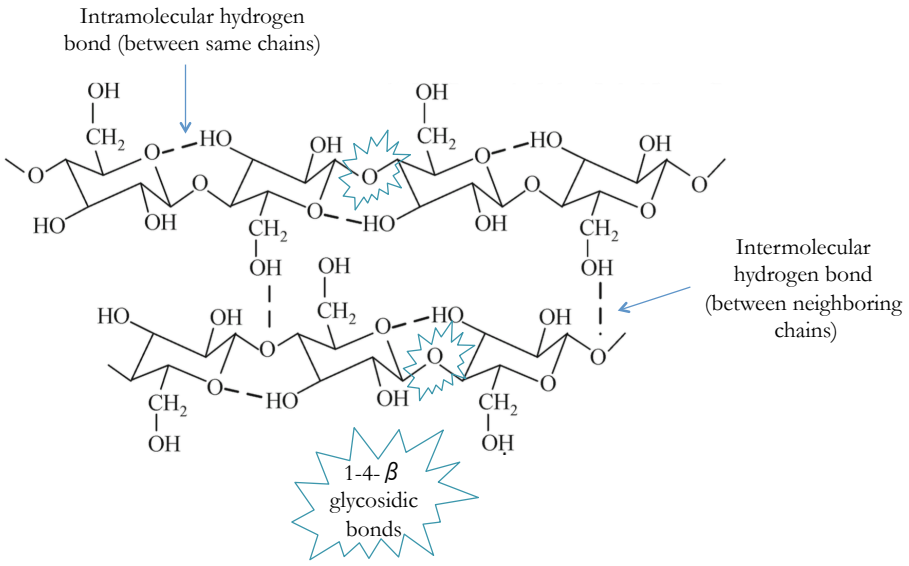

Figure 1.3. Chemical structure of cellulose chains. Adapted from [27]

Hemicellulose is constituted by a group of polysaccharides and represents a 25 wt% of the total lignocellulosic biomass. It is composed by both hexose (glucose, mannose and galactose) and pentose sugar rings (xylose and arabinose), with different functionalities. Hemicellulose polymers can be formed through α and β glycosidic bonds, the later

determining its branched structure. Figure 1.4. A) shows one of the main chains of hemicellulose, galactoglucomannan.

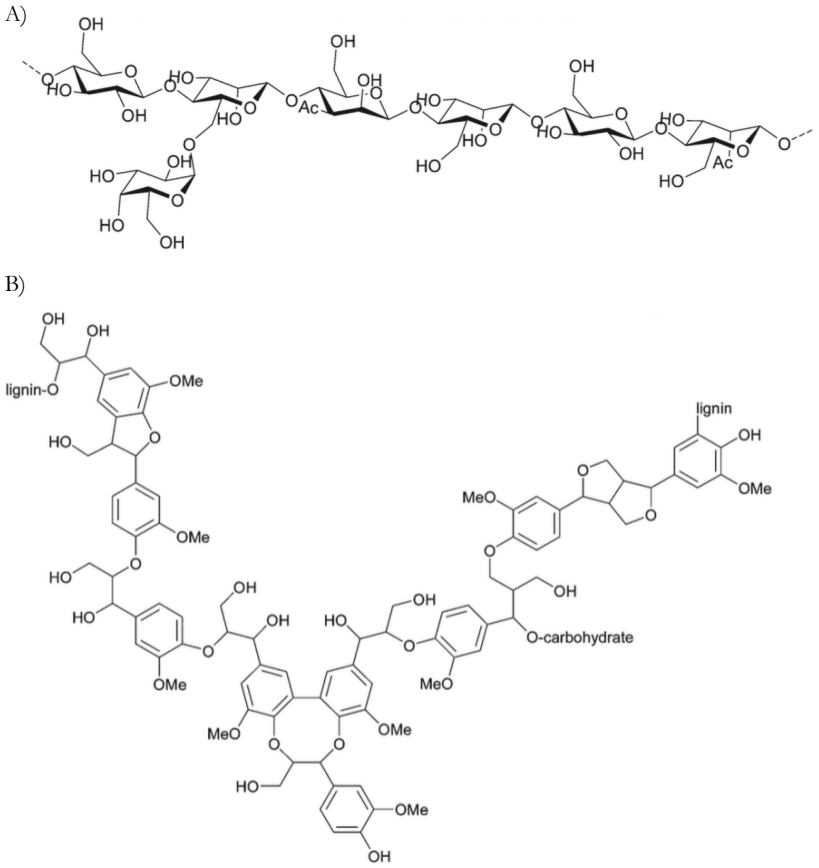

Figure 1.4. Chemical structures of A) galactoglucomannan and B) lignin. Adapted from [24]

Lignin is the more complex fraction and it is principally composed by aromatic six carbon rings, as shown in Fig. 1.4 B.

Cellulose is by far the easily usable fraction, since is a polymer formed by only one monosaccharide-type. The hydrolysis of cellulose, usually catalyzed by strong mineral acids such as H_2SO_4 and HCl, give rise to glucose, one of the most important platform chemicals derived from

biomass. Its utility lie on the high number of potential molecules in which glucose could convert. However, depolymerizing this high-weight polymer is not an easy task. Although the monomer and short oligomers are water-soluble, the pure cellulose is not. The later is derived from its high molecular weight (solubility is usually inversely proportional to the polymer length) and low chain flexibility [28]. Abundant presence of hydrogen bonds, both intramolecular and intermolecular, account for cellulose high crystallinity which, in addition to its most solvents insoluble character, difficult a lot the depolymerization. Nevertheless, in the last decade, a processes that allows cellulose deconstruction either in water or in sub-critical water [27] have been developed. Although its efficient conversion remains a challenge, recently, thee use of ionic liquids as solvents instead of water have been reported [24].

This Thesis is focused on the next step, i.e. the conversion of glucose unit (chosen as model molecule derived from the lignocellulosic biomass) to valuable biobased compounds.

1.3. Glucose as chemical precursor

It is really difficult to find literature reports that are able to summarize the huge amount of valuable chemicals that glucose can originate. Indeed, a search in Scopus Database with the keywords "Glucose conversion" and "platform chemicals" leads to a total of 7174 related documents being published 7096 papers since 2005 (Figure 1.5.). This analysis accounts for the increasing interest of the scientific community towards the valorization of biomass raw materials, in general, and in the use of glucose as building block, in particular. The increasing number of studies supplied numerous synthetic routes through which an extensive group of biomass-

based molecules can be obtained. The catalytic processes are more and more efficient as more knowledge literally every day is acquired.

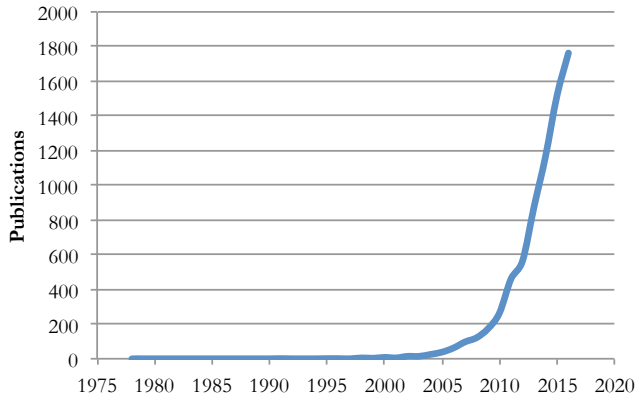

Figure 1.5. Number of publications, in Scopus database using "Glucose conversion" and "Platform chemicals", as search keywords for the 1978-2016 period

Therefore, it results suitable to focus topic to each valuable compound obtained from glucose and studied in the present Thesis separately. The studied routes are:

- Glucose epimerization to mannose (Scheme 1.1.)
- Glucose oxidation to gluconic acid (Scheme 1.2.)
- Glucose/fructose dehydration to 5-hydroxymethyl-2-furfural (HMF) (Scheme 1.3.)
- HMF oxidation to 2,5-Furandicarboxylic acid (FDCA) (Scheme 1.4.)

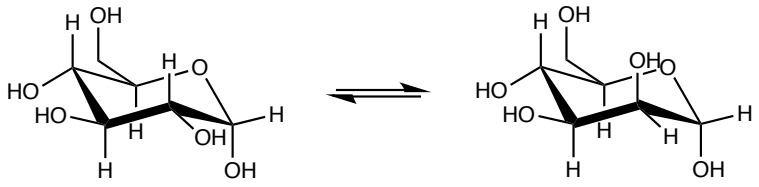

Scheme 1.1. Glucose epimerization to mannose

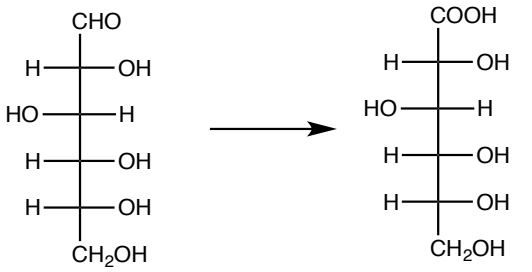

Scheme 1.2. Glucose oxidation to gluconic acid

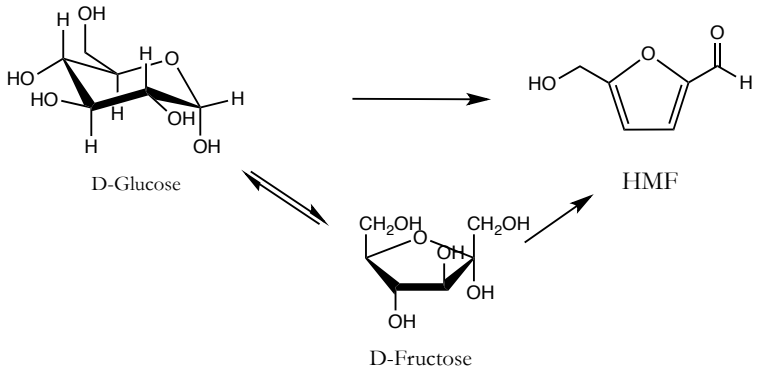

Scheme 1.3. Glucose/fructose dehydration to 5-hydroxymethyl-2-furfural (HMF)

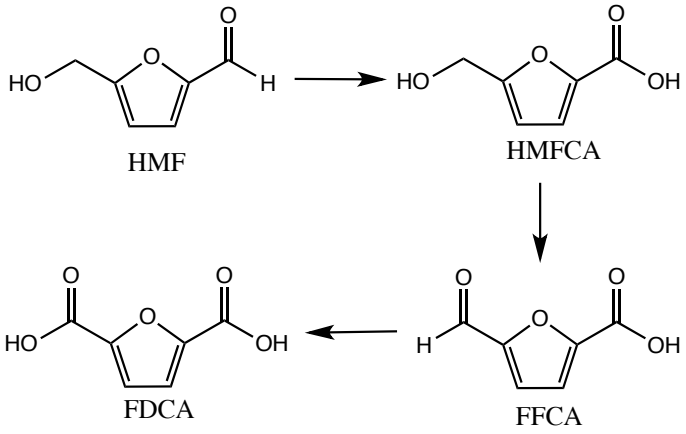

Scheme 1.4. HMF oxidation to 2,5-Furandicarboxylic acid (FDCA)

The state-of-art of every glucose transformation route will be addressed in the corresponding Chapters, where the bibliographic findings will be contrasted with the obtained results. Detailed Thesis organization will be proposed at the end of the present Chapter. Following the choice of catalytic materials will be introduced.

1.4. Biomass conversion via polyoxometalate-catalyzed reactions: new opportunities thought combination with ionic liquids

1.4.1. Polyoxometalates

1.4.1.1. General aspects

Polyoxometalates (POM) are a class of anionic metal-oxygen clusters built by the connection of $[MO]_x$ polyhedra of the early transition metals in their highest oxidation states [29–31]. Despite of the different nomenclature rules established [32], the polyoxometalate compounds are referred also as hetero- or isopolyacids and hetero- or isopolyanions or polyoxoanions. Among the different possibilities, the most studied structures are those based on molybdenum (VI) and tungsten (VI). Although the first polyoxometalates were reported over almost 200 years ago, new structures with unusual properties and/or applications are reported continuously. At this respect, there are a huge amount of papers and reviews that resume compounds main application fields, such as material science, medicine, or catalysis [33–36]. Derived from the different combinations and possibilities, thousands of compounds constitute the big "POM family", and different classifications over the years have been proposed. Recently, Long *et al.* [37] reported an useful classification, based essentially on the anionic metal-oxygen cluster type:

- Heteropolyanions: clusters including heteroatoms, such as $[XM_{12}O_{40}]^{n-}$ anion, where M is normally Mo^{VI} or W^{VI} and X is an heteroatom coordinated and situated in the core of the structure. Three different families could be distinguished inside this group, according to the different coordination of the heteroatom, Anderson $[XM_6O_{24}]^{n-}$, Keggin $[XM_{12}O_{40}]^{n-}$, and Dawson $[X_2M_{18}O_{62}]^{n-}$, octahedral for Anderson family and tetrahedral for the other two [37].
- Isopolyanions: clusters without heteroatoms.
- Molybdenum blue and molybdenum brown reduced POMs: a class of highly reduced POM clusters.

This classification is based only on the polyoxoanion, which is generally compensated by cations of different nature, inorganic such as H^+, Ca^+, Cs^+, or organic.

This Thesis is focused only on the Keggin structure polyoxometalates, concretely on those anions containing Mo, W and V. A representative scheme of the Keggin-type anion and $[PMo_{12}O_{40}]^{3-}$ structures are shown in Figure 1.6. As can be seen, the phosphorous atom form a tetrahedron with 4 oxygen atoms in the core of the cluster, to which the molybdenum atoms are directly liked (3 metal atoms per oxygen) resulting in 12 metal atoms in total, octahedrally coordinated. Two types of oxygen bridges, the edge-shared and the corner-shared connect the Mo atoms. There is one more type of oxygen, the terminal oxygen, bonded by double bond to the molybdenum atom.

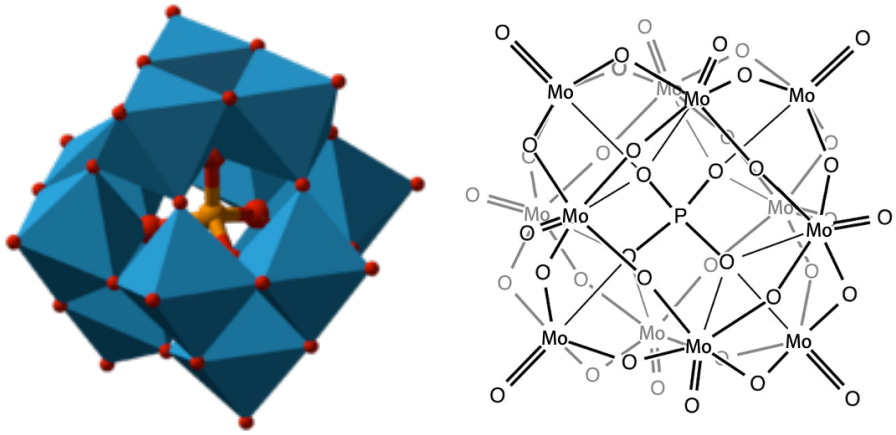

Figure 1.6. General Keggin type polyoxometalate anion (left) and $[PMo_{12}O_{40}]^{3-}$ structure (right)

It is well known that the proton compensated polyoxometalate anions have several advantages as homogeneous catalysts: i) their very strong Brönsted acidity (close to superacid region) and ii) their participation in fast reversible multielectron redox transformations that convert them in efficient oxidants. These acid-base and redox properties can be varied by changing POMs chemical composition [36]. The special acidity of the POMs originates from the fact that the negative change of the anion is shared over numerous external oxygen atoms (36 in Keggin structure), therefore producing much weaker attraction for its protons than the other mineral acids. Indeed, it has been demonstrated that most negative charge is situated on the oxygen bridges converting them in weak basic sites weakly attracting protons [38]. Aside from the Brönsted acidity, POM anions have metal centers in their highest oxidation states, which can act as Lewis acid centers. On the other hand, and due to their flexible redox behavior, they can act as electron reservoirs. The oxidized form may only accept electrons, however, their reduced forms may behave as donors or acceptors of several electrons while maintaining the original structure [39].

These fast redox transformations are reversible and, in some cases, lead to colored mixed valence species, known as heteropoly blues [40]. Additionally, they have good thermal and hydrolytic stability, also very important in liquid-phase catalytic reactions. Properties comparative for the most studied heteropolyacids are summarized below [36]:

- Acid strength: $[PW_{12}O_{40}]^{3-} > [PMo_{12}O_{40}]^{3-}$
- Oxidation potential: $[PMo_{12}O_{40}]^{3-} >> [PW_{12}O_{40}]^{3-}$
- Thermal stability: $[PW_{12}O_{40}]^{3-} > [PMo_{12}O_{40}]^{3-}$
- Hydrolytic stability: $[PW_{12}O_{40}]^{3-} > [PMo_{12}O_{40}]^{3-}$

1.4.1.2. Catalytic potential in biomass conversion

The catalytic potential of POMs derives from its multifunctionality, transforming this kind of compounds in suitable catalysts for reactions that needs Brönsted and/or Lewis acid sites, electron exchanges or a combination of them. The later becomes important in cascade-type reactions due to the possibility to reduce several processes to one-pot process, allowing its intensification. The list of polyoxometalate-catalyzed reactions is quite extensive. Wang and Yang [41] summarized the recent advances in an excellent review, where the reactions, mainly organic processes, are organized in several groups: oxidation, reduction, polymerization, acid-base catalysis, cycloadditions and coupling reactions. Without a doubt, the largest group is the oxidation reactions.

When focusing on biomass conversion reactions, most papers deal with cellulose depolymerization in water [42] and lignocellulosic biomass dissolution and delignification [43]. Attending to the prior, a glucose yield of approximately 55% was obtained over $H_3PW_{12}O_{40}$ after 3 h of reaction

at 453K. After that time, changes in selectivity and glucose yield were reported: glucose yield decreased in favor to HMF and levulinic acid [44]. The later is a clear example of cascade reaction. Driven by this result, several POMs have been applied to this reaction. Mizuno *et al.* [45] recently employed highly negatively charged heteropoly acids based on $[XW_{12}O_{40}]^{3-}$ where X = B, Al, Ga, Co exhibiting stronger acidity than $H_3PW_{12}O_{40}$ and mineral acids. The catalytic performance was better than mineral acids and $H_3PW_{12}O_{40}$, which suggests that stronger Brönsted acid is more efficient catalyst for the cellulosic β-1,4 glycosidic bonds cleavage.

As for the delignification, which is an oxidative degradation of the residual lignin in presence of O_2, POMs have resulted as excellent candidates [46,47]. The ideal polyoxometalate catalyst for such oxidative delignification should be strong enough to oxidize the residual lignin preferentially into CO_2 and H_2O without degrading the polysaccharides, and should re-oxidized by oxygen at the same time [46]. The POM compounds based on Mo and the combination of Mo and V demonstrated to be the most suitable ones.

It is evident that POMs are good candidates for the first steps of lignocellulosic biomass conversion; therefore, their use in glucose conversion reactions is also highly desirable.

1.4.2. Ionic Liquids

1.4.2.1. General aspects

Ionic Liquids (ILs) are ionic compounds with melting points below 100ºC [29]. Most typical structures are composed by organic cations (normally quaternary ammonium salts or based on cyclic amines) and inorganic anions (Cl^-, $AlCl_4^-$, PF_6^-, BF_4^-, among others), as is shown in Figure 1.7. Coulombic interactions are the dominant interactions between the ions;

however, intermolecular interactions like H bonding, π-π stacking and van der Waals interaction induce a supramolecular organization of ILs with high degree of directionality [48–52]. Their principal advantages could be resumed in high ionic mobility, good electric conductivity, low vapor pressure and good thermal and chemical stability [53,54]. Similarly to POMs, their properties could be tuned by introducing some changes in the ionic structures, such as different anions and cations or different functionalities [55].

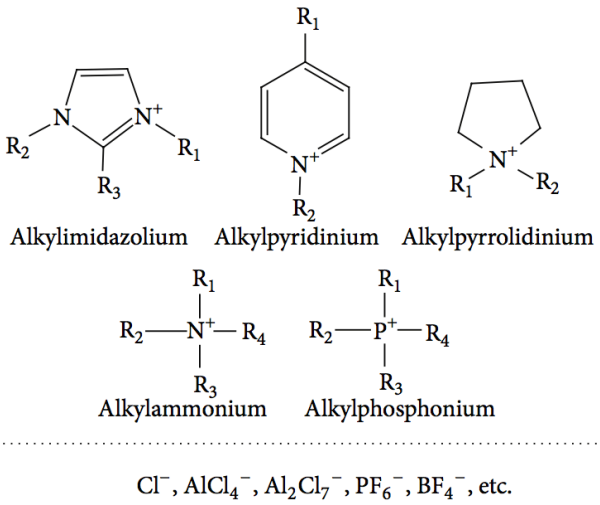

Figure 1.7. Most commonly used cations and anions forming the ILs. Reprinted from ref [29]

1.4.2.2. Catalytic potential in biomass conversion

The ILs have already found its application in catalysis as a solvents [56–59] in electrochemistry [60] and organic synthesis. However, its role in the chemical reactions is far away to be simple, it can act either as a solvent, as a catalyst or presenting a dual character: solvent and catalyst or co-catalyst [61]. There are numerous reviews dedicated to the use of ILs in either homogeneous, organometallic or heterogeneous catalysis [61–64].

Attending to biomass-involved reactions, the ILs have been mainly used as solvents in the dehydration of glucose/fructose to HMF, either alone or in presence of classical solvents forming biphasic systems [65–68]. Moreover, they have been use as solvent media during the delignification of lignocellulose [43]. In both cases, the exact role of the ILs remains unclear and it is though that the production of HMF in this kind of solvents is a "ionic liquid-mediated" [66]

It has been established, therefore, that both POMs and ILs can be used in biomass valorization with good results. The combination of both catalysts seems to be the next logical step, expecting that in the POM-IL hybrid remains the favorable effects provided by POM and ILs, to result in a system targeting higher multifunctionality and higher productivity.

1.4.3. Polyoxometalate/Ionic Liquids (POM-ILs) hybrid materials

Considering the obvious drawbacks of the homogeneous catalytic systems, such difficulties to recycle the catalysts and to purify the products, the exploration of heterogeneous POM catalysts attracts more and more attention in the last decade. The heterogeneization of the POM systems is given in most cases by the formation of salts after total or partial substitution of protons. It is evident, therefore, that there are an endless number of salt possibilities, whose specific properties will depend on the cation in the structure. Among the options, different organic-inorganic salts have been proposed [69]. Besides of their fascinating interest for crystallography, those salts are being explored in many catalysis areas.

First POM-ILs hybrids were synthetized in 2008 by Ranga Rao and coworkers [70–72]. They used the 1-butyl-3-methyl-imidazolium (C4mim)

bromide ionic liquid and several heteropolyacids to produce molecular salts with the formula $[C4mim]_3[PM_{12}O_{40}]$. The preparation method included a simple precipitation of the salts from aqueous solution of the initial acid and ionic liquid components. Single crystal structural analysis of phosphomolybdic hybrid suggests a compound crystalizing in orthorhombic structure in $Pca2_1$ space group, with one formula unit per unit cell. Additionally, Chen *et al.* [73] proposed the ionothermal method for the synthesis of transition metal containing polyoxotungstate ionic liquid hybrids. The single crystal analysis show that one cation is connected to three polyoxoanions via hydrogen bonds, resulting in the formation of square channels [73], with the later directly related with the presence of the ionic liquid. As proposed by Dupont [49], the ionic liquids have 3D arrangements in which cations and anions connect through hydrogen bonds and form an extended cooperative network.

For the alkyl imidazolium ILs used in this Thesis, the monomeric unit always consists of one imidazolium cation surrounded by at least three anions (like in the hybrid), an in turn each anion is surrounded by at least three cations. Two major 3D arrangements in the case of imidazolium ILs are then formed: (i) through the imidazolium rings chains (Figure 1.8 left) with anions accommodated in between and (ii) by columns consisting of alternating cations and anions (right). In both cases, high directionality is observed, a phenomenon known as ionic self-assembly (ISA). The similarity with the hybrids suggests that hybrid's structural organization is given by the ionic liquid.

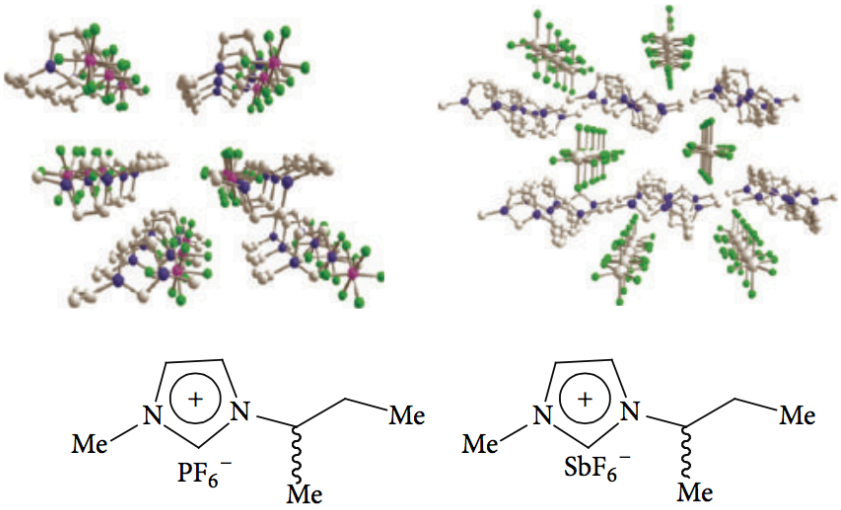

Figure 1.8. Representation of the two major 3-D arrangements of imidazolium ILs, taken from [49]

Some recent studies reported the catalytic activity of this kind of hybrid materials in different organic reactions [30,74–82]. Within the biomass valorization field, the hybrids were mostly reported for the cellulose processing, including delignification [83–85]. There is an important lack of studies on the glucose conversion to platform chemicals over these materials.

1.5. Objectives and Thesis organization

Several POMs and ILs are selected to provide the active sites needed for glucose transformation reactions. For example, the glucose epimerization reaction needs Lewis acid sites, the glucose/HMF oxidation a catalyst with good redox properties and the Glucose/Fructose dehydration a tandem of strong Lewis/Brönsted sites. For that purpose, our selection points to POMs based on Mo (high oxidation potential, Lewis acid

character and strong Brönsted acidity), on a combination of Mo and V to improve the redox properties of Mo and on W, possessing higher acid strength. The POMs properties are combined with those of three ionic liquids, based on alkyl-imidazolium cations and differing in the number of carbons of the ring substitute alkyl chains. The influence of both POM anion and the ILs cation nature will be studied in details during this thesis.

For all above, this PhD thesis will focus on the application of POM-ILs compounds in the transformation of glucose to different added-value chemicals. The main objective of the thesis is then to elaborate a multifunctional catalytic system able to participate in various cascade reactions starting from glucose as platform chemical.

This thesis is organized in 6 chapters, including the present one. Along the Chapter Two, the techniques and instrumentation employed to perform the experiments are presented. In Chapter Three, the synthesis and structural characterization of all POM-ILs structures is presented. In Chapter Four, the catalytic activity of all synthesized structures is evaluated in three different processes, glucose epimerization to mannose, glucose oxidation to gluconic acid and the glucose/fructose dehydration to 5-hydroxymethyl-2-furfural. Derived from the results in Chapter Three, Chapter Five and Chapter Six are born. Both chapters present more interesting alternative to POM-ILs catalysts for the biomass involved oxidation reactions, as the efficiency of the hybrids results low. As efficient alternative, gold supported catalysts were introduced due to metal high potential in oxidation reactions with molecular O_2. Chapter Five is then focused on the synthesis and characterization of two groups of gold catalysts; gold supported on different metal oxides and gold supported on active carbon. Finally, in Chapter Six the catalytic activity of both groups

of gold catalysts is evaluated in the glucose and HMF oxidation reaction. In both cases, the influence of support nature (by using the first group of gold catalysts) and the particle size (by using the second group of catalysts) are evaluated. A detailed study making special emphasis in gold catalyst recycling is also addressed in the last chapter.

This Thesis is developed under the International PhD normative. According to it, a brief summary containing some introduction, the objectives, the thesis organization, the conclusions and briefly some important results will be also presented in Spanish. In the same way, the general conclusions will be presented both in Spanish and English.

Finally, a list of already published papers and communication in congresses are included in annexes at the end of the present PhD Thesis.

References

[1] B. Kamm, M. Kamm, Principles of biorefineries, Appl. Microbiol. Biotechnol. 64 (2004) 137–145.

[2] P. Gallezot, Conversion of biomass to selected chemical products, Chem. Soc. Rev. 41 (2012) 1538–1558.

[3] F. Cherubini, The Biorefinery Concept: Using Biomass Instead of Oil for Producing Energy and Chemicals, Energy Convers. Manag. 51 (2010) 1412–1421.

[4] Biorefineries: adding value to the sustainable utilisation of biomass, IEA Bioenergy, (2009).

[5] S. J, S. E, W. R, M. H., Bio-refinery as the bio-inspired process to bulk chemicals, Macromol Biosci. 7 (2007) 105–117.

[6] J.J. Bozell, Feedstocks for the Future – Biorefinery Production of Chemicals from Renewable Carbon, Clean Soil Air Water. 36 (2008) 641–647.

[7] J.J. Bozell, G.R. Petersenb, Technology development for the production of biobased products from biorefinery carbohydrates—the US Department of Energy's "Top 10" revisited, Green Chem. 12 (2010) 539–554.

[8] A.L. Marshall, P.J. Alaimo, Useful products from complex starting materials: common chemicals from biomass feedstocks, Chem. Eur. J. 16 (2010) 4970–4980.

[9] http://www.roquette.com/documentation/roquette-group-communicationkit/swf_article=6790/;model_name:documentation_ request/, (n.d.).

[10] http://www.cognis.com, (n.d.).

[11] L.E. Manzer, Recent Developments in the Conversion of Biomass to Renewable Fuels and Chemicals, Top. Catal. 53 (2010) 1193–1196.

[12] K. B, K. M., Biorefineries--multi product processes, Adv Biochem Eng Biotechnol. 105 (2007) 175–204.

[13] M. Delmas, Vegetal Refining and Agrochemistry, Chem. Eng. Technol. 31 (2008) 792–797.

[14] S.S.Y. Tan, D.R. MacFarlane, J. Upfal, L.A. Edye, W.O.S. Doherty, A.F. Patti, et al., Extraction of lignin from lignocellulose at atmospheric pressure using alkylbenzenesulfonate ionic liquid, Green Chem. 11 (2009) 339–345.

[15] S. Fernando, S. Adhikari, C. Chandrapal, N. Murali, Biorefineries: Current Status, Challenges, and Future Direction, Energy Fuels. 20 (2006) 1727–1737.

[16] J.-P. Lange, Lignocellulose conversion: an introduction to chemistry, process and economics, Biofuels, Bioprod. Bioref. 1 (2007) 39–48.

[17] J.-P. Lange, Sustainable chemical manufacturing: a matter of resources, wastes, hazards, and costs, ChemSusChem. 2 (2009) 587–592.

[18] V. Dornburg, B. Hermann, M. Patel, Scenario projections for future market potentials of biobased bulk chemicals, Env. Sci Technol. 42 (2008) 2261–2267.

[19] T. Willke, K. Vorlop, Industrial bioconversion of renewable resources as an alternative to conventional chemistry, Appl Microbiol Biotechnol. 66 (2004) 131–142.

[20] P. Gallezot, Direct routes from biomass to end-products, Catal. Today. 167 (2011) 31–36.

[21] R. Rinaldi, F. Schüth, Design of solid catalysts for the conversion of biomass, Energy Environ. Sci. 2 (2009) 610–626.

[22] M.J. Climent, A. Corma, S. Iborra, M. Mifsud, A. Velty, New one-pot multistep process with multifunctional catalysts: decreasing the E factor in the synthesis of fine chemicals, Green Chem. 12 (2010) 99–107.

[23] H. Mehdi, V. Fábos, R. Tuba, A. Bodor, L.T. Mika, I.T. Horváth, Integration of Homogeneous and Heterogeneous Catalytic Processes for a Multi-step Conversion of Biomass: From Sucrose to Levulinic Acid, γ-Valerolactone, 1,4-Pentanediol, 2-Methyl-tetrahydrofuran, and Alkanes, Top. Catal. 48 (2008) 49–54.

[24] A. Brandt, J. Gräsvik, J.P. Halletta, T. Welton, Deconstruction of lignocellulosic biomass with ionic liquids, Green Chem. 15 (2013) 550–583.

[25] A.C. O'Sullivan, Cellulose: the structure slowly unravels, Cellulose. 4 (1997) 173–203.

[26] H. Jørgensen, J.B. Kristensen, C. Felby, Enzymatic conversion of lignocellulose into fermentable sugars: challenges and opportunities, Biofuels, Bioprod. Bioref. 1 (2007) 119–134.

[27] Y. Zhao, W. Lu, J. Chen, X. Zhang, H. Wang, Research progress on hydrothermal dissolution and hydrolysis of lignocellulose and lignocellulosic waste, Front. Environ. Sci. Eng. 8 (2014) 151–161.

[28] C.D. Armeniades, E. Baer, ntroduction to Polymer Science and Technology. Ed. H. S. Kaufman and J. J. Falcetta, Wiley, New York, 1977.

[29] S. Ivanova, Hybrid organic-inorganic materials based on polyoxometalates, ISRN Chem. Eng. 2014 (2014) Article ID 963792, 13 pages.

[30] A. Dolbecq, E. Dumas, C.R. Mayer, P. Mialane, Hybrid organic-inorganic polyoxometalate compounds: from structural diversity to applications, Chem. Rev. 110 (2010) 6009–6048.

[31] P. Gouzerh, A. Proust, Main-group element, organic, and organometallic derivatives of polyoxometalates, Chem. Rev. 98 (1998) 77–111.

[32] Y.P. Jeannin, The nomenclature of polyoxometalates: how to connect a name and a structure, Chem. Rev. 98 (1998) 51–76.

[33] D.E. Katsoulis, A survey of applications of polyoxometalates, Chem. Rev. 98 (1998) 359–387.

[34] J.T. Rhule, C.L. Hill, D.A. Judd, R.F. Schinazi, Polyoxometalates in medicine, Chem. Rev. 98 (1998) 327–357.

[35] N. Mizuno, M. Misono, Heterogeneous Catalysis, Chem. Rev. 98 (1998) 199–218.

[36] I. V. Kozhevnikov, Catalysis by heteropoly acids and multicomponent polyoxometalates in liquid-phase reactions, Chem. Rev. 98 (1998) 171–198.

[37] D.-L. Long, R. Tsunashima, L. Cronin, Polyoxometalates: building blocks for functional nanoscale systems, Angew. Chemie Int. Ed. 49 (2010) 1736–1758.

[38] R. Tayebee, F. Nehzat, E. Rezaei-Seresht, F.Z. Mohammadi, E. Rafiee, An efficient and green synthetic protocol for the 24H2O, with emphasis on the catalytic proficiency of Wells- Dawson versus Keggin heteropolyacid, J. Mol. Catal. A. 351 (2011) 154–164.

[39] B. Keita, L. Nadjo, Polyoxometalate-based homogeneous catalysis of electrode reactions: recent achievements, J. Mol. Catal. A. 262 (2007) 190–215.

[40] M. Clemente-León, E. Coronado, A. Soriano-Portillo, C. Mingotaud, J.M. Dominguez-Vera, Langmuir-Blodgett films based on inorganic molecular complexes with magnetic or optical properties, Adv. Colloid Interface Sci. 116 (2005) 193–203.

[41] S. Wang, G. Yang, Recent Advances in Polyoxometalate-Catalyzed Reactions, Chem. Rev. 115 (2015) 4893–4962.

[42] W. Deng, Q. Zhang, Y. Wang, Polyoxometalates as efficient catalysts for transformations of cellulose into platform chemicals, Dalt. Trans. 41 (2012) 9817.

[43] F. Cheng, H. Wang, R.D. Rogers, Oxygen Enhances Polyoxometalate-based

Catalytic Dissolution and Deligni fi cation of Woody Biomass in Ionic Liquids, ACS Sustain. Chem. Eng. 2 (2014) 2859–2865.

[44] J. Tian, J. Wang, S. Zhao, C. Jiang, X. Zhang, X. Wang, Hydrolysis of cellulose by the heteropoly acid H3PW12O40, Cellulose. 17 (2010) 587–594.

[45] Y. Ogasawara, S. Itagaki, K. Yamaguchi, N. Mizuno, Saccharification of Natural Lignocellulose Biomass and Polysaccharides by Highly Negatively Charged Heteropolyacids in Concentrated Aqueous Solution, ChemSusChem. 4 (2011) 519–525.

[46] A.R. Gaspar, J.A.F. Gamelas, D. V. Evtuguinb, C.P. Neto, Alternatives for lignocellulosic pulp delignification using polyoxometalates and oxygen: a review, Green Chem. 9 (2007) 717–730.

[47] J. Zakzeski, P.C.A. Bruijnincx, A.L. Jongerius, B.M. Weckhuysen, The Catalytic Valorization of Lignin for the Production of Renewable Chemicals, Chem. Rev. 110 (2010) 3552–3599.

[48] J. Dupont, On the solid, liquid and solution structural organization of imidazolium ionic liquids, J. Braz. Chem. Soc. 15 (2004) 341–350.

[49] J. Dupont, From molten salts to ionic liquids: a"nano"journey, Acc. Chem. Res. 44 (2011) 1223–1231.

[50] C.S. Consorti, P.A.Z. Suarez, R.F. De Souza, Identification of 1,3-dialkylimidazoIium salt supramolecular aggregates in solution, J. Phys. Chem. B. 109 (2005) 4341–4349.

[51] J. Dupont, P.A.Z. Suarez, R.F. De Souza, R.A.B.- Row, J.-P. Kintzinger, C-H-? interactions in 1-n-butyl-3- methylimidazolium tetraphenylborate molten salt: solid and solution structures, Chem. A Eur. J. 6 (2000) 2377–2381.

[52] M. Antonietti, D. Kuang, B. Smarsly, Y. Zhou, Ionic liquids for the convenient synthesis of functional nanoparticles and other inorganic nanostructures, Angew. Chemie Int. Ed. 43 (2004) 4988–4992.

[53] J.P. Hallett, T. Welton, Room-temperature ionic liquids: solvents for synthesis and catalysis. 2, Chem. Rev. 111 (2011) 3508–3576.

[54] P. Wasserscheid, T. Welton, Ionic Liquids in Synthesis, Wiley-VCH, 2003.

[55] S. Werner, M. Haumann, P. Wasserscheid, Ionic liquids in chemical engineering, Annu. Rev. Chem. Biomol. Eng. 1 (2010) 203–230.

[56] C. DeCastro, Immobilised Ionic Liquids as Lewis Acid Catalysts for the Alkylation of Aromatic Compounds with Dodecene, J. Catal. 196 (2000) 86–94.

[57] R.S. Avellaneda, S. Ivanova, O. Sanz, F. Romero-Sarria, M.A. Centeno, J.A.

Odriozola, Ionic liquid templated TiO2 nanoparticles as a support in gold environmental catalysis, Appl. Catal. B Environ. 93 (2009) 140–148.

[58] M. Herbert, F. Montilla, A. Galindo, R. Moyano, A. Pastor, E. Álvarez, Influence of N-donor bases and the solvent in oxodiperoxomolybdenum catalysed olefin epoxidation with hydrogen peroxide in ionic liquids., Dalton Trans. 40 (2011) 5210–5219..

[59] M. Herbert, A. Galindo, F. Montilla, Catalytic epoxidation of cyclooctene using molybdenum(VI) compounds and urea-hydrogen peroxide in the ionic liquid [bmim]PF6, Catal. Commun. 8 (2007) 987–990.

[60] L. Zhang, Q. Zhang, J. Li, Electrochemical behaviors and spectral studies of ionic liquid (1-butyl-3-methylimidazolium tetrafluoroborate) based sol-gel electrode, J. Electroanal. Chem. 603 (2007) 243–248.

[61] H. Olivier-Bourbigou, L. Magna, D. Morvan, Ionic liquids and catalysis: recent progress from knowledge to applications, Appl. Catal. A. 373 (2010) 1–56.

[62] Q. Zhang, S. Zhang, Y. Deng, Recent advances in ionic liquid catalysis, Green Chem. 13 (2011) 2619–2637.

[63] V.I. Parvulescu, C. Hardacre, Catalysis in ionic liquids, Chem. Rev. 107 (2007) 2615–2665.

[64] Y. Gu, G. Li, Ionic liquids-based catalysis with solids: state of the art, Adv. Synth. Catal. 351 (2009) 817–847.

[65] F.D. Anna, S. Marullo, P. Vitale, C. Rizzo, P. Lo Meo, R. Noto, Applied Catalysis A : General Ionic liquid binary mixtures : Promising reaction media for carbohydrate conversion into 5-hydroxymethylfurfural, Appl. Catal. A Gen. 482 (2014) 287–293.

[66] M.E. Zakrzewska, E. Bogel-łukasik, R. Bogel-łukasik, Ionic Liquid-Mediated Formation of 5-Hydroxymethylfurfural s A Promising Biomass-Derived Building Block, Chem. Rev. 111 (2011) 397–417.

[67] J. Song, H. Fan, J. Ma, B. Han, Conversion of glucose and cellulose into value-added products in water and ionic liquids, Green Chem. 15 (2013) 2619–2635.

[68] S. Hu, Z. Zhang, J. Song, Y. Zhou, B. Han, Efficient conversion of glucose into 5-hydroxymethylfurfural catalyzed by a common Lewis acid SnCl4 in an ionic liquid, Green Chem. 11 (2009) 1746.

[69] Y. Ren, M. Wang, X. Chen, B. Yue, H. He, Heterogeneous Catalysis of Polyoxometalate Based Organic–Inorganic Hybrids, Materials (Basel). 8 (2015) 1545–1567.

[70] T. Rajkumar, G. Ranga Rao, Characterization of hybrid molecular material prepared by 1-butyl 3-methyl imidazolium bromide and phosphotungstic acid, Mater. Lett. 62 (2008) 4134–4136.

[71] G. Ranga Rao, T. Rajkumar, B. Varghese, Synthesis and characterization of 1-butyl 3-methyl imidazolium phosphomolybdate molecular salt, Solid State Sci. 11 (2009) 36–42. doi:10.1016/j.solidstatesciences.2008.05.017.

[72] T. Rajkumar, G.R. Rao, Investigation of hybrid molecular material prepared by ionic liquid and polyoxometalate anion, J. Chem. Sci. 120 (2008) 587–594.

[73] W.-L. Chen, B.-W. Chen, H.-Q. Tan, Y.-G. Li, Y.-H. Wang, E.-B. Wang, Ionothermal syntheses of three transition-metal-containing polyoxotungstate hybrids exhibiting the photocatalytic and electrocatalytic properties, J. Solid State Chem. 183 (2010) 310–321.

[74] Y. Leng, J. Wang, D. Zhu, X. Ren, H. Ge, L. Shen, Heteropolyanion-Based Ionic Liquids: Reaction-Induced Self-Separation Catalysts for Esterification, Angew. Chemie Int. Ed. 48 (2009) 168–171.

[75] X. Han, W. Yan, K. Chen, C.-T. Hung, L.-L. Liu, P.-H. Wu, et al., Heteropolyacid-based ionic liquids as effective catalysts for the synthesis of benzaldehyde glycol acetal, Appl. Catal. A Gen. 485 (2014) 149–156.

[76] J. Chen, L. Hua, W. Zhu, R. Zhang, L. Guo, C. Chen, et al., Polyoxometalate anion-functionalized ionic liquid as a thermoregulated catalyst for the epoxidation of olefins, Catal. Commun. 47 (2014) 18–21.

[77] H. Li, Y. Qiao, L. Hua, Z. Hou, B. Feng, Z. Pan, et al., Imidazolium Polyoxometalate: An Ionic Liquid Catalyst for Esterification and Oxidative Esterification, ChemCatChem. 2 (2010) 1165–1170.

[78] Y. Leng, J. Wang, D. Zhu, L. Shen, P. Zhao, M. Zhang, Heteropolyanion-based ionic hybrid solid: A green bulk-type catalyst for hydroxylation of benzene with hydrogen peroxide, Chem. Eng. J. 173 (2011) 620–626.

[79] R. Wang, D. Jia, Y. Cao, "Facile synthesis and enhanced electrocatalytic activities of organic-inorganic hybrid ionic liquid polyoxometalate nanomaterials by solid-state chemical reaction," Electrochim. Acta. 72 (2012) 101–107.

[80] W. Zhu, W. Huang, H. Li, M. Zhang, W. Jiang, G. Chen, et al., Polyoxometalate-based ionic liquids as catalysts for deep desulfurization of fuels, Fuel Process. Technol. 92 (2011) 1842–1848. doi:10.1016/j.fuproc.2011.04.030.

[81] S.-S. Wang, W. Liu, Q.-X. Wan, Y. Liu, Homogeneous epoxidation of lipophilic alkenes by aqueous hydrogen peroxide: catalysis of a Keggin-type

phosphotungstate-functionalized ionic liquid in amphipathic ionic liquid solution, Green Chem. 11 (2009) 1589. doi:10.1039/b913059b.

[82] E. Rafiee, S. Eavani, A new organic–inorganic hybrid ionic liquid polyoxometalate for biodiesel production, J. Mol. Liq. 199 (2014) 96–101.

[83] X. Chen, B. Souvanhthong, H. Wang, H. Zheng, X. Wang, M. Huo, Polyoxometalate-based Ionic liquid as thermoregulated and environmentally friendly catalyst for starch oxidation, Appl. Catal. B Environ. 138–139 (2013) 161–166.

[84] K. Volkan, O. Muhammad, Synthesis and characterization of a polyoxometalate-based ionic liquid catalyst for delignification of wood biomass, Wood Sci. Technol. 50 (2016) 1213–1226.

[85] J.A. Abia, R. Ozer, Development of Polyoxometalate-Ionic Liquid Compounds for Processing Cellulosic Biomass, Bioresources. 8 (2013) 2924–2933.

Chapter Two

EXPERIMENTAL TECHNIQUES

2.1. Introduction

Catalyst characterization is a lively and highly relevant discipline in Catalysis. Since the heterogeneous reaction occurs at the catalyst surface, the determination of catalyst composition, surface properties and chemical structure, among others, has become of vital importance to elucidate and establish a direct relationship between catalyst properties and behavior.

The materials' characterization should provide valuable information, not only to understand how active/inactive the catalyst is, but also to uncover the tools that allow improving its activity, selectivity and stability.

In the present chapter, the principles of some characterization techniques are briefly outlined together with the experimental procedures and methods used to evaluate the physicochemical properties of the samples. The experimental and analytical operation conditions of all catalytic measurements are also specified.

2.2. Characterization techniques

2.2.1. X-Ray based methods

2.2.1.1. X-Ray Diffraction (XRD)

X-rays with the wavelengths in the angstrom range, are sufficiently energetic to penetrate the solids and to probe their internal structure. In the X-ray diffraction phenomena, the X-rays interact with the atoms that constitute the crystallographic planes, and a coherent and elastic dispersion (Rayleigh scattering) take place. The diffracted waves are the result of the constructive and destructive interferences of the dispersed

waves of each atom present in the plane. Considering that both atoms' positions and properties influence the dispersion, each solid diffracts depending on its structure and composition.

Therefore, the XRD analysis is a non-destructive characterization technique used to determine the crystal phases present in a sample. It is used to identify bulk phases, to estimate particles sizes and, with some refining, permits the quantification of all present phases.

Identification of crystal phases. Bragg`s Law.

When an incident X-Ray beam interacts with the crystal surface, the surface atoms disperse part of the radiation. Non-dispersed fraction penetrates the second atoms layer where, again, partial dispersion takes place (Figure 2.1). The dispersion angle could be then correlated with the distance between planes in the crystalline sample by means of Bragg`s Law (Eq. 2.1).

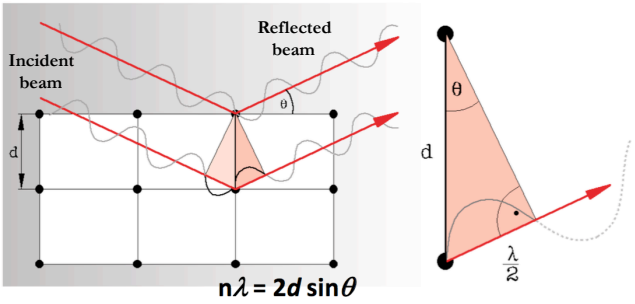

Figure 2.1. Diffraction phenomena. Basis of Bragg's Law.

$$n \cdot \lambda = 2 \cdot d \cdot sin\theta \qquad \text{Eq. 2.1}$$

Where λ is the wavelength of the employed X-rays, d is the distance between the lattice planes, θ is the angle between the incoming X-rays and

the normal to the reflecting lattice plane and n is an integer called the order of reflection.

The d parameter is characteristic of each crystal system, and allows the identification of all present crystal phases in the sample.

Estimation of crystallite size. Scherrer's equation.

The crystalline domain of all present phases (particle size estimation) could be calculated from the XRD analysis thought Scherrer equation (Eq. 2.2)

$$t = \frac{K \cdot \lambda}{\beta \cdot \cos\theta} \qquad \text{Eq. 2.2}$$

where t is the crystallite size; K is a shape factor (typically 0.9); λ is the wavelength of the incident radiation and β is the half-height width.

In this thesis, the conventional XRD experiments were carried out on an X'Pert Pro PANalytical diffractometer, using Cu K_α (40 mA, 45 kV) as source of radiation. The diffractograms were recorded over the 5 to 90° 2 θ range with 0.05° step size and acquisition time of 300 s.

The temperature dependent X-ray diffraction (TXRD) analysis was performed in a high temperature chamber Anton Paar HTK 1200 coupled with an X'Pert Pro Philips diffractometer with Cu anode. The diffractograms were recorded every 50 °C in the 30–750 °C temperature range from 5° to 65° 2 θ range (step size 0.05° and step time 50 s) in air. The heating ramp was fixed to 10 °C/min.

Small angle X-ray diffraction (SAXRD) experiments were also performed in the same X'Pert Pro Philips diffractometer equipped with Cu anode (K_α, 40 mA, 45 kV). The diffractograms were recorded over the 0.5 to 10.0° 2 θ range with 0.01° step size and acquisition time of 1.5 s.

2.2.1.2. Single Crystal X-Ray Diffraction (SCXRD)

X-ray diffraction technique applied to single crystals is one of the most powerful methods to identify the crystal and molecular structure of crystalline material. From collecting and data processing point of view, it is far more complex to use SCXRD than a conventional XRD analysis. The SCXRD analysis requires high specialization and deep knowledge. Typically, a small single crystal is placed on a diffractometer and data are collected under computer-controlled operation. From these data, the fractional coordinates describing the positions of the atoms within the cell, the cell dimensions, the crystal system type, the space group symmetry, the number of formula units per cell and the calculated density can be obtained. In this thesis, all single crystal analysis were performed on a Bruker-Nonius X8APEX-II CCD diffractometer using monochromated-graphite radiation λ (Mo K$\propto$) = 0.71073 Å by means of ω and ϕ scans. The structures were resolved using direct methods with a SIR 2004 [1] and refined using full-matrix least-squares procedures utilizing SHELXL-97 [2]. The SCXRD analysis was performed in collaboration with Dr. E. Álvarez from Instituto de Investigaciones Químicas de Sevilla.

2.2.1.3. X-Ray Fluorescence (XRF)

X-Ray fluorescence (XRF) is a characteristic secondary emission of the material when excited with high energy X-Rays. When an incident X-Ray beam penetrates a target material, some internal electrons are extracted from the inner shell creating a core hole, which is filled by electrons from higher-energy state. During this process, a characteristic X-ray wavelength (also called fluorescence) is emitted by the atom and directly correlated to its nature. Moreover, the XRF is sensitive to the amount of the present material since signal intensity is proportional to the element concentration. All these features make XRF suitable and useful technique to determinate the chemical composition of samples.

In this study, the chemical composition of the samples was evaluated using Panalitycal (AXIOS model) X-ray fluorescence spectrometer equipped with Rh tube of radiation. For the measurements, the samples were dispersed in boric acid pellets.

2.2.1.4. X-Ray Photoelectron Spectroscopy (XPS)

X-Ray Photoelectron Spectroscopy (XPS) is a characterization technique centered on the interaction of light photons with the solid surface. Based on the photoelectric effect, some electrons can be extracted when the photons reach the surface (Figure 2.2.). A photoemission takes places when the radiation energy exceeds the binding energy of the photoelectrons. The electrons absorb energy and are ejected with certain kinetic energy, depending of the incident radiation. As the incident energy is well known, it is possible to measure the kinetic energy, and to calculate

the binding energy of each electron. The binding energy is specific for each element in particular oxidation state. Thus, the XPS technique can provide information about the stoichiometry, oxidation state and electronic structure of all present elements on the solid surface.

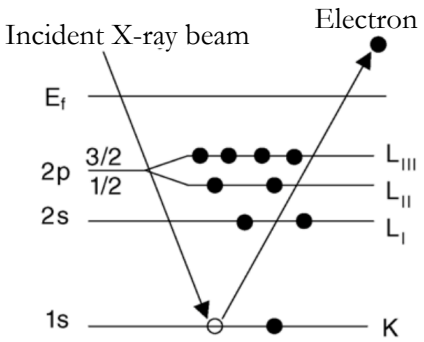

Figure 2.2. Schematic of the emission process of photoelectrons excited by X-rays. Adapted from [3]

In the present thesis, XPS is used to evaluate possible changes on the catalysts' active phase after the reaction process. The measurements were carried out on Leybold-Hereus LHS-1020 instrument coupled with EA200 detector and using non-monochromatic Mg K∝ (220W, 11kV, 1253,6 eV). Prior use the samples were pressed into pellet. The XPS spectra of all samples were recorded at room temperature and the binding energy was calibrated on C1s at 284.6 eV with an uncertainty of ±0.2 eV. The spectra were recorded with constant pass energy of 44 eV and 0.1 eV resolution for the studied zones.

2.2.2. Chemical composition analysis (ICP-AES)

Although XRF is a suitable method to determinate the chemical composition of some materials, it is not sensitive to elements like carbon. For this reason, the chemical composition of all carbon-based catalysts present in this thesis was determined by Inductively Coupled Plasma Atomic Emission Spectrometry (ICP-AES). This technique is based on the atomic absorption phenomena that take place when an atom or ion is illuminated with electromagnetic radiation, absorbs energy and becomes excited. During the excitation process, an electron from the low energy levels is promoted to high energy orbital. Such atom is less stable and will decay to less excited state by losing energy in form of electromagnetic (photon) radiation.

During the analysis, a liquid sample is transformed into a fine mist (inside the nebulization chamber) and decomposed by intense heat (plasma temperatures, between 5000-10000 K) into a cloud of hot gases containing excited free atoms and ions of the element of interest. The emitted radiation goes thought a monochromator and reaches the detector.

This technique facilitates qualitative and quantitative information. In general, the quantitative information (concentration) is related to the amount of electromagnetic radiation that is emitted while the qualitative information is related to the wavelengths at which the radiation is emitted.

In this thesis, ICP measurements were performed on Horiba Jobin Yvon spectrometer, after HF acid digestion of the samples. All the analysis were carried out at Centro de Investigación Tecnología e Innovación de la Universidad de Sevilla (**CITIUS**).

2.2.3. Transmission Electron Microscopy (TEM)

Electron microscopy is a straightforward technique to determine the size and shape of the supported particles. It can also reveal information of particles composition and internal structure, for example, by detecting the characteristic X-rays produced by the interaction of the electrons with the matter. This technique is known as Energy Dispersive X-ray spectroscopy (EDX) and allows to couple quantitative analysis with microscopic morphology measurements.

In TEM microscopy, the electron beam passes through an ultra-thin sample. The image is formed from the interaction of transmitted electrons with the studied system after magnification and focusing on imaging device, such fluorescent screen, photographic film or a CCD camera. TEM gives information about sample' micromorphology, the presence of different crystalline phases and allows analysis of nanometer size structures.

TEM micrographs of this study were acquired on PHILIPS CM-200. Samples were dispersed in ethanol by using an ultrasonic device and deposited on a holey carbon-coated copper grid.

High-Resolution Transmission Electron Microscopy (HRTEM) and High-Angle Annular Dark Field-Scanning Transmission Electron Microscopy (HAADF-STEM) images presented in this thesis were recorded on a JEOL2010F instrument. The spatial resolution at Scherrer defocus conditions in HRTEM mode is 0.19 nm, while the HAADF-STEM studies were performed using an electron probe of 0.5 nm of diameter and a diffraction camera length of 10 cm. The chemical composition of the samples was studied in STEM mode using an Energy-Dispersive X-

ray spectrometer (Oxford Instrument, Inca Energy-200). The samples were supported on a holey carbon-coated copper grid without using of solvents. The excess of sample was removed from the grids using a flow of N_2.

2.2.4. Z potential measurement: isoelectric point (IEP)

Potential Z and isoelectric point (IEP) measurements provide information about basicity and/or acidity of the materials in aqueous media. Taking into account that the catalytic studies are performed in liquid phase the acid/base properties could influence the overall process. The potential Z may then be used to compare the activity.

The net charge of the solid surface, as a result, of H^+ or OH^- absorption is defined as potential Z and the IEP as the pH value at which the net charge is equal to zero. The IEP is characteristic for each solid and independent of solution composition.

IEP measurements were carried out on a Malvern Zetamaster equipment. The samples were prepared by dispersion of 5 mg in 100 mL 0.01M NaCl solution using an ultrasonic device. From this starting solution, six more with different pH were prepared, by adjusting the pH between 3 and 12 with HCl and NaOH aqueous solutions and stabilizing it during 24 hours.

2.2.5. N_2 physisorption: specific surface area (BET surface area)

The solid materials present particular surface area through which they interact with the media. In catalysis, the determination of this area can be very useful for both synthesis and reaction processes.

The N_2 adsorption at its boiling temperature (-196 °C) is one of the most employed techniques for this purpose owed to the suitability of N_2 as probe molecule. Nitrogen presents a single physical adsorption with moderate strength; it has small molecular size and can access smaller pores and permits reproducible operation conditions (pressure and temperature).

The estimated surface area, expressed in m^2/g, represents the accessible surface of the material for molecule adsorption by gram of a sample. The specific surface is determined by Brunner Emmett Teller (BET) method and corresponds to the sum of internal pores surface and external surface of the grains.

The N_2 adsorption experiments were carried out on a Sorpty 1750 CE Instruments and the single-point BET analysis method employed. Before use the samples were pre-treated under vacuum conditions at 150 °C.

2.2.6. Temperature programmed reduction (TPR-H_2)

The temperature programmed reduction experiments (TPR) provides useful information about the reducibility of the species present in the solid. By using this techniques, information about the complete catalyst reduction, the interaction between the present species and their modification under external factors, such as catalytic reaction, can be elucidated.

The reduction experiments were performed using 5%H_2 in Ar under continuous temperature increase at atmospheric pressure (10 °C/min from room temperature to 900 ºC). The difference between the H_2 inlet and outlet is measured as a function of time by using a thermal

conductivity detector (TCD). Cryogenic mixture composed by liquid N_2 and ethanol was used as cold trap to retain the formed H_2O during the reduction. For the quantitative analysis the TCD signal was calibrated with CuO standart (Strem Chemicals 99.999 %).

2.2.7. Vibrational spectroscopies: Raman and Diffuse Reflectance Infrared Fourier Transform (DRIFT).

The energy of the molecules can be associated mainly to three components: a) the electron movement, b) the vibration of the constituent atoms and c) the rotation of the molecule. When a molecule absorbs a photon, the three processes take place, but at different time scale, being the electronic vibrations significantly faster than the rotational ones. Vibrational spectroscopies provide structural information for the studied material, its molecular symmetry and possible absorbed species and sites. It is important to mention that, the observed vibrational transitions are obtained when the radiation source used to excite the molecule has a specific wavelength (λ) comprised between 10^{-2}-10^{-4} nm. However, not all transitions are allowed for each molecule, the transitions number depends on its symmetry and selection rules.

Two vibrational spectroscopies were used to characterize the solid materials, Raman spectroscopy to obtain structural information and DRIFT spectroscopy to study the absorbed species on the catalyst surface after reaction processes.

The Raman study was performed on a dispersive Horiva Jobin Yvon® (HR800) microscope with confocal aperture of 1000 μm, and using an objective 50x, green laser (λ = 532.14 nm) and intensity filter D2.

DRIFT experiments were recorded at room temperature without sample dilution using a Thermo Nicolet Nexus FT-IR spectrometer equipped with a liquid nitrogen cooled MCT detector at 4 cm^{-1} resolution and average of 128 scans. The whole optical path was purged with CO_2 and H_2O-free nitrogen. About 50 mg of fresh or used catalyst finely grounded was loaded in the Praying Mantis™ cell for each measurement.

2.2.8. Ultraviolet-Visible (UV-Vis) spectroscopy

The UV-Vis spectroscopy measures the absorption or reflectance of the samples in visible or near-infrared range of the electromagnetic spectrum, where electronic transitions take place. The energy from incident light is absorbed by the molecules, which become excited after an electron transition to higher energy level. Subsequently, the electron decays to reach the most stable configuration, emitting radiation.

This technique provides qualitative information about the type of electron transition through the position of the absorption wavelength maximum, which can be also quantified by the Lambert-Beer law. However, its use is limited only to qualitative analysis, as will be explained in the following chapters.

UV–Vis measurements were carried out on UV–vis Avantes AvaLight-DH-S-BAL spectrometer equipped with optic fiber sensor for liquids at wavelengths between 100 to 1000 nm.

2.2.9. Nuclear magnetic resonance (NMR) spectroscopy

Nuclear magnetic resonance (NMR) spectroscopy is a characterization technique mainly employed to elucidate molecular structures and reaction mechanisms in liquid media by means of atom labeling. It provides qualitative and quantitative information about different molecules present in solution.

Some atomic nucleus can absorb radiation in the radiofrequency range under external magnetic field. The exact absorption frequency depends on nucleus environment, a fact that allows the determination of molecule structure. In order to employ NMR, nucleus must have a magnetic moment distinct to zero. The later is not fulfilled for nucleus with even atomic and mass numbers (like ^{12}C and ^{16}O). The most important nucleus used for NMR purpose are: ^{1}H, ^{13}C, ^{31}P, ^{19}F and ^{15}N.

The relative abundance of isotopes is also an important parameter. Greater abundance leads to higher signal intensity and therefore to more resolute peaks.

In this thesis, ^{1}H and ^{13}C NMR were employed to determinate the species in the liquid post reaction products. For this purpose, the final reaction mixture was lyophilized in a Flexi-Dry P FTS System lyophilizator and re-dissolved in deuterium oxide. This experiment was performed in a Bruker Avance DRX-400.

^{13}C and ^{31}P solid state NMR were employed to elucidate the molecular structure of some hybrid materials. The experiment was performed in a Bruker NMR Avance III WB 600 MHz. Phosphoric acid (85% in H_2O) was used as reference for ^{31}P NMR.

2.2.10. Oxygen storage complete capacity (OSSC) and oxygen storage capacity (OSC)

Surface migration of oxygen can be very important for the oxidation processes. The Oxygen Storage Complete Capacity (OSCC) and Oxygen Storage Capacity (OSC) provide very relevant information regarding the oxygen mobility and reducibility of the samples. In particular, the oxygen storage complete capacity (OSCC) provides information about the maximum reducibility of the samples, while the oxygen storage capacity (OSC) informs about the most reactive and immediately available oxygen atoms.

For the Oxygen Storage Complete Capacity (OSCC) 100 mg of catalyst were loaded into a U-shaped quartz reactor and the temperature raised in a 50 mL/min He flow. For each temperature, ten O_2 pulses of 1 mL were injected every 2 min. After that, the sample is submitted to ten equivalent CO pulses. The OSCC is obtained from the total CO_2 produced in all CO pulses. The sample is then degassed during 10 min in a He flow and subjected to a new series of oxidizing pulses (ten O_2 pulses) and subsequently to six alternating pulses ($CO–O_2–CO–O_2–CO–O_2$). The OSC is determined by the average amount of CO_2 per pulse formed after the first CO pulse of the alternated ones. This method is based on that proposed by Duprez *et al.* [4,5]. The gas composition at the exit of the reactor was analyzed by a mass spectrometer PFEIFFER Vacuum PrismaPlus controlled by Quadera® software.

2.3. Catalytic activity

2.3.1. Experimental device

The reactions were performed in a glass batch reactor of 50 mL capacity equipped with magnetic stirrer at atmospheric pressure. To maintain a constant temperature, both reactor and a thermocouple were submerged in oil bath and heated with an IKA® C-MAG HS 7 heater. The stirring rate was normally fixed to 600 rpm (position 2.5 of the above mentioned heater).

The reactions carried out under increased pressure were performed using two different models of Parr 4842/4848 autoclave reactor of 100/250 mL of capacity, equipped with mechanical stirrer (0-600 rpm) and temperature/pressure measurement tool (Figure 2.3). The stainless steel vessels were equipped with a reducing glass vessel, allowing a good stirring even if the total reaction volume is $\frac{1}{5}$ of the total volume. Both systems permit temperature control through a PID controller with K thermocouple situated inside the reactor. The reactors are closed between two semi-rings as a security element.

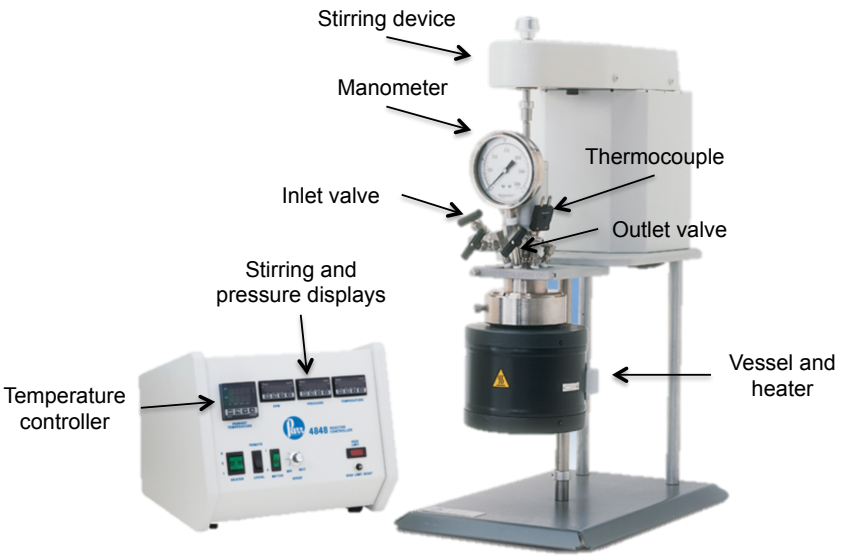

Figure 2.3. Autoclave reactor used in catalytic tests.

2.3.2. Catalytic activity tests

The operation conditions depend on the catalytic reaction and employed bifunctional catalyst.

The reaction studies concerning hybrid materials could be divided in three groups: i) glucose epimerization, ii) glucose/fructose dehydration and iii) glucose oxidation. Those catalytic tests were carried out at atmospheric pressure in a glass batch reactor of 50 mL at 600 rpm. The epimerization reaction was performed in 5 ml of total volume in which glucose (1 mmol, 0.1802 g) and hybrid catalyst in a Glucose:hybrid 256:1 molar ratio (0.0084 g) were mixed with 5 ml of H_2O at different temperatures. For the dehydration reaction, the reaction media was constituted by 1 mL of H_2O and 3 mL of organic solvent, 4-methyl-2-pentanona (MIBK) or diethyl ether (DEE) in which 1 mmol (0.1802 g) of sugar (glucose or fructose) was dissolved. The catalyst was added in Glucose:hybrid 360:1 molar ratio and the temperature maintained at 120 ºC. Finally, for the glucose oxidation process 2 mL of water, 1 mmol of glucose, 3 mmol of oxidant (hydrogen peroxide) and catalyst in Glucose:hybrid 360:1 molar ratio were mixed before the reaction. The reaction proceeds at fixed stirring rate of approximately 600 rpm and temperature at 60 ºC.

Similarly, the operation conditions for the reactions involving gold based catalysts are separated in two groups: j) base-free oxidation of glucose and jj) HMF oxidation to FDCA. The former was carried out at atmospheric pressure (glass batch reactor) with 5 mL of water, 1 mmol of glucose and catalyst in a Glucose:Au molar ratio of 100:1 at different temperatures and stirring rates, whereas, the later under 10 bar O_2 pressure (autoclave

reactor), in 25 mL total volume of water, 2 mmol (0.25 g) HMF and HMF:Au:NaOH molar ratio of 1:0.01:2 at 70 ºC and 400 rpm.

2.3.3. Analytical method

After every catalytic tests, a sample was taken, microfiltered (with a syringe filter of 0.45 μm) diluted in distilled water and analyzed by High Pressure Liquid Chromatography (HPLC), using a Varian 360 LC chromatograph equipped with a Varian Pro Star pump and Refractive index detector (RID). The used column was a Hi-Plex H 300 × 7.7 mm provided with a Hi-Plex H 50 × 7.7 mm pre-column. Water or 0.01M H_2SO_4 solution were used as eluents.

Liquid chromatography is one of the most used techniques to analyze carbohydrates. The main difficulties in the analysis of carbohydrates arise from their considerable number of isomeric forms due to various possible configurations of the monosaccharides. The most common stationary phase used for these purposes are cation exchange columns consisting of sulfonated polymer-based materials, which can be obtained in various degrees of cross-linking and various particles sizes. The used column is based on sulfonated poly(styrene-divinyl-benzene) (PS-DVB) copolymers in the H^+ form with a 8% of cross-linking. The degree of cross-linking limits the high molecular weight compounds detection, such as trisaccharides or oligomers; therefore, only simple sugars or disaccharides will be retained and eluted in this column. However, sulfonated resins in the protonated form are useful for profiling not only monosaccharides and sugar alcohols, but may be useful for analysis of a wide range of organic acids, alone or in combination with carbohydrates, short-chain

alcohols, aldehydes and ketones. The column selectivity can be alterated by changing the pH of the eluent, by using for instance, diluted acid. Those features make this column the most suitable for this study, due to the different processes that will be addressed. The compound identification was achieved by calibration using reference commercial samples. The standard HPLC configuration parameters used for the analysis of the majority of samples are summarized in Table 2.1.

Table 2.1. HPLC configuration parameters used in Varian 360 LC

Injector	Injection volume	20 μL
	Injection temperature	Room temperature
Column	Model	Hi-Plex H (300 × 7.7 mm)
	Column temperature	40 ºC
	Eluent	H_2O or 0.01M H_2SO_4
	Eluent flow rate	0.4 mL/min
Detector	Type	Refractive index (RID)
	Detector temperature	40 ºC

The study of HMF oxidation was carried out in the Industrial Chemical Department "Toso Montanari", Bologna University (Italy). In the same way, samples were analyzed by HPLC by using an Agilent Infinity 1260 liquid chromatograph equipped with a DAD detector and an Aminex HPX-87H (300 × 7.8 mm) column using a 0.005M H_2SO_4 solution as mobile phase. The standard HPLC configuration parameters used for the analysis of the HMF oxidation reactions are summarized in Table 2.2.

Table 2.2. HPLC configuration parameters used in Agilent Infinity 1260 LC

Injector	Injection volume	5 μL
	Injection temperature	Room temperature
Column	Model	Aminex HPX 87-H (300 × 7.8 mm)
	Column temperature	30 ºC
	Eluent	0.005M H_2SO_4
	Eluent flow	0.5 mL/min
Detector	Type	Diode array (DAD)
	Wavelengths of interest	251, 264 and 284 nm

The conversion, selectivity, products yield and carbon balance (CB) were calculated from the peak areas obtained through the HPLC analyses, according to the following equations:

$$Conversion\ (\%) = \frac{[Glucose]_I - [Glucose]_F}{[Glucose]_I} \times 100 \qquad \text{Eq 2.3.}$$

$$Selectivity\ (\%) = \frac{Carbon\ mol\ of\ specific\ product}{Carbon\ mol\ of\ glucose_I - Carbon\ mol\ of\ glucose_F} \times 100$$

Eq 2.4

$$Yield\ (\%) = \frac{Conversion\ (\%)}{100} \times Selectivity\ (\%) \qquad \text{Eq 2.5}$$

$$CB\ (\%) = \frac{Final\ carbon\ mols}{Initial\ carbon\ mols} \times 100 \qquad \text{Eq 2.6}$$

Where $[Glucose]_I$ and $[Glucose]_F$ are the initial and final concentration of starting material, respectively (glucose taken as example in this case).

References

The development of this chapter has been based on the book: J. W. Niemantsverdriet, Spectroscopy in Catalysis, An Introduction, Second Edition, Wiley-VCH

[1] M.C. Burla, R. Caliandro, M. Camalli, B. Carrozzini, G.L. Cascarano, L.G.C. De Caro, et al., No Title, J. Appl. Crystallogr. 38 (2005) 381.

[2] G.M. Sheldrick, No Title, Acta Crystallogr., Sect. A. 64 (2008) 112.

[3] P.K. Chu, L. Li, Characterization of amorphous and nanocrystalline carbon films, Mater. Chem. Phys. 96 (2006) 253.

[4] S. Kacimi, J.B. Jr., R. Taha, D. Duprez, Oxygen storage capacity of promoted Rh/CeC2 catalysts. Exceptional behavior of RhCu/CeO2, Catal. Letters. 22 (1993) 343–350.

[5] S. Royer, D. Duprez, Catalytic Oxidation of Carbon Monoxide over Transition Metal Oxides, ChemCatChem. 3 (2011) 24–65.

Chapter Three

SYNTHESIS and CHARACTERIZATION of POLYOXOMETALATE-IONIC LIQUID BASED CATALYSTS

Summary[1]

In this chapter the preparation of different polyoxometalate based organic-inorganic salts is described. As inorganic fraction, three POM anions based on molybdenum, tungsten and molybdenum-vanadium are used, and as organic fraction, three ionic liquids with different imidazolium substituted cations selected. A total of nine molecular salts were obtained by combination of one POM anion with each IL. The structure of the solids were fully characterized by means of XRD, temperature programmed XRD, Raman spectroscopy, small angle XRD and solid state $^{13}C\{^{1}H\}$ and ^{31}P NMR. The crystallographic parameters and structures of some molybdenum-based hybrids are also determined by single crystal XRD.

[1]Some results presented in this Chapter are published in:

C. Megías-Sayago *et al.* **Catalysis Today** 278 (2016) 82–90.

3.1. Introduction

Polyoxometalates (POMs) take part of a very big family of anionic molecular species consisting of transition metal ions and oxygen atoms. They are usually species with important molecular weight and good solubility in polar solvents. A wide range of applications arises from their unique properties being the super acidity and the excellent structural stability under multi-electron redox cycles the two most exceptional POMs features for catalytic applications. They are employed in several homogeneous industrial catalytic processes, demonstrating high potential guaranteed by high activity and low toxicity and corrosion. However, the difficulties in catalysts recycling and products separation and purification restrains the POMs application and makes the processes environmentally and economically unviable [1].

Several strategies to prepare heterogeneous POM catalysts have been applied, mainly based on the loading of the POM structure onto porous supports [2–5]. However, recently, the organic-inorganic hybrid POM compounds emerge as a promising way to form heterogeneous POMs [6–8] with tunable properties derived from the high number of possible organic ligands and resulting structures after combining them with the metal oxide cluster. Generally, the POMs structure is considered as potential Brönsted site, whereas the introduction of an organic ligand increases the porosity of the structure and provides a convenient way to modify the polarity of the framework.

From a crystallographic point of view, a wide variety of structures can be originated taking into account the diversity of conformations resulting from different organic fractions (with very different molecular weight, chemical composition and chain lengths) [9–13]. The formation of organic-inorganic hybrid POM is usually described as self-assembling

process difficult to predict in structure and composition [1,14] due to the complex behavior of POM - organic counterion interaction during crystallization. A controlled design and synthesis of this kind of hybrids is still an important challenge.

In various studies, Ranga Rao and coworkers [15–17] reported the preparation of Keggin POM based hybrid structures by using alkyl imidazolium ionic liquids as organic fraction supplier, concretely 1-butyl-3-methylimidazolim bromide, [Bmim]Br. The reaction between the organic and inorganic fraction gives rise to the formation of molecular salts with a general formula $[Bmim]_3[XM_{12}O_{40}]$ where X stands for P and M for Mo or W. The same simple method of preparation, hybrid precipitation, will be used in this thesis to obtain different salts by varying the type of alkyl imidazolium ionic liquid and the type of Keggin POM.

3.2. Catalysts synthesis

3.2.1. Synthesis of heteropolyacids

The proton compensated POM clusters, known as heteropolyacids (HPAs), were synthesized as previously reported by Wu [18]:

For the preparation of $\mathbf{H_3PW_{12}O_{40}}$ the used reactants were $Na_2WO_4 \cdot 2H_2O$ (Sigma Aldrich), 85 % H_3PO_4 (Panreac), 37% HCl (VWR) and diethyl ether (Panreac). $Na_2WO_4 \cdot 2H_2O$ (25 g) was dissolved under moderate heating in distilled water (25 ml). 85 % H_3PO_4 (2.5 ml) and HCl (20 ml) were then added to the W precursor. After four hours, the obtained precipitate was filtered and redissolved in water (30 ml). Diethyl ether (17 ml), HCl (10 ml) and the aqueous solution were mixed in a separatory funnel. The lowest layer was taken and distilled water (30 ml),

diethyl ether (12 ml) and HCl (10 ml) were added again. After separation, the lowest layer was taken, the solvent evaporated and white solid acid $H_3PW_{12}O_{40}$ finally obtained. From now the nomenclature used to denote this compound will be PWA.

In similar way, $\mathbf{H_3PMo_{12}O_{40}}$ was prepared as reported by Wu [18]. The $Na_2MoO_4 \cdot 2H_2O$ (Sigma Aldrich), 85% H_3PO_4 (Panreac), 37% HCl (VWR), diethyl ether (Panreac), and 65% HNO_3 (VWR) reactants were used.

$Na_2MoO_4 \cdot 2H_2O$ (25 g) was dissolved in 50 ml of distilled water, then H_3PO_4 (2.5 ml) and 25 ml HCl were added. The solution was transferred to separatory funnel and the active compound extracted in diethyl ether (37.5 ml). After shaking and cooling (about 15 minutes), three layers were formed. The lowest was transferred to another funnel and washed with distilled water (40 ml) several times and purified by the HCl (12.5 ml) and diethyl ether (20 ml) addition. Once again, the lowest layer was collected and washed with H_2O (40 ml) after separation. H_2O (7 ml) and a few drops of HNO_3 were added. The product was crystalized by evaporating excess water, which results in the appearance of yellow crystals. From this point, the PMoA abbreviation will be used to denote this compound.

Finally, for the $\mathbf{H_5PMo_{10}V_2O_{40}}$ preparation [19] MoO_3 (Riedel-de Haën), V_2O_5 (Sigma Aldrich) and 85% H_3PO_4 (Panreac) were used as reactants. MoO_3 (7.32 g) and V_2O_5 (1.03 g) were dissolved in 125 mL of distilled water and heated to 120ºC in a round bottom flask equipped with a reflux condenser. Reached 120ºC, H_3PO_4 (1 ml) was added and the mixture aged for 24 hours. An orange like colored viscous liquid was obtained. PMoVA will be used as abbreviation in the manuscript.

3.2.2. Synthesis of the hybrid structures (POM-IL)

For the hybrid synthesis, three commercial alkyl imidazolium ionic liquids were used, 1-ethyl-3-methylimidazolium methanesulfonate (Alfa Aesar), 1-butyl-3-methylimidazolium methanesulfonate (Sigma Aldrich) and 1-hexyl-3-methylimidazolium chloride (Alfa Aesar).

In all cases, the organic cations are constituted by 3-methyl substituted imidazolium ring, differing in the 1-alkyl substituent. The nomenclature used to denote them refers to the number of carbon atoms in the later, [C2mim], [C4mim] and [C6mim] for 1-ethyl-3-methylimidazolium, 1-butyl-3-methylimidazolium and 1-hexyl-3-methylimidazolium, respectively. The three synthesized HPAs were combined with each IL, resulting in three different hybrid structures per Keggin anion and, therefore, a total number of nine molecular salts. As reported by Ranga Rao [15,16], $[C4mim]_3[XM_{12}O_{40}]$ is the resulting molecular formula, where all protons are substituted by organic cations. The amount of HPA and IL was adjusted to preserve the 3:1 IL:POM molar ratio (when M = W, Mo) and 5:1 IL:POM molar ratio (in the case of M = Mo-V). The method of preparation is analogous for all solids. All used abbreviations are summarized in Table 3.1. The structures of three representative hybrids are presented in Figure 3.1.

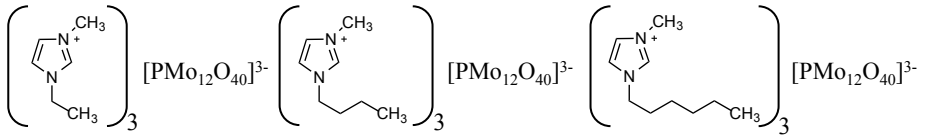

$[C2mim]_3[PMo_{12}O_{40}]$ $[C4mim]_3[PMo_{12}O_{40}]$ $[C6mim]_3[PMo_{12}O_{40}]$

Figure 3.1. Structure of representative POM-IL hybrids based on phosphomolybdic acid

For the [C2mim]PMo synthesis, as an example, appropriate quantities of

PMoA (0.9 g) and 1-ethyl-3-methylimidazolium methanesulfonate (0.34 g) were separately dissolved in distilled water. When mixed, a precipitate of the POM-IL hybrid appeared. The precipitate was separated by filtration and subsequently dried at room temperature. Following this procedure, three hybrid structures were obtained for each parent acid (Table 3.1.). All the hybrids were used as prepared without any additional treatment.

Table 3.1. List of synthesized compounds and their abbreviations.

Compound	Abbreviation
$H_3PW_{12}O_{40}$	PWA
$[C2mim]_3[PW_{12}O_{40}]$	[C2mim]PW
$[C4mim]_3[PW_{12}O_{40}]$	[C4mim]PW
$[C6mim]_3[PW_{12}O_{40}]$	[C6mim]PW
$H_3PMo_{12}O_{40}$	PMoA
$[C2mim]_3[PMo_{12}O_{40}]$	[C2mim]PMo
$[C4mim]_3[PMo_{12}O_{40}]$	[C4mim]PMo
$[C6mim]_3[PMo_{12}O_{40}]$	[C6mim]PMo
$H_5PMo_{10}V_2O_{40}$	PMoVA
$[C2mim]_5[PMo_{10}V_2O_{40}]$	[C2mim]PMoV
$[C4mim]_5[PMo_{10}V_2O_{40}]$	[C4mim]PMoV
$[C6mim]_5[PMo_{10}V_2O_{40}]$	[C6mim]PMoV

3.3. Structural characterizations of POM-IL catalysts

3.3.1. XRD study

The XRD diffraction patterns of all synthesized compounds are presented in Figure 3.2. In all cases, the XRD patterns of the hybrids are very similar to that of the parent acid, indicating the similarity of all structures. Nevertheless, a shift in the existing diffractions and some new ones are

detected, accounting for the presence of the organic cation and some modifications in the structure.

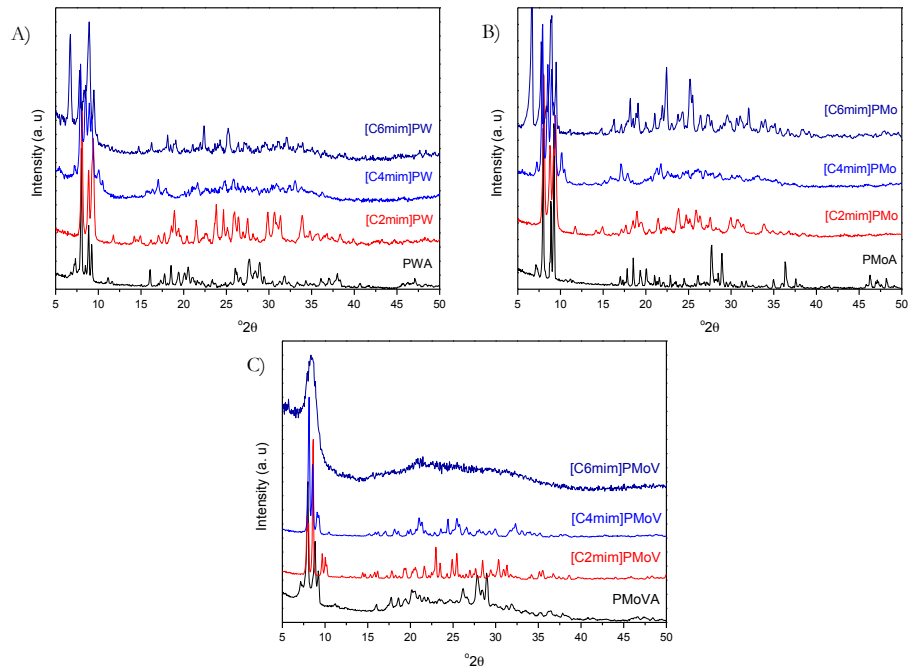

Figure 3.2. XRD patterns of A) PWA and its hybrids, B) PMoA and its hybrids and C) PMoVA and its hybrids.

The XRD pattern of the phosphotungstic acid (PWA, Fig. 3.2. A)) corresponds to hydrated acid $H_3PW_{12}O_{40} \cdot 14H_2O$ (JCPDS #00-050-0656) belonging to the triclinic system in agreement with literature [20]. It can be seen that PWA displayed a set of well-resolved diffractions for the secondary structure of a typical heteropolyacid (HPA) crystal with Keggin structure [21]. The introduction of different organic fractions leads to similar diffractions between 7° and 40°, which suggests that the Keggin structure remains intact in the hybrids. It should be noted that the longest alkylic chain hybrid [C6mim]PW present a sharp diffraction at small angles, around 6°, normally indicative for long-range ordering. As

reported [22], some ionic liquids in solid state form an extended cooperative network of cations and anions, connected through hydrogen bonds. This 3D arrangements in the case of imidazolium ILs give rise to "free" volumes with high degree of directionality, known as ionic self-assemblies (ISA) [14].

Similar results are obtained for the phosphomolydic acid series (Fig. 3.2. B)). The XRD pattern of PMoA corresponds to hydrated $H_3PMo_{12}O_{40} \cdot 13H_2O$ (JCPDS #01-075-1588) acid with triclinic system. In the same way, the changes of the XRD profiles appear to be related to the type of cation being the XRD profile of [C2mim]PMo more similar to the parent acid than [C4mim]PMo and [C6mim]PMo. Shorter the aliphatic chain, the smaller the modification of the parent acid diffractogram.

Finally, XRD patterns of PMoVA and its hybrids are presented in Fig. 3.2. C). Despite the formation of viscous liquid instead of a solid powder for this acid, the diffractogram shows the typical Keggin-structure organization. The XRD pattern agrees with $H_5PMo_{10}V_2O_{40} \cdot 36H_2O$ (JCPDS #01-084-0233) tetragonal system. Once again, the [C2mim]PMoV and [C4mim]PMoV diffractograms are very similar to the acid, leading to the same conclusions described to homologous hybrids and acids. Nevertheless, the [C6mim]PMoV hybrid presents only one broad reflection indicating the formation of a different structure. It is suggested that during the synthesis of [C6mim]PMoV, the HPAs crystal structure is rearranged to a self-assembly of cations and anions through electrostatic interaction, hydrogen bonds, and Van der Waals forces. Due to the introduction of long chain cation and originating higher steric impediments the resulting structure is semi-amorphous [19].

3.3.2. Thermogravimetric (TGA) analysis

The thermal stability of the synthesized structures is studied by TGA analysis in the presence of O_2 and the results are presented in Figure 3.3. Weight losses corresponding to physisorbed H_2O and structural H_2O removal (100-200ºC) area is observed for all acids as well as the destruction of the Keggin structure in the 250-600ºC range. It is worth mentioning that no initial low temperature weight loss was recorded for the hybrids (except for [C4mim]PMoV), indicating that the samples were water free. The later suggests that the water molecules are not involved in the hybrids 3D structure, unlike for the HPAs [23], reinforcing the idea that the self-assembly and, therefore, the final structure is directed probably by the ionic liquid.

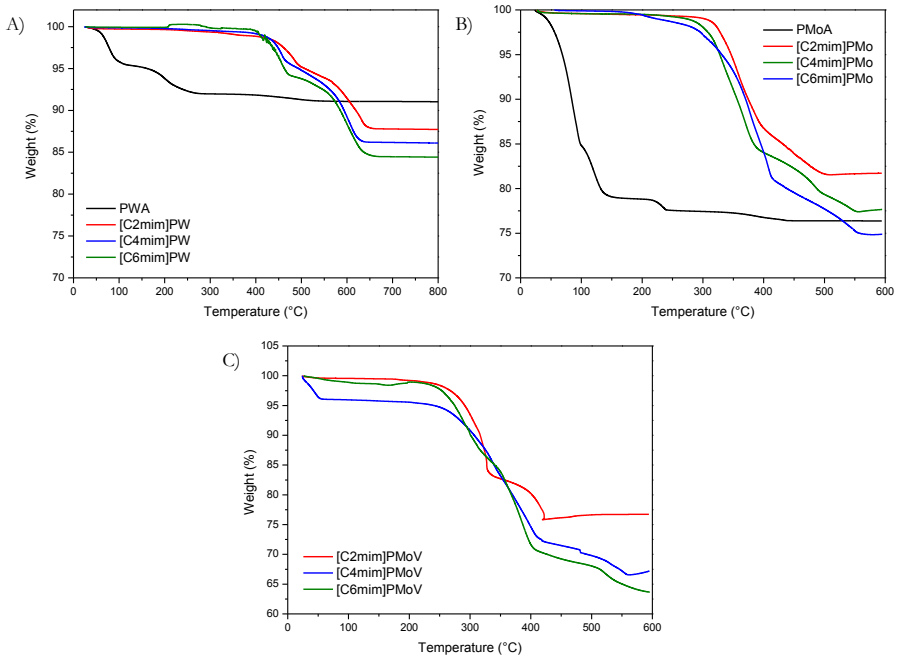

Figure 3.3. Thermogravimetric analyses of A) PWA and hybrids, B) PMoA and hybrids, C) hybrids based on PMoV

Generally, the hybrids based on PMoA (Fig. 3.3. B)) and PMoVA (Fig. 3.3. C)) exhibit lower thermal stability than PWA based ones (Fig. 3.3. A)). Regarding PWA series, the hybrids start to decompose in the range 400-435ºC being the less stable [C6mim]PW, followed by [C4mim]PW and [C2mim]PW. The organic part is lost in 3 successive steps up to 650ºC accompanied by a heat release (DTA curve not shown) due to the organic fraction combustion in the presence of air. The formed phases remain stable from 650 to 800ºC. Similar trend is observed for the PMoA series but at lower temperatures, indicating lower thermal stability. The hybrids start to decompose at around 300ºC following the tendency described for W hybrids. The PMoVA based hybrids decompose at lower temperatures starting at 250ºC.

It is well known, that the thermal stability of the HPAs follows the W > Mo trend [24]. This is confirmed for both, HPAs and its corresponding hybrids. For the hybrid structures formed by the same cation the W > Mo > MoV stability trend as for the parent acids is also obeyed. For the same Keggin anion, however, the thermal stability depends on the organic cation, and it is directly related with the number of carbon of the alkyl chain, and follows the tendency [C2mim]PM > [C4mim]PM > [C6mim]PM, where M = W or Mo.

3.3.3. XRD as function of temperature (TXRD)

In order to study in more details the phase transformation of both parent acids and hybrids, a XRD study as a function of temperature was undertaken. The XRD measurements were performed in flowing air from 30ºC to 750ºC with isotherms at every 50ºC. However, only the temperatures for which significant changes were detected appear in the figures.

- PWA series

The XRDiffractograms of PWA and its hybrids are summarized in Figure 3.4 and Table 3.2, where all corresponding phases at different temperatures are listed.

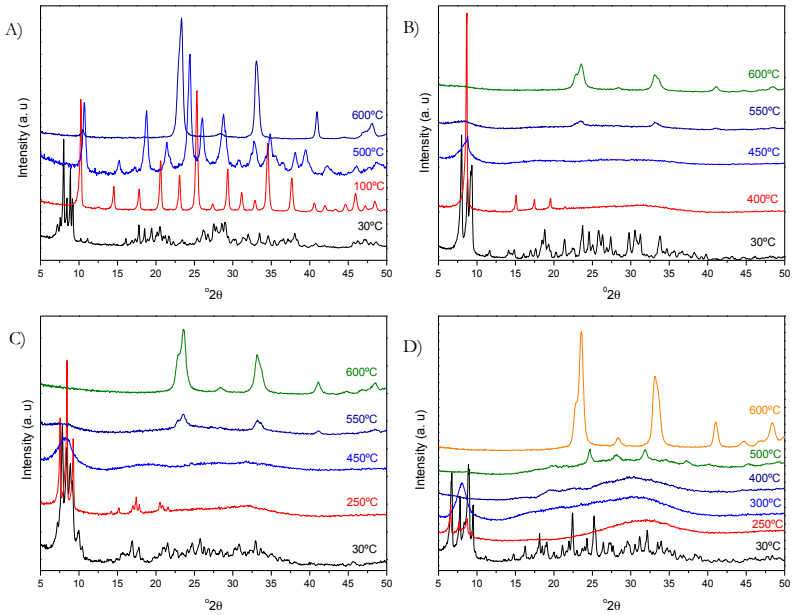

Figure 3.4. XRDiffractograms of PWA series as a function of temperature: A) PWA, B) [C2mim]PW, C) [C4mim]PW and D) [C6mim]PW.

The $H_3PW_{12}O_{40}\cdot 14H_2O$ (JCPDS #00-050-0656) loses hydration water in two steps resulting in $H_3PW_{12}O_{40}\cdot 6H_2O$ (JCPDS #00-050-0304) and anhydrous $H_3PW_{12}O_{40}$ (JCPDS #00-050-0657) at 100 and 300ºC, respectively. The mixture of anhydrous acid and $H_3PW_{12}O_{38}$ (JCPDS #00-050-0658) remains stable until 550ºC where starts the transformation into $WOPO_4$ (JCPDS #00-044-0349) and WO_3 (JCPDS #00-041-0905 + #01-071-0131) at 600ºC. WO_3 is the unique phase detected from this point to 750ºC.

As a confirmation of the TG study, the phase transformations of the hybrids, registered by XRD, show a dependence on the cation nature. Longer the substituted aliphatic chain of the imidazolium ring (ethyl, butyl or hexyl) lower the temperature of the first transformation. In addition, the hybrid structure transition to decomposition products is always accompanied by sample amorphization. [C2mim]PW structure is no longer confirmed at 350ºC. However, at 400ºC the diffractions in the 5-10° 2θ range remain indicating the presence of the Keggin anion, though some ionic liquid fraction probably disappears from the structure (represented as $[C2mim]_xPW_{12}O_{40}$ in the Table, where x accounts for some ionic liquid removal). At higher temperatures, the hybrid becomes amorphous until 550ºC where WO_3 starts to form. From 600ºC to the end temperature WO_3 (JCPDS #00-041-0905 + #01-071-0131) is only detected.

At temperatures above 200ºC, [C4mim]PW starts to change, and the typical Keggin structure diffractions appear indicating relocation of the ionic liquid, and appearance of a structure similar to that of the initial polyacid. This structure remains stable up to 400ºC where the sample becomes amorphous. At 550ºC WO_3 appears and at 600ºC WO_3 (JCPDS #00-041-0905 + #01-071-0131) is the only present phase. The [C6mim]PW hybrid exhibits the lowest thermal stability and becomes amorphous at 250ºC. In the same way, WO_3 (JCPDS #00-041-0905 + #01-071-0131) appears at 550ºC being the only detected phase between 600 and 750ºC.

Table 3.2. Identified crystal phases at different temperatures for PWA and hybrids.

T (ºC)	Phases PWA	Phases [C2mim]PW	Phases [C4mim]PW	Phases [C6mim]PW
RT	$H_3PW_{12}O_{40}\cdot 14H_2O$	$[C2mim]_3PW_{12}O_{40}$	$[C4mim]_3PW_{12}O_{40}$	$[C6mim]_3PW_{12}O_{40}$
50	$H_3PW_{12}O_{40}\cdot 14H_2O$	$[C2mim]_3PW_{12}O_{40}$	$[C4mim]_3PW_{12}O_{40}$	$[C6mim]_3PW_{12}O_{40}$
100	$H_3PW_{12}O_{40}\cdot 6H_2O$	$[C2mim]_3PW_{12}O_{40}$	$[C4mim]_3PW_{12}O_{40}$	$[C6mim]_3PW_{12}O_{40}$
150	$H_3PW_{12}O_{40}\cdot 6H_2O$	$[C2mim]_3PW_{12}O_{40}$	$[C4mim]_3PW_{12}O_{40}$	$[C6mim]_3PW_{12}O_{40}$
200	$H_3PW_{12}O_{40}\cdot 6H_2O$	$[C2mim]_3PW_{12}O_{40}$	$[C4mim]_3PW_{12}O_{40}$	$[C6mim]_3PW_{12}O_{40}$
250	$H_3PW_{12}O_{40}\cdot 6H_2O$	$[C2mim]_3PW_{12}O_{40}$	$[C4mim]_3PW_{12}O_{40}$	$[C6mim]_3PW_{12}O_{40}$ + Amorphous
300	$H_3PW_{12}O_{40}$ + $H_3PW_{12}O_{38}$	$[C2mim]_3PW_{12}O_{40}$	$[C4mim]_3PW_{12}O_{40}$	Amorphous
350	$H_3PW_{12}O_{40}$ + $H_3PW_{12}O_{38}$	$[C2mim]_3PW_{12}O_{40}$	$[C4mim]_3PW_{12}O_{40}$	Amorphous
400	$H_3PW_{12}O_{40}$ + $H_3PW_{12}O_{38}$	$[C2mim]_xPW_{12}O_{40}$	$[C4mim]_3PW_{12}O_{40}$	Amorphous
450	$H_3PW_{12}O_{40}$ + $H_3PW_{12}O_{38}$	Amorphous	Amorphous	Amorphous
500	$H_3PW_{12}O_{40}$ + $H_3PW_{12}O_{38}$	Amorphous	Amorphous	Amorphous
550	$H_3PW_{12}O_{40}$ + $H_3PW_{12}O_{38}$ + $WOPO_4$	Amorphous + WO_3	Amorphous + WO_3	Amorphous + WO_3
600	WO_3	WO_3	WO_3	WO_3
650	WO_3	WO_3	WO_3	WO_3
700	WO_3	WO_3	WO_3	WO_3
750	WO_3	WO_3	WO_3	WO_3

- *PMoA series*

In the same way, the phase transformation of phophomolybdic acid and its hybrids was studied as a function of temperature at identical measurement conditions (Figure 3.5.).

The parent acid $H_3PMo_{12}O_{40}\cdot 13H_2O$ (JCPDS #01-075-1588) loses hydration water and transforms to $H_3PMo_{12}O_{40}\cdot 6H_2O$ (JCPDS#01-070-1705) and $H_3PMo_{12}O_{40}\cdot 1.5\ H_2O$ (JCPDS#00-046-0482) at 100 and 150ºC, respectively. This phase remains intact up to 450ºC where transforms into

MoP_2O_7 (JCPDS#00-039-0026) and MoO_3 (JCPDS #00-001-0706 + #00-047-1081). From 550°C until the last measured temperature, only MoO_3 is detected. The acid based on Mo is less stable than W acid and its phase transformations occur at lower temperatures.

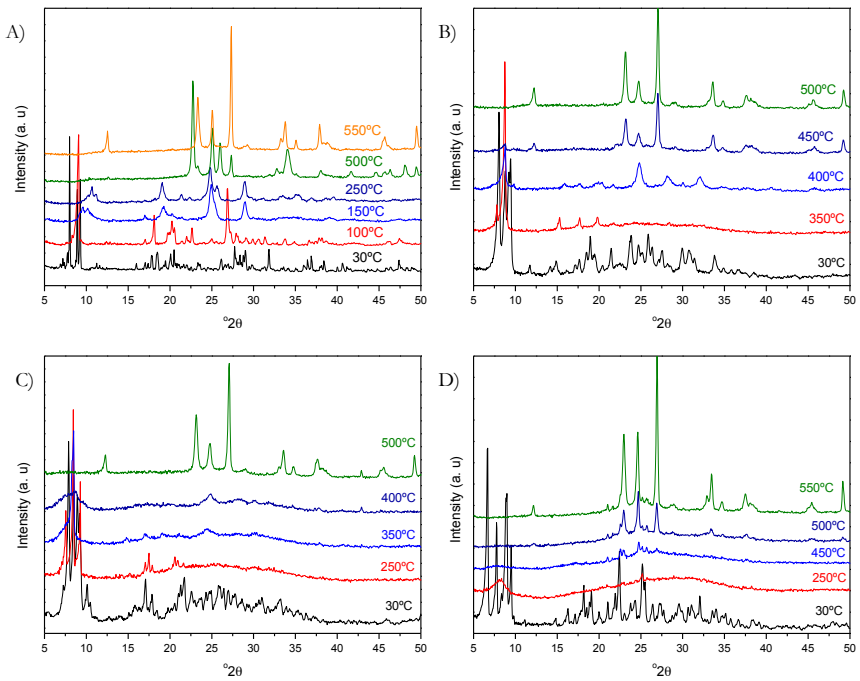

Figure 3.5. XRDiffractograms of PMoA series as a function of temperature: A) PMoA, B) [C2mim]PMo, C) [C4mim]PMo and D) [C6mim]PMo.

For the hybrids, the phase transformations depend also on the nature of cation. As discussed above, the temperature of the first phase transformation is higher for smaller aliphatic chains substituents (the most stable one being [C2mim] hybrid). The phase transformations starts always with samples amorphization. [C2mim]PMo maintains its structure up to 300°C and converts into MoO_3 at 500°C. [C4mim]PMo was not observed at temperature higher than 200°C, only products issued from the phosphomolybdic acid decomposition are detected: $H_3PMo_{12}O_{40} \cdot 13H_2O$

(JCPDS #01-075-1588), $10MoO_3 \cdot H_3PO_4 \cdot 24H_2O$ (JCPDS #00-001-0032), MoP_2O_7 (JCPDS #00-039-0020) and MoO_3 (JCPDS #00-001-0706, #00-047-1081). Similarly to the [C2mim]PMo, at 500 °C only MoO_3 is detected. [C6mim]PMo is observed till 200 °C where an amorphization occurs and directly MoO_3 appears at 550°C. In all cases MoO_3 crystallizes as monocrystal, indicating that the crystallization is directed by the presence of the ionic liquid probably playing a templating role.

All identified phases for hybrids and parent phosphomolybdic acid at every studied temperature are summarized in Table 3.3. The dependence of the hybrid's stability on the organic counter ion is easily observed. [C2mim]PMo is the most stable followed by [C4mim]PMo and [C6mim]PMo hybrids. The stability is structure sensitive in a way that lower the perturbation of the Keggin-structure higher the phase transformation stability and temperature. Additionally, it could be established that the stability of all hybrids strongly depends on the nature of the parent acid being the hybrids based on PWA more stable than those based on PMoA.

Table 3.3. Detected crystal phases at different temperatures for PMoA and hybrids.

T (ºC)	Phases (PMoA)	Phases [C2mim]PMo	Phases [C4mim]PMo	Phases [C6mim]PMo
RT	$H_3PMo_{12}O_{40}\cdot 13H_2O$	$[C2mim]_3[PMo_{12}O_{40}]$	$[C4mim]_3[PMo_{12}O_{40}]$	$[C6mim]_3[PMo_{12}O_{40}]$
50	$H_3PMo_{12}O_{40}\cdot 13H_2O$	$[C2mim]_3[PMo_{12}O_{40}]$	$[C4mim]_3[PMo_{12}O_{40}]$	$[C6mim]_3[PMo_{12}O_{40}]$
100	$H_3PMo_{12}O_{40}\cdot 6H_2O$	$[C2mim]_3[PMo_{12}O_{40}]$	$[C4mim]_3[PMo_{12}O_{40}]$	$[C6mim]_3[PMo_{12}O_{40}]$
150	$H_3PMo_{12}O_{40}\cdot 1.5H_2O$	$[C2mim]_3[PMo_{12}O_{40}]$	$[C4mim]_3[PMo_{12}O_{40}]$	$[C6mim]_3[PMo_{12}O_{40}]$
200	$H_3PMo_{12}O_{40}\cdot 1.5H_2O$	$[C2mim]_3[PMo_{12}O_{40}]$	$[C4mim]_3[PMo_{12}O_{40}]$	$[C6mim]_3[PMo_{12}O_{40}]$
250	$H_3PMo_{12}O_{40}\cdot 1.5H_2O$	$[C2mim]_3[PMo_{12}O_{40}]$	$H_3PMo_{12}O_{40}\cdot 13H_2O$ + $10MoO_3\cdot H_3PO_4\cdot 24H_2O$	Amorphous
300	$H_3PMo_{12}O_{40}\cdot 1.5H_2O$	$[C2mim]_3[PMo_{12}O_{40}]$	$H_3PMo_{12}O_{40}\cdot 13H_2O$ + $10MoO_3\cdot H_3PO_4\cdot 24H_2O$	Amorphous
350	$H_3PMo_{12}O_{40}\cdot 1.5H_2O$	$H_3PMo_{12}O_{40}\cdot 13H_2O$ + $10MoO_3\cdot H_3PO_4\cdot 24H_2O$	$H_3PMo_{12}O_{40}\cdot 13H_2O$ + $10MoO_3\cdot H_3PO_4\cdot 24H_2O$	Amorphous
400	$H_3PMo_{12}O_{40}\cdot 1.5H_2O$	$H_3PMo_{12}O_{40}\cdot 13H_2O$ + $10MoO_3\cdot H_3PO_4\cdot 24H_2O$ + MoP_2O_7	$H_3PMo_{12}O_{40}\cdot 13H_2O$ + $10MoO_3\cdot H_3PO_4\cdot 24H_2O$ + MoP_2O_7	Amorphous
450	$MoP_2O_7 + MoO_3$	$H_3PMo_{12}O_{40} + MoP_2O_7$ + MoO_3	$10MoO_3\cdot H_3PO_4\cdot 24H_2O$ + MoP_2O_7	Amorphous
500	$MoP_2O_7 + MoO_3$	MoO_3	MoO_3	Amorphous + MoO_3
550	MoO_3	MoO_3	MoO_3	MoO_3
600	MoO_3	MoO_3	MoO_3	MoO_3
650	MoO_3	MoO_3	MoO_3	MoO_3
700	MoO_3	MoO_3	MoO_3	MoO_3
750	MoO_3	MoO_3	MoO_3	MoO_3

- PMoVA series

XRD patterns as function of temperature for PMoVA based hybrids are presented in Fig. 3.6. In this case, the phase transformation of the liquid parent acid were not studied. As for the previous series, the crystallinity and stability of the hybrids depends on the counter cation. The hybrid with the longest alkyl chain [C6mim] becomes totally amorphous at 250

ºC, being its structure at low temperatures significantly different from that of [C2mim] and [C4mim]. [C6mim] sample amorphicity remains up to 550 ºC, giving way to MoO_3 (JCPDS #00-001-0706, #00-047-1081) and V_2O_5 (JCPDS #00-045-1074) formation. At 750 ºC, VO_2 (JCPDS #00-044-0253) is also detected.

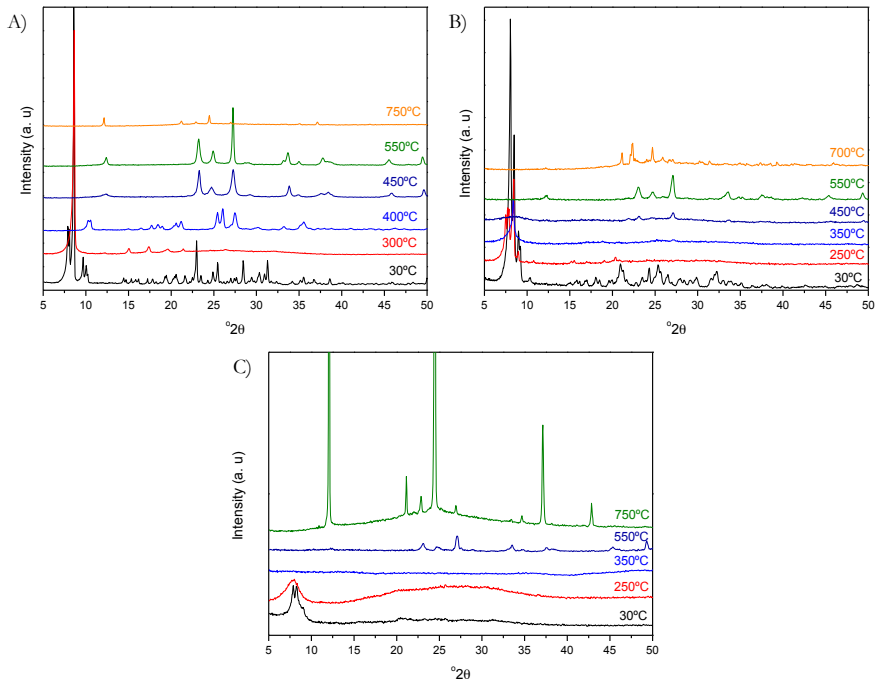

Figure 3.6. XRDiffractograms of PMoVA hybrids as a function of temperature: A) [C2mim]PMoV, B) [C4mim]PMoV and C) [C6mim]PMoV

On the contrary, [C2mim] and [C4mim] hybrids maintain their structures longer. All detected phases as a function of temperature appear in Table 3.4. For [C2mim]PMoV hybrid, some ionic liquid reorganization could be envisaged at 250 ºC, with the first decomposition products of the Keggin fraction appearing at 400 ºC, $H_4PMo_{11}O_{40}\cdot 2H_2O$ (JCPDS #00-046-0483), $V_8O_{16}\cdot 1.5H_2O$ (JCPDS #00-050-1797), $H_3PMo_{12}O_{40}\cdot xH_2O$ (JCPDS #00-043-0314) and $VO_{1.5}(OH)_{0.25}$ (JCPDS #00-037-0503). At 550 ºC the phase

transformations are identical to that described for [C6mim] hybrid. The phase transformations of [C4mim]PMoV hybrid are similar (Table 3.4.)

Table 3.4. Identified crystal phases at different temperatures for PWA and hybrids.

T (°C)	Phases [C2mim]PMoV	Phases [C4mim]PMoV	Phases [C6mim]PMoV
RT	$[C2mim]_5[PMo_{10}V_2O_{40}]$	$[C4mim]_5[PMo_{10}V_2O_{40}]$	Semi-amorphous
50	$[C2mim]_5[PMo_{10}V_2O_{40}]$	$[C4mim]_5[PMo_{10}V_2O_{40}]$	Semi-amorphous
100	$[C2mim]_5[PMo_{10}V_2O_{40}]$	$[C4mim]_5[PMo_{10}V_2O_{40}]$	Semi-amorphous
150	$[C2mim]_5[PMo_{10}V_2O_{40}]$	$[C4mim]_5[PMo_{10}V_2O_{40}]$	Semi-amorphous
200	$[C2mim]_5[PMo_{10}V_2O_{40}]$	$[C4mim]_5[PMo_{10}V_2O_{40}]$	Semi-amorphous
250	$[C2mim]_5[PMo_{10}V_2O_{40}]$	$[C4mim]_x[PMo_{10}V_2O_{40}]$	Amorphous
300	$[C2mim]_x[PMo_{10}V_2O_{40}]$	$[C4mim]_x[PMo_{10}V_2O_{40}]$	Amorphous
350	$[C2mim]_x[PMo_{10}V_2O_{40}]$	$[C4mim]_x[PMo_{10}V_2O_{40}]$	Amorphous
400	$H_4PMo_{11}O_{40}\cdot 2H_2O$ + $V_8O_{16}\cdot 1.5H_2O$ + $H_3PMo_{12}O_{40}\cdot xH_2O$ + $VO_{1.5}(OH)_{0.25}$	$[C4mim]_x[PMo_{10}V_2O_{40}]$	Amorphous
450	$MoO_3 + V_8O_{16}\cdot 1.5H_2O$	Amorphous + MoO_3	Amorphous
500	$MoO_3 + V_8O_{16}\cdot 1.5H_2O$		Amorphous
550	$MoO_3 + V_2O_5$	$MoO_3 + V_2O_5$	$MoO_3 + V_2O_5$
600	$MoO_3 + V_2O_5$	$MoO_3 + V_2O_5$	$MoO_3 + V_2O_5$
650	$MoO_3 + V_2O_5$	$MoO_3 + V_2O_5$	$MoO_3 + V_2O_5$
700	$MoO_3 + V_2O_5$	$MoO_3 + V_2O_5$	$MoO_3 + V_2O_5$
750	$MoO_3 + V_2O_5 + VO_2$	$MoO_3 + V_2O_5 + VO_2$	$MoO_3 + V_2O_5 + VO_2$

3.3.4. Raman spectroscopy

The XRD studies demonstrate the structural similarity of the hybrids to the parent acid and the changes induced by the aliphatic chain of the substituted imidazolium ring. These changes are also studied by Raman spectroscopy (Figure 3.7.). The Keggin structural units present four types of oxygen: terminal oxygen, Ot (M=O, where M denotes the metal in Keggin anion), two types of bridging oxygen atoms (M–O–M), edge

sharing oxygen Oe and corner sharing oxygen Ob, as well as corner sharing oxygen atoms between the central heteroatom and surrounding metal atoms Oa (P–O–M(x3)) [25]. Therefore, four oxygen bonds can be distinguished. The Raman spectra of the hybrids can be separated in two vibrational zones: the first one 100–1100 cm^{-1}, within the metal-oxygen bonds range, (Fig. 3.7. left) and the second one 2700–3200 cm^{-1} corresponding to the organic fraction vibrations (Fig. 3.7. right). The bands attribution and its comparison with some literature data are presented in Table 3.5.

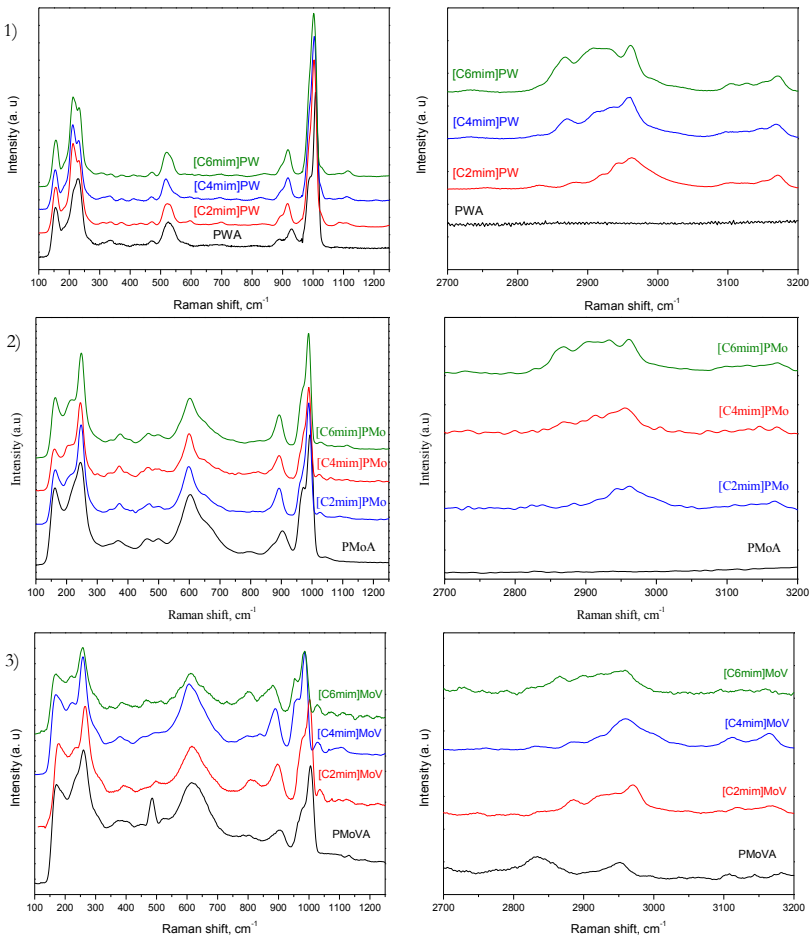

Figure 3.7. Raman spectra of HPAs and hybrids: 1) PWA series, 2) PMoA series and 3) PMoVA series

In general, the vibrational bands assigned to the metal-oxygen bonds do not change significantly in the presence of different imidazolium derivatives, the Keggin unit seems preserved, as confirmed by XRD. The M–Ob–M and M–Oe–Mo bands are slightly shifted for all hybrids: indicating that the organic cations situates near the bridging oxygens and affects their electronic density causing a blue shift.

For all hybrids, the CH vibrations are also present confirming the formation of hybrids with the preservation of the Keggin structure.

Table 3.5. Vibrational assignments for inorganic and organic fractions

Experimental Raman shift, cm^{-1}	Raman shift, cm^{-1} [26–29]	Assignment	Experimental Raman shift, cm^{-1}[30–33]	Assignment[a]
1008	1007[26]	ν_s (W=Ot)	2835	ν_s CH-CH
993	995[27]	ν_s (Mo=Ot)	2876	(imidazolium)
1004	992[28]	ν_s (V=Ot)	2919	ν_s CH R_2
				ν_s CH R_1
986	992[26]	ν_{as} (W=Ot)	2940	CH_3NHCH
969	981[27]	ν_{as} (Mo=Ot)	2968	ν_{as} CH R_1
978	930[28]	ν_{as} (V=Ot)	3018	ν_{as} CH R_2
928, 888	904[26]	ν_{as} (W-Ob-W)	3107	NC(H)N
901,878	909-	ν_{as} (Mo-Ob-Mo)	3170	ν_{as} CH-CH
906	876[29]	ν_{as} (V-Ob-V)		(imidazolium)
	693, 837,878[28]			
525	-	ν_s (W-Oe-W)		
600	603[29]	ν_s (Mo-Oe-Mo)		
618	523 [27]	ν_s (V-Oe-V)		
232, 212		ν_s (W-Oa)		
245, 222	251[29]	ν_s (Mo-Oa)		
260, 235		-		

[a] R_1 (ethyl, butyl or hexyl), R_2 (methyl)

3.3.5. SAXRD analysis of Mo based hybrids

The presence of low-angle diffractions for [C6mim]PM hybrids (where M = W, Mo) suggested the formation of species with certain long-order arrangements. In order to study this, small angle X ray diffraction

experiment was undertaken for the molybdenum compounds (Figure 3.8.). As observed by XRD, the lowest angle diffraction shifts from C2 to C6 hybrid, revealing the existence of facets with large interplanar spacing. According to the Bragg law, the spacings move from 11Å to 11.2Å and 13.3Å (Cu K-alpha = 1.5418 Å) for C2, C4 and C6, respectively, suggesting the formation of organic-inorganic compounds with relatively large cavities, as a function of alkyl chain. One interesting question arises at this point: Is it possible to predict the size of the cavities with the number of the aliphatic carbons?

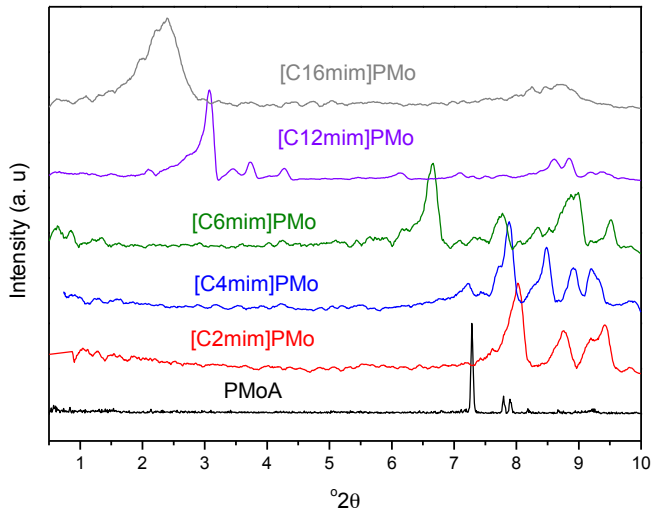

Figure 3.8. Small angle X ray diffractograms of Mo based hybrids (including C12 and C16)

In order to check that, two new Mo hybrids with C12 and C16 alkyl substitute chains are prepared. As shown in Fig. 3.8., small angle diffractions appear in both cases and the interplanar spacing move to 28.6Å to 36.8Å for C12 and C16, respectively. Therefore, it is clear that the structure organization is induced by the ionic liquid nature and bigger

cavities may be obtained by increasing the length of the cation' alkyl chain. Almost linear relation was obtained between the number of the carbons in the alkyl chain and *d*-spacing of the resulting hybrid (Figure 3.9.). At low carbon number the structure accommodates easily the alkyl substitute in a denser structure, whereas at higher number steric hindering becomes important and the arrangement is more open.

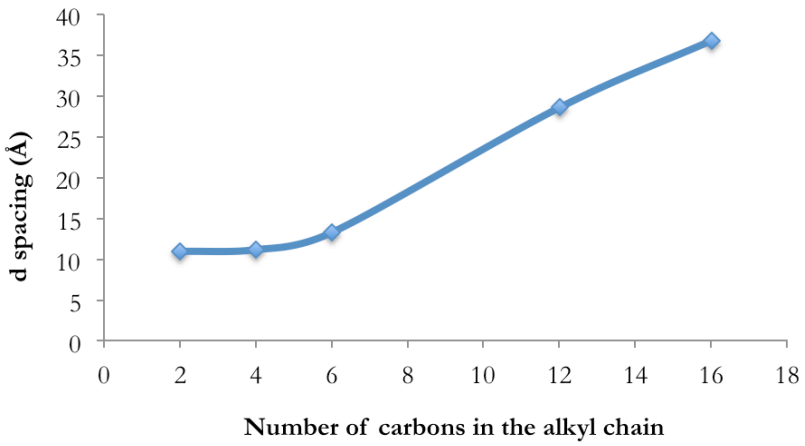

Figure 3.9. *d*-spacing/number of carbons correlation

3.3.6. Solid state $^{13}C\{^{1}H\}$ and ^{31}P NMR analysis of Mo based hybrids

$^{13}C\{^{1}H\}$ NMR is an important method for characterizing the organic fraction of the formed hybrids. While XRD, SAXRD and Raman spectroscopy give us information about the structure organization around the inorganic fraction, solid state ^{13}C coupled ^{1}H NMR provides the information about the possible changes around the imidazolium rings (Figure 3.10. left). The main disadvantage of the solid state $^{13}C\{^{1}H\}$ NMR is the difficulty, from a technical point of view, to obtain high resolution signals due to the long-range dipolar interactions in the solids. As a result,

the signals broaden; being almost impossible, in some cases, to detect their multiplicity. For this reason, only the carbon chemical shifts will be taken into account (Table 3.6.).

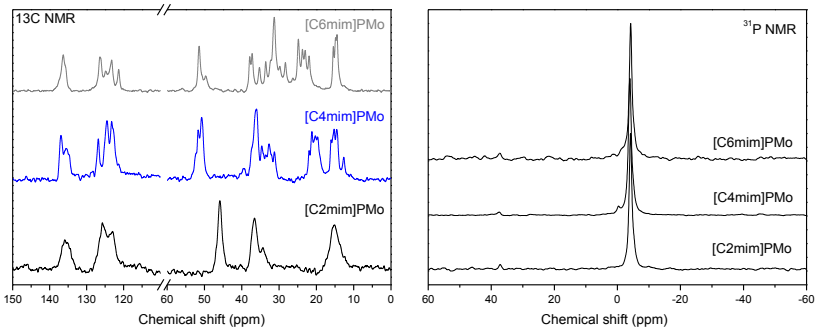

Figure 3.10. $^{13}C\{^{1}H\}$ NMR (left) and ^{31}P NMR (right) of [CXmim]PMo hybrids

Table 3.6. $^{13}C\{^{1}H\}$ NMR assignments [34–36]

	Chemical shift (ppm)		
Carbon	[C2mim]PMo	[C4mim]PMo	[C6mim]PMo
1	15.2	14.9	14.9
2	45.9	20.6	22.5
3	125.6	32.7	32.3
4	123.0	51.4	24.8
5	135.9	125.8	29.9
6	35.9	122.8	50.8
7	-	136.2	125.4
8	-	36.2	122.3
9	-	-	136.0
10	-	-	36.2

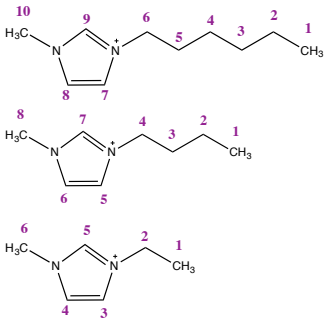

The ^{13}C chemical shifts agreed well with the reported for the parent ionic liquids [34–36], although shifts of 2-3 ppm are observed. The aliphatic carbons appear in the 0-70 ppm range, being shifted the carbons closely situated to the nitrogen atom of the ring, owing to the difference in the electronegativity (carbon 2, 4 and 6 in C2mim, C4mim and C6mim,

respectively). This region corresponds to sp^3 hybridization. The aromatic carbons appear in the 120-140 ppm range and correspond to the zone of sp^2 carbons. The similarity with literature data clearly suggests that the organic cations remain intact in the hybrid structure. Nevertheless, the local changes in their chemical environment, most probably due to the presence of neighboring M–O–M bond, as elucidated by Raman, causes the small observed shifts of the signals.

As for ^{31}P NMR, the single peak appearing below 0 ppm corresponds to one unique P present in the structure. No changes in this signal occurred, from acid to hybrids. This fact indicates stable chemical environment around phosphorous remaining unaltered by the presence of organic fraction.

3.3.7. Single crystal X-ray diffraction of Mo based hybrids

Single crystals of Mo based hybrids were obtained in order to determine the crystallographic parameters of the resulting structures. Completely dried hybrids were recrystallized from an equal volume (10 + 10 mL) mixture of acetone and acetonitrile. Solvents were carefully evaporated at room temperature for 7 days, and yellow monocrystals were formed and used for single crystal X-ray diffraction analysis. Table 3.7. includes all obtained crystallographic data, such as crystal system, space group, unit cell parameters (axes and angles), unit volume and number of molecular unit in the unit cell.

Table 3.7. Crystallographic data for the Mo Keggin molecular salts

	[C2mim]PMo	[C4mim]PMo	[C6mim]PMo
Formula	$C_{18}H_{33}Mo_{12}N_6O_{40}P$	$C_{24}H_{45}Mo_{12}N_6O_{40}P$	$C_{30}H_{57}Mo_{12}N_6O_4P$
M	2155.75	2239.91	2324.07
T [K]	193(2)	193(2)	193(2)
Wavelength [Å]	0.71073	0.71073	0.71073
Crystal system	triclinic	triclinic	orthorhombic
Space group	P -1	P -1	P b c a
a [Å]	14.9687(5)	12.9158(5)	22.3846(3)
b [Å]	15.0798(5)	21.2163(8)	20.9690(4)
c [Å]	21.8498(8)	21.6946(8)	26.0718(5)
α [°]	86.944(2)	95.876(2)	90.0
β [°]	88.681(2)	105.285(2)	90.0
γ [°]	85.622(2)	101.080(2)	90.0
V	4909.8(3)	5553.7(4)	12237.7(4)
Z	4	4	8

The single-crystal structural analysis suggests that the three compounds have three-dimensional structure containing $[Cxmim]_3PMo_{12}O_{40}$ frameworks withou water molecules included. The ORTEP representations of the molecular salts are presented in Fig. 3.11. A), Fig. 3.12. A) and Fig. 3.13. A), respectively. [C2mim]PMo crystallizes in space group P-1, with 4 molecular units per unit cell (Fig. 3.11. B)). The expanded packing is shown in Fig. 3.11. C).

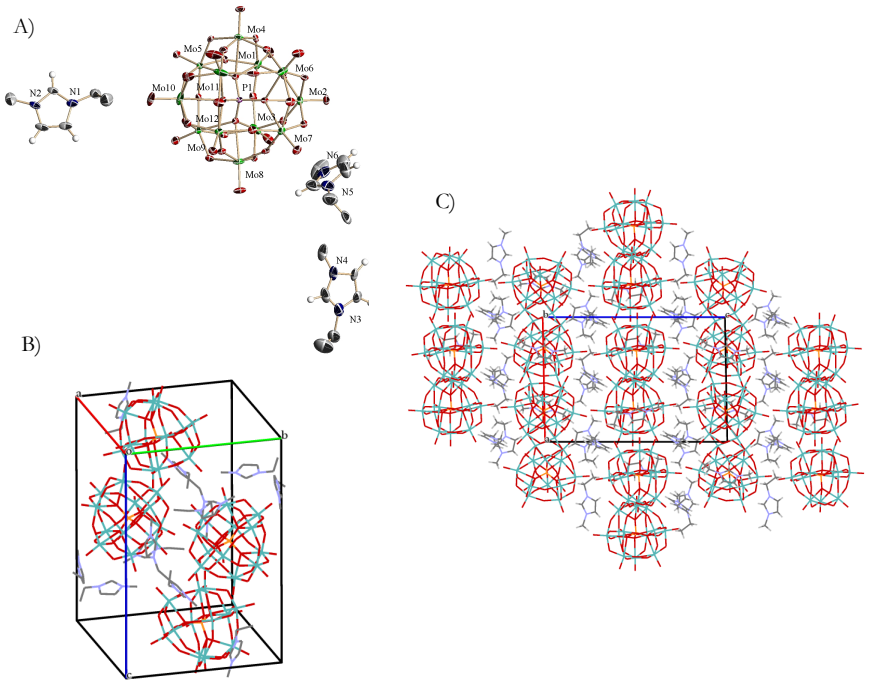

Figure 3.11. A) ORTEP representation, B) Unit cell and C) Expanded structure (b view) of [C2mim]PMo

[C4mim]PMo crystallizes in space group P-1, with 4 molecular units per unit cell (Fig. 3.12. B)). In all cases, for each phosphomolybdate anion there are three Cxmim cation moieties.

[C6mim]PMo crystallizes in space group Pbca, with 4 molecular units per unit cell (Fig. 3.13. B)). It seems that longer the aliphatic chain of the cation (or higher the weight or volume), higher the symmetry of the final compounds.

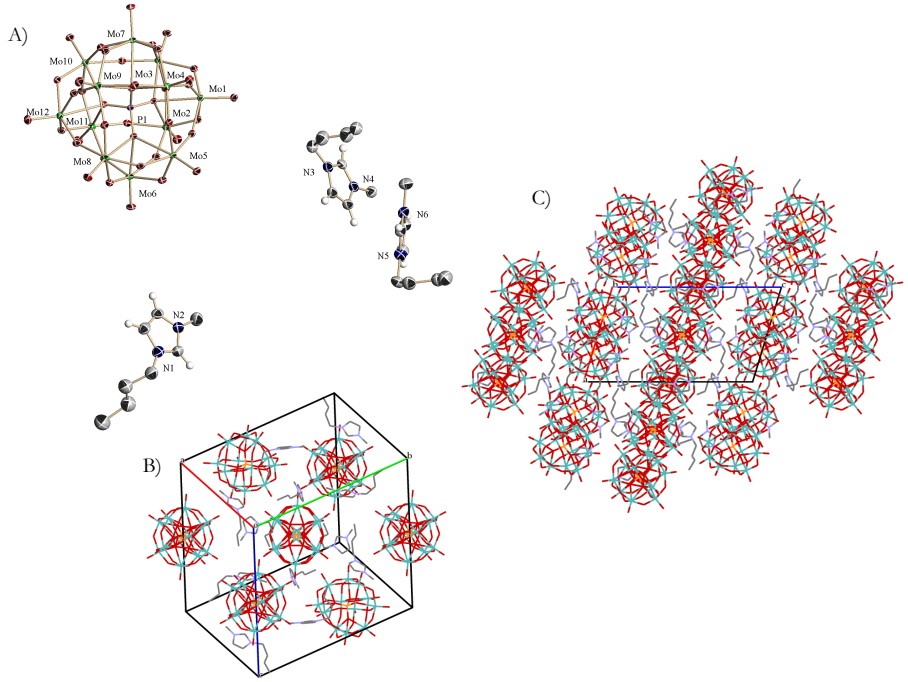

Figure 3.12. A) ORTEP representation, B) Unit cell and C) Expanded structure (b view) of [C4mim]PMo

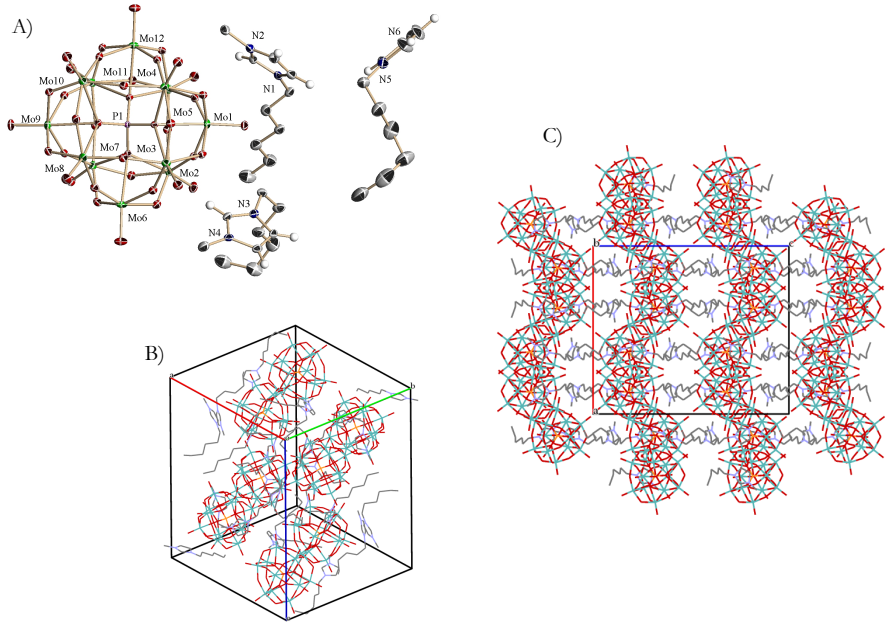

Figure 3.13. A) ORTEP representation, B) Unit cell and C) Expanded structure (b view) of [C6mim]PMo

As mentioned during SAXRD discussion, there is certain directionality caused by the organization of cations and anions. The type of directionality is different for C2mim, C4mim (Fig. 3.12. C)) and C6mim (Fig. 3.13. C)), different channels exist formed upon cations – anions arrangement. For instance, [C2mim]PMo and [C4mim]PMo presents parallel channels along *a* direction, whereas the channels of the [C6mim]PMo structure appeared in a zig-zag way. The cation introduction to the Keggin anion lead to the formation of different tridimensional structures, whose features follows a trend directly related with the number of carbons present in the imidazolium ring substitutes. Lower aliphatic chain length gives rise to more open channels and cavities, resulting in less compact final structure. The later could be accurately demonstrated by measuring the distance between two atoms of phosphorous belonging to different parallel chains of anions. The distances are 13.540 Å, 12.385 Å and 11.758 Å for [C2mim]PMo, [C4mim]PMo and [C6mim]PMo, respectively.

3.4. Partial conclusions

Three different HPAs with W, Mo and Mo-V metal centers and their corresponding hybrids materials obtained by mixing the acids with three commercial ionic liquids were synthesized.

The samples were fully characterized by XRD (conventional, upon temperature and small angle analysis), TGA, Raman spectroscopy, solid-state $^{13}C\{^{1}H\}$-NMR and ^{31}P NMR and single crystal X-ray diffraction.

The most important conclusions extracted from this chapter could be summarized as follows:

The hybrids formed by inorganic anions and organic cations interactions are structurally new materials with preserved Keggin structure. A long-range order exists for those compounds and becomes more evident on increasing the imidazolium ring substituents alkyl chain length. Unlike Keggin frameworks, the hybrids structures do not include water molecules and their space arrangement takes place through electrostatic interactions between the organic cation and the terminal and bridging Keggin oxygen atoms. In all cases, the imidazolium based structure remains in the hybrid.

The thermal stability of HPAs and their corresponding hybrids follows the trend W > Mo > Mo-V. The organic cations are lost around 300 ºC, remaining further only the Keggin structure.

Crystallographic data reveals three-dimensional structure containing $[Cxmim]_3PMo_{12}O_{40}$ frameworks, in which channels and cavities are formed due to the alternate organization of cations and anions. The later is directly related with the number of carbon atoms in the alkyl chain present in the imidazolium ring: shorter chains results in open channels and cavities and less compact structure.

References

[1] Y. Ren, M. Wang, X. Chen, B. Yue, H. He, Heterogeneous Catalysis of Polyoxometalate Based Organic–Inorganic Hybrids, Materials (Basel). 8 (2015) 1545–1567.

[2] K.U. Nandhini, J.H. Mabel, B. Arabindoo, M. Palanichamy, V. Murugesan, The influence of phosphotungstic acid acidity on Al-MCM-41 in t-butylation of phenol with t-butyl alcoholitle, Micropor. Mesopor. Mater. 96 (2006) 21–28.

[3] G.S. Kumar, M. Vishnuvarthan, M. Palanichamy, V. Murugesan, BA-15 supported HPW: Effective catalytic performance in the alkylation of phenol, J. Mol. Catal. A Chem. 260 (2006) 49–55.

[4] Y.Y. Liu, K. Murata, M. Inaba, N. Mimura, Selective oxidation of propylene to acetone by molecular oxygen over Mx/2H5−x[PMo10V2O40]/HMS (M = Cu2+, Co2+, Ni2+), Catal. Commun. 4 (2003) 281–285.

[5] G. Karthikeyan, A. Pandurangan, Heteropolyacid (H3PW12O40) supported MCM-41: An efficient solid acid catalyst for the green synthesis of xanthenedione derivatives., J. Mol. Catal. A Chem. 311 (2009) 36–45.

[6] J. Arichi, M.M. Pereira, P.M. Esteves, B. Louis, Synthesis of Keggin-type polyoxometalate crystals, Solid State Sci. 12 (2010) 1866–1869.

[7] X. Han, W. Yan, K. Chen, C.-T. Hung, L.-L. Liu, P.-H. Wu, et al., Heteropolyacid-based ionic liquids as effective catalysts for the synthesis of benzaldehyde glycol acetal, Appl. Catal. A Gen. 485 (2014) 149–156.

[8] J. Chen, L. Hua, W. Zhu, R. Zhang, L. Guo, C. Chen, et al., Polyoxometalate anion-functionalized ionic liquid as a thermoregulated catalyst for the epoxidation of olefins, Catal. Commun. 47 (2014) 18–21.

[9] W. He, S. Li, H. Zang, G. Yang, S. Zhang, Z. Su, et al., Entangled structures in polyoxometalate-based coordination polymers, Coord. Chem. Rev. 279 (2014) 141–160.

[10] H.N. Miras, L. Vila-Nadal, L. Cronin, Polyoxometalate based open-frameworks (POM-OFs), Chem. Soc. Rev. 43 (2014) 5679–5699.

[11] A. Mirzaei, M.; Eshtiagh-Hosseini, H.; Alipour, M.; Frontera, Recent developments in the crystal engineering of diverse coordination modes (0–12) for Keggin-type polyoxometalates in hybrid inorganic–organic architectures., Coord. Chem. Rev. 275 (2014) 1–18.

[12] B. Santoni, M.-P.; Hanan, G.S.; Hasenknopf, Covalent multi-component systems of polyoxometalates and metal complexes: Toward multi-functional organic–inorganic hybrids in molecular and material sciences., Coord. Chem. Rev. 281 (2014) 64–85.

[13] E. Du, D.; Yan, L.; Su, Z.; Li, S.; Lan, Y.; Wang, Chiral polyoxometalate-based materials: From design syntheses to functional applications., Coord. Chem. Rev. 257 (2013) 702–717.

[14] S. Ivanova, Hybrid organic-inorganic materials based on polyoxometalates, ISRN Chem. Eng. 2014 (2014) Article ID 963792, 13 pages.

[15] G. Ranga Rao, T. Rajkumar, B. Varghese, Synthesis and characterization of 1-butyl 3-methyl imidazolium phosphomolybdate molecular salt, Solid State Sci. 11 (2009) 36–42.

[16] T. Rajkumar, G. Ranga Rao, Characterization of hybrid molecular material prepared by 1-butyl 3-methyl imidazolium bromide and phosphotungstic acid, Mater. Lett. 62 (2008) 4134–4136.

[17] T. Rajkumar, G.R. Rao, Investigation of hybrid molecular material prepared by ionic liquid and polyoxometalate anion, J. Chem. Sci. 120 (2008) 587–594.

[18] H. Wu, Contribution to the chemistry of phosphomolybdic acids, phosphotungstic acids, and allied substances., J. Biol. Chem. 43 (1920) 189–220.

[19] Y. Leng, J. Wang, D. Zhu, L. Shen, P. Zhao, M. Zhang, Heteropolyanion-based ionic hybrid solid: A green bulk-type catalyst for hydroxylation of benzene with hydrogen peroxide, Chem. Eng. J. 173 (2011) 620–626.

[20] U.B. Mioč, R.Ž. Dimitrijević, M. Davidovic, Z.P. Nedic, M.M. Mitrovic, P. Colomban, Thermally induced phase transformations of 12-tungstophosphoric acid 29-hydrate: synthesis and characterization of PW8O26-type bronzes, J. Mater. Sci. 29 (1994) 3705–3718.

[21] J.F. Keggin, The Structure and Formula of 12-Phosphotungstic Acid, Proc. R. Soc. London Ser. A. 144 (1934) 75.

[22] J. Dupont, On the solid, liquid and solution structural organization of imidazolium ionic liquids, J. Braz. Chem. Soc. 15 (2004) 341–350.

[23] I. V. Kozhevnikov, a. Sinnema, H. van Bekkum, Proton sites in Keggin heteropoly acids from17O NMR, Catal. Letters. 34 (1995) 213–221.

[24] M. Misono, Acidic and catalytic properties of heteropoly compounds, Mater. Chem. Phys. 17 (1987) 103–120.

[25] S. Ganapathy, M. Fournier, J.F. Paul, L. Delevoye, M. Guelton, J.P. Amoureux, Location of protons in anhydrous keggin heteropolyacids H3PMo12O40 and H3PW12O40 by 1H{31P}/31P{1H} REDOR NMR and DFT quantum chemical calculations, J. Am. Chem. Soc. 124 (2002) 7821–7828.

[26] S.R. Matkovic, L.E. Briand, A. Bañares, Investigation of the thermal stability of phosphotungstic Wells-Dawson heteropoly-acid through in situ Raman spectroscopy, Mater. Res. Bull. 46 (2011) 1946–1948.

[27] J.-M. Tatibouet, C. Montalescot, K. Bruckman, J. Haber, M. Che, A Two-Step Transformation of the Magnesium Salt of Phosphomolybdic Acid HMgPMo 12 O 40 Supported on Silica, J. Catal. 169 (1997) 22–32.

[28] G.G. Nunes, A.C. Bonatto, C.G. De Albuquerque, A. Barison, R.R. Ribeiro, D.F. Back, et al., Synthesis , characterization and chemoprotective activity of polyoxovanadates against DNA alkylation, J. Inorg. Biochem. 108 (2012) 36–46.

[29] C. Rocchiccioli-Deltcheff, A. Aouissi, M.M. Bettahar, S. Launay, M. Fournier, Catalysis by 12-Molybdophosphates, J. Catal. 164 (1996) 16–27.

[30] N.E. Heimer, R.E. Del, Z. Meng, J.S. Wilkes, W.R. Carper, Vibrational spectra of imidazolium tetrafluoroborate ionic liquids, J. Mol. Liq. 124 (2006) 84–95.

[31] K.M. Dieter, C.J. Dymek, N.E. Heimer, J.W. Rovang, J.S. Wilkes, Ionic Structure and Interactions in 1-Methyl-3-ethylimidazolium Chloride-A1C13 Molten Salts, J. Am. Chem. Soc. 110 (1988) 2122–2126.

[32] E.R. Talaty, S. Raja, V.J. Storhaug, A. Dölle, W.R. Carper, Raman and Infrared Spectra and ab Initio Calculations of C 2 - 4 MIM Imidazolium Hexafluorophosphate Ionic Liquids, J. Phys. Chem. B. 108 (2004) 13177–13184.

[33] S. a Katsyuba, E.E. Zvereva, A. Vidis, P.J. Dyson, Application of density functional theory and vibrational spectroscopy toward the rational design of ionic liquids., J. Phys. Chem. A. 111 (2007) 352–370.

[34] M. Imanari, H. Tsuchiya, H. Seki, K. Nishikawaa, M. Tashirob, Characterization of the molecular reorientational dynamics of the neat ionic liquid 1-butyl-3-methylimidazolium bromide in the super cooled state using 1H and 13C NMR spectroscopy, Magn. Reson. Chem. 47 (2009) 67–70.

[35] E.P. Grishina, L.M. Ramenskaya, M.S. Gruzdev, O.V. Kraeva, Water effect on physicochemical properties of 1-butyl-3-methylimidazolium based ionic liquids with inorganic anions, J. Mol. Liq. 177 (2013) 267–272.

[36] S. Hesse-Ertelt, T. Heinze, B. Kosan, K. Schwikal, F. Meister, Solvent Effects on

the NMR Chemical Shifts of Imidazolium-Based Ionic Liquids and Cellulose Therein, Macromol. Symp. 294 (2010) 75–89.

Chapter Four

CATALYTIC VIABILITY of POM-IL HYBRIDS in BIOMASS VALORIZATION

Summary[1]

This chapter is devoted to catalytic evaluation of the obtained hybrid structures in different glucose transformation reactions. The studied processes are glucose epimerization to mannose, glucose oxidation to gluconic acid and glucose/fructose dehydration to 5-hydroxymethyl-2-furfural (HMF). For each reaction, an introduction detailing the process, needed active sites and reaction state-of-art is presented. In all cases, the influence of different reaction parameters is evaluated, as well as the influence of different organic cations and anion metal centers. In each section, experimental part, discussion of results and partial conclusions are included.

[1]Some of the presented results in this Chapter are published in:

C. Megías-Sayago *et al.* **Catalysis Today** 278 (2016) 82–90

The selective production of valuable chemicals derived from biomass resources using heterogeneous catalysts recently received much attention due to higher reaction rates reached when compared to the current applied biotechnological processes [1–3]. Unlike homogeneous catalysts, the use of heterogeneous systems allows their recovery and reutilization in several catalytic cycles, improving the overall efficiency of the processes. As described in Chapter One, both heteropolyacids and ionic liquids separately have demonstrated high capacity/potential for biomass-involved transformations. However, their ionic nature and ability to dissociate in aqueous media, diminishes their productivity in the catalytic reactions. The later can be solved though the synthesis of POM's molecular salts, mainly based on partially substituted acids with Cs^+ counter cation. These salts present similar catalytic properties which can be modified targeting a concrete reaction.

From a general point of view, the conversion of lignocellulosic biomass to added value chemicals involves several steps such as i) separation of cellulose, hemicellulose and lignin in single fractions, ii) depolymerization of carbohydrates in smaller molecules and iii) conversion of monomeric units in desirable sugar derived chemicals. In this study, the cellulose is chosen as model raw material. Cellulose depolymerization leads to the formation of only one monomer, glucose, a compound that will be used as biomass chemical representative for all catalytic tests. Despite that this thesis does not focus on the depolimerization process, it is worthy to mention the high capability of polyoxometalates to catalyze it. The difficulty of this reaction lies in the intrinsic characteristics of the polymer, including a robust crystalline structure, inaccessible β-1,4-glycosidic bonds and water-insolubility [4]. Because the Brönsted acidity of POMs can be stronger than that of the typical mineral acids [5–7], it is expected to be more efficient acid catalyst for the hydrolysis of cellulose, as demonstrated

by Shimizu and coworkers [8]. In their study, the catalytic activities of $H_3PW_{12}O_{40}$ and several mineral acids were compared in the hydrolysis of cellobiose, the simplest model molecule of cellulose formed by two glucose units. The results showed that the conversion of cellobiose decreased in the order: $H_3PW_{12}O_{40} > HClO_4 > H_2SO_4 > H_3PO_4$. On the other hand, Tian *et al.* optimized the reaction conditions for the same HPA, using microcrystalline cellulose as reactant, obtaining 50% glucose yield in 2 hours at 180 ºC [9]. Those one-pot transformation of cellulose into platform chemicals, make even more suitable and desirable the use of POMs in the reactions involving subsequent glucose transformation.

In this Chapter, the POM-IL hybrid structures detailed in Chapter Three are screened as catalysts in different catalytic transformation reactions of glucose. Different temperatures, reaction times and reactant-to-catalyst ratios in water or organic/aqueous mixtures, in presence or absence of oxidants such as H_2O_2, were tested depending on the reaction process. The results are organized in three parts, corresponding to each studied reaction, i.e. epimerization, oxidation and dehydration of glucose.

4.1. Glucose epimerization

4.1.1. Introduction

The epimerization of aldoses, such as glucose, arabinose or xylose, at C2 involves the transformation of the sugar to its quiral counterpart, the epimer. This transformation, leading to mannose in the case of glucose (Scheme 4.1.), has received much less attention than the isomerization into fructose, a fact explaining that only few chemocatalytic systems have been discovered for selective epimerization [10]. Similarly to isomerization, the epimerization occurs in presence of basic or Lewis acids catalysts [11–13], although the formation of the corresponding

ketose predominates over both systems. The formation of fructose via isomerization requires a little reorganization of the intermediate, whereas the formation of mannose takes place through rotation around the C2-C3 bond (see Scheme 4.1.). The different reorganization may be the reason why the formation of mannose is slower in comparison with glucose to fructose reaction [14]. Both reactions, however, are limited by thermodynamics, being 50:50 the reported isomerization equilibrium and 70:30 Glucose/Mannose equilibrium ratio.

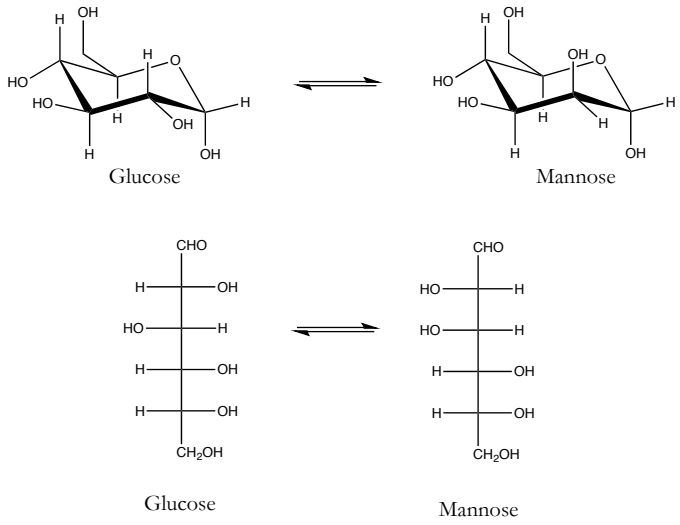

Scheme 4.1. Schematic of the Epimerization of D-Glucose to D-Mannose

The epimerization is widely used for different processes, including mainly the production of rare sugars and pharmaceuticals [15–17]. Currently, epimer production is assured by epimerases, which are highly selective in the epimerization of carbohydrates at different carbon positions. However, the number of drawbacks derived from the use of enzyme-catalyzed processes at industrial level promotes the search for solid inorganic catalysts. The most important disadvantages are the sensitivity

of enzymes to temperature and pH, which restricts the operating window, and difficults the post reaction separation [18].

As commented before, basic catalysts such as $Ca(OH)_2$ and NaOH can epimerize glucose to mannose reaction though the formation of molecular complexes [10]. However, it has been demonstrated that, in basic conditions, a series of 50 different secondary products can be formed, diminishing selectivity to the desired epimer. In a similar way, the epimerization process may occurs via complexation of the substrate with Ni/diamines complexes [19], being the reaction limited by the thermodynamics of the complexes, not saccharides, which implies the use of large quantities of catalyst.

The most studied process to epimerize aldoses without ketose formation is known as Bilik reaction. In 1970s Bilik discovered that molybdate anions under acidic conditions can epimerize glucose to the thermodynamic equilibrium at 90 ºC after 3h of reaction [13], without formation of fructose. The activity of the molybdate anions, however, was strongly influenced by the pH: the maximum yields were registered at pH 2.0-3.5 [20], being this pH necessary to maximize the concentration of dimeric Mo^{VI} [20], considered as the active species. The rate of epimerization drastically decreases on increasing pH, which entails the use of a strong Brönsted acid.

The epimerization follows a carbon-shift mechanism through coordination of the substrate to Mo^{VI} dimer (Scheme 4.2), simultaneous cleavage of the C_2-C_3 carbon bond and the formation of new C_1-C_3 carbon bond, all steps confirmed by ^{13}C NMR studies [21]. Through this mechanism, a large amount of compounds can be selectively epimerized, under some limitations: the alkylic chain should present a minimum of four carbons and hydroxyl groups in C_2, C_3 and C_4 positions.

The importance of the Bilik reaction was rapidly recognized and scaled up to pilot plant running in Bratislava. At this point, the challenge to make more efficient the overall process is to find an active and stable molybdate solid acid catalyst.

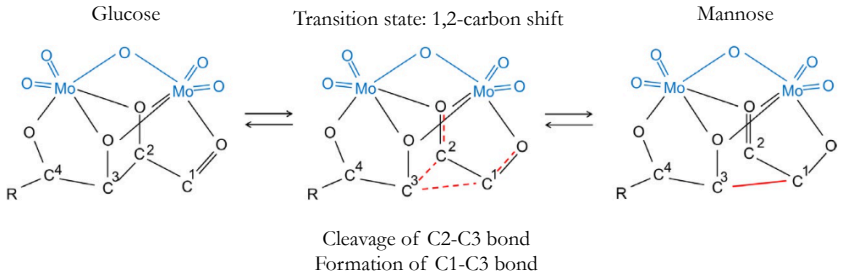

Scheme 4.2. Reaction mechanism of Mo-catalyzed epimerization of glucose. Adapted from Ref. [22]

VanderVelde and coworkers [18] recently reported for the first time the use of phosphomolybdic acid and Ag/Sn based salts in the above mentioned reaction, resulting in near-equilibrium conversions with high selectivity within 60 min. The registered conversions are independent of the nature of the cation in the structure (H^+, Ag^+, Sn^{4+}), which suggests that the cation does not participate in the process. The isotope-labelling ^{13}C NMR confirms that the reaction follows the above mentioned 1,2-carbon shift mechanism.

Along this section, the catalytic behavior of the synthesized hybrid structures in glucose epimerization reaction is studied. All Mo, W and MoV based hybrids are tested and the catalytic behavior related to the nature of the organic fraction and inorganic metal center nature. Reaction parameters such as reaction time and temperature are evaluated and the activation energies for the three PMoA based hybrids calculated.

4.1.2. Experimental

The catalysts were used as prepared (see the preparation section in Chapter 3). The catalytic tests were performed in a glass batch reactor of 50 mL equipped with magnetic stirrer. 1 mmol of glucose (Sigma Aldrich, 0.1802 g) and 0.4 mol% catalyst, referred to the sugar reactant, were introduced to H_2O until a total volume of 5 mL. The mixture was heated in paraffin oil bath with carefully controlled temperature and stirring rate of approximately 600 rpm. The product analysis was performed in a Varian 360 Liquid Chromatograph, using 0.01M H_2SO_4 as eluent. The specific operation conditions are summarized in Chapter 2, Analytical methods section. As an example, a typical chromatogram obtained during the epimerization is presented in Figure 4.1.

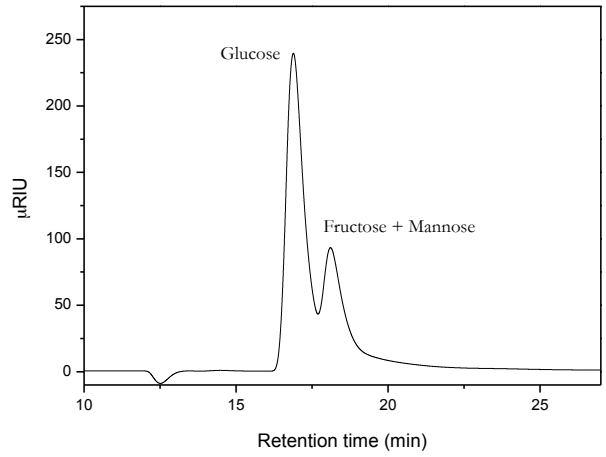

Figure 4.1. Typical chromatogram obtained during the epimerization analysis

4.1.3. Catalytic activity: results and discussion

Aldose conversions for the three hybrids based on phosphomolybdic acid as a function of the reaction temperature are presented in Figure 4.2. An

increase of glucose conversion with temperature is observed. When compared to literature data (Table 4.1; entries 2, 3 and 4) the results observed for [C2mim]PMo correspond to the equilibrium conversions at 80, 90 and 100 ºC within 60 min reaction. Irrefutably, glucose conversion is strongly dependent on organic cation nature, in a way that the longer the aliphatic chain of the imidazolium cation, the lower the glucose conversion, following the trend [C2mim]PMo > [C4mim]PMo > [C6mim]PMo.

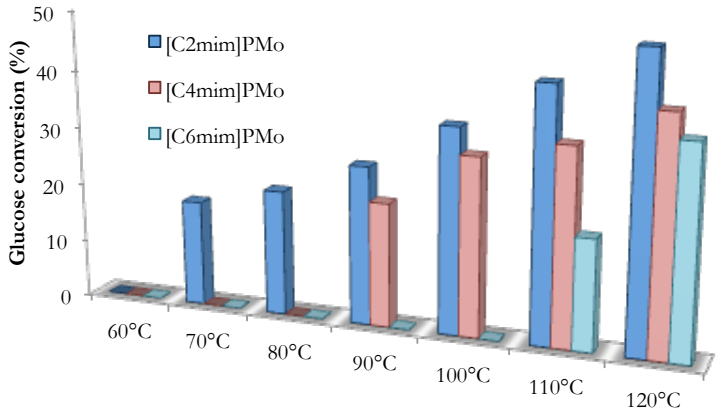

Figure 4.2. Glucose conversion (%) as function of the reaction temperature for the PMoA based hybrids.

Table 4.1. Comparison of glucose to mannose equilibrium data for [C2mim]PMo

Entry	Temperature (ºC)	Conversion (%) over [C2mim]PMo [a]	Equilibrium conversion (ref.)
1	70	18	-
2	80	21	26 [23]
3	90	27	30 [24]
4	100	34	32 [18]
5	110	43	-
6	120	49	-

[a] Reaction conditions: 5 mL of 0.2 M glucose solution, 0.4 mol% of catalyst referred to glucose (1:0.05 Glucose:Metal ratio), 60 min and 600 rpm.

It seems that the longer chain hybrids attain the equilibrium conversion at higher temperatures. This result suggests either that the IL cations are participating directly in the reaction or that the global hybrid organization is responsible for the catalytic differences. The first hypothesis entails participation of the cation, which should be different in the case of the H^+ substituted PMoA catalyst. However, the catalytic performance of PMoA leads to identical conversion data (Table 4.2; entry 1) as the corresponding [C2mim]PMo salt (Table 4.2; entry 2). The pure ionic liquid does not catalyze any glucose transformation reaction (Table 4.2; entry 7) which leads to the conclusion that the IL cation is not involved in the reaction.

As for the global hybrid organization, it is convenient to discuss in terms of crystallographic structure. Attending to the Mo hybrids expanded structure exposed in Chapter 3 (Fig. 3.11., Fig. 3.12. and Fig. 3.13.), the [C2mim]PMo presents the less compact structure of cations, with large cavities. The later should provide better aldose diffusion to the active sites and less steric impediments for the formation of molybdenum-glucose complex. Therefore, the different catalytic activities are directly correlated with the availability of Mo^{VI} active centers, as reported by VanderVelde for homologous POMs. Based on the later, the activity trend [C2mim]PMo > [C4mim]PMo > [C6mim]PMo is also congruent with [C4mim]PMo and [C6mim]PMo long-range structures and cavities dimensions restriction (see Figures 3.11., 3.12. and 3.13. on Chapter 3).

The catalytic performance of PW and PMoV based hybrids are compared to those of PMo at 120 ºC and summarized in Table 4.2. Despite the fact that 1,2-carbon shift has been only reported for Mo compounds, it is interesting to check if W and V could become potential alternatives as they form also iso- and hetero-polyanions with the same structure as Keggin PMoA. The study is also motivated by the fact that all molybdates, tungstates and also vanadates are very effective for the glucose

metabolism *in vivo*. The use of these metals results in lowering of the glucose blood levels and helps to control the diabetes [25,26]. Metal to glucose sensitivity lies on the fact that all metals form similar Me-glucose complexes [25] with similar characteristics to that of molybdate complexes [27] and logically should catalyze one or more glucose transformation reactions.

For [C2mim]PW and [C2mim]PMoV hybrids (Table 4.2., entries 5 and 6, respectively) the influence of the anion' metal center is evident. Whereas replacing Mo with W resulted in activity loss the replacing of two Mo with V leads to higher conversion. Nevertheless, the selectivity to mannose decreases in favor to glyceraldehyde (27 % selectivity). As it will be explained in the last section of the present chapter, glyceraldehyde is a product of fructose retro-aldolic condensation, reaction which takes place also on Lewis acid sites [28] under acidic conditions. The glyceraldehyde formation at this point indirectly suggests the formation of fructose.

Table 4.2. Catalytic performance of different hybrids in the epimerization of glucose

Entry	Catalyst [a]	Conversion (%)	Selectivity [b] (%)	pH before reaction [c]
1	PMoA	48	100	1.87
2	[C2mim]PMo	49	100	2.72
3	[C4mim]PMo	40	100	-
4	[C6mim]PMo	35	100	-
5	[C2mim]PW	0	0	2.62
6	[C2mim]PMoV	55	73	3.80
7	$[C2mim](SO_3)CH_3$ [d]	0	0	-

[a] Reaction conditions: 5 mL of 0.2 M glucose solution, 0.4 mol% of catalyst referred to glucose (1:0.05 Glucose:Metal ratio), 120 ºC, 60 min and 600 rpm. [b] Selectivity reported as mannose+fructose selectivity. [c] pH not controlled, the final pH value is measured at the end of the reaction. [d] The IL amount is equivalent to the corresponding hybrid loading in this conditions.

At this point, it is very important to deserve attention to selectivity. As shown in Fig. 4.1., under our operation conditions, mannose and fructose are eluted at the same retention time, which makes impossible the proper calculation of the selectivity. In spite of numerous publications that molybdate-based compounds are 100% selective toward epimerization at low reaction times, it is necessary to contrast it. In order to confirm it, a catalytic test at 80 ºC over [C2mim]PMo was carried out in distilled water. After catalyst separation and water lyophilization the resulted product was re-dissolved in deuterium oxide and characterized by means of ^{13}C {^{1}H} NMR (Figure 4.3.). The obtained chemical shifts are contrasted with reported values as summarized in Table 4.3.

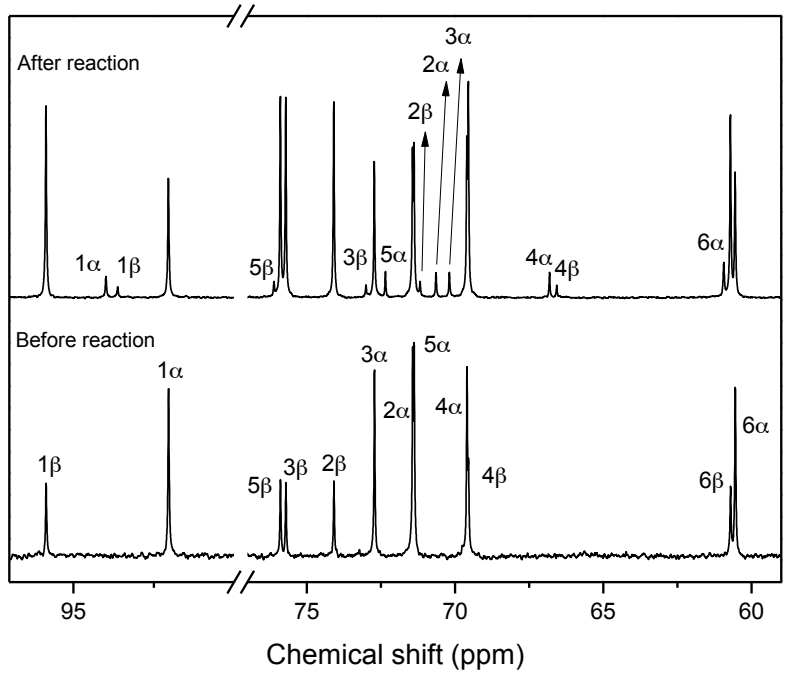

Figure 4.3. ^{13}C {^{1}H} NMR spectra of unlabeled glucose in aqueous solution before and after the reaction at 80 ºC for 60 min

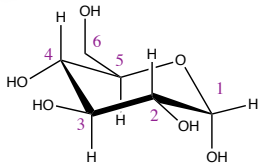

α-glucose

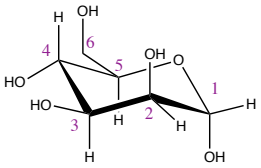

α-mannose

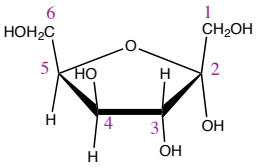

α-fructose

Table 4.3. ^{13}C {^{1}H} NMR chemical shifts

Entry	**Literature** [29]	C1	C2	C3	C4	C5	C6
1	α–glucose	92.9	72.5	73.8	70.6	72.3	61.6
2	β–glucose	96.7	75.1	76.7	70.6	76.8	61.7
3	α–mannose	95.0	71.7	71.3	68.0	73.4	62.1
4	β–mannose	94.6	72.3	74.1	67.8	77.2	62.1
5	α–fructose	63.8	105.5	82.9	77.0	82.2	61.9
6	β–fructose	63.6	102.6	76.4	75.4	81.6	63.2
	Experimental	C1	C2	C3	C4	C5	C6
7	α–glucose	92.1	71.4	72.7	69.6	71.4	60.55
8	β–glucose	95.9	74.1	75.7	69.55	75.9	60.7
9	α–mannose	94.0	70.6	70.2	66.8	72.3	60.9
10	β–mannose	93.6	71.2	73.0	66.6	76.1	*

* Overlaps with C6 of glucose

Before the reaction, only glucose is labeled in Fig. 4.3, while after reaction, only the new signals are identified. In all cases, both α– and β–conformations are presents due to the existing equilibriums between axial and equatorial substituents in aqueous solution [30]. The new signals agree with the presence of α– and β–mannose. There is not evidence for the presence of fructose within the reacted mixture, this on the basis of the missing signals corresponding to α– and β– fructose (Table 4.3., entries 5 and 6). The absence of resonances at 100 ppm (Table 4.3.,

entries from 7 to 10) corresponding to fructose C2 and also the lack of signals in the 80-90 ppm range, corresponding to C3 (α–conformation) and C5 (α– and β– conformation) confirms mannose as the only reaction product, i.e. the selectivity to the epimer is 100 %. This result is consistent with the study of Hayes and coworkers [31] where 100 % of selectivity over molybdenum systems is observed at short reaction times. However, at longer reaction times secondary products can be formed. Glucose conversion over [C2mim]PMo as a function of reaction time at the same reaction conditions (80 ºC, 600 rpm), is presented in Figure 4.4.

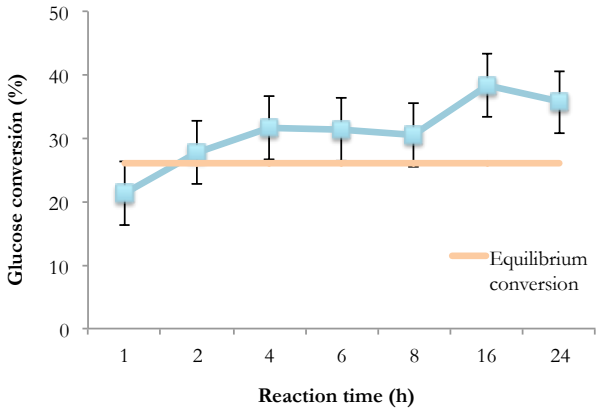

Figure 4.4. Glucose conversion (%) as a function of the reaction time. Reaction conditions: 1 mmol of glucose, 0.4 mol% of [C2mim]PMo, 80 ºC and 600 rpm

After 60 min of reaction, the conversion almost attains the equilibrium, reached in 2 hours. From this time on, all registered conversions exceed the equilibrium value, entailing most probably the formation of secondary products. From the HPLC measurements could be deduced that the secondary product corresponds probably to fructose, since no new products appear but the intensity of the mannose+fructose HPLC signal increases, in agreement with the reports of Hayes *et al.* [31] and Bilik [32]. Once the epimerization equilibrium is reached, the unconverted glucose

can undergo an intramolecular hydride shift in the presence of the molybdate-glucose complex [32]. As described previously, both glucose epimerization and isomerization take place over Lewis acid and basic catalysts, although in the majority of cases, the isomerization prevails over epimerization.

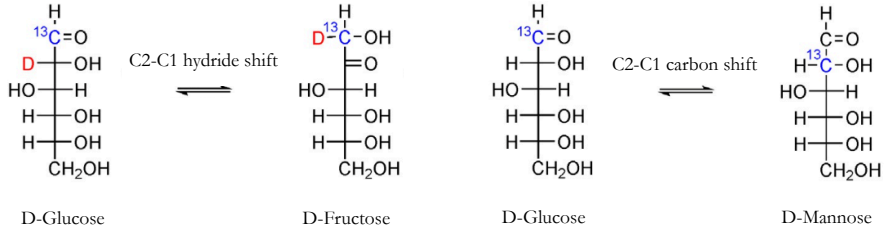

Scheme 4.3. Mechanism of fructose formation over Lewis acid site [33] (left) and mechanism of mannose formation over Mo^{VI} [18]

The mechanism of isomerization is normally described as 1,2-hydride shift over common Lewis acids such as Sn-Beta zeolites [33] and $CrCl_3$ [34] (Scheme 4.3.). Therefore, taking into account the Lewis acid character of Mo^{VI}, it is possible to claim that over [C2mim]PMo hybrid, the epimerization prevails during the first two hours of reaction. Once the equilibrium is attained and, due to the formation of glucose-molybdate complex, a hydride shift takes place, giving rise to the formation of fructose at higher reaction times. However, more studies are required and will be the object of future works.

The experiments conducted within 60 min as a function of the reaction temperature over [C2mim]PMo, [C4mim]PMo and [C6mim]PMo are used to determine the apparent activation barriers for glucose epimerization for these systems. Figure 4.5. shows the Arrhenius plots for each hybrid. As expected, and according to the catalytic results showed in Fig. 4.2. the apparent activation energies follows the trend [C2mim]PMo <

[C4mim]PMo < [C6mim]PMo. These results, reinforce the fact that large cavities and less compact structure facilitates the diffusion of reactants and offer less steric impediment for active complex formation. The increase of temperature rearranges the structure, boosting the active site availability and facilitating molybdate-glucose interaction. The calculated activation barriers, however, are much lower than those obtained for similar polyoxomolybdate based catalysts used by VanderVelde *et al.* [18] (96 kJ/mol) and suggests that the calculated energy barriers should account for two different processes, if only the anions are considered for the reaction. The final energy barriers should correspond to the contribution of the activation energy for the rate limiting 1,2-carbon shift and the necessary energy to rearrange the hybrid structure and to allow glucose diffusion to the active site. The later is especially important since the involved Keggin anion is the same for the three structures. Therefore, the hybrid activity depends on the compactness of the structure and on the type of channels that are formed. Both [C2mim]PMo and [C4mim]PMo presents similar type channel and therefore similar activation energy, whereas the zig-zag channels of the [C6mim]PMo hybrid increases the impediments for reactant access and therefore presents higher energy barrier.

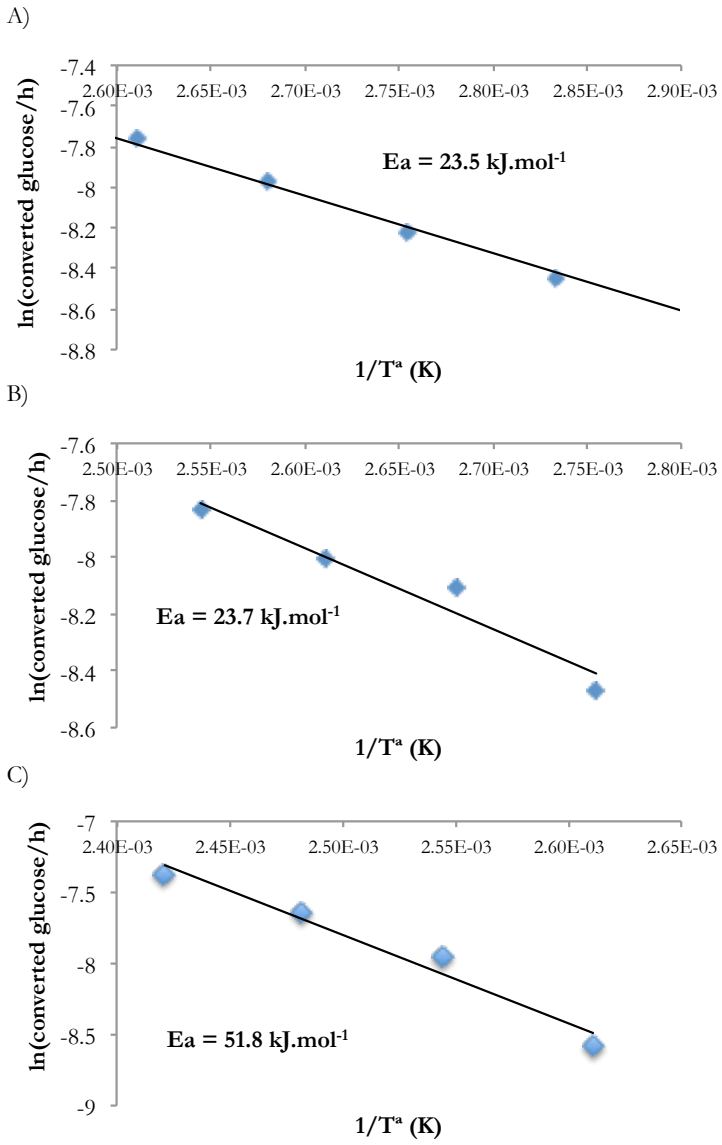

Figure 4.5. Arrhenius plots for the epimerization of glucose over A) [C2mim]PMo, B) [C4mim]PMo and B) [C6mim]PMo

One of the great challenges of homogeneous catalysis is catalyst separation and reutilization, an essential requisite to make any process economically viable. Despite that the organic cations seem to act as spectators during the epimerization, its role is as important as the anions

action. Their presence converts the used materials in solids, insoluble in aqueous solvents, feature that makes possible their separation and reutilization. So the catalyst should be stable under reaction conditions in order to be reutilized. When the Mo hybrid catalyst is employed and the reaction starts, the solids of yellow tonality, becomes blue after 5-10 min (Figure 4.6. c)). The literature reports that the color change associates with the formation of reduced Keggin anion form, $PMo_{12}O_{40}^{3-}$ (also known as heteropoly blue), in equilibrium with its oxidized parent (equation 4.1.) [35].

$$PMo^{VI}_{12}O_{40}^{3-} + ne^- \leftrightarrow PMo^{V}_{n}Mo^{VI}_{(12-n)}O_{40}^{(3+n)-} \qquad \text{Eq. 4.1.}$$

This change of molybdenum oxidation state only happens upon interaction with glucose. The inorganic fraction, $PMo^{VI}_{12}O_{40}^{3-}$, withdraws electrons from glucose, the reducing sugar, changing its oxidation state from +6 to +5, demonstrated by XPS in previous studies [18]. The electron transfer could have an interesting effect in glucose activation during the epimerization reaction. The possible changes in [C2mim]PMo structure induced by the reaction are studied by XRD (Figure 4.6. a)). Despite certain changes in the relative intensity of the diffractions between 5-10 º2**Θ**, no important structural changes and/or decomposition of the hybrid structure is detected after one hour of reaction at 80 ºC. The partial reduction of Mo is reversible and the initial structure can be recovered after treatment with 30% v/v H_2O_2 solution (Figure 4.6. b) and c)).

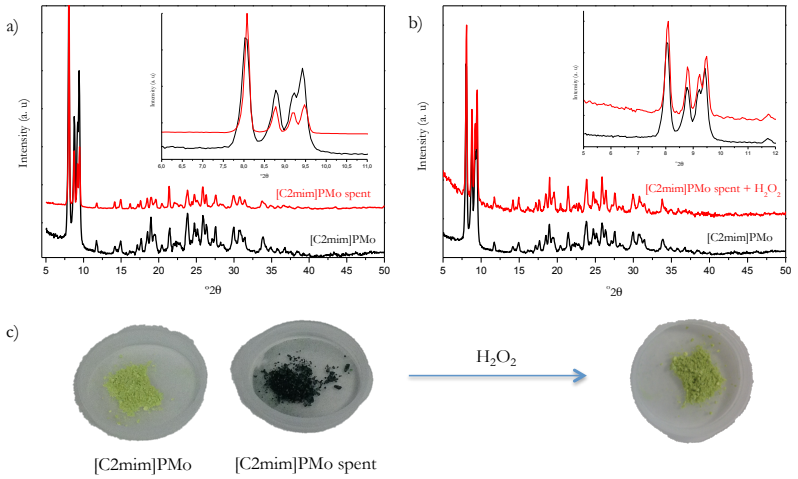

Figure 4.6. a) Comparison of the X ray diffractograms of [C2mim]PMo fresh and spent, b) Comparison of the X ray diffractograms of [C2mim]PMo fresh and spent (after treatment with H_2O_2 solution) and c) Color differences between partially reduced and oxidized species.

Finally, the stability of the [C2mim]PMo catalyst was evaluated by reusing it three times at 80 ºC during 60 min, without any treatment between the cycles. The results are presented in Figure 4.7. In all cases, the water-glucose-catalyst ratio was kept constant to ensure exactly the same reaction conditions. The recycled catalyst exhibits similar activity to that of the original sample, suggesting that hybrid's decomposition does not occur under specific reaction conditions. Slight improvement of activity was observed in the 2nd and 3^{d} cycle, due probably to the partial reduction of Mo after the first cycle, thus facilitating the first step of the reaction, i.e. the electron transfer. However, this statement is not enough clear and needs additional study.

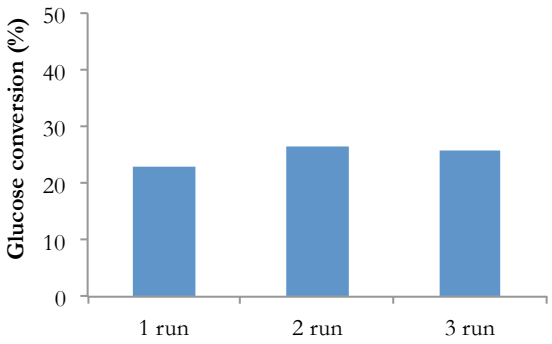

Figure 4.7. Recycling experiments over [C2mim]PMo.

4.1.4. Partial conclusions

In this section, the activity, selectivity and stability of POM-ILs hybrids were evaluated and all results discussed. It has been demonstrated that molybdenum-based hybrids are highly active and selective for the epimerization of glucose at low reaction times. This process involves electron transfer from aldose to the Mo octahedral units of the Keggin anion and subsequent intramolecular C1-C2 carbon shift. The organic cations do not participate in the carbon shift mechanism; however, their presence influences the overall process indirectly by the organization of hybrid' structure and channel system. Smaller cations give rise to less compact structures with large cavities and channels with improved glucose diffusion and metal availability, whereas longer chain cations exerts negative effect on metal-glucose complex formation and glucose epimerization activity. This effect is reflected in the calculated apparent activation energies, significantly lower than the reported for other molybdate-based catalysts in the case of the less compact structures and twice higher for the long chain hybrid (23.5, 23.7 and 51.8 kJ/mol for [C2mim]PMo, [C4mim]PMo and [C6mim]PMo, respectively).

On the other hand, the presence of different metal centers in the Keggin anion strongly influences the activity and selectivity of the systems. The substitution of Mo with W leads to important activity loss whereas the substitution of two atoms of Mo by V entails the formation of other products like glyceraldehyde, suggesting that secondary reactions take place on the additional V centers.

Finally, it has been demonstrated that the structures of molybdenum-based hybrids are stable and do not decompose under the proposed reaction conditions. The catalyst can be easily extracted from the solution and recycled in a number of cycles. These findings pave the way for the implementation of molybdenum based POM-ILs hybrids as single, easy to separate, and recyclable catalytic systems for the epimerization of aldoses under aqueous conditions.

4.2. Glucose oxidation

4.2.1. Introduction

Within all added-value chemicals issued from glucose, the gluconic acid (GA), obtained via oxidation of the glucose aldehyde group (Scheme 4.4.), is very useful in pharmaceutical, chemical, food, beverage and textile industries, either as additive, chelating agent for cleaning purposes or for the extraction of metal traces in solutions [36]. Its current production lays on enzymatic process, in the presence of glucose oxidase. However, this method presents several drawbacks such as high amounts of expensive enzyme, its irreversible deactivation, long reaction times for acceptable yields, need of exhaustive control of process parameters (such as pH and temperature) and several pre-reaction purification processes to remove impurities [37]. All this disadvantages stimulates the pursuit of new

efficient, environmentally friendly catalysts and processes to improve carbohydrate conversion and, therefore, biomass exploitation.

The production of gluconic acid has been studied over catalysts of different nature, including enzymatic [38] and heterogeneous, based on platinum [39,40] and, more recently, on gold [41,42], either with O_2 or H_2O_2 as oxidants. To the best of our knowledge, POM based material has not been studied for this reaction, although the application of POMs in the liquid phase oxidation reactions is widely known. The POM suitability is normally due to its redox nature based on its fast capacity of storage and release of electrons. The activity of those systems principally depends on the metal centers, nearly all oxidative reactions describes at least one W/Mo-based compounds [43]. The aptness of these materials is also derived from their strong resistance to oxidative degradation and hydrolysis, which makes possible their use in presence of strong oxidants like H_2O_2. In addition, their capability to catalyze the oxidation reactions by means of H_2O_2 activation makes overall process environmentally benign, due to the fact that only H_2O is produced as byproduct. There is an extensive list of liquid phase reactions in which POMs have been successfully applied [43], including alkene oxidation [44,45], alkane oxidation [46,47], the oxidation of alcohols [48] and carbonyl compounds [49]. In the same way and due to the continuous efforts to immobilize/heterogenize the catalyst, POM-ILs based solid hybrids have been recently introduced in the oxidation of organic molecules [50–54].

Along this section, the activity of the synthesized hybrid structures will be studied in the glucose oxidation reaction, using H_2O_2 as oxidant. The effects produced by the organic cations and Keggin' metal center nature changes will be also discussed. Parameters such us reaction time and catalyst loading will be evaluated.

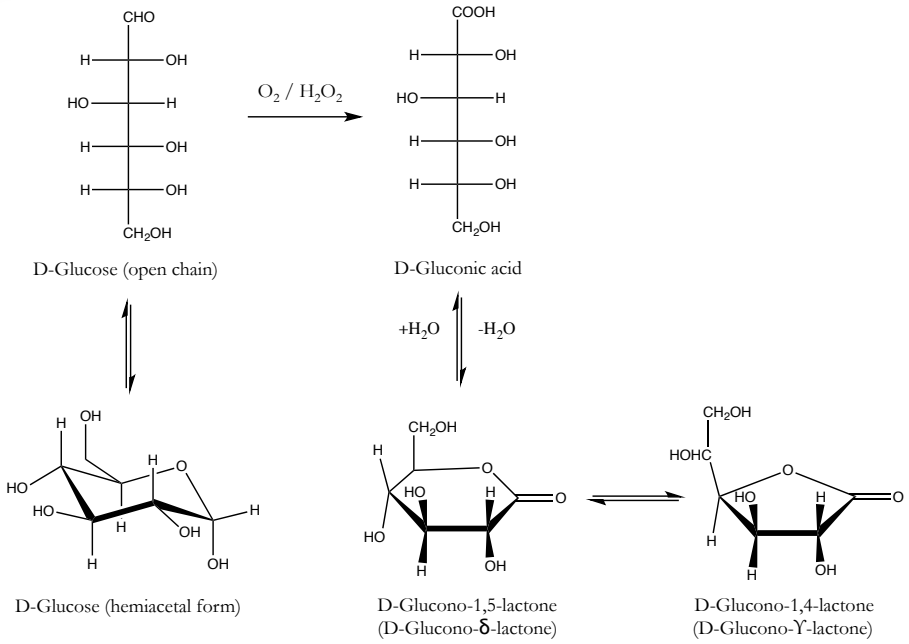

Scheme 4.4 Oxidation of D-Glucose to D-Gluconic acid (GA). Chemical equilibrium of D-Glucose to its hemiacetalic form. Chemical equilibrium of GA and its lactones in aqueous solution.

4.2.2. Experimental

The hybrids were used as synthesized without any treatment. The reactor (50 mL vessel equipped with Young valve and stirrer flea) was charged with 1 mmol of α-D-Glucose (Sigma Aldrich, 0.1816 g), the oxidant (30 % aqueous H_2O_2, 340 μL, 3 mmol), hybrid catalyst (0.25 or 2.5 mol% related to glucose) and 2 mL of water, resulting in a final glucose concentration of 0.5M. The reactor was sealed and the solution reacted under constant stirring (approximately 600 rpm) in thermostated oil bath (60 °C) during 18 hours. After that, the reactor was immediately cooled to 0 ºC, the sample taken, diluted in ultra-pure water (500 μL of sample + 500 μL of H_2O) and analyzed by HPLC, using MilliQ water as mobile phase. The specific operation conditions are summarized in Chapter 2,

Analytical methods section. As an example, a typical chromatogram (Figure 4.8.) obtained during the oxidation analysis evidence the presence of gluconic acid and lactones, according dehydration equilibrium presented in Scheme 4.4.

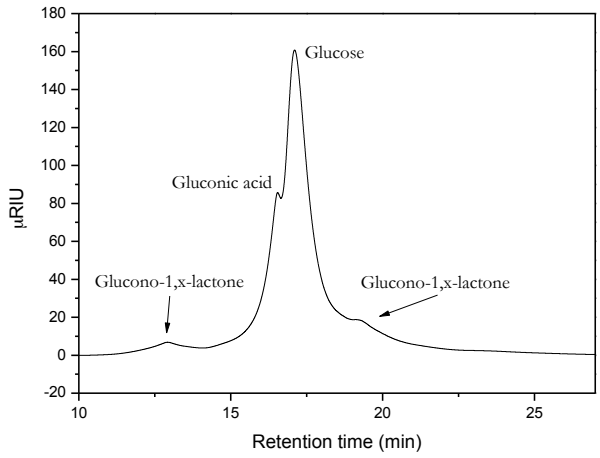

Figure 4.8. Typical chromatogram obtained after the oxidation reaction

4.2.3. Catalytic activity: results and discussion

The catalytic performances of PMoA and its hybrids in presence of H_2O_2 under mild conditions are presented in Table 4.4. Approximately 21% of glucose is converted in absence of catalyst (Table 4.4.; entry 1), with the formation of gluconic acid and some glucaric acid traces. This result changes slightly in presence of PMoA acid (Table 4.4.; entry 2), only 25% glucose conversion is achieved. The switch to the hybrid structure adds another improvement, resulting in a final difference of 10% glucose conversion, which regarding to the blank sample activity represents 50% more conversion for the hybrids. In all cases, gluconic acid was the only product, indicating that in the presence of catalyst the formation of glucaric acid is inhibited. The nature of the organic cations does not

influence the catalyst behavior, being the conversions 30%, 32% and 28% for [C2mim]PMo, [C4mim]PMo and [C6mim]PMo, respectively, within the same range. Again, the organic fraction does not seem to influence directly the catalytic results. Contrary to the epimerization reaction, the hybrid's structure organization is not so important; the reaction occurs always in the same manner and leads to the same glucose conversion. One important difference for both reactions can be deduced; whereas the epimerization needs more space for accommodating the metal-glucose complex, the oxidation reaction only needs access to the active sites, i.e. the Keggin anion. The role of the organic fraction is unclear, probably participates in some intermediate stabilization. Although the last assumption stays only a supposition at this stage, the increase of the glucose conversion from 25 to 30 % from acid to hybrid clearly suggests the existence of some positive role of the organic fraction.

Table 4.4. Oxidation of glucose by H_2O_2 over Mo-based compounds

Entry	Catalyst	Amount, mol% (referred to glucose)	Conversion (%)	GA selectivity (%)
1	-	-	21	99
2	PMoA	0.25	25	100
3	[C2mim]PMo	0.25	30	100
4		2.5	40	100
5	[C4mim]PMo	0.25	32	100
6		2.5	39	100
7	[C6mim]PMo	0.25	28	100
8		2.5	38	100

The influence of the amount of catalyst was also studied and catalyst's loading was increased by ten (2.5 mol% vs 0.25mol%), with the same reaction conditions described above. The glucose conversion slightly

increases (Table 4.4.; entries 4, 6 and 8) for all samples. This results motivates further the study and the catalyst loading was increased gradually to 5mol.% for the [C2mim]PMo sample (Figure 4.9.). The corresponding conversion increases from 0.25 mol% to 2.5 mol%, where a maximum is reached and after that the values oscillate around this point.

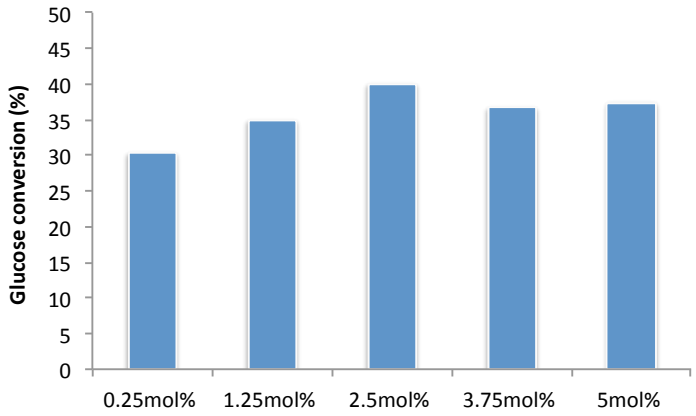

Figure 4.9. Influence of the catalyst loading on glucose conversion (%)

The oxidation process over the hybrids could be tentatively explained by using one already reported reaction mechanism, the free radical mechanism, generally, recognized for the oxidation of organic molecules [50]. As evidenced in the previous section, the change of catalyst' color (from yellow to greenish blue) informs about the coexistence of Mo^{6+} and Mo^{5+} species, resulting from the reducing ability of glucose over the hybrid. The return to yellow occurs when the hybrid is put in contact with H_2O_2 and implies reversible redox process from $Mo^{5+}$to Mo^{6+}. Taking into account that the resulting radical from H_2O_2 can be only OH their participation in the mechanism should be taken into consideration. Hydroxyl radicals (OH·) are oxidizing agents with extremely high-potential and short life and can oxidize various organic substrates generating other free radicals [55]. Some previous studies suggest this

mechanism as possible for the POM-ILs catalyst [43]. Taking into account the fast electron exchange between glucose and hybrid and assuming classical radical reaction mechanism, the process could be tentatively described (Scheme 4.5.), in a similar way to that proposed by Leng *et al* [54] for the hydroxylation of benzene over MoV based hybrid.

Initially, there is an electron exchange between the catalyst and glucose, resulting in coexisting Mo^{5+}/Mo^{6+} species within the Keggin anion and a free glucose radical formation. Then, this mixed valence [C2mim]$PMo^{6+}Mo^{5+}$ species can react with H_2O_2 to form the hydroperoxy radical ($HOO^{\cdot}$) by storing both an electron and a proton, the later probably over the terminal Keggin anion oxygens. The reaction of the $HOO^{\cdot}$ with another H_2O_2 molecule produces $HO^{\cdot}$ radical which can attack the carbonylic group of glucose, incorporating the –OH group to form the final acid. This reaction is rather slow at low pH due to the higher energy needed for the transfer of an electron from the HO_2 πg^* orbital to the empty σ_u^* orbital of H_2O_2 and results from the decomposition of hydrogen peroxide [56]. The later occurs upon heating; is a step of the peroxide decomposition reaction and could explain the conversion obtained in the blank experiment. On the other hand, transition metal complexes are able to catalyze this step. The [C2mim]$HPMo^{6+}Mo^{5+}$ species re-oxidizes and lost the proton with the formation of an additional $HO^{\cdot}$ radical and water. All those reactions result in the $HO^{\cdot}$ radical concentration increase and positive effect on glucose conversion.

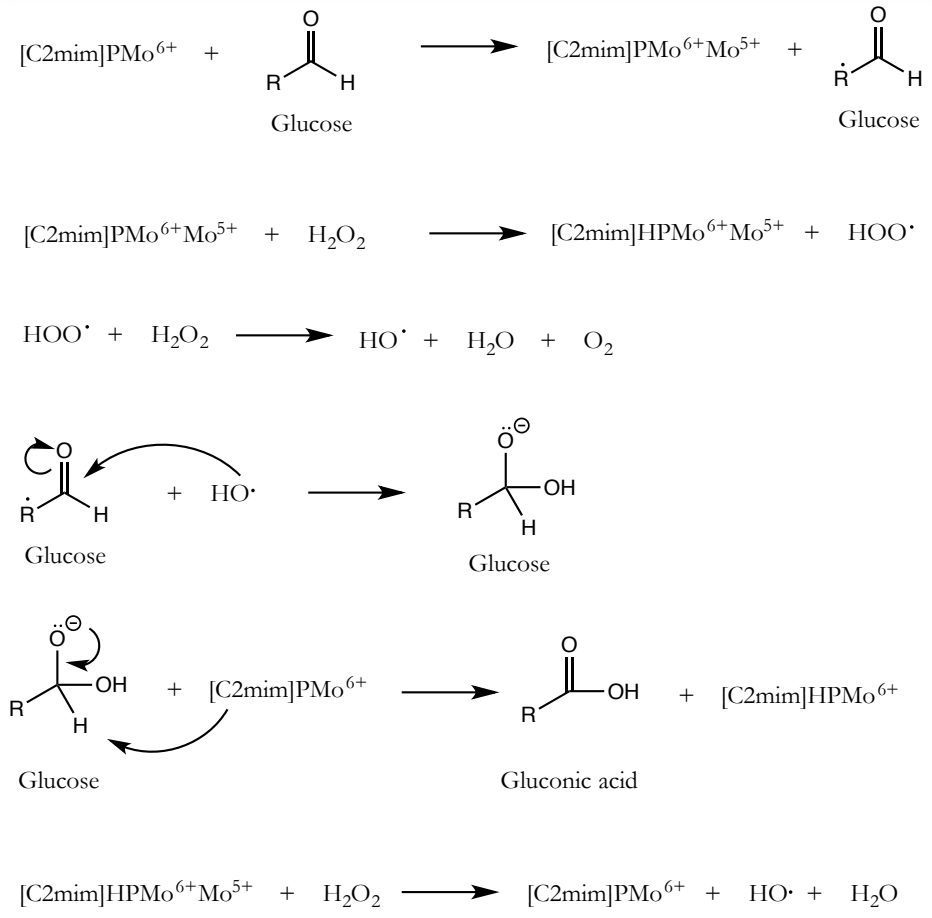

Scheme 4.5. Tentative reaction mechanism for oxidation of glucose with H_2O_2 over [C2mim]PMo.

This is, however, only a plausible mechanism and not yet proven experimentally. Nevertheless, this mechanism could explain the absence of differences between the hybrids, since only the Keggin anion is involved in the reaction. The cation, however, could stabilize some radical intermediates and this stabilization could be the key to explain the higher conversion registered for the hybrids in comparison with that of the acids.

As for the influence of the catalyst loading, the existence of optimal value (2.5 mol% of catalyst) suggests that the formed HO · radicals are rapidly consumed either by the reaction or for re-oxidizing Mo. It is possible then, that the 3 mmol H_2O_2 equivalent was not enough to cover both process and the conversion slightly decreases for the highest catalyst loadings, as a consequence of H_2O_2 deficiency. The later could be also the reason for the low gluconic acid yields. A detailed study of H_2O_2 amount variation is needed to confirm the speculatively elucidated mechanism.

Table 4.5. . Oxidation of glucose by H_2O_2 over different POM based hybrids

Entry	Catalyst	Amount, mol% (referred to glucose)	Conversion (%)	GA selectivity (%)	FA selectivity (%)
1	[C2mim]PMo	0.25	30	100	0
2		2.5	40	100	0
3	[C2mim]PMoV	0.25	44	78	22
4		2.5	51	89	11
5	[C2mim]PW	0.25	35	100	0
6		2.5	35	100	0

The influence of the metal center in the Keggin anion was also evaluated. Table 4.5. lists the obtained results as a function of the catalyst amount (0.25 mol% vs 2.5 mol%) and metal center nature. The substitution of Mo by W leads to some glucose conversion increase at lower catalyst charge, but, this conversion does not increase for higher loadings, suggesting a different catalyst charge-activity dependence. The substitution of two atoms of Mo by V, leads to the highest observed conversion, 44%, increasing with the catalyst loading to 51%. However, not only the activity but also the selectivity is influenced, the GA yield decreases in favor to

Formic Acid (FA) production as a result of total oxidation of glucose molecule.

The catalytic behavior of the [C2mim]PMo was also studied as a function of reaction time (Figure 4.10.). Neither glucose conversion nor GA selectivity undergo important changes from 1 to 18 hours of reaction, having a conversion of 25% after 1 hour, and 30% after 6 hours.

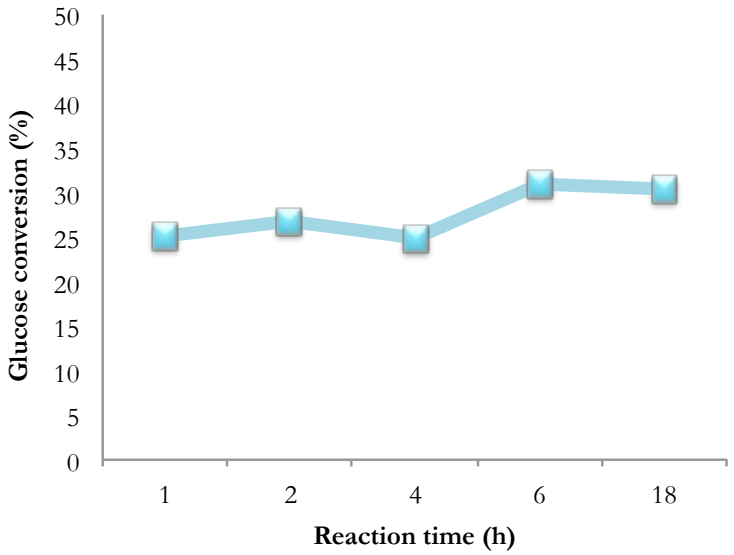

Figure 4.10. Catalytic behavior in glucose oxidation reaction as a function of reaction time (h) over [C2mim]PMo

The last study was used to demonstrate the stability of the structures at long reaction times, by means of X Ray Diffraction (Figure 4.11.). All diffractions of fresh [C4mim]PMo appears for the spent catalyst analysis, and correspond exactly to the same initial structure pointing to the possible reutilization of the catalyst in increased number of cycles.

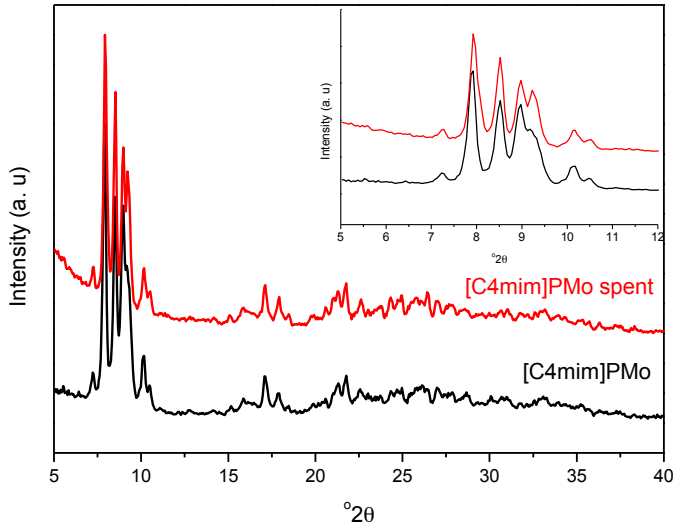

Figure 4.11. XRDiffractograms of [C4mim]PMo fresh and spent (after 18 hours of reaction)

4.2.4. Partial conclusions

This section demonstrates that POM-ILs compounds are also active for mild glucose oxidation reaction with hydrogen peroxide. Despite that 21% of glucose conversion is achieved in absence of catalyst to gluconic acid and traces of glucaric acid, higher conversions are obtained with the hybrid with 100% selectivity to GA. The different organic cations do not influence directly the catalytic performance, but probably participates indirectly in the stabilization of intermediates of the proposed mechanism. The later is proposed on the base of free radical organic molecule oxidation mechanism and the Haber-Weiss cycle of hydrogen peroxide decomposition/activation. The Keggin structure change produces higher impact on activity/selectivity balance. The substitution of Mo by W results in higher catalytic performance, but with different catalyst loading/activity dependence. Higher conversions are also obtained upon 2

atoms Mo by V substitution. However, the selectivity to GA suffers and the formation of formic acid is observed. The reaction time effect shows that the reaction occurs in the first few hours and the structure of the hybrid remains intact after the oxidation process, a promising result for possible recycling. Although more work needed, this study serves as first approximation to the application of the POM-ILs materials in organic molecules oxidation reaction with hydrogen peroxide under mild conditions.

4.3. Glucose/Fructose dehydration

4.3.1. Introduction

The production of 5-hydroxymethylfurfural (HMF) from lignocellulosic derivatives is one of the top studied processes involved in the field of biomass valorization. Most research focused on the conversion of fructose to HMF [57–59]. Fructose dehydration is fairly easy to perform and is catalyzed by homogeneous and heterogeneous Brönsted acid catalysts [60–62]. In contrast, it is hard to convert glucose to HMF in acidic aqueous media, the product selectivity is low unless the used catalyst converts firstly glucose to fructose [63,64]. The transformation of glucose to fructose involves an isomerization reaction, which entails the hydride shift between C2 and C1, and ketone formation in C2 position. The fructose hemiacetal form is a five member furanic ring, whose general structure is very similar to that of HMF (see Scheme 4.6.), a detail that seems to be the key difference between glucose and fructose dehydration process. In a complete report, R. J. van Putten and coworkers [64] combined experimental and DFT studies to find out the differences between aldose and ketose dehydration including the rate limiting step of the process. They demonstrated that there is no differences in the

dehydration rates between the aldoses (glucose and mannose), however, for the five membered furanic ring ketoses the dehydration is promoted due to the dehydration mechanism that implies cyclic species (see Scheme 4.7, for fructose).

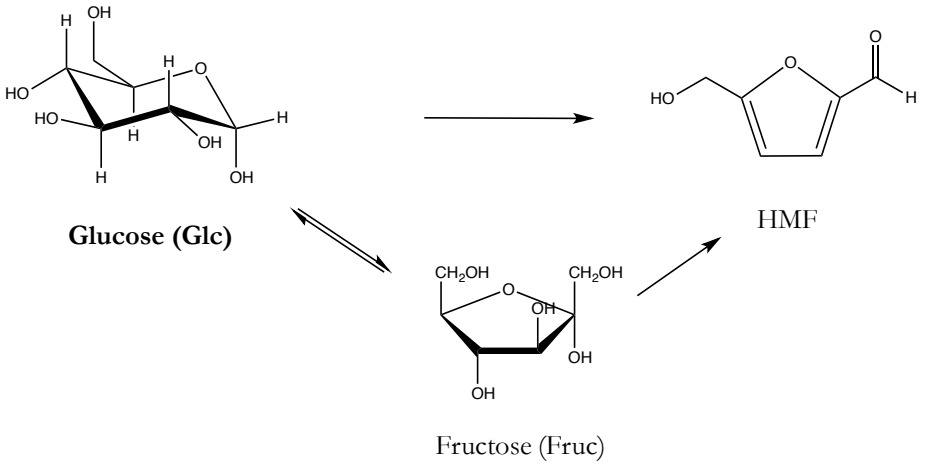

Scheme 4.6. Overall schematic of the glucose/fructose dehydration to HMF

Glucose isomerization to fructose has been widely studied over different Lewis acid catalysts [33,34,65] and zeolites [66–68], being the H2-H1-hydride shift widely accepted as isomerization mechanism. This mechanism implies the formation of glucose-Lewis center adduct in the open form that gives rise to the corresponding ketone (Scheme 4.7.).

As summary of the active sites involved, the glucose isomerization requires Lewis acid sites whereas the fructose dehydration Brönsted acid ones. Therefore, the fructose dehydration needs only one active site while the glucose dehydration needs a Lewis / Brönsted acid tandem sites.

The general pathway of glucose dehydration to HMF is presented in Scheme 4.7. The mechanism, implicates the formation of fructose as intermediate. However, the transformation of glucose to HMF has been

also studied over Brönsted acid catalysts, with different mechanism [69], in which fructose does not appear as intermediate.

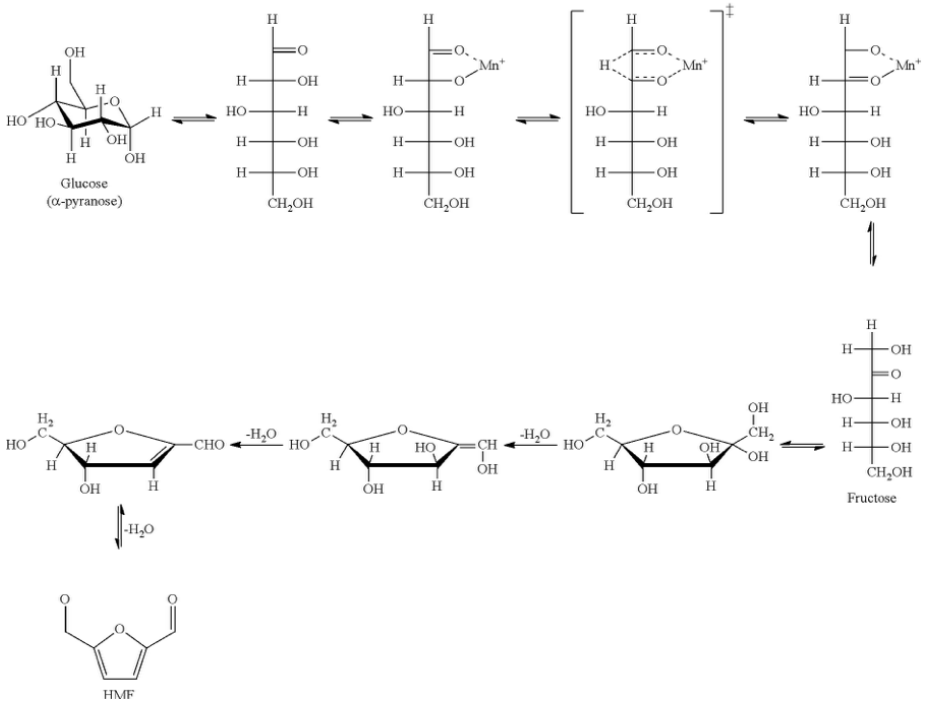

Scheme 4.7. Reaction scheme for the conversion of glucose to HMF catalyzed by the tandem Lewis/Brönsted acid sites.

One of the main factors to consider in this process is the high number of secondary reactions that could take place in acidic aqueous media [70]. The most important are the rehydration of HMF to levulinic acid (LA) and formic acid (FA) and the formation of polymerization products as a result of successive aldolic condensations, widely known as humins (see Scheme 4.8.). The rehydration rate is directly related with the water content in the media, being the HMF production in aqueous solution not a viable option, presumably due to the slow rate of HMF formation and rapid rehydration to furan opening-ring products, levulinic and formic acid [71]. This selectivity problem motivates the continuous extraction of

HMF from the reaction mixture by using biphasic systems composed by immiscible aqueous and organic solutions [72].

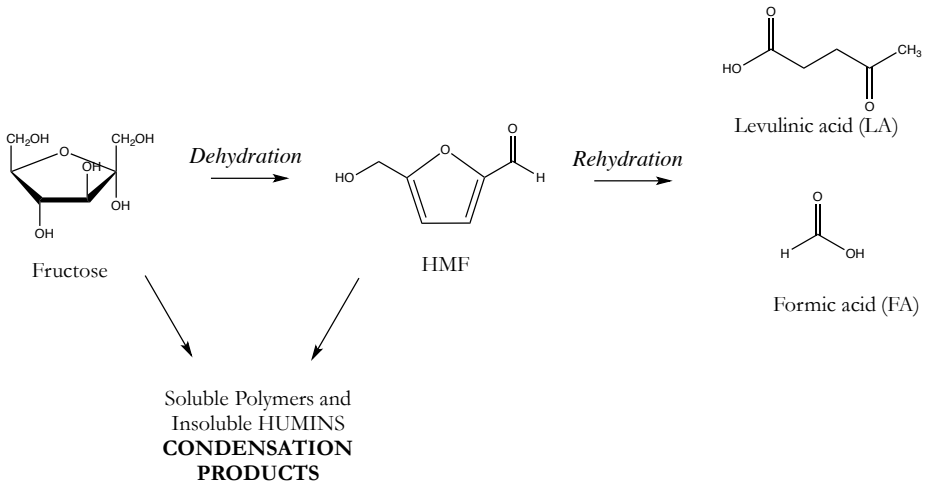

Scheme 4.8. Main secondary reactions during the dehydration of fructose to HMF in acidic media.

The organic layer should act also as extracting phase, a continuous accumulation of HMF into the organic phase immediately after its formation in the reactive phase is expected. That way, lower concentration of HMF in the aqueous phase limits the rate of side reactions and thereby improves HMF yields [73]. In this context, the partition coefficient (*R*) is an important parameter in determining the overall effectiveness of the biphasic media. Higher partitioning of the HMF into the organic layer improves the effective extraction and hence increases the HMF selectivity. In addition, the HMF can be easily separated by simple evaporation of the organic solvent, and low boiling point solvents are highly desired. A great number of solvents have been studied, alone or in combination with different phase additives to improve the partition coefficient [74,75]. In the same way, a great number of Brönsted acid catalysts have been tested, alone or in combination with Lewis acid catalysts [69,72,76].

Along this section, the catalytic activity of the synthesized hybrid structures will be studied in the glucose/fructose dehydration to HMF. Biphasic system composed by water and methyl isobutyl ketone (MIBK), a low boiling point organic solvent with good HMF partition coefficient will be used.

The influence of the starting material (Glucose *vs.* Fructose), reaction time, catalyst loading and water/organic solvent volume ratio will be investigated. The catalytic differences between hybrid and corresponding acid will be also discussed as well as the influence of metal center change.

4.3.2. Experimental

The catalysts were used as prepared according to the experimental part of Chapter 3. The catalytic tests were performed in a glass batch reactor of 50 mL equipped with a magnetic stirrer, where 1 mmol of glucose/fructose (Sigma Aldrich, 0.1802 g) and the catalyst, in a 0.25 mol% or 2.5 mol% (amount referred to the sugar reactant) were introduced to a H_2O:MIBK mixture in 1:3 volume ratio. The mixture was then heated in a paraffin oil bath to 120 ºC at a stirring rate of 600 rpm approximately. After the reaction, the reactor was cooled down in ice bath and the phase was separated from the organic phase. A sample was taken from the aqueous phase, diluted in ultra-pure water and analyzed by HPLC. All analyses were performed in Varian 360 Liquid Chromatograph, using H_2SO_4 as eluent. The specific operation conditions are summarized in Chapter 2, Analytical methods section. A typical chromatogram obtained during the dehydration analyses is exposed in Figure 4.12 , as an example. Conversion, selectivity and yields were calculated as exposed in Chapter 2. However, owing to the large amount of formed products and

presence of byproducts, the equations are summarized specifically in this section, taking fructose as starting sugar:

$$Conversion\ (\%) = \frac{[Fructose]_i - [Fructose]_f}{[Fructose]_i} x\ 100 \qquad \text{Eq. 4.2.}$$

$$HMF\ Selectivity\ (\%) = \frac{HMF\ mol}{Fructose\ mol_i - Fructose\ mol_f} x\ 100 \qquad \text{Eq. 4.3.}$$

$$Byproducts\ Selectivity\ (\%) = 100 - Total\ selectivity \qquad \text{Eq. 4.4.}$$

$$HMF\ yield\ (\%) = \frac{Conversion\ (\%)\ x\ Selectivity\ (\%)}{100} \qquad \text{Eq. 4.5.}$$

$$C\ Balance\ (\%) = \frac{Final\ C\ mols}{Initial\ C\ mols} x\ 100 \qquad \text{Eq. 4.6.}$$

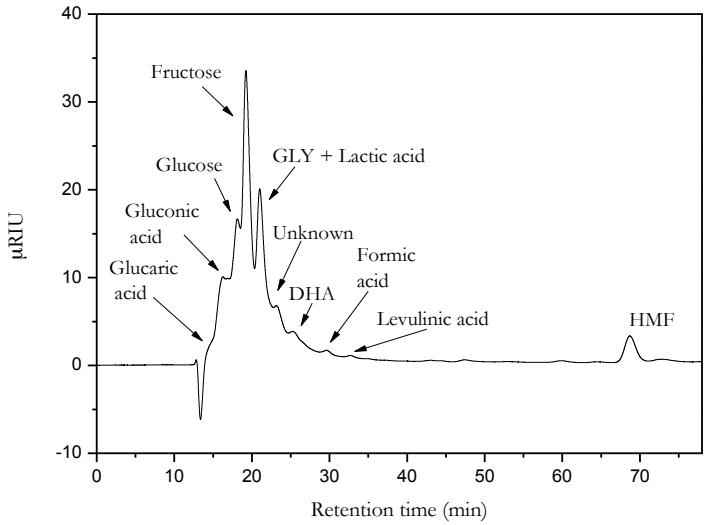

Figure 4.12. Typical chromatogram obtained during the dehydration analysis. Note: GLY (Glyceraldehyde), DHA (Dihydroxyketone), HMF (5-hydroxymethylfurfural).

4.3.3. Catalytic activity: results and discussion

The partition coefficient (*R*) of HMF in an immiscible mixture of H_2O:MIBK was calculated experimentally by dissolving a determined amount of HMF in 1 mL of H_2O on which 3 mL of MIBK were added. The mixture was heated at 120 ºC during an hour, after that, a sample from each layer were taken and analyzed by HPLC. The partition coefficient is calculated from the HMF concentration ratio in each layer, as presented in Eq 4.7.

$$R = \frac{[HMF]_{org}}{[HMF]_{aq}} \qquad \text{Eq. 4.7.}$$

Despite that most experiences were carried out using MIBK, the influence of H_2O:organic solvent ratio was studied also with diethyl ether (DEE). Analogously, the partition coefficient of HMF in diethyl ether (DEE) was calculated. Both are listed in Table 4.6.

Table 4.6. Calculated partition coefficients in MIBK and DEE

Solvent	*R*
MIBK	1.11
DEE	0.14

After these experiments, only the aqueous phase is analyzed, being the amount of HMF in the organic phase obtained from the partition coefficient *R*.

The visual aspect of the catalytic system, once the reactants contacted and reacted for 15 minutes, is shown in Figure 4.13.

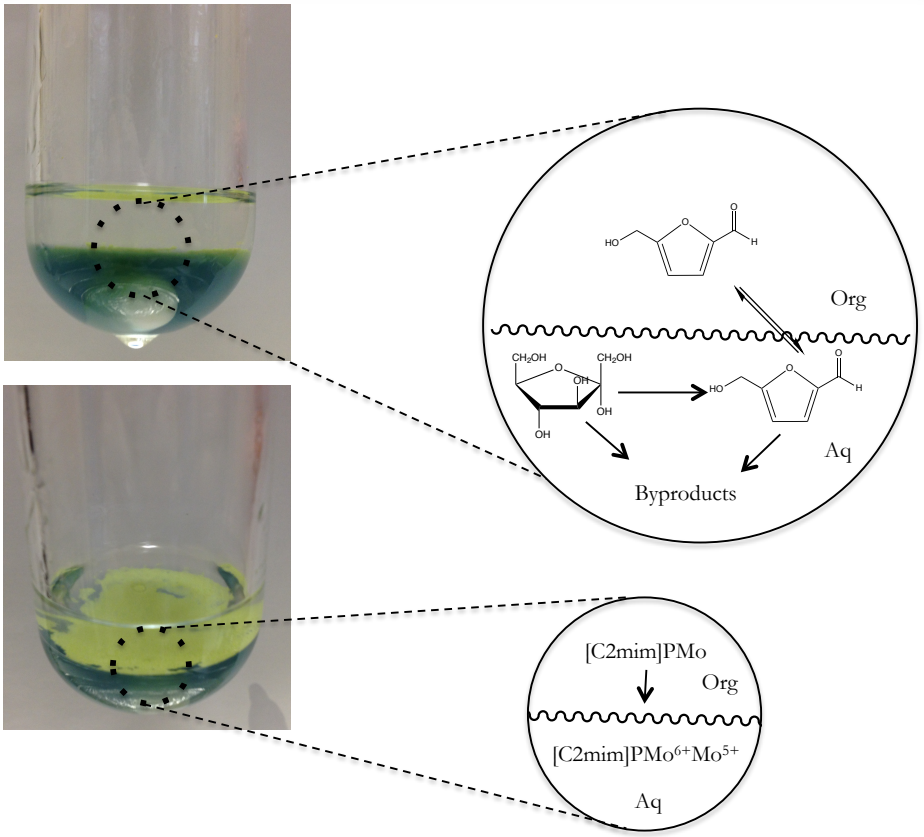

Figure 4.13. Catalytic system for fructose dehydration. Reaction conditions: 1 mmol of fructose (0.1802 g), 1mL of H_2O, 0.25 mol% of [C2mim]PMo, 3 mL of MIBK, 15 min, 120 ºC.

The hybrid is situated at the interphase, because of its dual nature, it is compatible with the organic phase through the organic cation and compatible to the aqueous one due to Keggin anion presence. The organic cations are probably oriented toward organic phase contrary to the anions. The electron exchange between glucose and Keggin anion takes place firstly in the hybrid oriented towards aqueous phase (see Figure 4.13.). If the reaction happens near the interphase, the HMF migration from aqueous to organic phase is boosted, remaining less time in the former. However, if the HMF is produced mainly in the aqueous

phase, the presence of hybrid at the interphase could hinder the HMF migration, increasing its spent time in aqueous phase and the probability for byproducts formation.

Table 4.7. lists the obtained results for PMoA and [C2mim]PMo. In both cases, the influence of the starting sugar, glucose or fructose, is evaluated. As expected, the catalytic performance strongly depends on the reactant, being the conversion below 100% in the case of glucose and 100% when the starting sugar is fructose. The selectivity and byproducts formation are also influenced by the sugar type.

Generally, in the case of glucose (Table 4.7. entries 1 and 3), high selectivity toward Fructose/Mannose (32% and 20% for PMoA and [C2mim]PMo, respectively) is observed and expected according the epimerization study. Most probably, both compounds are present, since the glucose isomerization to fructose is enhanced at longer reaction times. The HMF selectivity, however, is very low, 3% and 4% for PMoA and [C2mim]PMo respectively, suggesting that both hybrid and acid are scarcely active in glucose dehydration. Moreover, the presence of different products and byproducts informs about the undesired reactions. In the case of PMoA (Table 4.7. entry 1), some glucose is oxidized to Gluconic (GA, 18% of selectivity) and Glucaric Acid (GcA 13% of selectivity), the HMF is rehydrated toward Formic (FA, 4%) and Levulinic Acid (LA, 2%) and some produced fructose undergo retro-aldol condensation to form Glyceraldehyde (GLY, 13% of selectivity) and dihydroxyacetone (DHA, 7%). The formation of non-identified byproducts is also taking place (8%). The formation of some oxidation products could be related with the oxidant atmosphere used during the catalytic tests, since no air is removed from the reactor.

Table 4.7. Transformation of glucose/fructose over PMoA and [C2mim]PMo catalysts (2.5 mol% of starting material): influence of starting sugar

Entry	Catalyst	Starting material	Conversion (%)	Selectivity (%)								
				GcA	GA	Glc*/Fruc+Mann	FA	LA	**HMF**	GLY	DHA	Byproducts (non analyzed)
1	PMoA	**Glc**	**69**	13	18	32	4	2	**3**	13	7	8
2	PMoA	**Fruc**	**100**	11	5	3*	3	4	**23**	5	1	45
3	[C2mim]PMo	**Glc**	**83**	0	6	20	2	0	**4**	8	2	52
4	[C2mim]PMo	**Fruc**	**100**	0	2	3*	2	1	**21**	7	8	61

Legend: Glc (Glucose), Fruc (Fructose), GcA (Glucaric acid), GA (Gluconic acid), Mann (Mannose), FA (Formic acid), LA (Levulinic acid), HMF (5-hydroxymethylfurfural), GLY (glyceraldehyde), DHA (dihydroxyacetone).

* The selectivity corresponds to Glc when the starting sugar is Fruc and corresponds to Fruc + Mann when starting with Glc.

Reaction conditions: 1 mmol of starting sugar (0.1802 g), 2.5 mol% of catalyst (0.06 g), 1 mL of H_2O, 3 mL of MIBK, 18 hours at 120 ºC and 600 rpm.

The overall reaction pathway is summarized in Scheme 4.9.

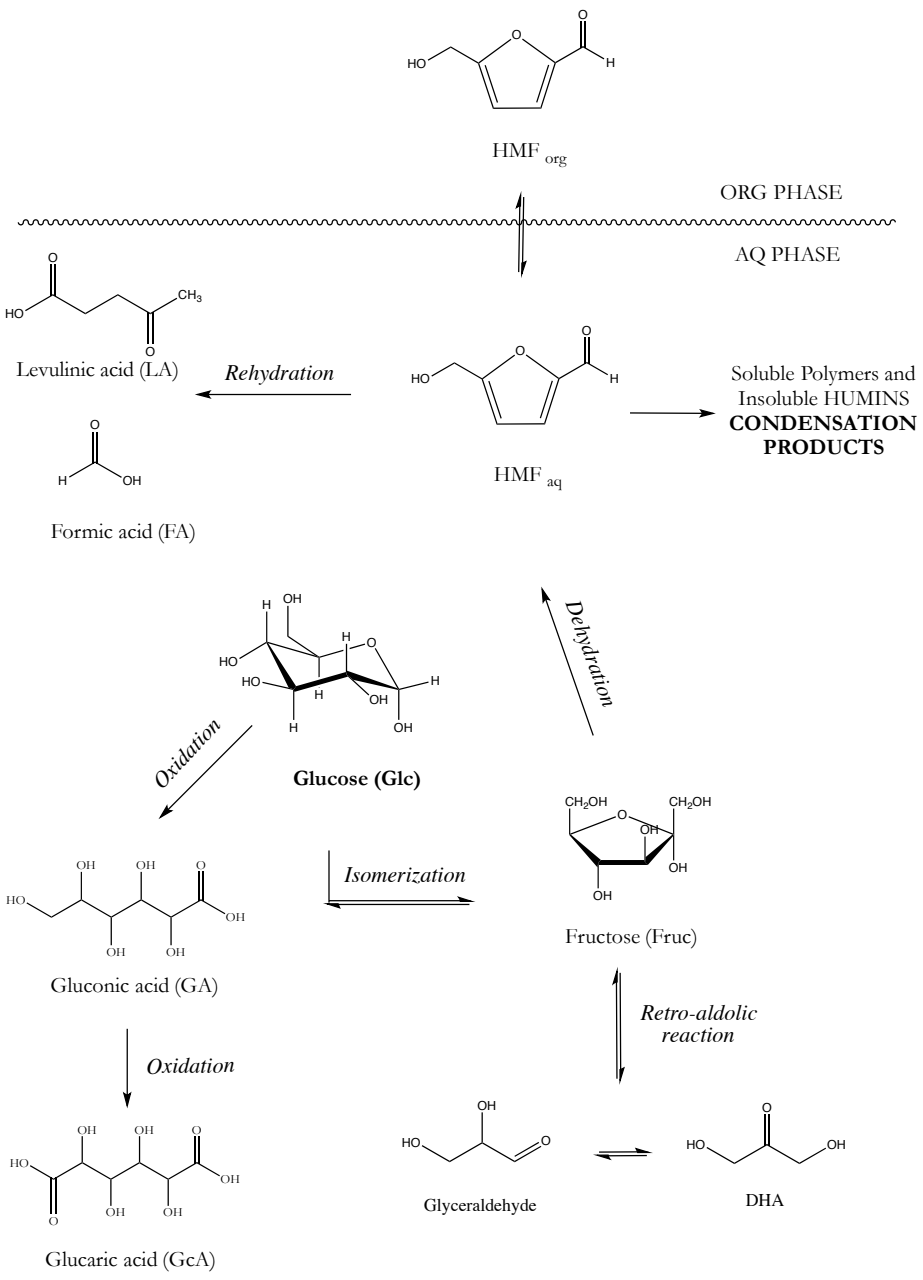

Scheme 4.9. Proposed pathway during glucose/fructose dehydration reaction over studied catalysts

Glucose is in equilibrium with fructose/mannose as a consequence of the isomerization/epimerization reaction over the Lewis acid sites available from the Mo dimer species. Some glucose is also oxidized to form firstly gluconic acid and, after glucaric acid. Once the fructose is formed, it undergoes a consecutive loss of water leading to HMF formation. If the later was not rapidly extracted in the organic phase, rehydrates to form open chain products, such as formic and levulinic acid. Also the presence of HMF in the aqueous phase could provoke rapid polymerization, leading to the production of soluble polymers and insoluble humins, both undetected by our HPLC method. However, the humin presence could be intuited by the carbon balance calculation. A balance lower than 90% suggests C atoms loss in non-identified products, such as humins. Our balances ranges between 40 and 80% depending on the catalysts and reaction condition and accounts for the byproducts fraction. Moreover, the presence of solid fraction is also evident in the post reaction mixture (Figure 4.14). The presence of GLY and DHA, on the other hand, account for the C-C cleavage, through reverse aldol reaction, also possible in acidic media [70].

As for fructose as reagent (Table 4.7. entries 2 and 4), higher selectivity to HMF is reached (23% and 21% for PMoA and [C2mim]PMo, respectively), being 3% the registered selectivity to glucose in both cases. Again partially oxidized products issued from glucose are detected. On the other hand, part of fructose suffers reverse aldol reaction and the HMF is also rehydrated to FA and LA. These undesired side reactions occur in the same extent, no matter the starting sugar. However, the polymerization/condensation byproducts are strongly enhanced when fructose is used as raw material. The formation of humins in acidic media occurs *via* aldol addition and condensation, as proposed by Horvat [77]. Once the HMF is formed, its rehydration leads to the formation of LA

and FA (see Scheme 4.9.) or to the ring opening to form 2,5-dioxo-6-hydroxy-hexanal (see Scheme 4.10.). The later can react with the remaining HMF, undergoing a series of consecutives aldol addition/condensation reactions to form conjugated molecules of high molecular weight, which become insoluble in acidic media. Under the reaction conditions described in this section, the formation of insoluble polymers seems evident not only on the basis of the carbon balance (Figure 4.14.)

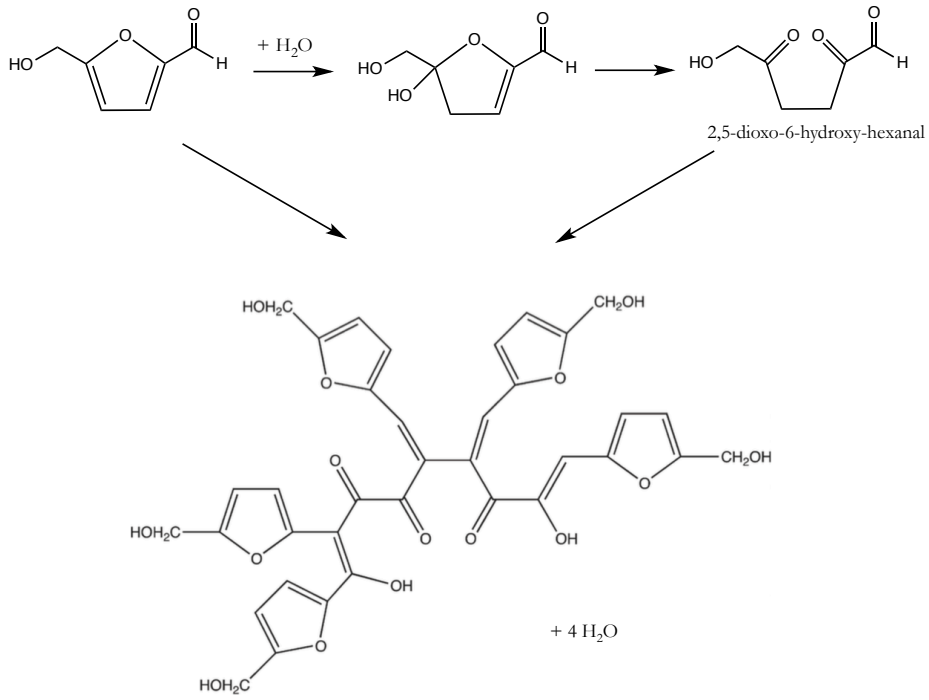

Scheme 4.10. HMF conversion pathway to humins formation, suggested by Horvat [77]

Humins have coiled conformations, cross-linked by weak Van der Waals forces, and strongly dependent on the pH. In acidic media, these polymerization products became insoluble due to both, formation of intermolecular hydrogen bonds and rearrangement of the conformations.

However, when the pH increased, the degree of cross-linking diminishes, and the polymeric structures become soluble [78]. The obtained solid was separated from the post reaction mixture and manually stirred 5 seconds in a diluted solution of NaOH (Figure 4.14). The precipitate starts to dissolve immediately in basic media, corroborating the high selectivity to polymeric byproducts presented in Table 4.7.

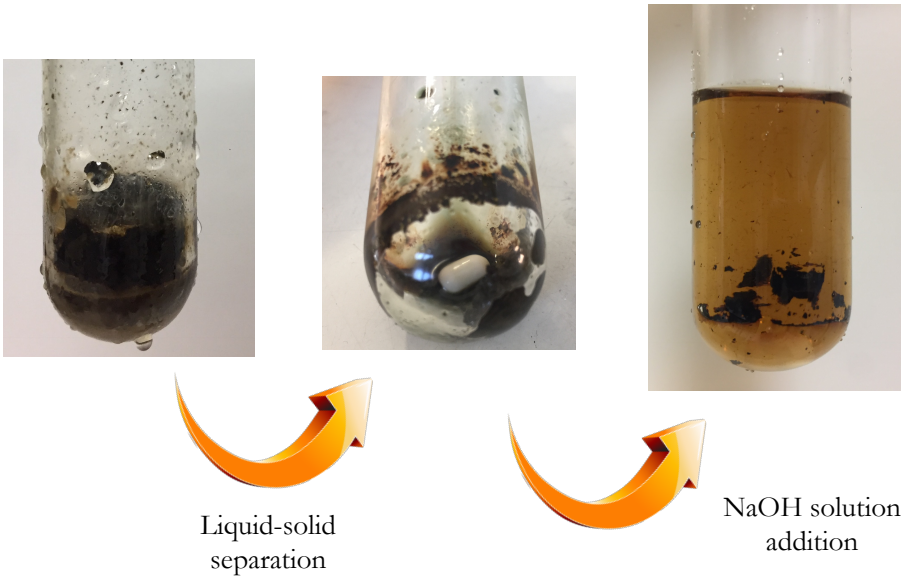

Figure 4.14. Formation of solid byproducts during the fructose dehydration (post reaction mixture)

Going back to Table 4.7., it should be underlined that the amount of byproducts is always higher for the hybrid than for the bare acid, for a similar HMF selectivity. This suggests that the hybrid is more active in the dehydration reaction (for both glucose and fructose), since more HMF should be formed to produce a higher amount of humins. Evidently, this is not an exceptional result but serves to consider the viability of both compounds in the mentioned reaction. It is clear that the dehydration occurs, however, the formation of byproducts should be inhibited either by change of the catalytic material or by means of *R* improvement, faster

the HMF transfer to the organic phase lower the humins formation rate. The later will be one of the point to consider for future research.

Another factor that could inhibit the amount of formed byproducts is the reaction time. As demonstrated by Zhao *et al.* [79] the production of HMF from fructose normally presents a maximum as function of time, situated around 60 min of reaction in their catalytic system. From this point, the selectivity to HMF diminishes in favor to the byproducts. Table 4.8. summarizes the results obtained in the transformation of fructose over [C2mim]PMo at different reaction times. As expected, the fructose conversion increases with the reaction time as well as the formation of byproducts. It is interesting that, at shorter reaction times the amount of byproducts is higher than expected whereas the rehydration to FA and LA is totally inhibited. The later suggest that the HMF rehydration and cycle opening reaction is faster and occurs immediately once HMF formed. The byproducts formation reaches a maximum in 2 hours reaction, and after that the formed HMF remains as HMF, as observed in Table 4.8.

As for the reverse aldol reaction, it is also interesting that at shorter reaction times, the GLY and DHA selectivities are greater. It is known that in acid media the aldolisation of DHA and GLY towards HMF formation could take place [70], which may be the reason of the obtained selectivities after 18 hours.

Table 4.8. Transformation of fructose over [C2mim]PMo catalyst at different reaction times.

Entry	Time (h)	Conversion (%)	Selectivity (%)									pH before	pH after
			GcA	GA	Glc	FA	LA	**HMF**	GLY	DHA	Byproducts (non analyzed)		
1	1	44	2	2	9	0	0	**5**	27	7	49	2.72	-
2	2	55	4	6	17	0	0	**7**	25	6	60	2.72	-
3	18	100	0	2	3	2	1	**21**	7	2	61	2.72	2.0

Legend: Glc (Glucose), GcA (Glucaric acid), GA (Gluconic acid), FA (Formic acid), LA (Levulinic acid), HMF (5-hydroxymethylfurfural), GLY (glyceraldehyde), DHA (dihydroxyacetone).

Reaction conditions: 1 mmol of fructose (0.1802 g), 2.5 mol% of catalyst (0.06 g), 1 mL of H_2O, 3 mL of MIBK, at 1, 2 and 18 hours, respectively, at 120 ºC and 600 rpm

Table 4.9. Transformation of fructose over PMoA and [C2mim]PMo catalysts: influence of catalyst amount.

Entry	Catalyst	Amount, mol% (referred to fructose)	Conversion (%)	Selectivity (%)									pH before	pH after
				GcA	GA	Glc	FA	LA	**HMF**	GLY	DHA	Byproducts (non analyzed)		
1	PMoA	0.25	100	0	3	3	2	1	**22**	7	4	58	-	-
2		2.5	100	11	5	3	3	4	**23**	5	1	45	1.87	1.84
3	[C2mim]PMo	0.25	90	0	2	13	3	1	**27**	15	3	36	-	-
4		2.5	100	0	2	3	2	1	**21**	7	2	61	2.72	2.0

Legend note: Glc (Glucose), GcA (Glucaric acid), GA (Gluconic acid), FA (Formic acid), LA (Levulinic acid), HMF (5-hydroxymethylfurfural), GLY (glyceraldehyde), DHA (dihydroxyacetone).

Reaction conditions: 1 mmol of fructose (0.1802 g), 0.25mol% or 2.5 mol% of catalyst (0.006 g or 0.06 g), 1 mL of H_2O, 3 mL of MIBK, were reacted during 18 hours, respectively, at 120 ºC and 600 rpm

The influence of the catalyst loading was studied varying from 0.25 mol% to 2.5 mol% the catalyst charge. The obtained results for the [C2mim]PMo hybrid and its corresponding acid are presented in Table 4.9.

For the PMoA, the fructose conversion is not influenced by the amount of catalyst, 100% conversion is obtained in both cases. However, the products distribution is slightly different, for a similar HMF selectivity. Higher acid amount lead to more oxidation products (5% and 11% selectivity to GA and GcA, respectively) and less byproducts formation (45% for 2.5 mol% *vs.* 58% for 0.25mol%).

For the hybrid (Table 4.9. entries 3 and 4) the variation of the catalyst amount results in more evident changes. When the catalyst decreased by 10 times, the fructose conversion is 90% whereas complete conversion is reached for 2.5 mol% of catalyst. Regarding the product distribution, lower hybrid amount give rise to higher HMF selectivity, 27% instead of 21%, and lower byproducts formation 36% vs. 61% with ten times more catalyst.

At this point, it is possible to ensure that the hybrid is superior to the bare acid for the dehydration of fructose, although more research is needed to reach the optimum operation conditions.

The influence of the Keggin anion was also evaluated for both sugars. The three parent acids, PWA, PMoA and PMoVA, and their corresponding C2mim based hybrids, [C2mim]PW, [C2mim]PMo and [C2mim]PMoV, were tested in standard reaction conditions. The obtained results are presented in Table 4.10. Reaction conditions: 1 mmol of sugar (0.1802 g), 2.5 mol% of catalyst (0.06 g), 1 mL of H_2O, 3 mL of MIBK, were reacted during 18 hours, respectively, at 120 ºC and 600 rpm

Table 4.10. Transformation of glucose/fructose over different catalysts (2.5 mol% of catalyst referred to the corresponding sugar)

Entry	Catalyst	Starting material	*X* (%)	Selectivity (%)									pH before	pH after
				GcA	GA	Glc*	FA	LA	HMF	GLY	DHA	Byproducts (non analyzed)		
1	PMoA	Glc	**69**	13	18	32	4	2	**3**	13	7	8	1.87	1.84
2		Fruc	**100**	11	5	3*	3	4	**23**	5	1	45	1.87	1.84
3	[C2mim]PMo	Glc	**83**	0	6	20	2	0	**4**	8	2	52	2.72	2.0
4		Fruc	**100**	0	2	3*	2	1	**21**	7	8	61	2.72	2.0
5	PWA	Glc	**10**	0	100	0	0	0	**0**	0	0	0	1.80	1.80
6		Fruc	**88**	0	16	0*	3	3	**6**	5	4	63	1.80	1.80
7	[C2mim]PW	Glc	**8**	0	100	0	0	0	**0**	0	0	0	2.62	2.62
8		Fruc	**41**	0	9	11*	0	0	**53**	0	0	27	2.62	2.36
9	PMoVA	Glc	**62**	0	13	37	0	0	**4**	11	5	30	2.12	1.80
10		Fruc	**74**	0	3	9*	3	0	**15**	14	3	53	2.12	1.67
11	[C2mim]PMoV	Glc	**67**	0	2	47	0	0	**4**	10	9	28	3.80	2.43
12		Fruc	**90**	0	4	6*	2	1	**19**	8	3	55	3.80	2.42

* The selectivity corresponds to Glc when the starting material is Fruc and corresponds to Fruc + Mann when the starting sugar is Glc.

Generally, the conversion and HMF selectivity are higher when the starting sugar is fructose, which is concordant with the proposed reaction mechanisms. Taking into account only these results (Table 4.10. entries 2, 4, 6, 8, 10 and 12), the differences in both, activity and selectivity, as a function of the catalyst nature can be discussed. For the HPAs (Table 4.10. entries 2, 6 and 10), fructose conversion follows the trend PMoA > PWA > PMoVA; and the HMF selectivity the trend PMoA > PMoVA > PWA and the byproducts selectivity PWA > PMoVA > PMoA. The later means that the PMoA is the most efficient in these reaction conditions, since the higher conversion and selectivity and lower byproducts selectivity is achieved. The high byproducts formation is registered for PWA, with a 63% of selectivity, which can be associated to its stronger acidity that promotes the fast rehydration in favor to humins formation. The substitution of two Mo atoms by V in the PMoVA leads only to less active catalyst in fructose dehydration with lower conversion.

The H^+ exchange by $[C2mim]^+$ entails certain change in the catalytic behavior when comparing hybrids to parent acids. The observed tendencies differ from the previous ones with regards to fructose conversion, [C2mim]PMo > [C2mim]PMoV > [C2mim]PW, HMF selectivity, [C2mim]PW > [C2mim]PMoV > [C2mim]PMo and byproducts selectivity [C2mim]PMo > [C2mim]PMoV > [C2mim]PW. In the case of the Mo based hybrids, it seems to be less efficient in these reaction conditions. Although the highest conversion is achieved, the lowest HMF selectivity and the highest byproducts formation is attained. Here the [C2mim]PW hybrid presents the best conversion/selectivity ratio with 41% conversion and 53 % HMF selectivity.

From these experiments, one can conclude that the catalytic behavior strongly depends on the metal nature in the Keggin anion. The differences between the Mo and W based systems may be related to their different

acidity, higher in the case of PWA. The presence of the organic cations also influences the catalytic behavior as a function of the Keggin to which is bonded. In the case of Mo based compounds, the presence of alkylimidazolium cations scarcely influence the overall process, whereas for MoV related structures, a decrease of the activity is observed. As for the PW compounds, the proton exchange with organic cation leads to more selective catalyst, achieving the highest HMF selectivity in this study and the lowest amount of humins. This is a very good starting point encouraging the future investigations in order to find out the true potential of POM-ILs for the fructose dehydration.

The dehydration reaction is a complex process where a lot of parameters should be taken in account to optimize a process with a new catalytic system. This optimization should entail a complete study of the effect of the initial fructose concentration on its conversion and product distribution, demonstrated as a key factor to control the byproducts formation [79]. Also the reaction time, the amount of catalyst, the temperature, the type of solvent, the volume ratio of aqueous and organic phases, the presence of modifiers to improve the partition coefficient [72] have to be studied in details.

In this thesis, only a part of the above-mentioned features were studied, but in a "superficial way" just to have a clue for future research. The influence of the organic and aqueous phases volume ratio was evaluated for MIBK and DEE. The conversion (%) and the HMF yield (%) for H_2O:MIBK systems are represented in Figure 4.15. In the same way, the HMF selectivity (%) is compared with byproducts selectivity (%) as function of H_2O:MIBK ratio is summarized in Table 4.11.

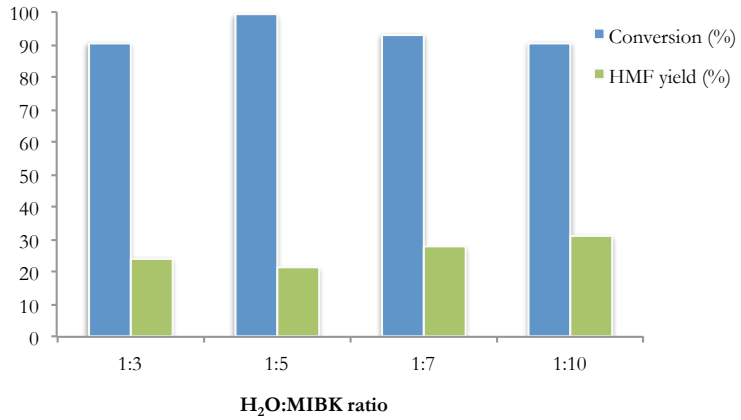

Figure 4.15. Fructose conversion (%) and HMF yield (%) as function of H_2O:MIBK ratio

Table 4.11. HMF and byproducts selectivities (%) as function of H_2O:MIBK ratio

Entry	H_2O:MIBK volume ratio	Selectivity (%)	
		HMF	Byproducts (non analyzed)
1	1:3	**27**	36
2	1:5	**21**	56
3	1:7	**30**	44
4	1:10	**34**	19

Reaction conditions: 1mmol of fructose (0.1802 g), 0.25 mol% of catalyst (0.006 g), 1 mL of H_2O and 3, 5, 7 and 10 mL of MIBK, respectively, at 120 ºC, 600 rpm after 18h

The increased MIBK volume does not influence the fructose conversion (Figure 4.15.). On the contrary the HMF and byproducts selectivity's dependent strongly on the amount of organic solvent (Table 4.11.), the higher MIBK, the higher HMF selectivity and lower byproducts selectivity. The later is consistent in terms of HMF migration to the organic phase, higher organic volume implies higher HMF concentration in the organic phase per ml of solvent. It should be noted that under these

reaction conditions, the highest HMF selectivity is 34% with 19% of byproducts selectivity, when the H_2O:MIBK is 1:10.

As for DEE, the conversion (%) and the HMF yield (%) are represented in Figure 4.16. The HMF selectivity (%) compared with byproducts selectivity (%) as function of H_2O:DEE ratio is summarized in Table 4.12. Contrary to the MIBK systems, the conversion depends strongly by the H_2O:DEE ratio, in a way that higher the DEE volume, lower the fructose conversion (Figure 4.16.). The HMF and byproducts selectivity's do not follow a clear trend but is always very low for HMF and high for byproducts.

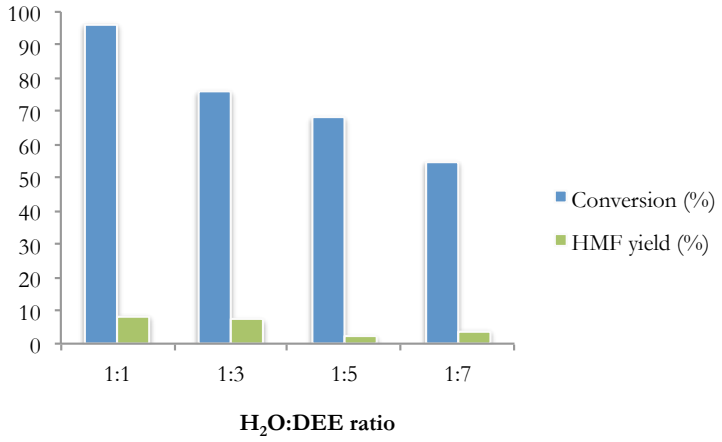

Figure 4.16. Fructose conversion (%) and HMF yield (%) for different H_2O:DEE ratio

Table 4.12. HMF and byproducts selectivities (%) as function of H_2O:DEE ratio

Entry	H_2O:DEE volume ratio	Selectivity (%)	
		HMF	Byproducts (non detected)
1	1:1	**8**	75
2	1:3	**10**	51
3	1:5	**3**	67
4	1:7	**7**	40

Reaction conditions: 1mmol of fructose (0.1802 g), 0.25 mol% of catalyst (0.006 g), 1 mL of H_2O and 3, 5, 7 and 10 mL of DEE, respectively, 120 ºC, 600 rpm after 18h

The inefficiency of DEE as extraction solvent is probably related with its low boiling point (34.6 ºC) and the high reaction temperature (120 ºC). The system H_2O:MIBK is then more suitable to extract HMF and inhibit byproducts formation.

4.3.4. Partial conclusions

Along this section, the activity and selectivity of the prepared POM-ILs hybrids have been evaluated in the reaction of glucose/fructose dehydration.

The dual nature of the organic-inorganic hybrids make possible the accommodation of the catalyst at the interphase. However most probably due to the lack of interphase area, some hybrid remains in the bulk aqueous phase, and reacts first with glucose/fructose. The later is evident due to the electron exchange from glucose/fructose to the bulk hybrid, resulting in hybrid reduction and change of color.

The dehydration of fructose is easier to that of glucose. The HMF selectivity is higher when the starting sugar is fructose, but also the byproducts selectivity is higher, accounting for secondary undesired reactions in aqueous phase. The overall pathway for insoluble byproducts formation is deduced after the reaction products analysis. Several effects as the reaction time, amount of catalyst and nature of the Keggin anion were also evaluated.

To sum up, the viability of the hybrids structures in the glucose/fructose dehydration should be considered not at this stage but after additional optimization of reaction parameters in order to reveal the true potential of these materials for the mentioned reaction. Nevertheless the first approximation is done.

References

[1] M.J. Climent, A. Corma, S. Iborra, Converting carbohydrates to bulk chemicals and fine chemicals over heterogeneous catalysts, Green Chem. 13 (2011) 520.

[2] P. Gallezot, Conversion of biomass to selected chemical products, Chem. Soc. Rev. 41 (2012) 1538–1558.

[3] H. Kobayashi, A. Fukuoka, Synthesis and utilisation of sugar compounds derived from lignocellulosic biomass, Green Chem. 15 (2013) 1740–1763.

[4] W. Deng, Q. Zhang, Y. Wang, Polyoxometalates as efficient catalysts for transformations of cellulose into platform chemicals, Dalt. Trans. 41 (2012) 9817.

[5] N. Mizuno, M. Misono, Heterogeneous Catalysis, Chem. Rev. 98 (1998) 199–218.

[6] I. V. Kozhevnikov, Catalysis by heteropoly acids and multicomponent polyoxometalates in liquid-phase reactions, Chem. Rev. 98 (1998) 171–198.

[7] T. Okuhara, Water-Tolerant Solid Acid Catalysts Water-Tolerant Solid Acid Catalysts, 102 (2002) 3641–3666.

[8] K. Shimizu, H. Furukawa, N. Kobayashi, Y. Itaya, A. Satsuma, Effects of Brønsted and Lewis acidities on activity and selectivity of heteropolyacid-based catalysts for hydrolysis of cellobiose and cellulose, Green Chem. 11 (2009) 1627–1632.

[9] J. Tian, J. Wang, S. Zhao, C. Jiang, X. Zhang, X. Wang, Hydrolysis of cellulose by the heteropoly acid H3PW12O40, Cellulose. 17 (2010) 587–594.

[10] I. Delidovich, R. Palkovits, Catalytic Isomerization of Biomass-Derived Aldoses : A Review, ChemSusChem. 9 (2016) 547–561.

[11] R. Yanagihara, S. Osanai, S. Yoshikawa, C-1,C-2 Stereospecific Rearrangements of Aldohexoses by Calcium Ion in Basic Solution, Chem. Lett. 19 (1990) 2273–2276.

[12] S. Osanai, R. Yanagihara, K. Uematsu, A. Okumura, S. Yoshikawa, Epimerization of aldoses catalysed by self-organized metallomicelles in an aqueous solution, J. Chem. Soc. Perkin Trans. 2. (1993) 1937–1940.

[13] V. Bilik, Reactions of Saccharides Catalized by Molybdate Ions. II. Epimerization of D-Glucose and D-Manose, Chem. Zvesti. 26 (1972) 183–186.

[14] G. De Wit, A.P.G. Kieboom, H. van Bekkum, Enolisation and isomerisation of

monosaccharides in aqueous, alkaline solution, Carbohydr. Res. 74 (1979) 157–175.

[15] T. Granström, G. Takata, M. Tokuda, I. K., Izumoring: a novel and complete strategy for bioproduction of rare sugars., J. Biosci. Bioeng. 97 (2004) 89–94.

[16] G. Gumina, G.-Y. Song, C.K. Chu, l-Nucleosides as chemotherapeutic agents, Microbiol. Lett. 202 (2001) 9–15.

[17] B. Kamm, Production of Platform Chemicals and Synthesis Gas from Biomass, Angew. Chemie Int. Ed. 46 (2007) 5056–5058.

[18] F. Ju, D. Vandervelde, E. Nikolla, Molybdenum-Based Polyoxometalates as Highly Active and Selective Catalysts for the Epimerization of Aldoses, ACS Catal. 4 (2014) 1358–1364.

[19] S.J. Angyal, The Lobry de Bruyn-Alberda van Ekenstein Transformation and Related Reactions, Top. Curr. Chem. 215 (2001) 1–14.

[20] B.K. Chethana, D. Lee, S.H. Mushrif, First principles investigation into the metal catalysed 1 , 2 carbon shift reaction for the epimerization of sugars, J. Mol. Catal. A. Chem. 410 (2015) 66–73.

[21] V. Bilik, I. Knezek, Reactions of saccharides catalyzed by molybdate ions XL. Inhibition of the epimerization of aldoses, Chem. Pap. 44 (1990) 89–96.

[22] A. Takagaki, S. Furusato, R. Kikuchi, S.T. Oyama, Efficient Epimerization of Aldoses Using Layered Niobium Molybdates, ChemSusChem. 6 (2015) 3769–3772.

[23] S.J. Angyal, The composition and conformation of sugars in solution, Angew. Chemie - Int. Ed. 8 (1969) 157–166.

[24] A. Cybulski, B.F.M. Kuster, G.B. Marin, The kinetics of the molybdate-catalysed epimerization of D-glucose and D-mannose in aqueous solutions, J. Mol. Catal. 68 (1991) 87–103.

[25] A. Kiersztan, K. Winiarska, J. Drozak, M. Przedlacka, M. Wegrzynowicz, T. Fraczyk, et al., Differential effects of vanadium, tungsten and molybdenum on inhibition of glucose formation in renal tubules and hepatocytes of control and diabetic rabbits: Beneficial action of melatonin and N-acetylcysteine, Mol. Cell. Biochem. 261 (2004) 9–21.

[26] Y. Karlish, D.S.J. Shechter, Insulin-like stimulation of glucose oxidation in rat adipocytes by vanadyl (IV) ions, Nature. 284 (1980) 556–558.

[27] M.T. Pope, A. Müller, Polyoxometalate chemistry: an old field with new dimensions in several disciplines, Angew. Chem., Int. Ed. 30 (1991) 34–48.

[28] M. Watanabe, Y. Aizawa, T. Iida, C. Levy, T.M. Aida, H. Inomata, Glucose reactions within the heating period and the effect of heating rate on the reactions in hot compressed water, Carbohydr. Res. 340 (2005) 1931–1939.

[29] K. Bock, H. Thogersen, Nuclear Magnetic Resonance Spectroscopy in the Study of Mono- and Oligosaccharides, Annu. Reports NMR Spectrosc. 13 (1983) 1–57.

[30] M.J. King-Morris, A.S. Serianni, Carbon-13 NMR studies of [1-13C]aldoses: empirical rules correlating pyranose ring configuration and conformation with carbon-13 chemical shifts and carbon-13/carbon-13 spin couplings, J. Am. Chem. Soc. 109 (1987) 3501–3508.

[31] M.L. Hayes, N.J. Pennings, A.S. Serianni, R. Barker, Epimerization of Aldoses by Molybdate Involving a Novel Rearrangement of the Carbon Skeleton, J. Am. Chem. Soc. 104 (1982) 6764–6769.

[32] V. Bilik, L. Petrus, No Title, Chem. Zvesti. 33 (1979) 114–117.

[33] Y. Román-Leshkov, M. Moliner, J. a. Labinger, M.E. Davis, Mechanism of glucose isomerization using a solid lewis acid catalyst in water, Angew. Chemie - Int. Ed. 49 (2010) 8954–8957.

[34] S. Jia, K. Liu, Z. Xu, P. Yan, W. Xu, X. Liu, et al., Reaction media dominated product selectivity in the isomerization of glucose by chromium trichloride: From aqueous to non-aqueous systems, Catal. Today. 234 (2014) 83–90.

[35] N.N. Greenwood, A. Earnshaw, Chemistry of the Elements, 2nd Edition, 1997.

[36] S. Ramachandran, P. Fontanille, A. Pandey, C. Larroche, Gluconic Acid : Properties , Applications and Microbial Production, Food Technol. Biotechnol. 44 (2006) 185–195.

[37] K. Buchholz, J. Seibel, Industrial carbohydrate biotransformations, Carbohydr. Res. 343 (2008) 1966–1979.

[38] S. Anastassiadis, H.J. Rehm, Continuous gluconic acid production by the yeast-like Aureobasidium pullulans in a cascading operation of two bioreactors, Appl. Microbiol. Biotechnol. 73 (2006) 541–548.

[39] M. Besson, F. Lahmer, P. Gallezot, P. Fuertes, G. Fléche, Catalytic Oxidation of Glucose on Bismuth-Promoted Palladium catalysts, J. Catal. 152 (1995) 116–121.

[40] I. Nikov, K. Paev, Palladium on alumina catalyst for glucose oxidation: reaction kinetics and catalyst deactivation, Catal. Today. 24 (1995) 41–47.

[41] P. Beltrame, M. Comotti, C. Della Pina, M. Rossi, Aerobic oxidation of glucose, Appl. Catal. A Gen. 297 (2006) 1–7.

[42] U. Prüße, M. Herrmann, C. Baatz, N. Decker, Gold-catalyzed selective glucose

oxidation at high glucose concentrations and oxygen partial pressures, Appl. Catal. A Gen. 406 (2011) 89–93.

[43] S. Wang, G. Yang, Recent Advances in Polyoxometalate-Catalyzed Reactions, Chem. Rev. 115 (2015) 4893–4962.

[44] C. Venturello, E. Alneri, M. Ricci, A new, effective catalytic system for epoxidation of olefins by hydrogen peroxide under phase-transfer conditions, J. Org. Chem. 48 (1983) 3831–3833.

[45] S. Pathan, A. Patel, Transition-Metal-Substituted Phosphomolybdates: Catalytic and Kinetic Study for Liquid-Phase Oxidation of Styrene, Ind. Eng. Chem. Res. 52 (2013) 11913–11919.

[46] I.C.M.S. Santos, M.M.Q.S. Filipe A. Almeida Paz, M.G.P.M.S. Neves, J.A.S. Cavaleiro, J. Klinowski, A.M.V. Cavaleiro, Catalytic homogeneous oxyfunctionalization with hydrogen peroxide in the presence of a peroxotungstate, Appl. Catal. A Gen. 351 (2008) 166–173.

[47] A.M. Khenkin, R. Neumann, Low-Temperature Activation of Dioxygen and Hydrocarbon Oxidation Catalyzed by a Phosphovanadomolybdate: Evidence for a Mars–van Krevelen Type Mechanism in a Homogeneous Liquid Phase, Angew. Chem., Int. Ed. 39 (2000) 4088–4090.

[48] A.M. Khenkin, L.J.W. Shimon, R. Neumann, Preparation and Characterization of New Ruthenium and Osmium Containing Polyoxometalates, [M(DMSO)3Mo7O24]4- (M = Ru(II), Os(II)), and Their Use as Catalysts for the Aerobic Oxidation of Alcohols, Inorg. Chem. 42 (2003) 3331–3339.

[49] O.A. Kholdeeva, M.P. Vanina, M.N. Timofeeva, R.I. Maksimovskaya, T.A. Trubitsina, M.S. Melgunov, et al., Co-containing polyoxometalate-based heterogeneous catalysts for the selective aerobic oxidation of aldehydes under ambient conditions, J. Catal. 226 (2004) 363–371.

[50] X. Chen, B. Souvanhthong, H. Wang, H. Zheng, X. Wang, M. Huo, Polyoxometalate-based Ionic liquid as thermoregulated and environmentally friendly catalyst for starch oxidation, Appl. Catal. B Environ. 138–139 (2013) 161–166.

[51] E. Rafiee, F. Mirnezami, Keggin-structured polyoxometalate-based ionic liquid salts: Thermoregulated catalysts for rapid oxidation of sulfur-based compounds using H2O2 and extractive oxidation desulfurization of sulfur-containing model oil, J. Mol. Liq. 199 (2014) 156–161.

[52] B.S. Chhikara, R. Chandra, V. Tandon, Oxidation of alcohols with hydrogen

peroxide catalyzed by a new imidazolium ion based phosphotungstate complex in ionic liquid, J. Catal. 230 (2005) 436–439.

[53] H. Li, Y. Qiao, L. Hua, Z. Hou, B. Feng, Z. Pan, et al., Imidazolium Polyoxometalate: An Ionic Liquid Catalyst for Esterification and Oxidative Esterification, ChemCatChem. 2 (2010) 1165–1170.

[54] Y. Leng, J. Wang, D. Zhu, L. Shen, P. Zhao, M. Zhang, Heteropolyanion-based ionic hybrid solid: A green bulk-type catalyst for hydroxylation of benzene with hydrogen peroxide, Chem. Eng. J. 173 (2011) 620–626.

[55] Idil Arslan-Alatona, J.L. Ferryb, Application of polyoxotungstates as environmental catalysts: wet air oxidation of acid dye Orange II, Dye. Pigment. 54 (2002) 25–36.

[56] W.H. Koppenol, J. Butler, J.W. van Leeuwen, The Haber-Weiss cycle, Photochem. Photobiol. 28 (1978) 655–658.

[57] Y. Xiao, Y.-F. Song, Efficient catalytic conversion of the fructose into 5-hydroxymethylfurfural by heteropolyacids in the ionic liquid of 1-butyl-3-methyl imidazolium chloride, Appl. Catal. A Gen. 484 (2014) 74–78.

[58] Y. Qu, C. Huang, J. Zhang, B. Chen, Efficient dehydration of fructose to 5-hydroxymethylfurfural catalyzed by a recyclable sulfonated organic heteropolyacid salt, Bioresour. Technol. 106 (2012) 170–172.

[59] Y. Liu, L. Zhu, J. Tang, M. Liu, R. Cheng, C. Hu, One-pot, One-step Synthesis of 2,5-Diformylfuran from Carbohydrates over Mo-Containing Keggin Heteropolyacids, ChemSusChem. 7 (2014) 3541–3547.

[60] J.S. Kruger, V. Nikolakis, D.G. Vlachos, Carbohydrate dehydration using porous catalysts, Curr. Opin. Chem. Eng. 1 (2012) 312–320.

[61] J.S. Kruger, V. Nikolakis, D.G. Vlachos, Aqueous-phase fructose dehydration using Brønsted acid zeolites: Catalytic activity of dissolved aluminosilicate species, Appl. Catal. A Gen. 469 (2014) 116–123.

[62] J.C. Serrano-Ruiz, R.M. West, J.A. Dumesic, Catalytic Conversion of Renewable Biomass Resources to Fuels and Chemicals, Annu. Rev. Chem. Biomol. Eng. 1 (2010) 79–100.

[63] E. Nikolla, Y. Román-Leshkov, M. Moliner, M.E. Davis, "One-Pot" Synthesis of 5-(Hydroxymethyl)furfural from Carbohydrates using Tin-Beta Zeolite, ACS Catal. 1 (2011) 408–410.

[64] R. Van Putten, J.N.M. Soetedjo, E.A. Pidko, J.C. Van Der Waal, Dehydration of Different Ketoses and Aldoses to 5- Hydroxymethylfurfural, ChemSusChem. 6

(2013) 1681–1687. doi:10.1002/cssc.201300345.

[65] M. Moliner, Y. Roman-Leshkov, M.E. Davis, Tin-containing zeolites are highly active catalysts for the isomerization of glucose in water, Proc. Natl. Acad. Sci. 107 (2010) 6164–6168.

[66] S. Saravanamurugan, M. Paniagua, J. a. Melero, A. Riisager, Efficient isomerization of glucose to fructose over zeolites in consecutive reactions in alcohol and aqueous media, J. Am. Chem. Soc. 135 (2013) 5246–5249.

[67] C. Moreau, R. Durand, A. Roux, D. Tichit, Isomerization of glucose into fructose in the presence of cation-exchanged zeolites and hydrotalcites, Appl. Catal. A Gen. 193 (2000) 257–264.

[68] M. Liu, S. Jia, C. Li, A. Zhang, C. Song, X. Guo, Facile preparation of Sn-β zeolites by post-synthesis (isomorphous substitution) method for isomerization of glucose to fructose, Chinese J. Catal. 35 (2014) 723–732.

[69] Y.J. Pagán-Torres, T. Wang, J.M.R. Gallo, B.H. Shanks, J.A. Dumesic, Production of 5-Hydroxymethylfurfural from Glucose Using a Combination of Lewis and Brønsted Acid Catalysts in Water in a Biphasic Reactor with an Alkylphenol Solvent, ACS Catal. 2 (2012) 930–934.

[70] M.B. Fusaro, V. Chagnault, D. Postel, Reactivity of D-fructose and D-xylose in acidic media in homogeneous phases, Carbohydr. Res. 409 (2015) 9–19.

[71] F.S. Asghari, H. Yoshida, Kinetics of the Decomposition of Fructose Catalyzed by Hydrochloric Acid in Subcritical Water: Formation of 5-Hydroxymethylfurfural, Levulinic, and Formic Acids, Ind. Eng. Chem. Res. 46 (2007) 7703–7710.

[72] B. Saha, M.M. Abu-omar, Advances in 5-hydroxymethylfurfural production from biomass in biphasic solvents, Green Chem. 16 (2014) 24–38.

[73] E.I. Gürbüz, S.G. Wettstein, J.A. Dumesic, Conversion of Hemicellulose to Furfural and Levulinic Acid using Biphasic Reactors with Alkylphenol Solvents, ChemSusChem. 5 (2012) 383 – 387.

[74] Y. Román-Leshkov, J. a. Dumesic, Solvent effects on fructose dehydration to 5-hydroxymethylfurfural in biphasic systems saturated with inorganic salts, Top. Catal. 52 (2009) 297–303.

[75] Y. Román-Leshkov, J.N. Chheda, J.A. Dumesic, Phase Modifiers Promote Efficient Production of Hydroxymethylfurfural from Fructose, Science (80-.). 312 (2006) 1933–1937.

[76] V. V. Ordomsky, J. van der Schaaf, J.C. Schouten, T.A. Nijhuis, Fructose

Dehydration to 5-Hydroxymethylfurfural over Solid Acid Catalysts in a Biphasic System, ChemSusChem. 5 (2012) 1812–1819.

[77] S.K.R. Patil, C.R.F. Lund, Formation and Growth of Humins via Aldol Addition and Condensation during Acid-Catalyzed Conversion of 5-Hydroxymethylfurfural, Energy Fuels. 25 (2011) 4745–4755.

[78] A. Piccolo, P. Conte, A. Cozzolino, Effects of mineral and monocarboxylic acids on the molecular association of dissolved humic substances, Eur. J. Soil Sci. 50 (1999) 687–694.

[79] Q. Zhao, L. Wang, S. Zhao, X. Wang, S. Wang, High selective production of 5-hydroymethylfurfural from fructose by a solid heteropolyacid catalyst, Fuel. 90 (2011) 2289–2293.

Chapter Five

INTRODUCTION of GOLD CATALYSTS for BIOMASS-INVOLVED OXIDATION REACTIONS: SYNTHESIS and CHARACTERIZATION

Summary[1]

In this chapter the preparation of two groups of gold supported catalysts, as POM-IL alternative for oxidation reactions, is described. Within the first group, an optimized method was used to obtain similar gold sizes over different metal oxides supports. For the second group, another synthetic method was used, which leads to the preparation of a series of gold on carbon catalysts with different metal sizes. All solids were characterized by means of XRD, XRF, TEM microscopy, N_2 adsorption and TPR-H_2, UV-Vis spectroscopy and ICS-AES. Prepared solids are tested in the glucose and HMF oxidation reactions, being the results presented in the next chapter.

[1]Some of the results presented in this Chapter have been published in:

C. Megías-Sayago *et al.* **Catalysis Today** 279 (2017) 148–154

C. Megías-Sayago *et al.* **Catalysis Today** (2017) *In press*
http://dx.doi.org/10.1016/j.cattod.2017.03.022

C. Megías-Sayago *et al.* **Catalysis Today** (2017) *In press*
http://dx.doi.org/10.1016/j.cattod.2017.01.007

5.1. Introduction

Among the previous chapter, the potential of POM-ILs hybrids in biomass-involved reactions has been discussed. Despite their wide applicability in different reactions by means of tuning the reaction parameters, their catalytic behavior in oxidation reactions remains insufficient, using H_2O_2 as oxidant. In addition the hybrids do not catalyze glucose oxidation in presence of molecular oxygen.

As will be discussed in the next chapter, the oxidation processes that involve the conversion of biomass raw materials to value-added chemicals require active and especially selective catalysts, the later being of primordial importance, due to the wide oxidation products that can result. For this reason, the use of POM-IL hybrid catalyst is not suitable and the search for other heterogeneous alternatives becomes necessary.

When searching active oxidation catalysts, the choice of cheap and ecofriendly oxidant becomes an important issue. Air is the cheapest possible oxidant and the most desired one for large industrial catalytic operations. However, in most cases for an effective catalytic reaction pure oxygen is preferred. The reasons are many: (i) faster reactions and greater reactor productivity; (ii) improved yield and better energy efficiency, avoiding oxygen dilution with nitrogen; (iii) smaller, lower capital cost plants; (iv) lower energy consumption and (v) environmental improvements due to significant reduction in the amount of purge gas [1].

In spite of all advantages derived from the use of O_2 as green oxidant, such as low cost, H_2O formation as the only byproduct and atom efficiency of 50/100% (depending of the number of atoms involved in the oxidation) [2,3], the oxygen molecule have to be activated by properly selected catalysts, which is not an easy task.

The first studies concerning the application of gold catalysts in aerobic oxidation reactions were reported many years ago, focusing on CO oxidation and liquid phase oxidation of diols [4–8]. The low temperature CO oxidation, H_2O_2 synthesis from H_2 and O_2 [9–11], water gas shift [12], C-C coupling reactions [13] and conversion of carbohydrates and alcohols to corresponding carbonylic and carboxylic compounds [8,14–18] are some of the most successful applications of this type of catalysts. Regarding exclusively the liquid phase oxidation of organic compounds, the application list of gold catalysts is also extensive, from the oxidation of hydrocarbons through alkanes, alkenes, alcohols, polyalcohols, benzyl compounds, amines, heterocycles to any carbohydrate derived from biomass resources [19,20].

Within biomass-involved oxidation reactions, the oxidation of glucose, as the simplest monomer derived from lignocellulosic biomass, and the oxidation of HMF, one of the top building blocks, have received special attention in the last decade [21–24]. In both reactions, the great activity and selectivity of Pt, Pd and Au catalysts have been demonstrated, being gold the most suitable mainly due to its higher resistance to overoxidation, avoiding catalyst active phase deactivation. More detailed bibliographic review of the mentioned reactions will be included in each section in Chapter 6 dedicated to the oxidation activity results, and only a brief resume is proposed here.

In general, the activity and selectivity of gold catalysts in liquid or gas phase oxidation reactions are strongly influenced by the employed preparation method and the resulting gold particle size. Several methods are available for preparing supported gold-based catalysts, among them, deposition-precipitation and deposition/immobilization of colloidal gold particles onto supports are the most commonly used [25].

In this Chapter, two different preparation methods are applied for the preparation of gold supported catalysts, depending on the support nature and on the object of the study.

The direct anionic exchange technique is used to prepare gold particles with similar size supported on several pure and mixed oxides.

The deposition/immobilization of colloidal gold was selected for preparing two series of gold catalysts supported on active carbon. In this case, the support is kept the same, being the gold particle size varied by means of the change of synthetic parameters. Both series are characterized and the results presented in this chapter. The catalysts activity/selectivity/stability in the glucose and HMF oxidation reactions will be presented in details in the next chapter.

5.2. Gold supported on different metal oxides

5.2.1. Why metal oxides?

Based on literature reports, the activity/selectivity of gold supported catalysts in the liquid phase oxidation of carbohydrates strongly depend on parameters such as gold particle size and support nature. Focusing on the base-free oxidation of glucose, several studies have reported good activity/selectivity results over gold supported on different metal oxides, including ZrO_2 and CeO_2 [26,27]. As for the HMF oxidation, similar systems have been investigated, mainly CeO_2 [23], TiO_2 [24] and ZrO_2 [28]. However, the effect of the support nature has not been systematically studied. Based on this, we decided to study the influence of the support nature on the catalyst behavior using the systems prepared by the direct anionic exchange method. For these systems the gold particle size is similar. For this reason, an optimized preparation method has to be

used [29], in order to keep the gold particle sizes in the 3-4 nm range in a reproducible way.

5.2.2. Synthesis of catalysts

Many commercial supports were used without any previous treatment to prepare different catalysts such as Al_2O_3, CeO_2(20wt%)/Al_2O_3 (both from Sasol), CeO_2, CeO_2(50wt%)/ZrO_2 and CeO_2(25wt%)/ZrO_2 (last three available from Daiichi Kigenso Kagaku Kogio Co., Ltd.).
In order to simplify, the adopted nomenclature is Al for Al_2O_3, CeAl for CeO_2(20wt%)/Al_2O_3, Ce for CeO_2, Ce50Zr for CeO_2(50wt%)/ZrO_2 and Ce25Zr for CeO_2(25wt%)/ZrO_2.

Irrespective of the support nature the same gold deposition method was utilized, the direct anionic exchange (DAE) assisted by ammonia [29,30]. Aqueous solutions of the gold precursor $HAuCl_4$ (Johnson Matthey) $2 \cdot 10^{-4}$ M and the support were used in order to obtain a final Au loading of 2 wt.%. The solution was heated to 70 ºC and aged 20 min with the corresponding support amount. After, the suspension was cooled down to 40 ºC and 50 mL of NH_3 (30 % Aldrich) were added and aged for another 20 min.* The slurry was then filtered, washed with water, dried at 100 ºC overnight and finally calcined in air at 300 °C for 4 h.
Similar to the supports, in the adopted nomenclature the real gold loadings are omitted for simplification. As an example, the used nomenclature for the gold deposited on alumina catalyst is AuAl.

* Caution/safety note: The contact of ammonia with gold solution may result in the formation of gold ammonia complexes ("fulminating gold"), which are explosive. The use of this preparation procedure is not dangerous when the gold complexes are strongly attached to the support by the DAE.

5.2.3. Physicochemical characterization

5.2.3.1. XRD of the prepared solids

The diffraction patterns of the prepared catalysts compared to their corresponding supports are presented in Fig. 5.1.

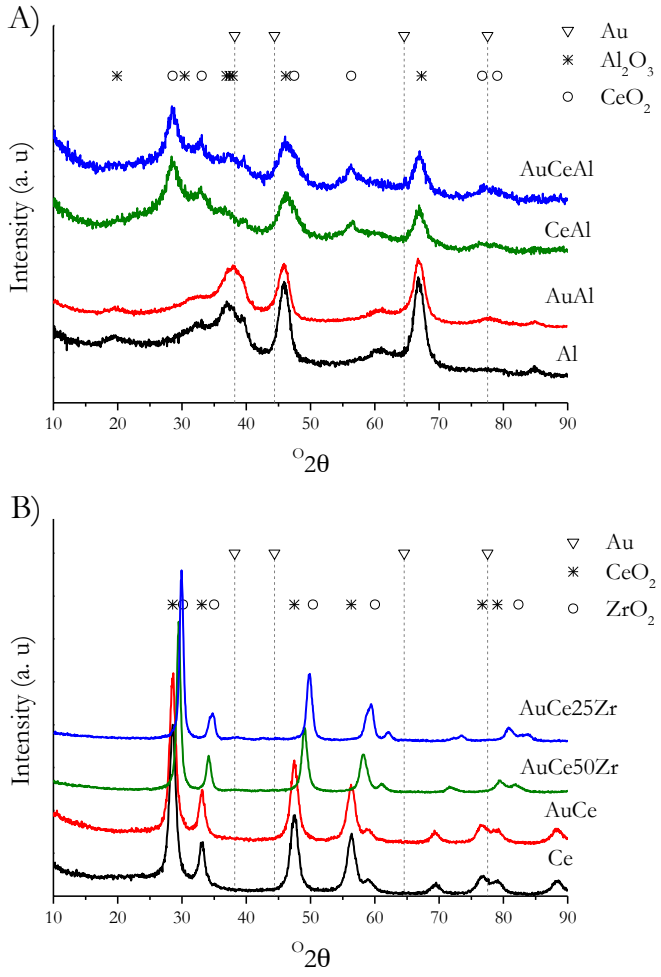

Figure 5.1. XRD of the supported systems: A) Al_2O_3 containing supports, B) CeO_2 containing supports

The diffraction peaks corresponding to gold metal phase are, in general, not observed for the ceria containing catalysts, suggesting an average size of the gold crystallites under the detection limit of the technique (4 nm). Nevertheless, and despite the lower crystallinity of the bare alumina support, a low intensity diffraction line that may be attributed to gold at 77º 2θ, is observed for AuAl sample. This suggests an average gold particle size slightly above 4 nm, which cannot be properly quantified by using Scherrer equation since its low intensity. It is worth mentioning the formation of CeO_2 - ZrO_2 solid solution (Fig. 5.1. B), whatever the Ce/Zr molar ratio, as confirmed by the shift of the diffraction lines toward higher 2θ on increasing the Zr content.

5.2.3.2. Textural properties and gold loadings

The actual gold loadings and textural properties of the fresh catalysts are listed in Table 5.1. For AuAl catalyst, a metal loss of around 18 % was detected, due to incomplete gold deposition. On the other hand, all ceria-containing solids, present experimental values close or even higher than the targeted ones. This suggests that although a complete metal deposition occurs some support loss is also possible. In the case of the bare ceria support, almost the double of gold loading is detected suggesting that the use of strongly basic media during gold deposition may result in the partial dissolution of the support. Moreover, the support losses increase on increasing the ceria content within the support composition. In the preparation process the amount of gold precursor is always slightly higher than required to account for metal losses; nevertheless, the greater values observed are probably due to incident blends, or to the fact that the commercial support could contain other components, which are removed after calcination.

Table 5.1. Gold loadings (%) and textural properties of the prepared catalysts

Sample	% Au	S_{BET} (m^2/g)	Average pore size (nm)	Pore volume (cm^3/g)
AuAl	1.64	187	8.7	0.474
AuCeAl	2.36	158	7.6	0.396
AuCe	3.94	57	13.4	0.200
AuCe50Zr	2.39	55	8.9	0.161
AuCe25Zr	2.31	57	11.8	0.201

As for the textural properties, all solids are mesoporous materials with average pore sizes ranging between 5 nm and 13.5 nm. Alumina containing solids have bigger areas than those of the mixed CeZr and bare Ce systems.

5.2.3.3. TEM microscopy

Transmission electron microscopy (TEM) was used to evaluate the average gold particle size for all samples. The corresponding micrographs and particle size distributions for the alumina containing samples are presented in Figure 5.2. In the same way, the data corresponding to AuCe and AuCeZr catalysts are showed in Figure 5.3.

As detected by XRD, the AuAl catalyst presents an average particle size slightly superior to 4 nm unlike the rest of the samples. The particle size distribution follows a typical Gaussian curve except for AuCe and AuCeZr samples, a possible cause being the low TEM contrast between gold and cerium, which complicates the detection of gold nanoparticles smaller than 2 nm.

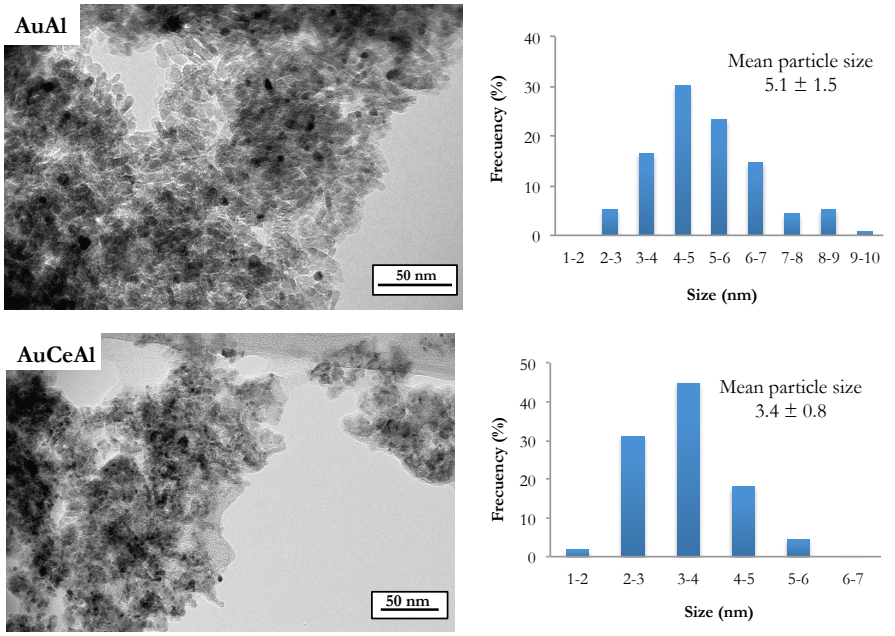

Figure 5.2. TEM images and particle size distribution of alumina containing catalysts

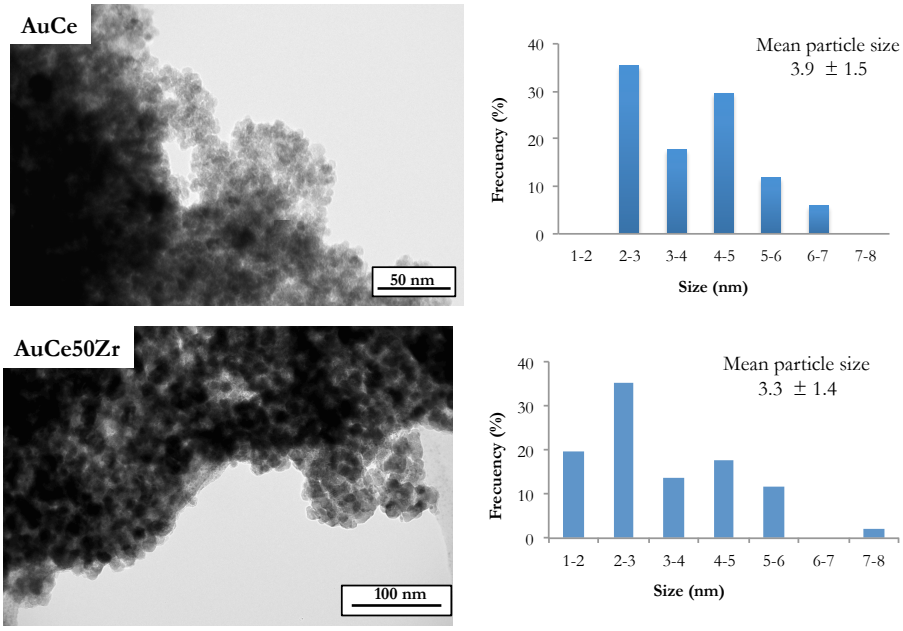

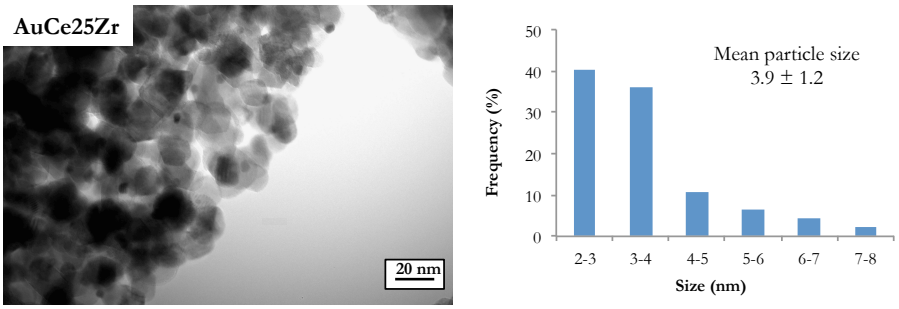

Figure 5.3. TEM images and particle size distribution of Ce and CeZr based catalysts

Based on the calculated average particle size for the fresh catalysts, gold dispersion can be estimated on the basis of particle modeling proposed by Polisset [31]. Just briefly, in this model the dispersion D is defined as:

$$D = \frac{N_s}{N_t} \qquad \text{Eq. 5.1.}$$

Where N_s is the number of atoms on the surface and N_t is the total number of atoms. Ns is corrected considering the contact surface (N_c) between the metallic particle and the support leading to N_s' ($N_s' = N_s - N_c$) and therefore:

$$D = \frac{N'_s}{N_t} \qquad \text{Eq. 5.2.}$$

The dispersion depends on the metal particle size as follows:

$$d_{rel} = \frac{d_{sph.}}{d_{at.}} = \frac{1}{d_{at.}} \sqrt[3]{\frac{6}{\pi} N_t \frac{V_{m.el.}}{n_{m.el.}}} \qquad \text{Eq. 5.3.}$$

where $d_{sph.}$ is the diameter of the sphere with a volume equal to the volume occupied per atom in the unit cell, $d_{at.}$ is the diameter of the considered metallic atom (gold in our case), $n_{m.el.}$ is the number of atoms

in the unit cell and $V_{m.el.}$ is the volume of the unit cell. In the case of gold considering the FCC the calculation is simplified to:

$$d_{rel} = 1.105\sqrt[3]{N_t} \qquad \text{Eq. 5.4.}$$

Finally the calculation of N_t, N_s and N_s' depend on the selected geometry. In our case the cuboctahedral model was used, where:

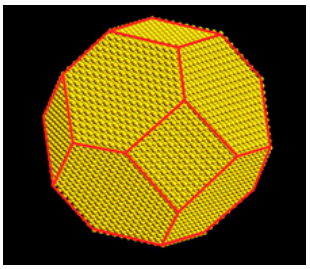

$N_t = 16n^3 - 33n^2 + 24n - 6$

$N_s = 30n^2 - 60n + 32$

$N_s' = 27n^2 - 51n + 25$: corrected surface of one hexagonal face (minus the atoms on the six edges)

The calculated dispersions are listed in Table 5.2. In all cases the dispersion varies within the 25-40 % range.

Table 5.2. Estimated particle size and dispersion for the samples

Sample	Average particle size, nm	Dispersion, %
AuAl	5.1±1.5	26
AuCeAl	3.4±0.8	38
AuCe	3.9±1.5	33
AuCe50Zr	3.3±1.4	39
AuCe25Zr	3.9±1.2	33

5.2.3.4. Isoelectric point analysis (IEP)

The isoelectric point (IEP) determination could be used as basicity/acidity measurement of the solid materials in water solutions. The IEP of the prepared samples is presented in Table 5.3.

Table 5.3. IEP of the samples

Sample	IEP
AuAl	7.6
AuCeAl	6.8
AuCe	6.5
AuCe50Zr	7.3
AuCe25Zr	6.2

AuAl catalyst exhibits the more basic IEP, 7.6. The introduction of ceria in AuCeAl catalyst decreases the value to 6.8, being the IEP for the bare AuCe of 6.5. The introduction of 50% of zirconia in the lattice illogically increases the value up to 7, but when the zirconia content reaches 75% the IEP decreases with respect to bare ceria, accounting for the more acid character of zirconia in aqueous solution.

5.2.3.5. TPR-H_2

The redox properties of the catalysts were investigated with the TPR technique. H_2 TPR profiles of the prepared samples are presented in Figure 5.4. Due to the non-reducible character of alumina, bare Al and AuAl are not included in this study. The CeAl presents two reduction zones, attributed to Ce^{4+} to Ce^{3+} reduction; one at lower temperature (495º C) attributed to superficial ceria reduction, and another corresponding to bulk ceria reduction at higher temperatures (860º C). Similarly, bare ceria

present both contributions at slightly lower temperature intervals (452 and 757º C). The TPR profiles of the Ce-Zr mixed systems, differ from the previous ones, there is only one reduction zone that shifts to higher temperature with Ce content decrease. This shift can be related to the lower ceria content and, in consequence, to its low availability for the reduction process being the Ce bulk reduction out of the applied temperature zone.

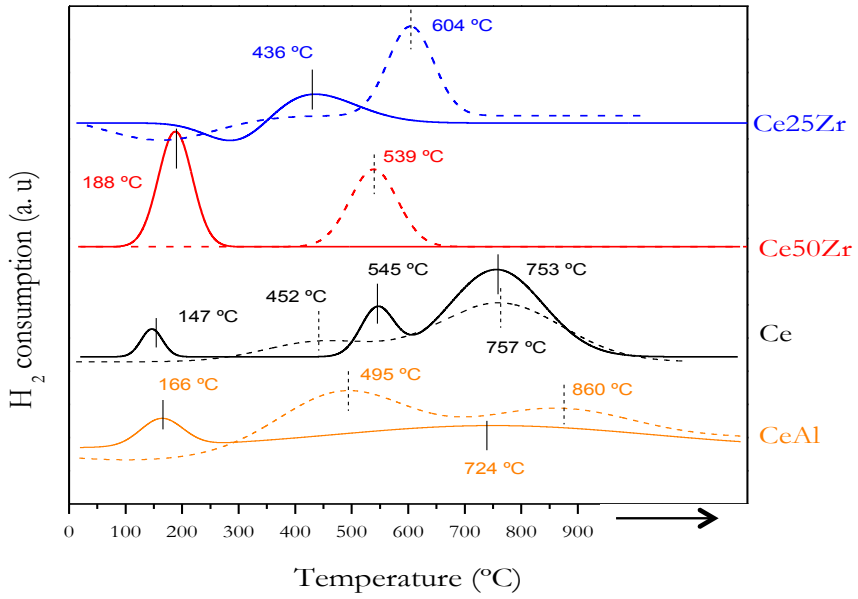

Figure 5.4. TPR-H_2 profiles of the supports (dashed lines) and their corresponding gold catalysts (full lines)

Regarding gold catalysts, in all studied cases gold addition favors oxide reduction by increasing H_2 mobility on the solid surface and decreasing the temperature of the reduction zone center. Generally, the low temperature reduction zone is the most influenced by the noble metal and it is assigned to the surface reduction [32]. In AuCeAl catalyst, the surface reduction is centered at 166 ºC whereas the bulk reduction originates a

very broad zone virtually centered at 724º C. As for the AuCe catalyst the situation is a bit different. The surface reduction takes place at 147 ºC, and two more zones appear, centered at 545º C and 753º C, the former attributed to the surface ceria not in contact with gold and the later to the bulk ceria. As for the CeZr systems, the surface reduction of ceria depends on the ceria content in a way that, higher the ceria content lower the temperature of its surface reduction. The AuCe50Zr catalyst present lower temperature of reduction, which suggests better gold-support interaction. On the contrary, AuCe25Zr, presents high-temperature reduction, centered at 436º C, caused probably by the low availability of ceria and the weak ceria-gold interaction. From a quantitative point of view, the presence of gold shifts the surface reduction of ceria to much lower temperatures due to a decrease of the Ce-O bonds strength when adjacent to gold. The smaller bond strength leads to higher mobility of surface lattice oxygen and therefore higher reactivity of the oxygen species [33]. Oxygen mobility correlates with the interaction of gold and surface lattice oxygen in such a way that oxygen mobility reduces on increasing the metal-support interaction [33,34].

It is also possible to evaluate qualitatively the reduction degree calculating the reducibility percentage for all samples by using the Eq. 5.5.

$$RP = \frac{E_{HC}}{T_{HC}}\, x\, 100 \qquad \text{Eq. 5.5.}$$

The RP relates the experimentally measured H_2 consumption (E_{HC}) to the total theoretical H_2 consumption (T_{HC}). The T_{HC} depends on the oxidation state considered for the reducible species. For all samples, Ce^{4+} species were assumed as the initial oxidation state for ceria, which reduces to Ce^{3+} in presence of H_2 according to Eq. 5.6. Zr^{4+} and Al^{3+} are considered non-

reducible species. As for gold, due to the auto-reduction capability of gold species during the calcination process, gold is presumably metallic, and therefore non-reducible species.

$$2\,CeO_2 + H_2 \rightarrow Ce_2O_3 + H_2O \qquad \text{Eq. 5.6.}$$

100% of RP is obtained for CeAl and AuCeAl samples, accounting for a total reduction of Ce^{4+} species to Ce^{3+}. In this case, the ceria (20wt.% over 80 wt.% of alumina), seems to be totally accessible. For the rest of samples, the RP are lower, accounting for the existence of bulk ceria not reduced during the experiment. The reducibility of both catalysts and supports are similar.

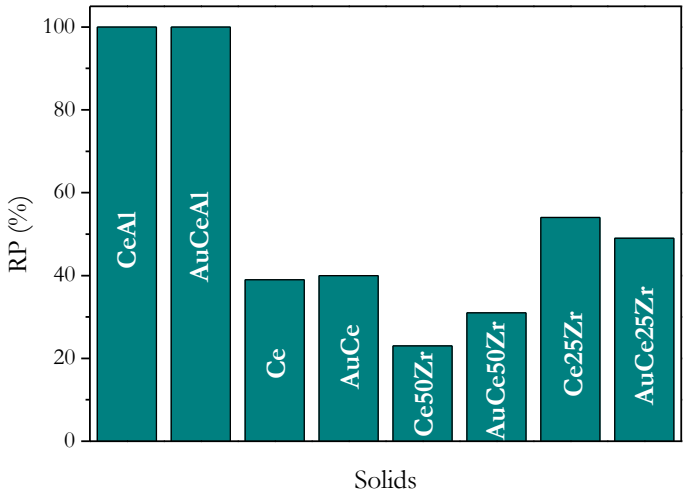

Figure 5.5. Reducibility percentage (RP) of the prepared solids

In summary, a series of gold catalysts supported on different oxide supports was prepared by DAE method and characterized. Gold contents are close to 2wt.% and the supported particles show nanometer size

ranging between 3-5 nm and corresponding to dispersions higher than 25%. The IEP was obtained as indicator for the sample' acidity/basicity and TPR-H_2 for the estimation of catalysts redox properties.

5.3. Gold supported on active carbon

5.3.1. Why active carbon?

The substantial importance of active carbon as metal support in industrial catalysis is well recognized. Its stability in bot,h acidic and basic media, its tunable pore structure and stability at high temperatures, the easiness of metal phase recovery by carbon burn and its lower costs in comparison to conventional supports such as alumina or silica [35,36] convert it in a versatile material for heterogeneous catalysis.

However, the real relevance of carbon in aqueous phase oxidation reactions derives from its hydrophobicity, which difficult active metal phase leaching, thus improving catalyst's inherent activity. In fact, higher activity of the hydrophobic catalysts, in glucose oxidation, compared to hydrophilic ones has been reported [37,38]. This difference in activity was assigned to a stronger adhesion between hydrophobic catalyst grains and oxygen bubbles leading to an increase of the available catalyst grains at the gas-liquid interface and, therefore, to enhance the gas transfer rate toward the catalyst [39]. The only disadvantage of using hydrophobic support is that the conventional methods for gold nanoparticles preparation, such as deposition-precipitation or direct anionic exchange are useless resulting in important gold losses and low reproducibility. Within the existing gold nanoparticles preparation methods, the gold colloidal route seems the most appropriated to obtain a homogeneous and reproducible gold nanoparticle size distribution. By using this method a direct particle size/activity correlation is allowed.

Opposite to the first section, the support, carbon in this case, is the same during the overall study but the gold particle size, is varied by means of a fine control of the synthesis parameters, as discussed below.

5.3.2. Synthesis of catalysts

Activated charcoal powder DARCO® (Sigma Aldrich, 100 mesh particle size) and $HAuCl_4$ (Johnson Matthey) gold precursor were used as received.

The deposition of gold (2 wt.% nominal value) on the carbon support was carried out according to the colloidal method assisted by polyvinyl alcohol (PVA) where $NaBH_4$ (Sigma Aldrich) was used as reducing agent [40]. The necessary amount of gold precursor was dissolved in water to a final concentration of 5.10^{-4} M and the corresponding quantity of PVA (1wt. % aqueous solution) was added and stirred for 20 min. After that, the appropriate amount of 0.1M freshly prepared $NaBH_4$ solution was quickly added to reduce the gold precursor. After 20 min stirring, a sample of 5 mL was taken to characterize the colloid. The solution is then mixed with the adequate amount of the commercial activated carbon in order to have a theoretical gold loading of 2wt.%. After stirring for 45 min, the final mixture was centrifuged at 15000 rpm for 20 minutes in order to ensure the anchorage of the totality of gold nanoparticles. The resulting samples were filtered and dried at 100 ºC for 2 hours and finally calcined at 300 ºC for 2 hours. Following this procedure, 11 samples, were prepared as a function of PVA:Au weight ratio (Series 1) and $NaBH_4$:Au molar ratio (Series 2). Table 5.4. summarizes the synthesis parameters of both gold samples series. Gold colloids and their corresponding catalysts were named as 'Col X' and 'AuC X' respectively, being X a distinctively roman number of order.

Table 5.4. Code and Au/PVA/$NaBH_4$ ratios of the prepared gold samples

	Sample	PVA:Au ratio[a]	$NaBH_4$:Au ratio[b]
Series 1	Col I / AuC I	0	5
	Col II / AuC II	0.5	5
	Col III / AuC III	**0.85**	**5**
	Col IV / AuC IV	3	5
	Col V / AuC V	5	5
	Col VI / AuC VI	10	5
Series 2	Col VII / AuC VII	0.85	0.5
	Col VIII / AuC VIII	0.85	1
	Col IX / AuC IX	0.85	2
	Col X / AuC X	0.85	3
	Col III / AuC III	**0.85**	**5**
	Col XII / AuC XII	0.85	10

[a] Weight ratio, [b] molar ratio

5.3.3. Characterization

5.3.3.1. Colloids characterization: UV-Vis spectroscopy and TEM microscopy

The influence of PVA:Au and $NaBH_4$:Au ratios on gold particle size and morphology was studied by both UV-Vis spectroscopy and TEM microscopy. Figure 5.6. presents the UV-Vis absorption spectra of all synthesized colloids. All samples present an intense absorption with maxima in the 502-530 nm region. This absorption is characteristic of the surface plasmon resonance of Au metal nanoparticles and its position, intensity and width is strongly dependent on the size and shape of the Au

particles and on the dielectric properties of the surrounding environment [41].

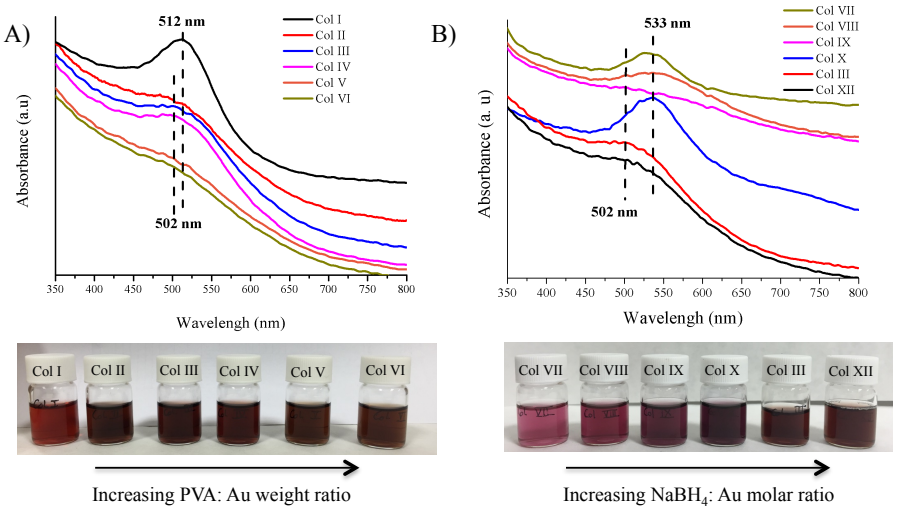

Figure 5.6. UV-Vis spectra of gold colloids. A) Series 1, B) Series 2

For both colloidal series, a modification in the position, shape and width of the gold plasmon band is observed from one colloid to another, indicating differences in the average gold particle size and/or morphology. In good agreement, changes in the color of the colloidal solutions are also observed (see Figure 5.6.), all of them in the reddish mauve spectra. The color of gold colloids is also indicative for the resulting gold particle size and depends on the support (if used), on gold concentration, morphology and size distribution [25]. In particular, colloidal gold is reddish when the corresponding particles are smaller than 20 nm. So far from the color we can deduce that our gold particles independently on the synthetic parameters present sizes always below/around 20 nm.

From Fig. 5.6.A is obvious that an increment in PVA:Au ratio during the preparation leads to a blue shift of around 10 nm in the position of the

gold plasmon and reduction of its intensity, both phenomena suggest a continuous decrease of the particle size from Col I to Col VI.

This size variation was also confirmed by TEM (Figure 5.7.) and the calculated average gold particle size decreases constantly from 3.6 nm (Col I) to 1.8 nm (Col VI) with the increase of the PVA concentration for series 1 (Table 5.5.). In all cases, the obtained particle shape is similar, as deduced from the particle size distributions and TEM micrographs.

The average gold particle size was estimated considering the surface distribution calculation, expressed in Eq. 5.7.

$$D\,[3,2]=\frac{\sum_1^n D_i^3 v_i}{\sum_1^n D_i^2 v_i} \qquad \text{Eq. 5.7.}$$

where D_i is the geometric diameter of the i^{th} particle, and v_i the number of particles with this diameter. For every distribution the total number of measured particles overcomes 200 particles per sample (colloid or catalyst).

It is well known, that the metal particle size variation is based on a fine balance between the nucleation and particle growth rates, both controlled by the nanoparticle synthesis parameters. Many theories exist to explain the mechanisms of nucleation and growth. The rates of gold nanoparticle nucleation and growth generally depends on the pH of the solution, on the reducing agent nature and concentration and on the presence of surfactants [42]. Ji et al. [43] reported that the pH dependence could be ascribed to the existence of differently hydrolyzed gold complexes and their reactivity towards reducing agent. When very diluted gold precursor solutions (as in our case) are employed, the pH of the solution neighbors that of distilled water (6-6.5). At this pH, Ivanova et al. [44] reported that

70 % of Au could be found as $[Au(OH)_2Cl_2]^-$ and $[Au(OH)_3Cl]^-$ complexes. These complexes get reduced with slower nucleation time (60 s) than the less hydrolyzed ones and show lower growth rate. The nature of the reducing agent is also very important, stronger the reductive potential of the agent lower the time of nucleation. The use of $NaBH_4$ indicates quasi-instantaneous nucleation, within a seconds, to an average radius of 2 nm which then undergo coalescence up to 4 nm [45] in the first 20 min, the case of Col I when no stabilizing agent is used. The fast nucleation of gold could be then considered as a separate process from the particle size growth, which will mainly depend on colloidal stability, i.e. on the increase of the aggregation barrier [42]. The later could be achieved by the use of a stabilizing agent (PVA in our case). Indeed the stability of the colloidal solution as a function of time showed interesting differences between the samples. Whereas Col I and II samples agglomerate and precipitate after two days, the Col III to VI remain stable. The correlation between colloidal stability and gold particle size suggests that stable gold colloids could be obtained at PVA/Au ratios superior to 0.85 with resulting particle size of 2.3±0.5 nm. Because of this observation, the series 2 (Col VII to Col XII colloids) was prepared at a fixed PVA:Au ratio of 0.85 and varying the $NaBH_4$:Au proportion. For this series, the increment of the $NaBH_4$:Au ratio leads to a blue shift of the gold plasmon (see Fig. 5.6.A), pointing out the formation of smaller nanoparticles at high concentration of the reductant agent (Table 5.5.).

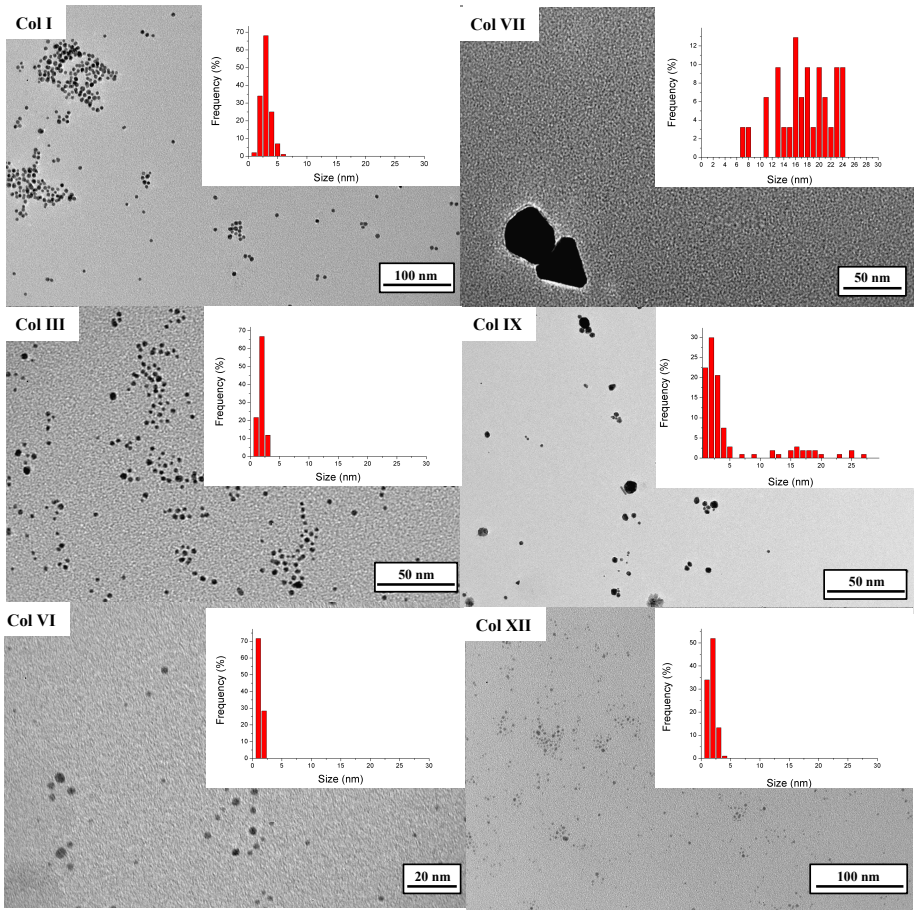

Figure 5.7. Representative TEM micrographs and gold size distribution for selected prepared gold colloids

However, the TEM analysis (Fig. 5.7.) put in evidence that the variation $NaBH_4$:Au ratio affects also the shape and size heterogeneity of the produced nanoparticles. At low ratios (low concentration of reductant agent) a wide particle size distribution is obtained, generating gold particles between 7 and 25 nm and as a consequence higher average particle size. Besides this, a change of particle morphology from spherical to triangular and/or irregular shapes is evidenced (Figure 5.8.). Narrower particle size distribution and lower mean particle size were observed with the increase of $NaBH_4$ /Au ratio. For Col IX an important contribution

of particles in the 1 - 5 nm range is observed, with very few agglomerates. $NaBH_4$ /Au ratio of 3 seems to be the limiting value above which stable colloids of gold particles of 2.3 nm are obtained.

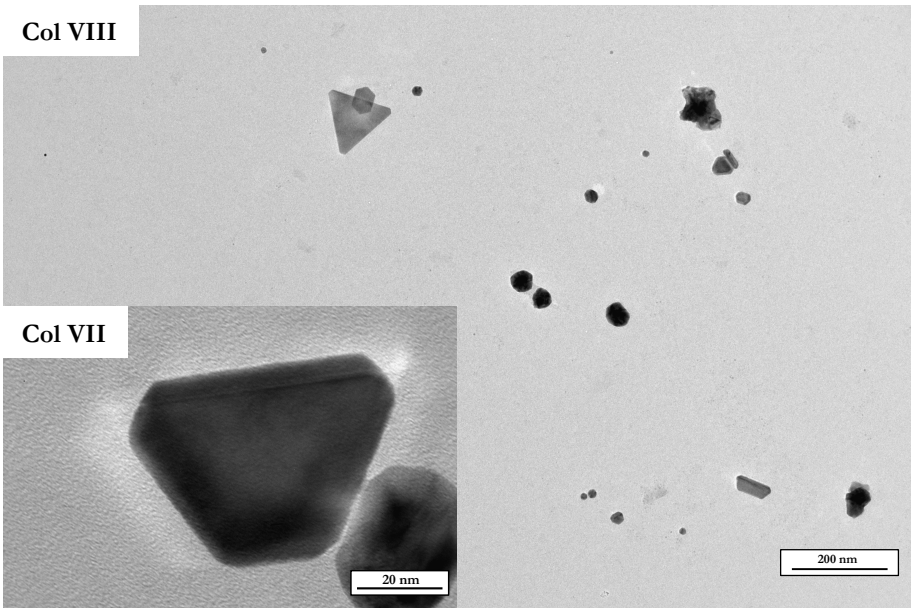

Figure 5.8. Shape and size heterogeneity of the obtained gold nanoparticles at increasing $NaBH_4$:Au ratio

Table 5.5. Average gold particle size of the prepared colloids

	Sample	Average particle size (from TEM), nm
Series 1	Col I	3.6
	Col II	3.3
	Col III	**2.3**
	Col IV	2.8
	Col V	2.3
	Col VI	1.8
Series 2	Col VII	18.9
	Col VIII	3.7
	Col IX	7.6
	Col X	4.9
	Col III	**2.3**
	Col XII	2.2

5.3.3.2. AuC characterization

5.3.3.2.1. ICP and UV-Vis spectroscopy

The pre-formed colloids were immobilized on activated carbon targeting Au loading of 2 wt.%. After the calcination treatment (300ºC, 2h), no significant modification of the textural properties of the parent carbon support was observed. Diffuse Infrared Fourier Transform Spectroscopy (DRIFTS) study evidenced total removal of the PVA protective layer on the surface of the gold nanoparticles (figure not shown). The real gold loadings measured by ICP are summarized in Table 5.6.

The deposited amount of gold is slightly over 2 wt.% in most samples indicating the successful immobilization of the colloid on the carbon surface. However, for the samples prepared with the highest PVA/Au ratios (Au/C V and Au/C VI), a lower gold uptake is obtained, in such a way that higher the used PVA/Au ratio, lower the immobilized gold loading. Considering that, the stability of the colloids is proportional to the PVA concentration the anchoring of gold becomes probably more difficult and responsible for the lower gold uptake. UV-Vis analyses of the post filtration liquid, Fig. 5.9, evidences this difficulty. Regarding the Series 1 (Fig. 5.9. A) gold remains as colloid after gold-carbon slurry filtration from Col IV to VI, being the gold plasmon detected by UV-Vis spectroscopy, at 520 nm. Opposite, the increment of the $NaBH_4$:Au ratio results in proper gold anchorage (Fig. 5.9. B) with gold undetectable by UV-Vis.

From here, and despite the low average gold particle size obtained for these colloids, PVA/Au ratios higher than 3 must be avoided in order to assure total immobilization of the gold nanoparticles.

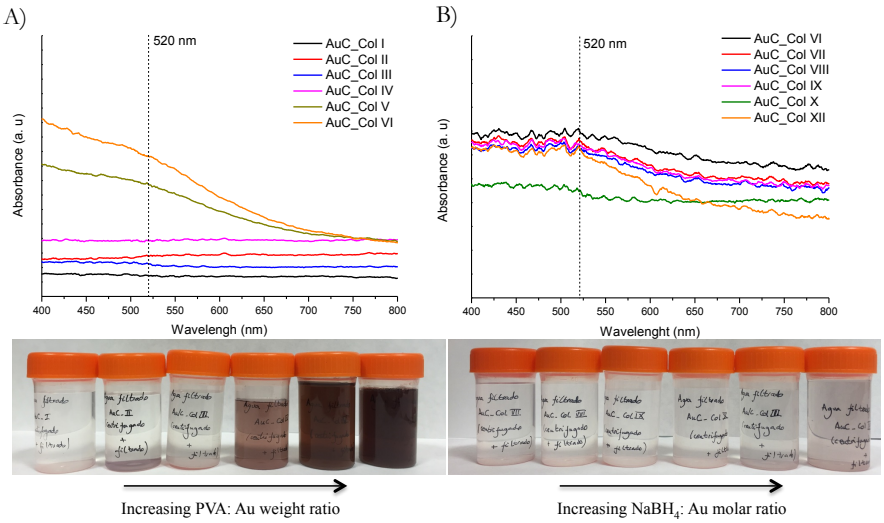

Figure 5.9. UV-Vis analyses of post filtration liquids: effect of PVA:Au ratio in the gold uptake

Table 5.6. Gold loadings of the prepared samples

	Sample	% Au [ICP]
Series 1	Col I / AuC I	2.0
	Col II / AuC II	2.3
	Col III / AuC III	2.4
	Col IV / AuC IV	2.3
	Col V / AuC V	1.1
	Col VI / AuC VI	0.5
Series 2	Col VII / AuC VII	2.1
	Col VIII / AuC VIII	2.3
	Col IX / AuC IX	2.3
	Col X / AuC X	2.2
	Col III / AuC III	2.4
	Col XII / AuC XII	2.3

5.3.3.2.2. XRD and TEM microscopy

The average gold particle sizes of the supported gold samples were calculated from both TEM and XRD measurements. All prepared samples

lead to the same diffraction pattern (Figure 5.10.), being the only difference the gold diffraction intensity, derived for the supported systems, and as expected after the TEM colloids analyses.

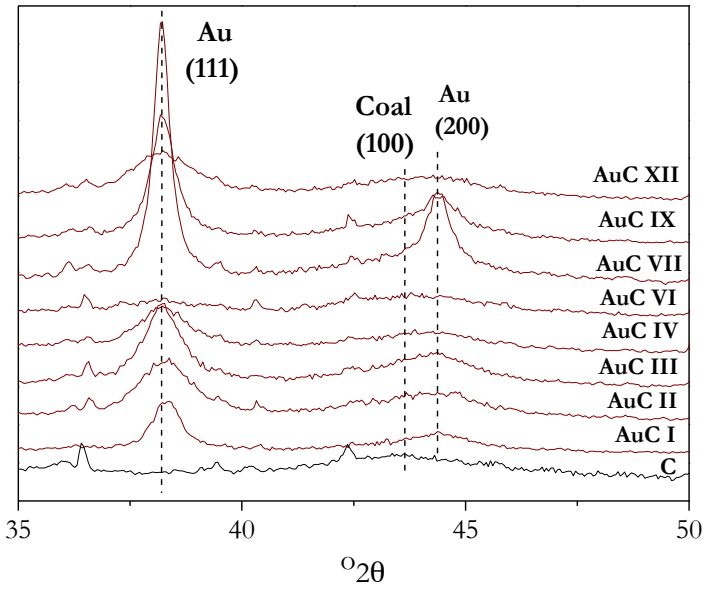

Figure 5.10. Representative X Ray diffractograms for selected AuC catalysts

The average gold particle sizes of the supported gold samples (Table 5.7.) present similar trends compared to the parent colloids. Figure 5.11. shows representative TEM micrographs and gold particle size distribution for Au/C samples. For all samples, a 3 to 4-fold increase of gold particle size was observed, which can be assigned to particle agglomeration occurred after the thermal treatment carried out over the supported systems (calcination at 300 ºC for 2 hours). An almost linear correlation was found between the metal particle size in the colloids and corresponding supported solid (Figure 5.12.), being only the sample corresponding to the Col VII falling off this tendency due to the already aggregated state obtained in the initial colloid. On the other hand, good linear relationship

was also achieved between the average gold particle size determined by TEM and XRD (Figure 5.13.).

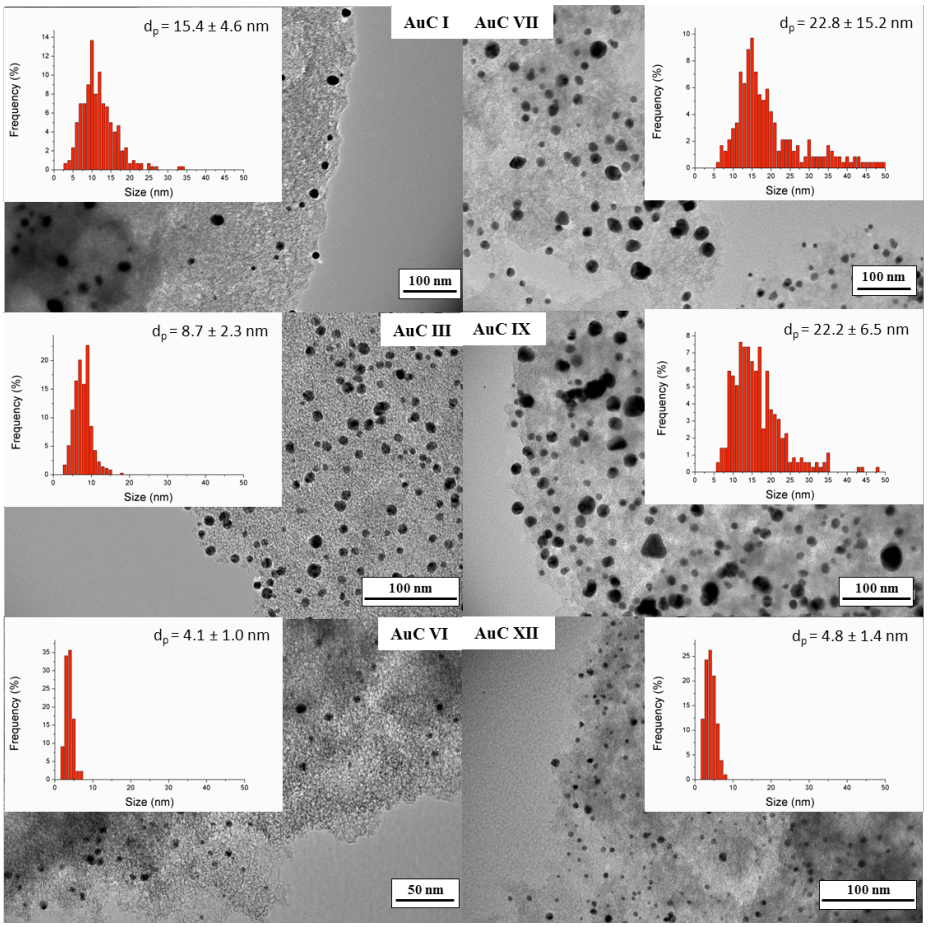

Figure 5.11. Representative TEM micrographs and gold size distribution for selected Au/C catalysts

Table 5.7. Mean Au particle size (colloids and catalysts) and dispersion of the supported gold catalysts.

	Sample	Average particle size of colloids (from TEM), nm	Average particle size (from TEM), nm	Average particle size (from XRD), nm	Dispersion (%)
Series 1	Col I / AuC I	3.6	15.4	14.9	10
	Col II / AuC II	3.3	9.3	9.3	15
	Col III / AuC III	**2.3**	8.7	10.4	16
	Col IV / AuC IV	2.8	10.1	11.1	14
	Col V / AuC V	2.3	6.8	6.6	20
	Col VI / AuC VI	1.8	4.1	4.4	32
Series 2	Col VII / AuC VII	18.9	22.8	28	7
	Col VIII / AuC VIII	3.7	20.1	25.4	7.5
	Col IX / AuC IX	7.6	22.2	22.5	7
	Col X / AuC X	4.9	20.4	16.1	7.4
	Col III / AuC III	**2.3**	8.7	10.4	16
	Col XII / AuC XII	2.2	4.8	5.2	27

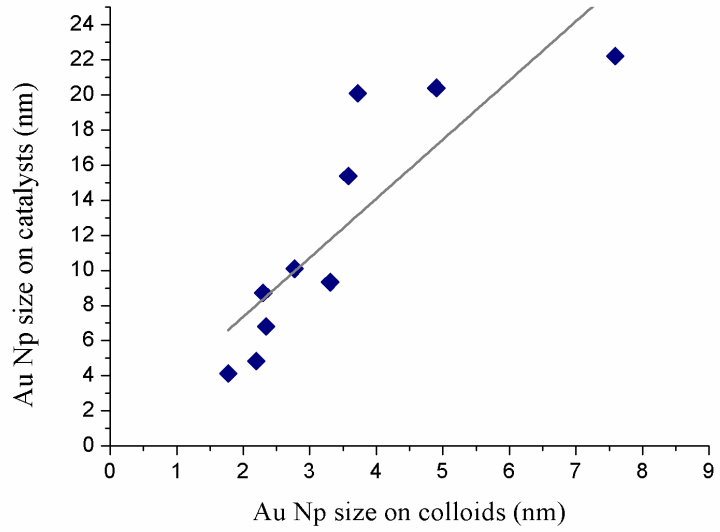

Figure 5.12. Correlation between the average gold particle size in colloids and corresponding Au/C catalysts.

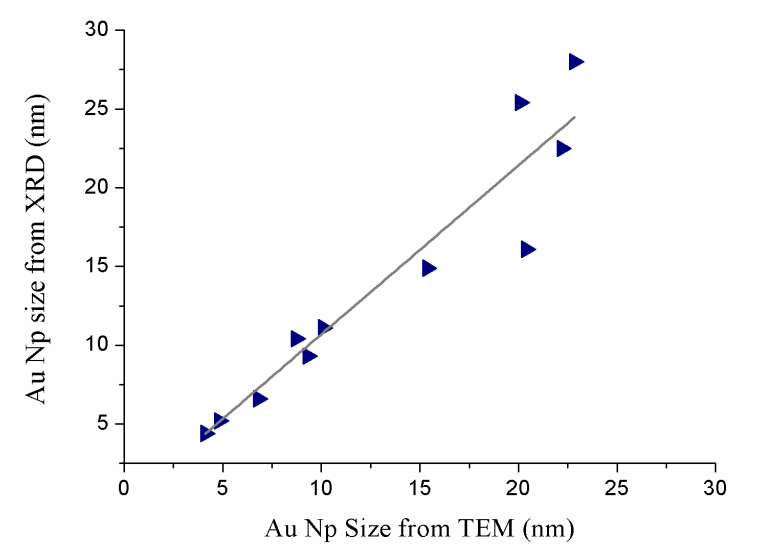

Figure 5.13. Correlation between the average gold particle size determined by TEM and XRD

The immobilization of the pre-formed colloids resulted in a series of Au/C catalysts with average gold particle sizes ranging from 4 to 20 nm. Most of the samples presented a similar gold content (close to 2 wt.%) and gold particle shape (spherical), with a narrow gold size distribution, and will be used to determine the influence of the gold particle size on the catalytic oxidation of glucose and HMF, respectively. Only samples prepared at high PVA/Au ratios (>3) or very low $NaBH_4$:Au ratio (<1) must be carefully applied, due to their lower gold content or different gold particles shape and wide size distribution, respectively.

5.4. Partial conclusions

The introduction of gold catalysts for efficient oxidation of carbohydrates becomes necessary since the POM-ILs structures resulted to be scarcely efficient. Among the different alternatives and based on different

literature reports, gold was chosen as active and selective oxidation catalyst.

Two groups of catalysts were prepared, characterized and organized in order to study the influence of the support nature and gold particle size in glucose and HMF oxidation reaction. The partial conclusions for the two groups are organized as follows:

1) Gold on metal oxides. A series of gold on different bare and mixed oxides supports were prepared by using the DAE method for gold deposition and further fully characterized. This preparation resulted in catalysts with comparable gold loading (2 wt.%), particle size (3-5 nm) and dispersion (20-40 %). The similarity in the gold particle size makes possible their use to determine the influence of support on the catalytic oxidation of glucose and HMF. The IEP was used as indicator of sample's acid/basic properties and TPR-H_2 for the redox ones. The obtained results will be used in the next chapter in order to relate the catalyst activity to the catalyst properties.

2) Gold on carbon. Two series of AuC catalysts have been prepared by immobilization of the pre-formed colloids, with variable gold particle sizes between 4 and 20 nm. Most of the samples present similar gold contents (close to 2 wt.%), gold particle shape (spherical), narrow gold size distribution.

References

[1] G. Strukul, A. Scarso, Liquid Phase Oxidation via Heterogeneous Catalysis: Organic Synthesis and Industrial Applications, 2013.

[2] T. BM, The atom economy--a search for synthetic efficiency, Science (80-.). 254 (1991) 1471–1477.

[3] Trost BM, Atom Economy—A Challenge for Organic Synthesis: Homogeneous Catalysis Leads the Way, Angew. Chem., Int. Ed. 34 (1995) 259–281.

[4] M. Haruta, T. Kobayashi, H. Sano, N. Yamada, Novel Gold Catalysts for the Oxidation of Carbon Monoxide at a Temperature far Below 0 °C, Chem. Lett. 16 (1987) 405–408.

[5] M. Haruta, N. Yamada, T. Kobayashi, S. Iijima, Gold catalysts prepared by coprecipitation for low-temperature oxidation of hydrogen and of carbon monoxide, J. Catal. 115 (1989) 301.

[6] M. Haruta, Size- and support-dependency in the catalysis of gold, Catal. Today. 36 (1997) 153–166.

[7] M. Haruta, No Title, Stud. Surf. Sci. Catal. 110 (1997) 123–134.

[8] L. Prati, M. Rossi., Gold on Carbon as a New Catalyst for Selective Liquid Phase Oxidation of Diols, J. Catal. 176 (1998) 552–560.

[9] G.J. Hutchings, Nanocrystalline gold and gold palladium alloy catalysts for chemical synthesis, Chem. Commun. 2008.

[10] J.K. Edwards, A.F. Carley, A.A. Herzing, C.J. Kiely, G.J. Hutchings, Direct synthesis of hydrogen peroxide from H2 and O2 using supported Au–Pd catalysts, Faraday Discuss. 138 (2008) 225–239.

[11] J. Edwards, B. Solsona, E. N, A. Carley, A. Herzing, K. CJ, et al., Switching off hydrogen peroxide hydrogenation in the direct synthesis process, Science (80-.). 323 (2009) 1037–1041.

[12] T. Ramírez Reina, M. González Castaño, S. Palma, S. Ivanova, J.A. Odriozola, Twenty years of golden future in the water gas shift reaction, in: Heterog. Gold Catal. Catal., 2014: pp. 111–139.

[13] A.S.K. Hashmi, J.P. Weyrauch, M. Rudolph, E. Kurpejović, Gold Catalysis: The Benefits of N and N,O Ligands, Angew. Chem., Int. Ed. 43 (2004) 6545 –6547.

[14] C. Bianchi, S. Biella, A. Gervasini, L. Prati, M. Rossi, Gold on carbon: influence of support properties on catalyst activity in liquid-phase oxidation, Catal. Letters.

85 (2003) 91–96.

[15] M. Comotti, C. Della Pina, R. Matarrese, M. Rossi, The catalytic activity of "naked" gold particles, Angew. Chemie - Int. Ed. 43 (2004) 5812–5815.

[16] M. Comotti, C. Della Pina, E. Falletta, M. Rossi, Aerobic oxidation of glucose with gold catalyst: Hydrogen peroxide as intermediate and reagent, Adv. Synth. Catal. 348 (2006) 313–316.

[17] Y. Önal, S. Schimpf, P. Claus, Structure sensitivity and kinetics of D-glucose oxidation to D-gluconic acid over carbon-supported gold catalysts, J. Catal. 223 (2004) 122–133.

[18] P. Beltrame, M. Comotti, C. Della Pina, M. Rossi, Aerobic oxidation of glucose, Appl. Catal. A Gen. 297 (2006) 1–7.

[19] C. Della Pina, E. Falletta, L. Prati, M. Rossi, Selective oxidation using gold, Chem. Soc. Rev. 37 (2008) 2077–2095.

[20] C. Della Pina, E. Falletta, M. Rossi, Update on selective oxidation using gold, Chem. Soc. Rev. 41 (2012) 350–369.

[21] C. Baatz, U. Prüße, Preparation of gold catalysts for glucose oxidation by incipient wetness, J. Catal. 249 (2007) 34–40.

[22] U. Prüße, M. Herrmann, C. Baatz, N. Decker, Gold-catalyzed selective glucose oxidation at high glucose concentrations and oxygen partial pressures, Appl. Catal. A Gen. 406 (2011) 89–93.

[23] A. Lolli, S. Albonetti, L. Utili, R. Amadori, F. Ospitali, C. Lucarelli, et al., Insights into the reaction mechanism for 5-hydroxymethylfurfural oxidation to FDCA on bimetallic Pd – Au nanoparticles, Appl. Catal. A, Gen. 504 (2015) 408–419..

[24] S. Albonetti, T. Pasini, A. Lolli, M. Blosi, M. Piccinini, N. Dimitratos, et al., Selective oxidation of 5-hydroxymethyl-2-furfural over TiO 2 -supported gold – copper catalysts prepared from preformed nanoparticles : Effect of Au / Cu ratio, 195 (2012) 120–126.

[25] G.C. Bond, D.T. Thompson, Catalysis by Gold, Catal. Rev. Sci. Eng. 41 (1999) 319–388.

[26] P. Qi, S. Chen, J. Chen, J. Zheng, X. Zheng, Y. Yuan, Catalysis and Reactivation of Ordered Mesoporous Carbon-Supported Gold Nanoparticles for the Base-Free Oxidation of Glucose to Gluconic Acid, ACS Catal. 5 (2015) 2659–2670.

[27] Y. Wang, S. Van de Vyver, K.K. Sharma, Y. Román-Leshkov, Insights into the

stability of gold nanoparticles supported on metal oxides for the base-free oxidation of glucose to gluconic acid, Green Chem. 16 (2014) 719–726.

[28] A. Zro, F. Menegazzo, T. Fantinel, M. Signoretto, F. Pinna, M. Manzoli, On the process for furfural and HMF oxidative esterification over, J. Catal. 319 (2014) 61–70.

[29] S. Ivanova, C. Petit, V. Pitchon, A new preparation method for the formation of gold nanoparticles on an oxide support, Appl. Catal. A Gen. 267 (2004) 191–201.

[30] S. Ivanova, V. Pitchon, C. Petit, Application of the direct exchange method in the preparation of gold catalysts supported on different oxide materials, J. Mol. Catal. A Chem. 256 (2006) 278–283.

[31] M. Polisset, Ph. D. Thesis University of Paris VI, 1990.

[32] G. Jacobs, E. Chenu, P.M. Patterson, L. Williams, D. Sparks, G. Thomas, et al., Water-gas shift: comparative screening of metal promoters for metal/ceria systems and role of the metal, Appl. Catal. A Gen. Gen. 258 (2004) 203–214.

[33] S. Scirè, S. Minicò, C. Crisafulli, C. Satriano, A. Pistone, Catalytic combustion of volatile organic compounds on gold/cerium oxide catalysts, Appl. Catal. B Environ. 40 (2003) 43–49.

[34] S. Scirè, P.M. Riccobene, C. Crisafulli, Ceria supported group IB metal catalysts for the combustion of volatile organic compounds and the preferential oxidation of CO, Appl. Catal. B Environ. 101 (2010) 109–117.

[35] C.L. Bianchi, S. Biella, A. Gervasini, L. Prati, M. Rossi, Gold on carbon : influence of support properties on catalyst activity in liquid-phase oxidation, 85 (2003).

[36] F. Rodriguez-Reinoso, The role of carbon materials in heterogeneous catalalysis, Carbon N. Y. 36 (1998) 159–175.

[37] J.H. Vleeming, B.F.M. Kuster, G.B. Marin, Effect of platinum particle size and catalyst support on the platinum catalyzed selective oxidation of carbohydrates, Catal. Letters. 46 (1997) 187–194.

[38] K.C. Ruthiya, J. van der Schaaf, B.F.M. Kuster, J.C. Schouten, Modeling the effect of particle-to-bubble adhesion on mass transport and reaction rate in a stirred slurry reactor: influence of catalyst support, Chem. Eng. Sci. 59 (2004) 5551–5558.

[39] I. V. Delidovich, B.L. Moroz, O.P. Taran, N. V. Gromov, P. a. Pyrjaev, I.P.

Prosvirin, et al., Aerobic selective oxidation of glucose to gluconate catalyzed by Au/Al2O3 and Au/C: Impact of the mass-transfer processes on the overall kinetics, Chem. Eng. J. 223 (2013) 921–931.

[40] J. Luo, W. Chu, S. Sall, C. Petit, Facile synthesis of monodispersed Au nanoparticles-coated on Stöber silica, Colloids Surfaces A Physicochem. Eng. Asp. 425 (2013) 83–91.

[41] P. Bera, M.S. Hedge, No Title, Catal. Letters. 79 (2002) 107.

[42] J. Polte, Fundamental Growth Principles of Colloidal Metal Nanoparticles - a new Perspective, CrystEngComm. 17 (2015) 6809–6830.

[43] X. Ji, X. Song, J. Li, Y. Bai, W. Yang, Size Control of Gold Nanocrystals in Citrate Reduction : The Third Role of Citrate, (2007) 1957–1962.

[44] S. Ivanova, V. Pitchon, C. Petit, H. Herschbach, A. Van Dorsselaer, E. Leize, Preparation of alumina supported gold catalysts: Gold complexes genesis, identification and speciation by mass spectrometry, Appl. Catal. A Gen. 298 (2006) 203–210.

[45] N.T.K. Thanh, N. Maclean, S. Mahiddine, Mechanisms of Nucleation and Growth of Nanoparticles in Solution, Chem Rev. 3 (2014) 7610.

Chapter Six

AEROBIC OXIDATION of GLUCOSE and HMF: CATALYTIC SCREENING

Summary[1]

In this chapter the catalytic activity of two groups of gold catalysts has been evaluated in the base-free oxidation of glucose to gluconic acid and in the oxidation of 5-hydroxymethyl-2-furfural to 2,5-furandicarboxylic acid, using O_2 as oxidant. For both reactions, the influence of the support is studied using metal oxide-supported gold catalysts. The influence of Au particle size is assessed using carbon-based supports. The effect of several reaction parameters, such as temperature, reaction time and stirring rate are also considered. Finally, the catalyst stability is evaluated by reusing the solids several times, paying special attention to Au/carbon catalysts. For these catalysts a deep study focused on the possible causes of deactivation is presented.

[1]Some of the results presented in this Chapter have been published in:

C. Megías-Sayago *et al.* **Catalysis Today** 279 (2017) 148–154

C. Megías-Sayago *et al.* **Catalysis Today** (2017) *In press*
http://dx.doi.org/10.1016/j.cattod.2017.03.022

C. Megías-Sayago *et al.* **Catalysis Today** (2017) *In press*
http://dx.doi.org/10.1016/j.cattod.2017.01.007

6.1. Base-Free oxidation of glucose

6.1.1. Introduction

The oxidation of D-Glucose to D-Gluconic acid (Scheme 6.1.) over metal supported catalysts has received much attention in the last two decades, principally due to the complexity of the current industrial fermentation processes through which a production of about 100.000 tons is registered annually [1–3]. In addition to the limitations derived from the use of enzymes, it has been reported that the accumulation of gluconic acid inhibits microbial function leading to lower yields and slow overall reaction rates [3,4].

Several studies focused on gluconic acid production over platinum group metals (PGM) catalysts [5–7] being the main drawback of these systems their deactivation due to oxygen poisoning of the metal surface [8]. In order to improve PGM catalysts activities, bimetallic Bi-Pt and trimetallic Bi-Pd-Pt catalysts were reported with higher activity and selectivity [6,9]. However, Bi is prone to leaching converting these catalysts in inadequate candidates for the production of chemicals for food and pharmaceutical industries.

Gold, however, has been successfully used in aerobic oxidation of carbohydrates [10,11]. More specifically, aerobic oxidation of glucose carried out over different unsupported and supported gold catalysts, showed important activity and very good resistance to oxygen poisoning. However, an important drawback of these processes is the strong dependence of gold activity on the reaction pH value, which entails the use of base, usually sodium hydroxide [12,13]. Biella et al. [14] have demonstrated that the use of alkaline conditions improves the activity and increases the catalyst stability during recycling tests. Additionally, basic conditions (pH at 9.5) seems to avoid gold nanoparticle leaching and

sintering, and therefore, prevents catalyst deactivation. Another cause of deactivation could be also the strong interaction between gold nanoparticles and the resulting carboxylic compounds, normally suppressed in the presence of base due to salt formation. Despite all the advantages of using base in glucose oxidation reactions, base-free processes are highly desired in order to simplify the treatment of the post-reaction mixture and to obtain pure acid instead of gluconate salts. In addition, glucose isomerization to fructose occurs catalyzed by the presence of base and usually lowers the selectivity to gluconic acid.

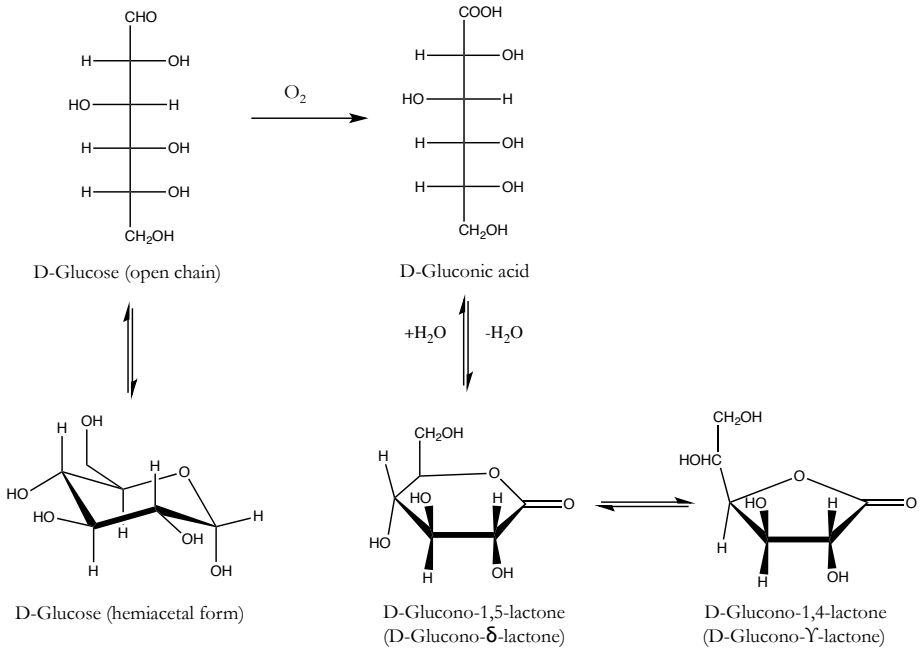

Scheme 6.1. Scheme of the D-Glucose to D-Gluconic acid (GA) oxidation. Chemical equilibrium of D-Glucose to its hemiacetalic form. Chemical equilibrium of GA and its lactones in aqueous solution.

Some recent studies report the base-free oxidation of glucose over gold supported catalysts under mild conditions. Qi *et al.* [15] studied glucose oxidation over gold supported on structured carbon and ZrO_2 at 110 ºC

and 0.3MPa $P(O_2)$. A high initial glucose conversion was reported over Au/C catalyst (92.4%) in comparison to zirconia based one (12.7%), decreasing of approx. 20% after 4 runs. Wang *et al.* [16] also investigated the base-free oxidation of glucose over different CeO_2 and ZrO_2 supported gold catalysts at 65 ºC and 0.23 MPa $P(O_2)$ and reported an activity dependence on gold loading, being the catalysts with lower gold content the most active. Approximately 30% to 60% decrease of glucose conversion over Au/CeO_2 catalysts after 5 runs was also observed. To palliate this effect the authors proposed a catalyst treatment, calcination and/or base washing before the reuse cycles. In general, any change of the support state, particle size or catalyst's acid-base properties influence in a great extent the activity and selectivity of the systems.

In this first section of this Chapter 6, the catalytic activity of several gold supported catalysts is evaluated in the base-free oxidation of glucose under mild conditions.

Firstly, various gold catalysts supported on mineral metal oxides are screened. γ -Al_2O_3, and CeO_2 are chosen as simple oxides and CeO_2(20%wt)/Al_2O_3, CeO_2(25%wt)/ZrO_2, and CeO_2(50%wt)/ZrO_2 as mixed oxides combinations. The effect of the support nature, reaction time, temperature and stirring rate on the catalytic activity and product distribution is evaluated and the catalyst reusability discussed.

Secondly, two series of gold catalysts supported on active carbon with different particle sizes and shapes are studied, being the gold particle size directly correlated to the activity and product distribution. Special emphasis is payed to catalyst recyclability under repeated, taking into account all possible deactivation causes.

6.1.2. Gold supported on metal oxides: influence of support

6.1.2.1. Experimental

All catalytic tests were performed in a glass batch reactor (50 mL) saturated with oxygen at atmospheric pressure (approximate $P(O_2)$ of 0.1 MPa) with 5 ml 0.2M glucose solution and Glucose/Au molar ratio of 100. In a typical experiment, a 20 mL/min pure oxygen flux was introduced in the reactor in order to supply an oxygen rich atmosphere. Then, the reactor was closed and the mixture stirred at 600 rpm at various times and temperatures (0ºC to 120ºC temperature range) without base addition. After reaction, 500 μL of sample was taken from the final mixture, diluted in 500 μL of MilliQ water and immediately analyzed by HPLC. The specific operation conditions are summarized in Chapter 2, Analytical methods section. As an example, a typical chromatogram obtained during the oxidation reaction is presented in Figure 6.1. The presence of gluconic acid and its lactones is evidenced during the analysis, according to the dehydration equilibrium shown in Scheme 6.1.

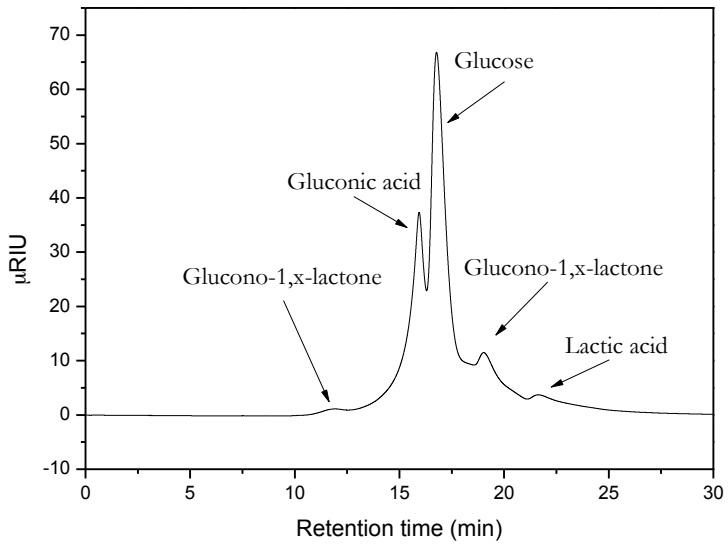

Figure 6.1. Typical chromatogram obtained during the oxidation analysis

6.1.2.2. Catalytic activity: results and discussion

Firstly was studied the influence of the support nature and on the base of the obtained results, few samples are chosen for reaction parameters adjustment.

Effect of the support

The conversion of glucose after 18 h of reaction does not seem to be influenced by the nature of the support being over 75% in all cases (Fig. 6.2.A). As the catalysts, present different gold loadings, a normalization of the activity to the available surface gold atoms should be done for proper comparison of the samples. The TOF is calculated on the basis of Au dispersion (Equation 6.1.) and presented in Table 6.1.

$$\text{TOF} = \frac{moles\ Glucose\ converted}{moles\ Au{*}s{*}dispersion} \qquad \text{Eq. 6.1.}$$

Table 6.1. Estimated particle size, dispersion and TOF

Sample	Average particle size, nm	Dispersion, %	TOF, $s^{-1} * 10^3$
AuAl	5.1±1.5	26	5.44
AuCeAl	3.4±0.8	38	2.64
AuCe	3.9±1.5	33	1.66
AuCe50Zr	3.3±1.4	39	2.53
AuCe25Zr	3.9±1.2	33	2.87

The AuAl sample doubles the activity of almost all ceria-containing samples, which within its series obey the following order:

AuCe25Zr > AuCeAl > AuCe50Zr > AuCe

It looks like the activity is inversely proportional to the ceria loading, the higher the ceria loading the lower the TOF. Nevertheless, below 50 % of ceria, the activity maintains the same order, suggesting that the activity is related to the support nature and more particularly to its Lewis acidity. Using the Pearson concept for hard and soft Lewis acids and bases, the relative Lewis acids hardness can be calculated by considering all ions in its real proportions. The acidity hardness decreases almost in the same order as the activity AuAl>AuCeAl> AuCe25Zr> AuCe50Zr> AuCe indicating that the change of the support nature plays some role during the reaction [17,18].

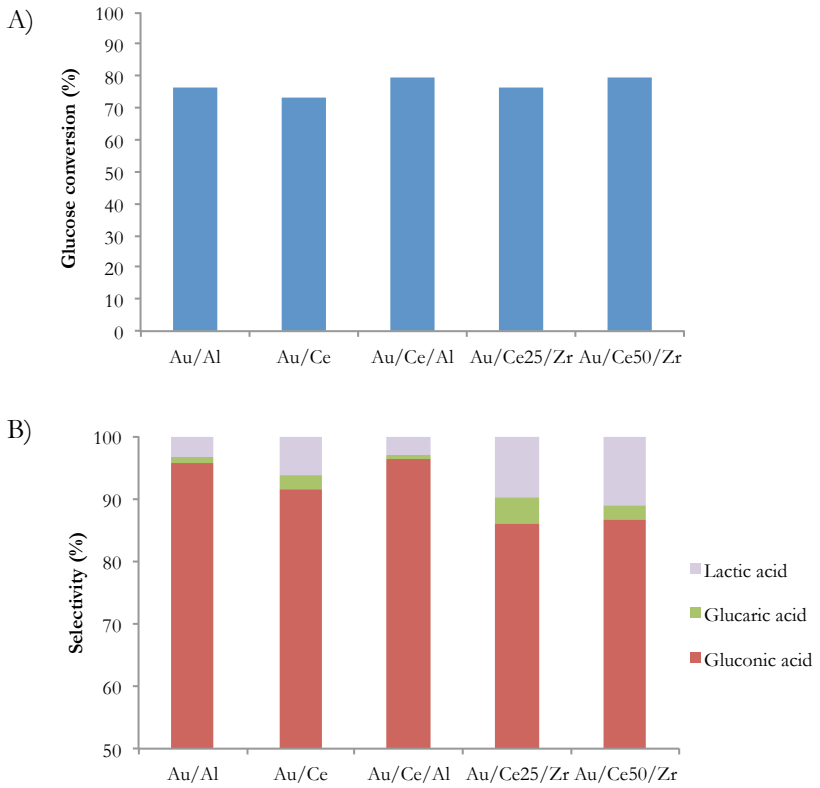

Figure 6.2. A) Glucose conversion (%) over different gold supported catalysts (18 h, 120ºC, 600 rpm), B) Selectivity (%)

The products distribution (Fig. 6.2. B) is also influenced by the support nature. The alumina supported sample presents the highest selectivity to gluconic acid (95%) followed by the AuCeAl sample and AuCe. The zirconia containing samples show the lowest selectivity to gluconic acid, favoring some lactic acid formation (10%) in comparison to AuAl (3%) and AuCe (6%) based catalysts. The formation of glucaric acid seems to follow the same trend. In general, the formation of lactic acid involves several reactions such as isomerization [19] retro-aldol reaction [20], and secondary isomerization reaction, which normally occurs in the presence of Lewis acid sites. However, it looks like the lactic acid formation is not guided by acid strength of sites as the opposite tendency is observed. The presence of some specific acid sites and more probably their density on the support changes the product distribution and leads to lactic acid formation. For zirconia-containing solids, the glucose conversion and product distribution follows the same trend, the lowest selectivity and activity in terms of TOF are registered. It is obvious that the support plays an important role in the process and further research about support acidity, type and strength is required.

Based on the results only three samples are selected for further study of the reaction time effect, AuAl, AuCe and AuCeAl.

Effect of the reaction time

As expected, the conversion increases with the reaction time (Fig. 6.3.), and insignificant differences between the catalysts are observed. No matter the reaction time, the selectivity is clearly governed by the support.

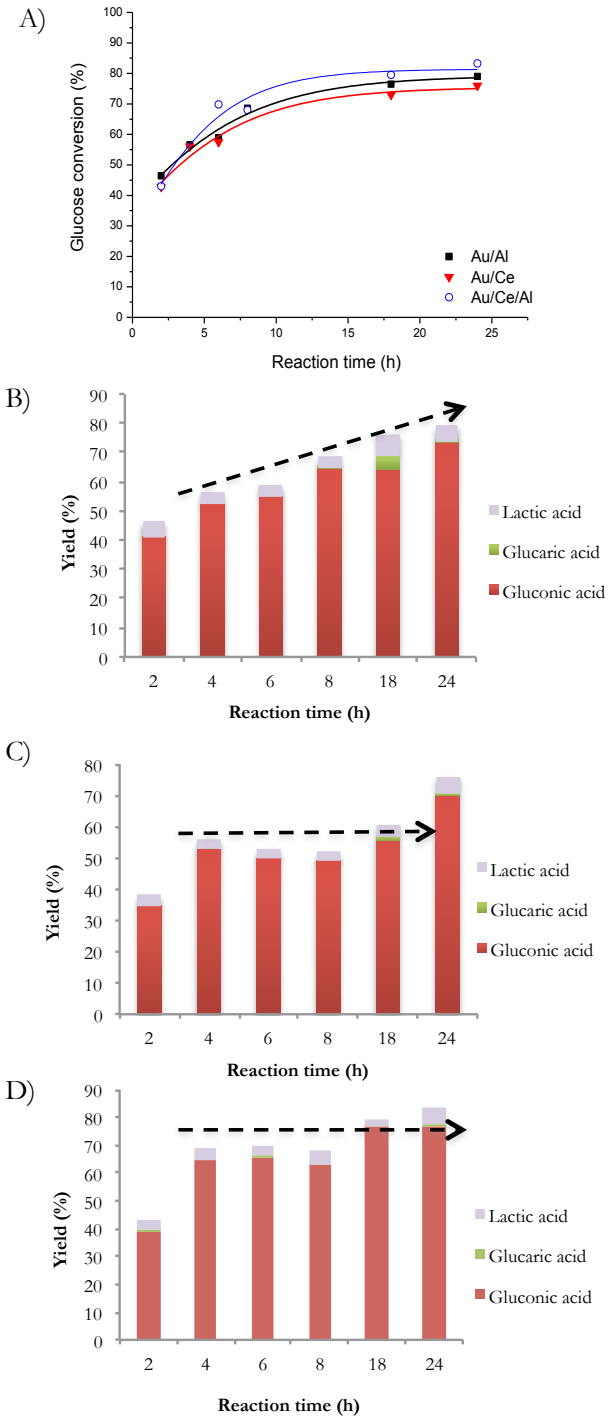

Figure 6.3. A) Glucose conversion (%) vs. reaction time (120ºC, 600 rpm), B) Yield over AuAl, C) Yield over AuCe, D) Yield over AuCeAl.

Gluconic acid yield (Fig. 6.3.B) for the AuAl catalyst increases linearly with reaction time unlike for AuCe and AuCeAl (Fig. 6.3. C, D) catalysts where the yield attains a constant value in the first 4 hours of reaction. The presence of ceria in both samples suggests that the oxidation of glucose might involve labile surface oxygen available for this oxide. Therefore the oxidation process is improved, especially at short reaction times probably by the participation of its lattice oxygen and oxygen vacancies [21].

Effect of reaction temperature

All other experiments are carried out over AuAl catalyst. The temperature effect is studied in the 0-120 ºC range with 2 hours of reaction at every temperature and the results are shown in Fig. 6.4. A.

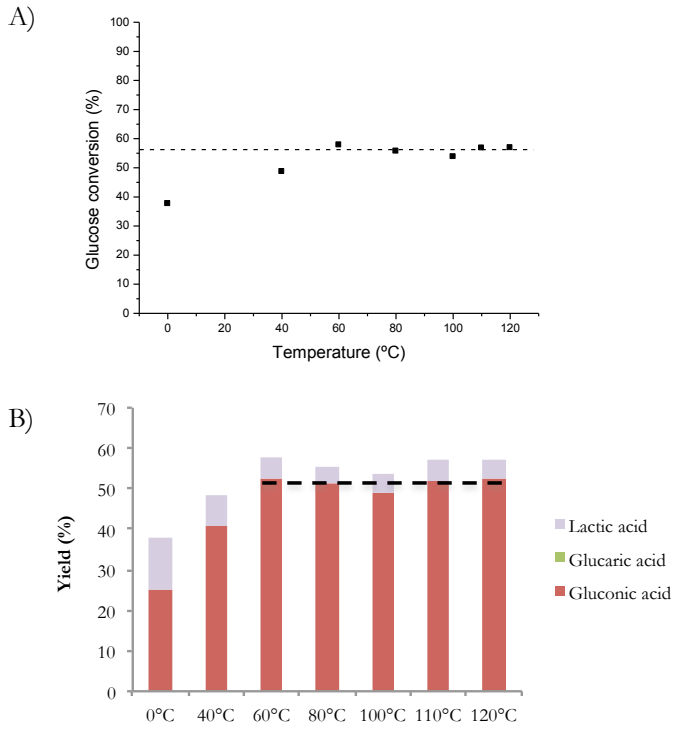

Figure 6.4. A) Glucose conversion (%) as a function of temperature over AuAl (600 rpm, 2h) B) Yield (%)

The glucose conversion rises with the temperature till a constant value at around 55% at 60 ºC. This result is expected as the oxygen solubility in water decreases with the temperature [22]. The solubility of oxygen reaches the lowest point at 60 ºC and does not change significantly when the temperature increases [22]. To achieve then a higher activity the oxygen pressure has to be risen. It is interesting to underline that relatively high glucose conversion is achieved at 0 ºC (35%) which indicates that AuAl could work successfully at atmospheric pressure, low temperatures and in absence of base. The product distribution also changes with temperature (Fig. 6.4. B), favoring lactic acid formation at low temperatures. Low temperatures imply low reaction rates for the glucose oxidation and higher selectivity to lactic acid formation.

Stirring rate dependence

It is well known for the liquid-phase reactions, that the diffusional processes of either reactants arrival to the active sites or products desorption from the catalyst surface depend on the mixing degree. For this reason, some experiments were carried out over AuAl sample at 120º C (2h reaction time) varying the stirring rate from 300 to 900 rpm. As expected, higher the stirring rate, higher the conversion of glucose (Figure 6.5.) and higher the gluconic acid yield (47% vs. 59%).

Besides glucose conversion, the lactic acid yield also relates to the mixing degree, being higher at low stirring rates (6% of yield at 300 rpm vs. 3% at 900 rpm). This result could be tentatively explained by the higher residence time of the reactants on the surface of the catalyst at lower mixing and/or by lower oxygen concentration in solution, both allowing the secondary reaction to lactic acid formation. As observed above in the reaction temperature effect, the lower the reaction rate of oxidation the higher the selectivity towards lactic acid. The formation of lactic acid at

low conversions and low mixing rate suggests that great glucose coverage on the catalyst surface is one of the key factors for a proper product distribution.

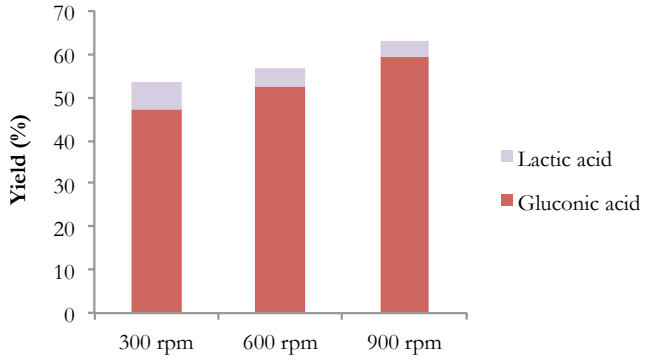

Figure 6.5. Yield (%) as a function of the stirring rate over AuAl (120ºC, 2h)

On the other hand, the limited conversions above 60ºC and the fact that higher conversions can be reached by increasing the stirring rate might also suggest some mass-transfer limitations. However, as reported by Delidovich et al. [23] the diffusional processes limiting the glucose oxidation reaction rate on Au/Al_2O_3 strongly depend on the Glucose:Au molar ratio. It was reported in this study that for low Glucose:Au molar ratios (below 750:1) the apparent reaction rate is only limited by the rate of oxygen dissolution. Therefore, we can consider that in our study (Glucose:Au 100:1) the limitations due to the mass-transfer process although existing are not so important as those caused by oxygen dissolution processes.

Catalyst reusability

The reuse experiments are carried out over AuAl catalyst in 4 successive runs. A clear drop of the glucose conversion is observed (Figure 6.6.).

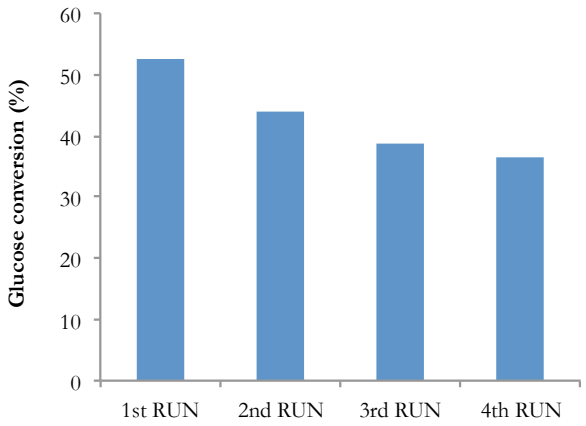

Figure 6.6. Catalyst reuse, conversion of glucose (%) over AuAl (120ºC, 2h, 600 rpm)

The initial conversion of 53% achieved in the first run (120ºC, 2 h) drops to 44% in the second and 39% and 37% in the third and fourth runs, respectively. The slope of activity loss becomes smaller with the number of runs. On the other hand, the change of the reaction solution color occurs, turning to mauve and pointing to a gold leaching process. Indeed, the X ray fluorescence (XRF) analysis of the spent sample shows that after 18 hours of reaction at 120 ºC, the metal loading drops to 1.14% instead 1.64% for the initial catalyst. Generally, in the literature, the gold particle size growth during the reaction is reported as one of the main reasons for gold catalysts deactivation. Comotti *et al.* [24] observed that the rate of glucose oxidation is inversely proportional to the gold particle diameter, being especially detrimental to increase the size above 10 nm. In our case, upon reaction, the average gold particle size hardly changes. The estimated particle size of fresh and spent catalysts and particle size distribution of AuAl, AuCe and AuCeAl after 18 hours reaction time are shown in Figures 6.7; 6.8 and 6.9.

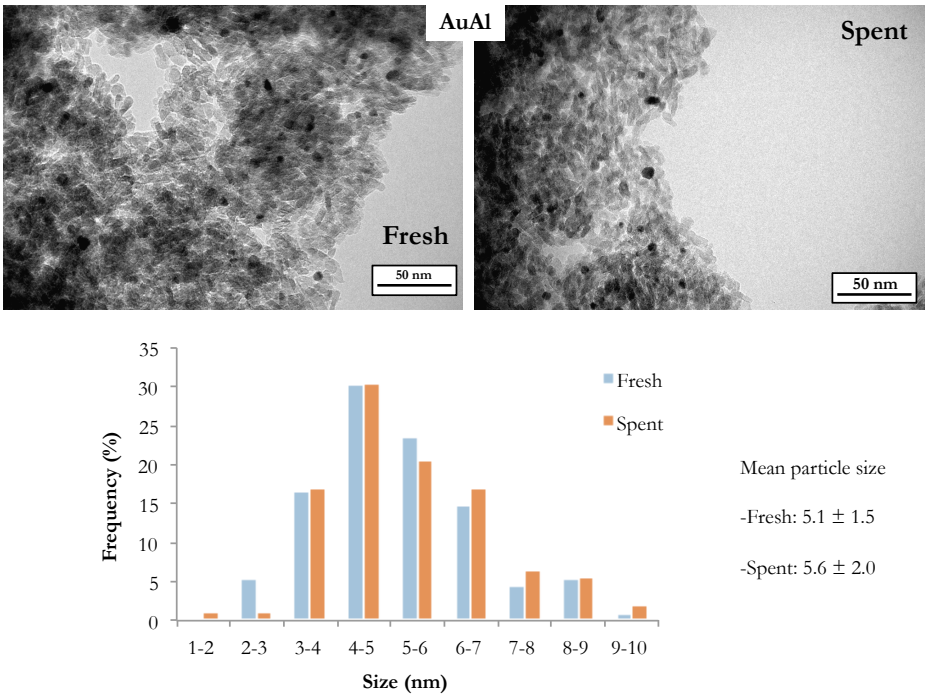

Figure 6.7. TEM images and particle size distribution of fresh and spent AuAl catalyst

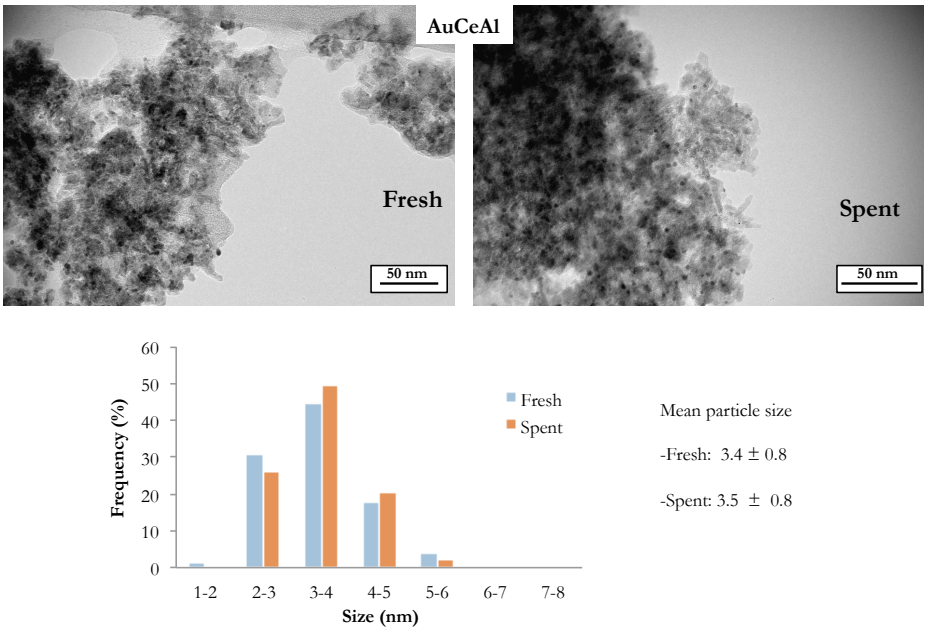

Figure 6.8. TEM images and particle size distribution of fresh and spent AuCeAl catalyst

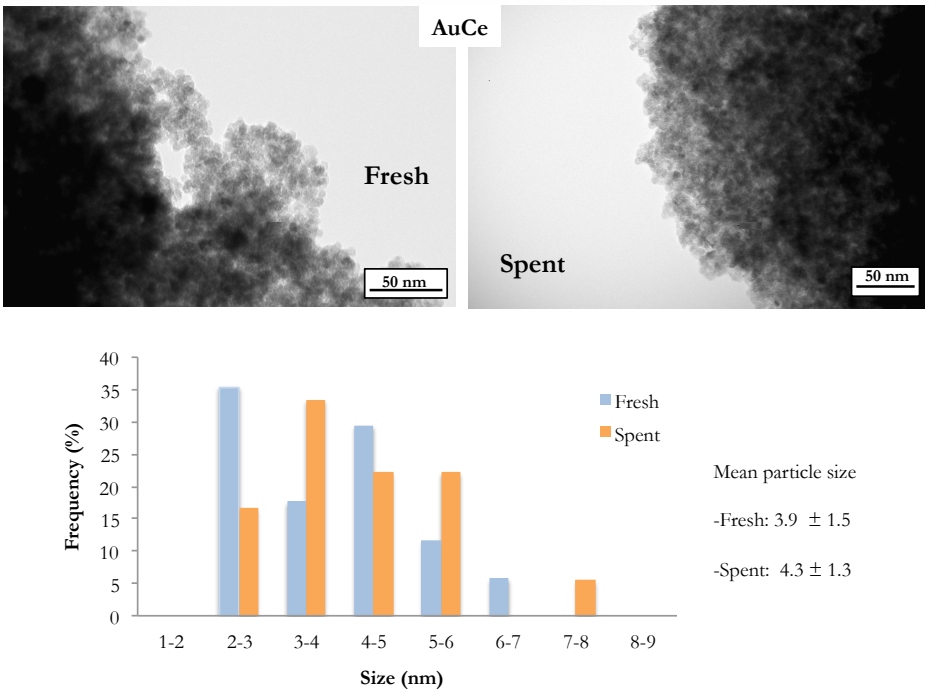

Figure 6.9. TEM images and particle size distribution of fresh and spent AuCe catalyst

Although, there is an increase of the average gold particle size upon reaction, the size difference is insignificant and might not be the cause of the observed activity loss. This suggests that leaching of gold should be the problem to solve in order to avoid catalyst deactivation.

In order to verify this assumption, AuAl was reload at the same reaction conditions (120ºC, 600 rpm) for 4 hours. After this time, the catalyst was microfiltered, oxygen re-introduced the reaction continued to total reaction time of 18 hours but without solid catalyst. In this way, the change of the activity in the last 14 h is caused only by the leached gold particles. The obtained results (in red) compared with those of typical experience at 4 and 18h (in blue) are shown in Fig. 6.10.

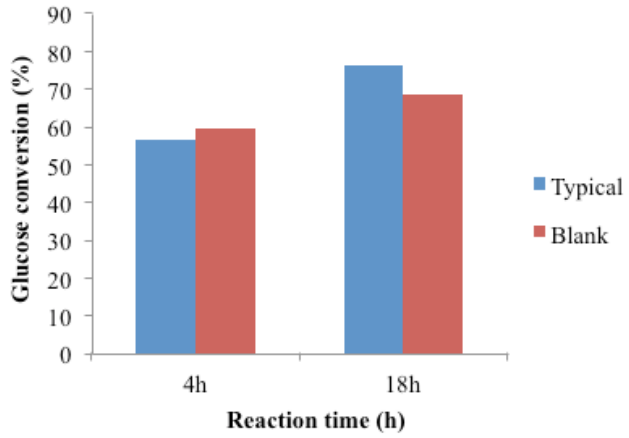

Figure 6.10. Typical vs. Blank experiments over AuAl at different reaction time.

In a typical experiment after 4 hours run, the obtained conversion is 57 % that increases to 77% after 18 hours, being the difference in the conversion directly attributed to the presence of supported catalyst and increase of the reaction time. On the other hand, in the blank test, 59 % of conversion is reached after 4 hours with catalysts while 69 % is measured after 18 hours over the leached gold solution. Hence, this 10 % can be ascribed to both leached gold and reaction time increase. As the reaction time is the same, we can consider that the difference is due to the different gold present, in one case supported and leached in other. These results confirm that the leached gold is also participating in the reaction although lower conversions are obtained. However, the color of the leached gold solution changes dramatically from purple to black after 18 h, indicating detrimental particles agglomeration in absence of support. This color change was not observed for the other typical experiments including supported gold.

Even though leached gold can participate in the oxidation process, a higher activity is observed for the supported catalysts. With these experiments we can affirm that the loss of activity during reuse runs is due

mainly to gold metal leaching and active sites lost during catalysts recuperation and also that the presence of the support is necessary for particles stabilization against agglomeration.

6.1.2.3. Partial conclusions

All screened catalysts show high glucose conversion and important selectivity to gluconic acid in base-free conditions. Both, selectivity and activity, depend on support nature, in a way, that the presence of ceria promotes the oxidation reaction at lower reaction times and the presence of zirconia promotes the secondary reactions to lactic acid formation. Higher the zirconia concentration, lower the glucose conversion and higher the selectivity to lactic acid. The secondary reaction is also promoted at low reaction temperatures and stirring rates.

When exposed to various catalytic cycles the AuAl catalyst fails to maintain constant conversion, with the reason being the gold metal leaching.

6.1.3. Gold supported on carbon: influence of particle size

6.1.3.1. Experimental

The catalytic tests were carried out in a similar way to the above described. The reactor (glass batch reactor equipped with Young valve and magnetic stirrer) was charged with a 0.2M glucose solution, catalyst in Glucose/Au molar ratio of 100 and oxygen, in the aforementioned order. The oxygen diffusion through solution was assured by 20 mL/min pure oxygen flux bubbling for few minutes. Afterwards, the reactor was closed and the mixture stirred at 600 rpm, at 40º C during 18 hours in base-free conditions. Once the reaction finished, 500 μL of sample taken from the final reaction mixture and diluted in 500 μL of ultra-pure water was immediately analyzed by HPLC, in the same conditions described previously.

The recycling study was carried out in a similar manner separating the catalyst from the products by filtration between the runs and re-using it maintaining Glucose/Au molar ratio of 100 at every run. Some reactivation treatments were considered: washing with distilled water, 0.1M NaOH solution or thermally treated (calcined) at 300º C for 2h before every run.

6.1.3.2. Catalytic activity: results and discussion

An important difference with the catalysts from the first section should be underlined, due to the higher activity of the Au/carbon catalysts at 60ºC, the reaction temperature is decreased to 40 ºC in order to study the particle size effect. As discussed in the previous section, the oxygen dissolution in water is a function of the temperature, being limited over 60 ºC. The later implies that the maximum temperature would be limited to

60 ºC, unless the oxygen pressure is increased. The activity registered for carbon-based catalysts at 60 ºC is higher than those obtained for the metal oxides supported catalysts, but no differences were observed between AuC I, II and III. Based on the later, we decide to decrease the temperature below 60 ºC, to detect the maximum differences and to discern between the different gold particle sizes and shapes. The oxidation of glucose is carried out, therefore, under really mild conditions, 40 ºC, in presence of O_2 and in absence of base.

The catalytic activity in terms of glucose conversion of all synthesized AuC catalysts as a function of the average gold particle size determined from TEM are shown in Figure 6.11.

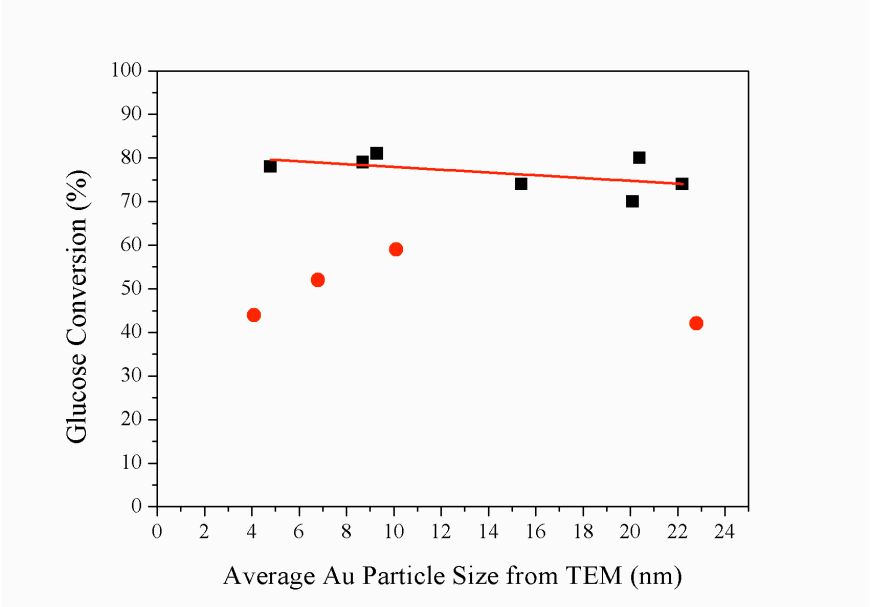

Figure 6.11. Glucose conversion as a function of average gold particle size determined by TEM (0.1 MPa O_2, 40ºC, 18h)

All samples showed 100 % of selectivity to gluconic acid without formation of other products. Excluding the samples with significantly lower gold content and different gold particles shape and wide size distribution (in red), a linear almost constant trend, is observed. A slightly

negative slope would indicate that smaller gold particles are more active than the bigger ones [25]. In fact, a maximum in activity for particles around 9 nm is observed, in agreement with the findings of Prati et al. during the last decade and resumed in a recent publication [26]. They found 7 nm as optimal gold nanoparticle size for highest activity and assigned it to the exercised embedding effect of carbon on smaller nanoparticles.

Nevertheless, if the activity is normalized to the exposed gold surface by using turn-over-frequency (TOF) values (see Eq. 6.1.) the observed size/activity relationship is somehow different, Figure 6.12. TOF was calculated taking into account the gold dispersion, estimated from the average gold particle size deduced from TEM by mathematical modeling for cuboctahedral particles [27] and the real Au contents measured from ICP (Table 6.2.).

Table 6.2. Experimental gold loadings, mean Au particle size, dispersion and TOF of the supported gold catalysts.

	Sample	% Au [ICP]	Average particle size (from TEM), nm	Dispersion (%)	TOF, $s^{-1}*10^3$
Series 1	Col I / AuC I	2.0	15.4	10	11.24
	Col II / AuC II	2.3	9.3	15	7.08
	Col III / AuC III	2.4	8.7	16	6.19
	Col IV / AuC IV	2.3	10.1	14	5.60
	Col V / AuC V	1.1	6.8	20	7.58
	Col VI / AuC VI	0.5	4.1	32	8.59
Series 2	Col VII / AuC VII	2.1	22.8	7	9.40
	Col VIII / AuC VIII	2.3	20.1	7.5	12.04
	Col IX / AuC IX	2.3	22.2	7	14.5
	Col X / AuC X	2.2	20.4	7.4	14.7
	Col III / AuC III	2.4	8.7	16	6.19
	Col XII / AuC XII	2.3	4.8	27	3.77

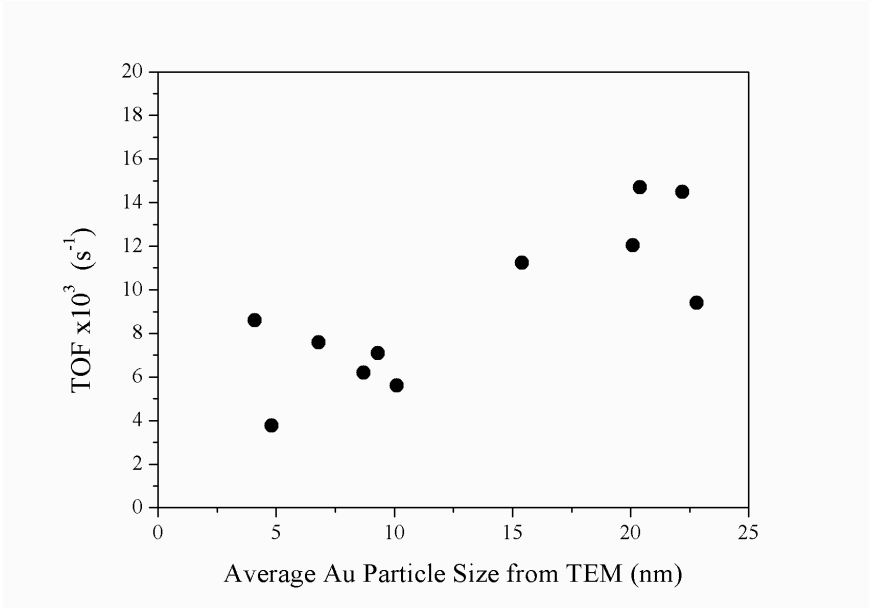

Figure 6.12. Glucose oxidation turn-over-frequency (TOF) values as a function of the average gold particle size determined from TEM (0.1 MPa O2, 40ºC, 18h)

Now, the samples could be organized in two groups, samples up to 10 nm showing similar trend and samples with particle size around 15-20 showing a higher activity. This result appears somehow contradictory as we consider that higher the particle size lower the gold atoms surface exposure. Anyway, this result suggests that glucose adsorption step should play an important role in the reaction mechanism and that the adsorption strength and activation mechanism are probably different on small and big size gold particles.

There is a serious lack of studies considering the glucose oxidation mechanism in base-free conditions. In alkaline conditions, Ishimoto et al. [28] proposed a theoretical mechanism in 4 steps, where i) glucose is adsorbed on OH adsorbed on Au, ii) OH^- from the solution react with the CHO group of glucose to iii) form and release water by proton transfer and finally iv) gluconic acid is formed by OH transfer from the Au surface. However, in base-free conditions the mechanism should

occur differently way. Normally it is considered that the liquid phase oxidation of alcohols and aldehydes adopts the oxidative dehydrogenation mechanism [29] where the reactants are deprotonated on the metal surface with metal hydrate formation, which subsequently reacts with dissociatively adsorbed oxygen to form water. However, for this mechanism the structure/size dependency is the opposite of that observed here, i.e. lower the particle size higher the adsorption/dehydrogenation of the CHO group and higher the activity toward acid formation. Taking into account both mechanisms, one can consider the adsorption of glucose over metal as the important first step of reaction. Indeed, the energy of adsorption of glucose directly on Au was calculated stronger than that of OH on the same metal [30]. On the other hand, the interaction between activated carbon and Au proceeds through electron transfer from carbon to the metal, inferring slightly negative charge on gold. It was reported, that negatively charged gold clusters easily dissociate oxygen [31]. Concurrently, the formation of hydrogen peroxide during glucose oxidation with gold has been reported in base-free [15] besides than in alkali conditions [32]. Comotti *et al.* [32] proved that the generated H_2O_2 would act as an oxidant to oxidize glucose and decompose to oxygen. However, apart from these two consumption reactions, hydrogen peroxide could also produce hydroxyl ions on the surface of Au by a series of chain reactions [33]. The later closes all possibilities for the oxidation mechanism in base-free conditions.

It is also the place to consider the role of carbon in the reaction. The activated carbon possesses a diversity of oxygen containing groups being the more important the phenolic groups which could influence by itself or when situated in the vicinity to gold particles the apparent reaction rate. Our blank test (using only activated carbon in the same reaction

conditions) show 8% of glucose conversion but without any detectable product formation, suggesting only glucose adsorption on the catalyst surface at this temperature.

6.1.3.3. Recycling study: results and discussion

The catalytic performance of three selected AuC catalysts has been used for the study recycling. All possible deactivation causes as gold leaching, sintering and chemical poisoning (active sites blocking by reaction intermediates) are contemplated and related to the variation of the initial gold particle size. The viability of some catalyst treatments between the operation cycles aiming to recover the initial activity have been also investigated.

The samples were chosen on the basis of their size disparity, avoiding those samples with no spherical shapes. Thereby, three samples were selected: AuC X, AuC III and AuC XII. Within the samples, the used PVA:Au ratio during the synthesis is kept the same, 0.85, meanwhile the $NaBH_4$:Au is varied from 3 to 5 and 10, respectively (see Table 5.6., Chapter 5).

The real gold loading measured by ICP and the mean particle size deduced from TEM of fresh and spent samples are presented in Table 6.3.

The catalyst activity of all samples at every cycle, expressed as glucose conversion, is shown in Figure 6.13. (a). The calculated carbon balance ranges between 86 and 95 % (first vs. last cycle) indicating possible non-accumulative adsorption of reactants or intermediates after the first cycle. The gluconic acid selectivity on the base of liquid non-adsorbed products was found 100% and will not be discussed from now on.

Table 6.3. Gold metal loadings and particle size for fresh and spent catalysts.

Sample	Au wt.% (fresh),	Au, wt.% (spent 4th cycle)	Au particle size, nm (fresh)	Au particle size, nm (spent 1st cycle)	Au particle size, nm (spent 4th cycle)
AuC_X	2.2	1.9	16.1	n.m.	20.4
AuC_III	2.4	1.9	8	17	16.6
AuC_XII	2.3	1.9	4.8	8.9	7.7

n.m. not measured

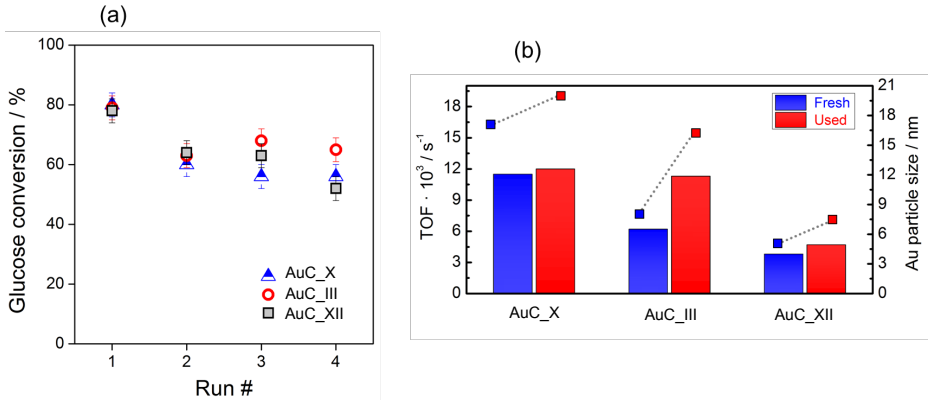

Figure 6.13. a) Glucose conversion on fresh and spent catalysts under 4 reaction cycles b) TOF (bars) and particle size (points) comparison in 1st and 4th cycles on fresh and spent catalysts.

No matter the gold particles size similar glucose conversions are obtained in all first cycles neighboring 80%. Systematically, the second cycle gives always less conversion than the first one, being the difference in the range of 20-25 %. The performed blank test with activated carbon shows that at this temperature only 8% of glucose could be adsorbed on the carbon surface and false the initially calculated glucose conversion. Anyway, the deactivation of the catalyst between the 1st and the 2nd cycle occurs unequivocally. It is also observed very similar 2nd and 3rd cycles and slightly different 4th cycle. The sample AuC_XII shows continuous decrease of

glucose conversion, while the AuC_X and AuC_III stabilized after the initial loss of activity. Nevertheless, from statistical point of view, within the series of samples only AuC_III behave differently (Figure 6.13. (a)).

The reasons for deactivation could be assembled in two groups, those altering directly the active sites, as sintering or metal loss, and those responsible for catalyst blocking or support modifications. The leaching of gold was checked by ICP analysis of the remaining gold on catalyst after accomplished recycling study (Table 6.3.) and in the filtration water before every cycle. No matter the starting catalyst and/or particle size, the same gold loss is detected averaging 15% of the initial gold loading and always the gold loss between 1st and 2nd cycle represents almost 80% of the total leaching.

On the other hand, gold particle size is also influenced (Table 6.3.). The sample AuC X does not change practically its initial particle size, only a slight increase is observed. AuC III and AuC XII doubled their size after the 1st run, after which, the size remains constant in the last two runs. The increase of the average particle size is caused by the identification of some agglomerates that reflect on wider particles distribution, as presented in Figure 6.14., using AuC III as representative sample. The specific activity can be recalculated for the 1st and 4th cycle for all catalysts, considering gold quantity and dispersion (see Table 6.2.). The estimations of the gold dispersion and specific activity in the 4th cycle compared to those in the 1st one are presented in Table 6.4.

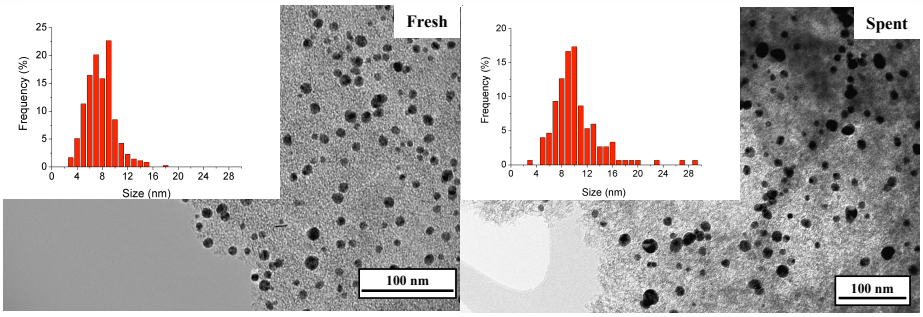

Figure 6.14. Representative TEM micrographs and gold size distributions for fresh and spent (4th cycle) AuC III samples.

Table 6.4. Gold particles dispersion and TOF for the fresh and spent samples (1st and 4th cycle of operation).

Sample	Au dispersion fresh, %	Au dispersion spent, %	TOF*10^3 (fresh), s^{-1}	TOF*10^3 (spent 4th cycle), s^{-1}
AuC X	9	7	11.5	12.0
AuC III	16	9	6.2	11.3
AuC XII	27	18	3.8	4.7

It is clear, that gold particle size increases during the 1st cycle of operation resulting in lower dispersion almost for all samples. Although negative influence on glucose oxidation activity for samples with gold particle size superior to 10 nm is reported [34,35] the specific activity in our case shows a maximal placed between 15-20 nm average gold particle size (Figure 6.13. (b). As long as the gold particles neighbor the optimum average size maximum specific activity is achieved. Prati et al. [26] found 7 nm as optimal gold nanoparticle size for uncalcined catalyst, slightly inferior to the size of our best fresh catalyst. This result shows that the observed decrease of glucose conversion is not reflected in a decrease of the specific activity indicating that particle sintering is not of primordial importance as activity inhibitor as the gold loading is for this reaction. Nevertheless, the gold metal particle size must be controlled in a range appropriate for the reaction. Wang et al. [16] found that gold particle size

alteration and leaching is more pronounced in acidic conditions and that a reasonable stability and activity could be achieved by the proper choice of support. However, the use of mineral supports as Al_2O_3 or CeO_2 based materials results in severe gold leaching converting the carbon-based supports in the most appropriate materials for these reaction conditions. The solution of the leaching problem still has to be found either by appropriate changes in the support (porosity and/or surface composition modifications) or by establishing an appropriate gold loading for high specific activity but with low leaching rate.

Outward gold metal state (loadings and size) possible active sites blocking during the reaction is also reported as the main reason for deactivation [16,36]. The surface properties of our fresh and spent catalysts were studied by XPS and DRIFT analysis. At this point, as representative sample, the AuC III is selected owed to the highest changes in specific activity observed for this sample between the cycles (Figure 6.13. (b).

The XPS spectra of fresh and spent (after 4th cycle) AuC III sample are presented in Figure 6.15.

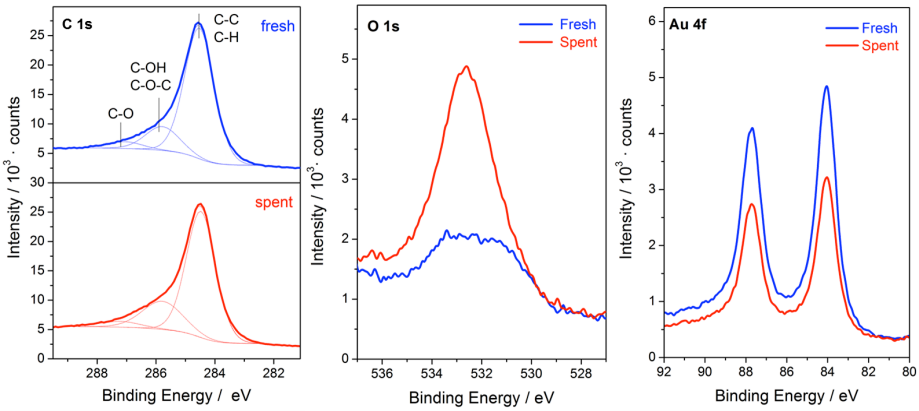

Figure 6.15. XPS spectra of fresh (1st cycle) and spent (4th cycle) AuC_III catalyst.

The C*1s* spectra of the fresh sample can be resolved into three peaks; one corresponding to graphitic carbon C-C sp^2 bond located at 284.5 eV, one of C-O single bond of phenols and esters at 285.8 eV and the C=O double bounded oxygen in ketones and quinones contribution at 287.0 eV. The three types of carbon are presented in the original activated carbon sample. After the 4th cycle the carbon contributions could be assigned also to the same groups, with major difference being observed for the second group. The relative contribution of the organic carbon issued from phenols and esters increases together with the O/C ratio (0.045 vs. 0.13 for fresh and spent sample, respectively). This increase could be related either to the oxidation of activated carbon surface or to the adsorption of some reaction products. The O*1s* of the fresh sample indicates the presence of only one type of oxygen – "organic oxygen" C-O at 532.6 eV found in phenols or esters and this contribution increases dramatically after catalyst recycling. Zope and Davis [36] reported as a possible cause for gold deactivation, low catalyst tolerance to strongly adsorbed ketones, enones or compounds with β-dicarbonyl structure issued from highly oxygenated biomass derivatives with OH groups bounded to the secondary C atoms. Those intermediate species interact eventually and adsorb strongly on the catalyst surface, producing active sites blocking. However, no oxygen contributions assigned to the C=O groups were observed in our XPS spectra indicating at this step, the absence of ketones on the surface. The activated carbon surface is just enriched in oxygen at the end of reaction.

On the other hand, the gold surface distribution, in both beginning and end of the reaction, shows the presence of metallic gold confirmed by the corresponding $4f_{5/2}$ and $4f_{7/2}$ transitions situated at 87.8 and 84.0eV, respectively. The Au/C and Au/O atomic surface ratio decreases from fresh to spent catalyst (0.016 to 0.009 and 0.35 to 0.07) indicating in the

first case gold particles size agglomeration (confirmed by TEM) and in the second one that the oxygen surface distribution originates more probably from the intermediates presence and not from oxidized gold metal centers.

In order to estimate the role of intermediates in catalyst's poisoning and possible ways for regeneration, different treatments (H_2O, 0.1M NaOH, calcination in static air at 300ºC or no treatment) were carried out over representative sample, AuC III. The results expressed in glucose conversion are presented in Figure 6.16.

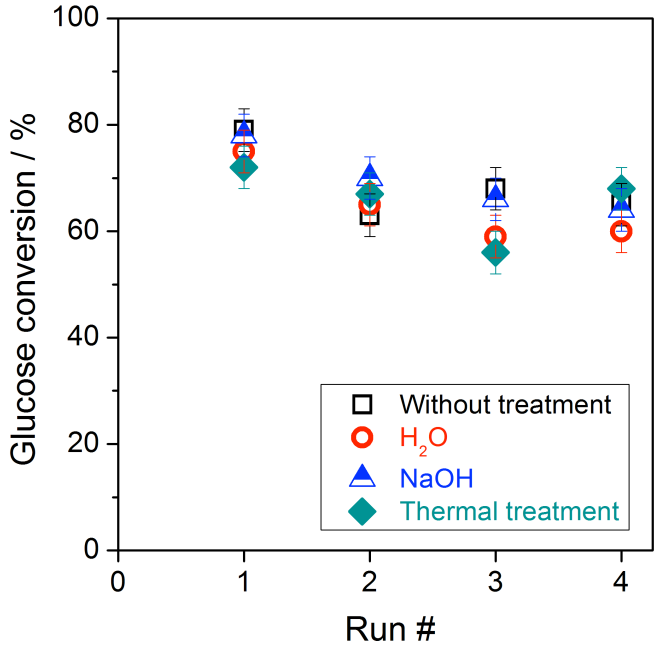

Figure 6.16. Activity of the AuC III sample after various regeneration treatments.

The analysis of the results leads to the conclusion that the treatments between the cycles do not influence excessively the catalyst performance. With or without treatments, the 2nd cycle is always affected negatively and no recuperation of initial activity is observed. Figure 6.17. presents the DRIFT spectra recorded to estimate the changes induced on the catalyst

surface during the first cycle of operation and during the regeneration treatments. In order to discern all formed or adsorbed species, the difference DRIFT spectra taking as a reference the fresh sample are considered.

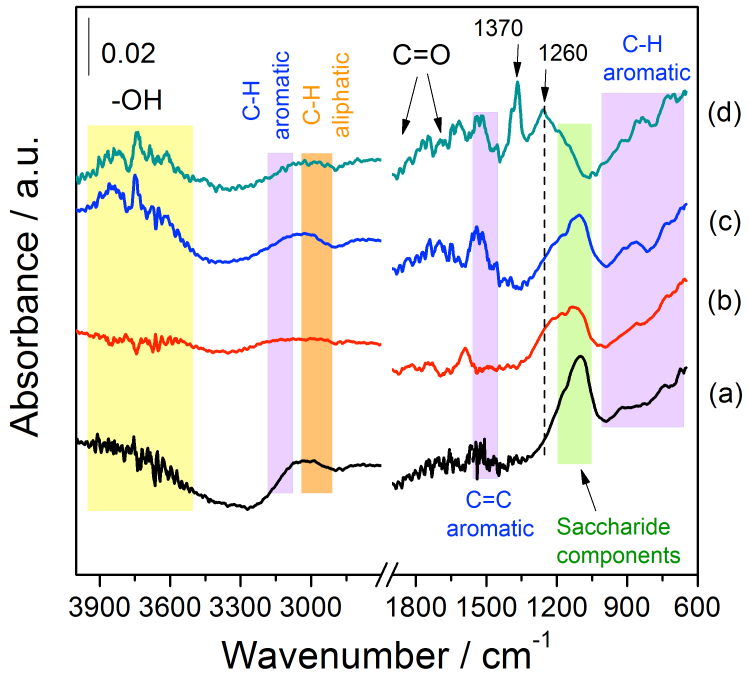

Figure 6.17. Difference DRIFT spectra (spent vs. fresh) under different regeneration treatments: (a) without treament, (b) H_2O, (c) NaOH and (d) thermal treatment.

As can be observed, the DRIFT spectra of the spent untreated catalysts clearly show the presence of adsorbed species or modification of the carbon support resulting after glucose oxidation. According to the literature data, all spectral features in the 900-650 cm^{-1} region could be attributed to the C-H out of the plane aromatic compounds vibrations, the bands in the 3100-3000 cm^{-1} region to the C-H ring stretching vibration, the bands in the 3000-2800 cm^{-1} region to the C-H aliphatic species stretching vibration and the bands in the 1600-1450 cm^{-1} region to

the ring carbon-carbon stretching vibration, all caused by the presence of activated carbon [37,38]. In addition, the broad band with several contributions observed in the 1150-1050 cm^{-1} region could be assigned to the presence of polysaccharide (highly oxygenated) compounds [39]. Also bands in the 1600-1850 cm^{-1} range are observed and attributed to the C=O stretching vibration of carbonyl groups in aldehydes, ketones, carboxylic acids, esters or acid anhydrides [40–42]. Both regions (1150-1050 cm^{-1} and 1600-1850 cm^{-1}) indicate the presence of intermediates and/or products adsorbed on the catalyst surface. The pronounced broad band in the 3900-3500 cm^{-1} indicates the presence of hydrogen bonds involved –OH groups. The assignment in this region, however, is of complex nature, since it includes contributions from various groups.

After regeneration, the samples treated with water and NaOH present similar bands to the untreated spent catalyst. Only a slight modification in the –OH stretching region seems to occur upon NaOH treatment. The saccharide like compounds remain adsorbed on the surface upon water and NaOH treatment. By contrast, the thermal treatment lead to polysaccharide bands vanishing and the appearance of two new bands. The first broad band centered at 1260 cm^{-1} could be assigned to the C-O stretching modes typical for ester/ether bridging groups, phenols and lactones [38] and the second at 1370 cm^{-1} to δ O-H vibrations and ν C=O vibrations [43]. The thermal treatment transformed the adsorbed polysaccharide species into new oxygen-containing compounds. Those compounds could result either from the subsequent oxidation of the initially adsorbed species or from the modification of the support and from its oxidation during the calcination treatment in static air. Therefore, it could be concluded that the adsorbed species during the reaction, strongly adsorbed on the catalyst surface, could not be removed without thermal treatment. Nevertheless, nor soft chemical treatments (H_2O and

NaOH) nor harder calcination treatment can regenerate the initial state of the catalyst. The adsorbed and remaining species on the surface formed after the 1st run (H_2O, NaOH or thermal treatments) do not change the catalyst activity (similar 2nd, 3rd and 4th cycle) indicating that nor the adsorbed intermediates nor the modification of the support play important role in catalyst deactivation. The similar 2nd, 3rd and 4th cycles demonstrate also that the presence of adsorbed intermediates or modifications of the support does not inhibit the reaction. It seems that gold metal state, i.e. gold particle size variation and metal leaching, is the most important parameter inducing loss of activity. On one hand the particles agglomeration could result in beneficial optimal particle size and specific activity increase (AuC III). And on the other, the leached gold participates in the reaction with around 10% conversion increase between the 4th and the 18th hour of reaction (see Figure 6.10. in the present Chapter) which together with the 8% of glucose adsorption on activated carbon accounts for the 20% of glucose conversion decrease between the 1st and the 2nd cycle. All this leads to the conclusion that the most important problem to solve is gold metal leaching.

This statement leads to the assumption that the carbon support is not a key parameter in this reaction and that the glucose oxidation occurs only on low defect surface gold particles with preferable average size of 15-20 nm. Ishida et al. [34] also suggested that the glucose oxidation reaction occurs preferably on gold particles surface and not on the gold/support interface or support. Our observations also support this idea, as the most important deactivation is produced by the gold state change.

6.1.3.4. Partial conclusions

Gold colloids particle size is influenced by the stabilizing and reducing agent/Au ratio. Two limiting values were found for stable colloid production and homogeneous particles size distribution: the PVA/Au ratio superior to 0.85 and $NaBH_4$/Au superior to 3.

The immobilization of colloids on the carbon support surface is effective and the resulted gold loading are similar to the nominal value. A series of Au/C samples with similar gold contents (close to 2% wt), gold particle shape (spherical) and narrow gold size distribution were prepared. After calcination treatment, an increment in the average gold particle size is observed, although a good correlation between colloids and supported gold particle sizes maintained.

All catalysts show very good activity in the oxidation of glucose under base free mild conditions with 100% selectivity to the desired product gluconic acid. The structure/size sensitivity shows optimal size for maximum conversion of around 9 nm, although the normalization to exposed surface gold atoms (TOF) moves this optimum to the 15-20 nm range, pointing to possible influence of the glucose adsorption step in the reaction mechanism.

Regarding the stability study, the recycling reveals that deactivation occurs after the 1st cycle independently on the initial gold particle size. Gold leaching is confirmed as primary reasons for catalyst deactivation. Also gold particles agglomeration occurs and results beneficial for the specific activity improvement when the size enters the optimal average. On the other hand, the support nature, its chemical state or adsorbed species do not seem to be very important. All reactivation treatments result in the same activity trend indicating that the catalyst operation is not affected by intermediates adsorption, removal or support modification. Therefore,

every loss of activity is due to gold metal leaching after the 1st cycle and when the leaching stops the activity remains constant (2nd, 3rd, 4th cycle).

6.1.4. General conclusion on the base-free oxidation of glucose

It has been demonstrated that gold nanoparticles are highly active and selective for the aerobic oxidation of glucose at anomeric position, even in absence of base. Both, support nature and gold particle size influence the overall process, as concluded in each section, respectively. No matter the group of catalysts gold leaching remains the main problem to be solved for gold supported on mineral oxides. The choice of partially hydrophobic support, as is the case of active carbon, reduces the leaching significantly, with gold loss observed only in the first cycle of operation.

6.2. HMF oxidation to FDCA

6.2.1. Introduction

Among the involved transformation of the lignocellulosic fraction into valuable chemicals, an important role is played by furfural derivatives with functional groups in position five [44,45]. Indeed, the 5-hydroxymethyl-2-furfural (HMF) molecule is considered a versatile platform chemical [46,47], directly produced from the six carbon sugars, via isomerization-dehydration reactions [48–50]. It is key precursor for the synthesis of many chemicals among which stand out those for fuel applications and polymers industry [51–53]. The dehydration of glucose/fructose towards HMF production was explained and studied over the POM-IL hybrids in Chapter 4.

The selective oxidation of both alcohol and aldehyde functions of the HMF molecule (see oxidation reaction network in Scheme 6.2.) leads to the formation of 2,5-furandicarboxilic acid (FDCA), which belongs, according to the US Department of Energy, to the top 12 high-potential bio-based products [54,55]. Actually, FDCA is considered as a possible replacement monomer of the terephthalic acid, used to produce polyethylene terephthalate (PET), to produce polyethylene furandicarboxylate (PEF) technology applied by Avantium [56]. Gandini *et al.* have shown that FDCA based polymers have many properties similar to PET [57]. Scheme 6.3. shows the structural similarity of terephthalic acid and FDCA.

FDCA is also a key intermediate for the synthesis of other polymers, fine chemicals, pharmaceuticals and agrochemicals [47,58,59].

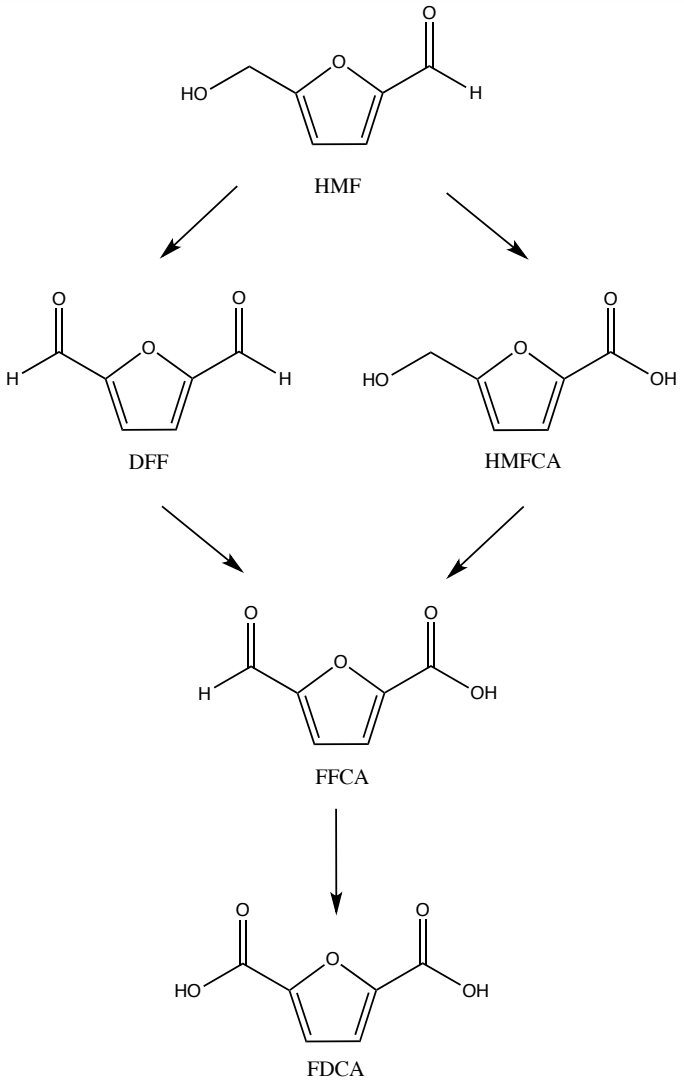

Scheme 6.2. General reaction network for HMF oxidation

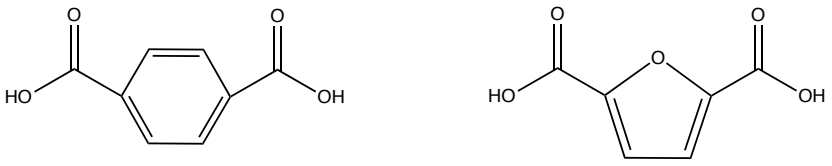

Terephthalic acid FDCA

Scheme 6.3. FDCA as a potential biorenewable replacement monomer for terephthalic acid in polyethylene terephthalate (PET) plastics.

The synthesis of 2,5-furandicarboxilic acid from 5-hydroxymethyl-2-furaldehyde has been widely studied during the last decades, using different catalysts and reaction conditions. The stepwise heterogeneously catalyzed transformation of HMF to FDCA using molecular oxygen is highly desirable [59], avoiding the need for stoichiometric oxidants such as $KMnO_4$ and homogeneous processes [60–62]. Recently, gold-supported catalysts were found to be very active for HMF oxidation to FDCA with many efforts focused in searching the best supports and reaction conditions to improve FDCA yield [63,64]. The base addition necessity as promoter is good established, expanding as general requirement for gold catalyzed alcohol oxidations [65,66]. Further, some investigations over Pt/TiO_2 [64] show that, if the reaction is carried out without addition of base, the process is blocked due to the precipitation of the formed carboxylic compounds under acidic conditions. Nevertheless, the strong alkali conditions needed in some cases to promote HMF oxidation (even 20 equivalents of NaOH) could make the process highly corrosive. For this reason, the development of more efficient catalyst in low base concentration are extremely recommended.

On the other hand, some studies suggests that support composition and a good metal-support interaction [67] plays an important role in the process, influencing FDCA yield [58,64]. As for the gold particle size, there is a lack of studies correlating it with the catalytic activity. However, a particle size ranging 2-7 nm is widely accepted as appropriate/optimum size.

It is well known, that both, metal-support interaction and particle size are strongly influenced by the preparation method. To the best of our knowledge, there are no studies applying DAE method for gold catalysts synthesis in this field. In most cases, performed colloidal particles are transferred to an oxidic carrier and then the solid is dried. The calcination step is often avoided to prevent nanoparticle sintering, nevertheless, the

presence of surfactants in the final solid difficults a proper metal-support interaction, affecting the catalytic behavior.

In this chapter section, the catalytic activity of several gold supported catalysts is evaluated for the selective HMF oxidation under mild conditions using molecular oxygen as oxidant.

Firstly, several gold supported on metal oxides are screened, using γ-Al_2O_3, CeO_2 as simple oxides and CeO_2(20%wt)/Al_2O_3, CeO_2(25%wt)/ZrO_2, and CeO_2(50%wt)/ZrO_2 as mixed oxides, the same catalysts presented in the first section of this Chapter. The influence of the support nature, HMF/NaOH ratio and reaction time on the product yield and distribution will be discussed in details. The catalyst stability is also assessed by repeated cycles under the same operation conditions.

Secondly, following the same structure to the proposed in "glucose oxidation section", representative gold on carbon catalysts with different particle sizes are studied, being the later directly correlated with the catalyst' activity and product distribution.

6.2.2. Experimental

The catalytic experiments in this chapter were performed during a research-training period of three months spend in the University of Bologna, Italy under the supervision of Prof. S. Albonetti.

The oxidation of HMF was performed in an autoclave reactor of 100 mL capacity, provided with a mechanical stirrer (0-600 rpm) and measurement tools for temperature and pressure. The reactor was charged with an aqueous solution of HMF (aprox. 25 mL), the necessary amount of NaOH and the catalyst in a HMF:Au:NaOH of 1:0.01:2.

Before test, the reactor was purged two times with pure O_2 (10 bar) and finally pressurized to 10 bar. Temperature was gradually increased to 70

ºC and the reaction mixture was stirred at approximately 400 rpm for 4 hours. The reaction starts (t = 0) when the temperature reached 70 ºC (about 10 min). After 4 hours, the reactor was cooled down to room temperature in ice bath and the reaction mixture centrifuged and filtered. After that, a sample was taken and diluted before analysis in Agilent Infinity 1260 liquid chromatograph equipped with a DAD detector and an Aminex HPX-87H 300 mm × 7.8 mm column using 0.005 M H_2SO_4 as eluent. The specific operation conditions are summarized in Chapter 2, Analytical methods section. As an example, typical chromatograms obtained during the oxidation analyses are shown in Figure 6.18. Each sample is detected at its own maximum absorbance wavelength, which is indicated in Table 6.6. Each compound has its own retention time with the exception of FDCA and BHMF. The later is formed when secondary reactions take place. All involved process taken into account are explained in the next section.

Table 6.6. Maximum absorbance wavelength for the calibrated compound.

Compound	Wavelength (nm)
HMF	284
DFF	284
FFCA	284
HMFCA	251
FDCA	264
BHMF	223

Stability studies carried out with the spent samples, were recovered from the post reaction mixture and dried at 120 ºC overnight. The HMF:Au:NaOH molar ratio was always constant. Conversion, selectivity and yield were calculated from the peak areas, after calibration using

reference commercial samples, according to the following equations (taking *FDCA* as example):

$$Conversion\ (\%) = \frac{[HMF]_F - [HMF]_I}{[HMF]_F}\ x\ 100 \qquad \text{Eq. 6.2.}$$

$$FDCA\ Selectivity\ (\%) = \frac{FDCA\ mols}{HMF\ mols_I - HMF\ mols_F} x\ 100 \qquad \text{Eq. 6.3.}$$

$$FDCA\ Yield\ (\%) = \frac{Conversion}{100} x\ Selectivity \qquad \text{Eq. 6.4.}$$

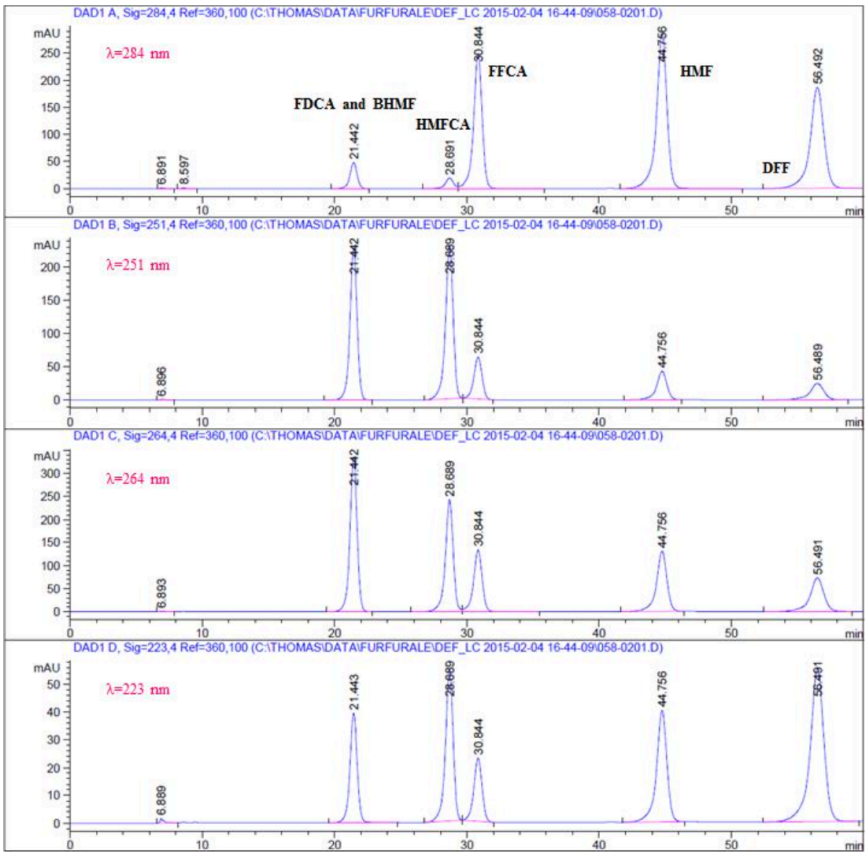

Figure 6.18. Typical chromatograms displaying the retention time of the compounds and wavelength of detection.

6.2.3. Gold supported on metal oxides: influence of support

6.2.3.1. Catalytic activity: results and discussion

The basic media required for HMF oxidation provides the perfect decor for different secondary reactions. HMF possesses different functionalities being the presence of alcohol and aldehyde groups the most important ones. Aldehydes with ∝-hydrogen(s) undergo self-condensation on warming with dilute or mild base to give β-hydroxy aldehydes called aldols. This transformation is widely known as aldol condensation and it is catalyzed by bases. Nevertheless, in presence of strong base, the aldehydes without ∝-hydrogen(s) (non-aldolizing aldehydes), as in our case, undergo disproportionation (self oxidation and reduction), also called Cannizzaro reaction. Scheme 6.4. shows the Cannizzaro reaction of HMF to 5-hydroximethyl-2-furancarboxilic acid (HMFCA) and 2,5-Bis(hydroximethyl)furan (BHMF).

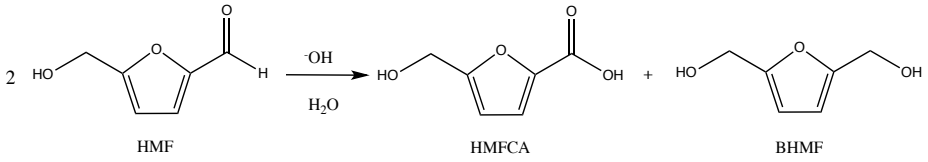

Scheme 6.4. Cannizzaro reaction of HMF under inert atmosphere in the presence of a base

In the reaction conditions described above, the degradation of pure HMF to HMFCA and BHMF cannot be ignored, Figure 6.19 [67]. The blank experiments carried out by Albonetti *et al.* evidenced that significant amount of HMF degrades in base conditions, 40% of HMF conversion is reached after 10 min at 70 ºC, without formation of oxidation products. The reaction mixture turns from colorless to yellow and then to red with the time. After 30 min, total HMF conversion is observed. The formed

degradation products are soluble in water at high pH (pH = 13) and insolubles in acidic conditions.

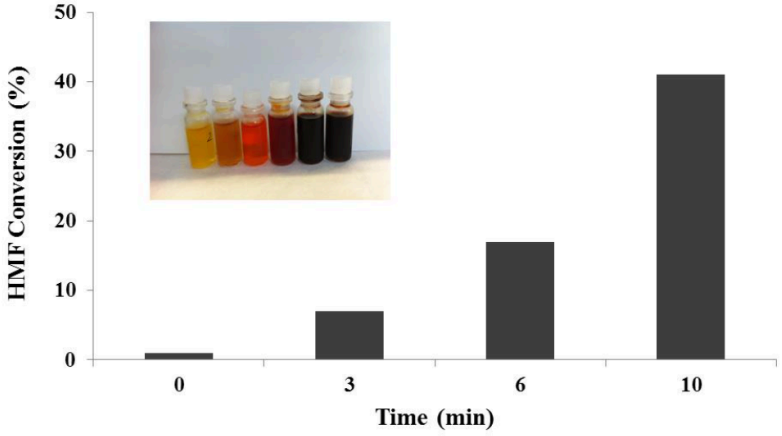

Figure 6.19. Effect of reaction time on HMF degradation. Reaction conditions: no catalyst, atmospheric O_2 pressure, 70 ºC, ambient pressure, HMF:NaOH 1:4 molar ratio. Adapted from Ref [67]

The later accounts for the formation of high molecular weight compounds, commonly called humins, as a result of multiple aldol condensations. The HMF molecule and derivatives do not present ∝-hydrogen(s) and the mechanism of humins formation in basic conditions is different to that in acidic media, which goes through furan ring hydrolysis and opening [68]. In a recent study Besson *et al.* also proposed that the formation of polymers occurs via Cannizzaro reaction in basic media as shown in Scheme 6.5. The products of the Cannizzaro reaction join further to form polymeric products when the temperature increase. Only the products formed at low temperature corresponds to those of the disproportionation reaction.

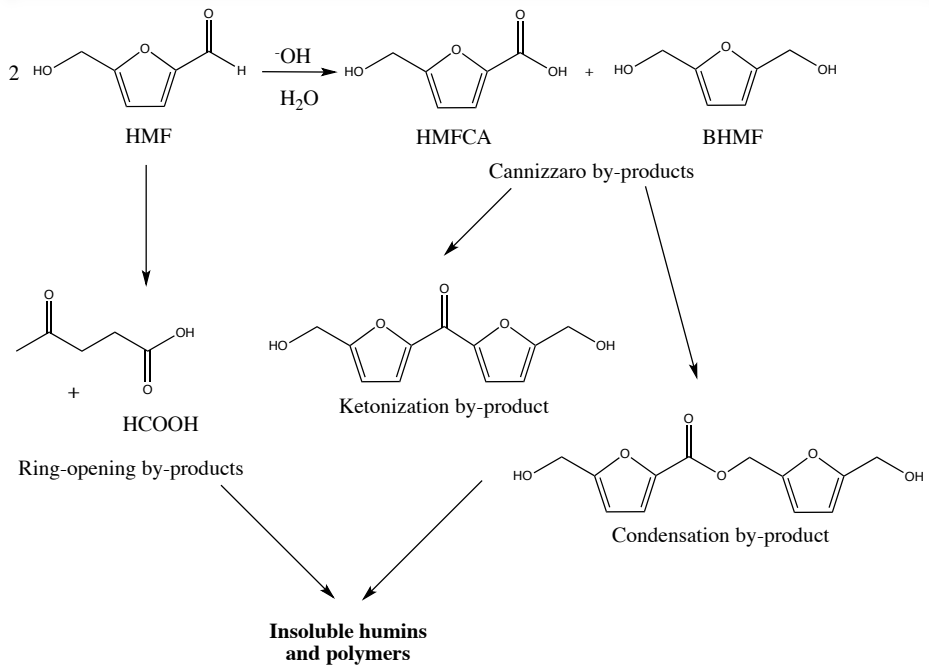

Scheme 6.5. Possible pathways of HMF degradation products during HMF oxidation at high temperature in presence of strong added base. Adapted from [64]

The scientific literature extensively reports the positive effects of the homogeneous base addition during HMF oxidation. Certainly, the HMF oxidation rate depends significantly on the presence of NaOH, and the later seems to promote the formation of 5-hydroxymethyl-2-furancarboxilic acid (HMFCA), which is further oxidized to 5-formyl-2-furancarboxilic acid (FFCA) and then to 2,5-furandicarboxilic acid (FDCA) [69]. However, in absence of active catalyst, the basic environment leads to the formation of the above-mentioned by-products. Therefore, it is important to develop an active catalyst that rapidly oxidizes HMF to intermediate products, avoiding their fast degradation in reaction conditions.

The first catalytic tests were carried out over AuAl sample and the effect of NaOH/HMF molar ratio (Figure 6.20) was studied. The HMF

conversion reaches 100 % after 4 hours of reaction, no matter the quantity of added base. However, unlike the conversion the product yields are completely dependent on NaOH amount, an effect already reported in the litterature [56,59,67,70]. The HMF transforms immediately in oxidation products only the disproportionation does not occur and the resulted solutions are clearly yellow (see Figure 6.20.) with carbon balances close to 100 %, accounting for the efficiency of the catalyst.

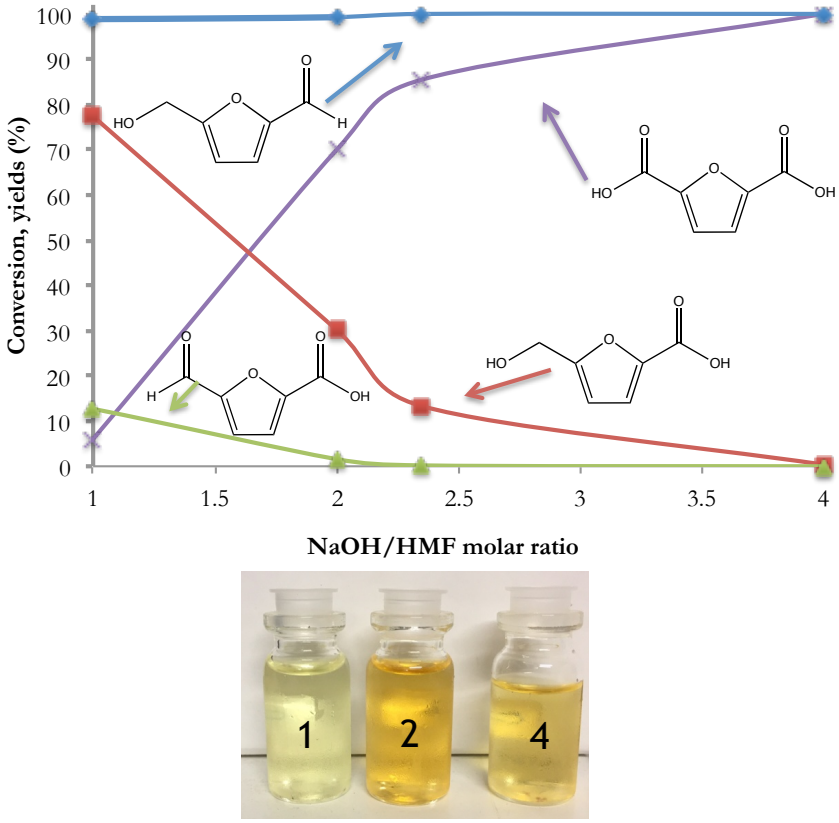

Figure 6.20. Conversion and product yields over AuAl catalysts at different NaOH/HMF molar ratio. Post reaction mixtures after catalyst separation, NaOH/HMF molar ratio of 1, 2 and 4.

Reaction conditions: HMF:Au molar ratio 100:1, 10 bar O_2, 70 ºC, 400 rpm, 4h.

As NaOH to HMF quantity increases, the first oxidation step towards HMFCA is promoted and the final FDCA yield results higher. The intermediate oxidation product, FFCA, is practically undetectable, due to its fast oxidation to the final FDCA. It was reported that the formation of HMFCA is a very fast reaction, while the subsequent transformation of the hydroxyl to aldehyde group is slower [58]. Therefore, the rate-limiting step will be the oxidation step from HMFCA to FFCA.

Two possible oxidation routes are possible for HMF oxidation (see Scheme 6.2.). HMFCA appears because of first step aldehyde selective oxidation, whereas DFF is formed by the oxidation of the HMF's alcohol group. During the reaction, DFF was not observed, suggesting that the reaction occurs via HMFCA formation (Scheme 6.6.). The later is also concordant with previous studies in presence of gold catalysts [56,70]. In fact, the formation of DFF is reported for Pd and Ru based catalysts used in absence of a base [71–73].

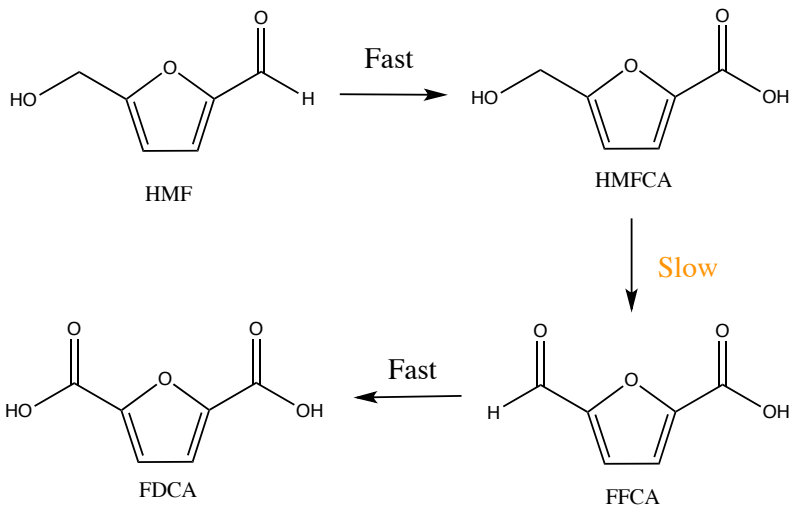

Scheme 6.6. Products of HMF oxidation via HMFCA

The real interest of the NaOH/HMF study comes from the detected final FDCA yield. Total conversion with >99 % FDCA yield is achieved by

using 4 equivalents of NaOH for 4 hours at only 70 ºC. To the best of our knowledge, this is the best result obtained over monometallic gold.

On the other hand, FDCA yield of 70 % is reached with only two NaOH equivalents, a result from comparable to better to other reported catalytic systems using large amount of base. The later demonstrates the excellent viability of Au/Al catalyst at this stage in terms of FDCA yield in low-corrosive conditions.

As the main goal of this study is to understand the effect that can produce the support nature on the overall catalytic activity, the NaOH/HMF ratio was decreased to 2 in order to achieve detectable differences between the samples. From this point all experiments are performed at HMF:Au:NaOH molar ratio of 1:0.01:2.

A typical reaction profile is shown in Figure 6.21., where HMF conversion and products yield are plotted as a function of the reaction time over AuAl catalyst at 70 ºC. In these conditions, a 100 % of conversion is achived after 10 min of reaction, being the HMFCA yield 94% with 4% FDCA yield. The later suggest that the HMF conversion complete in less than 10 minutes, since part of the formed HMFCA undergoes further oxidation. This observation is consistent with the described above, the HMF oxidation to HMFCA is a fast process and finishes in ten minutes. Moreover, no by-products are formed, confirmed by the calculated carbon balance.

From this time to the end of reaction (240 min), progressive oxidation of the hydroxyl group is taking place which, once oxidized to aldehyde, is rapidly converted into dicarboxylic acid, as deduced by the FFCA absence (FFCA yield around 1 %). As shown in Figure 6.21. the solution color also accounts for the progress of FDCA formation in a way that less colored the solution more FDCA is formed. Again, no byproducts are observed suggesting that the rapidly produced HMFCA (in 10 min) is

stable in basic conditions and does not suffer any degradation. Certainly, only aldehydes undergo Cannizzaro reaction, thus only HMF and FFCA could undergo self-oxidation reduction process. Nevertheless, the fast oxidation of FFCA to FDCA prevents FFCA degradation, being the process of byproduct formation only attributed to the HMF molecule. Therefore, once the HMF disappears from the basic media, the probability of Cannizzaro and further polymerization reactions decreases exponentially.

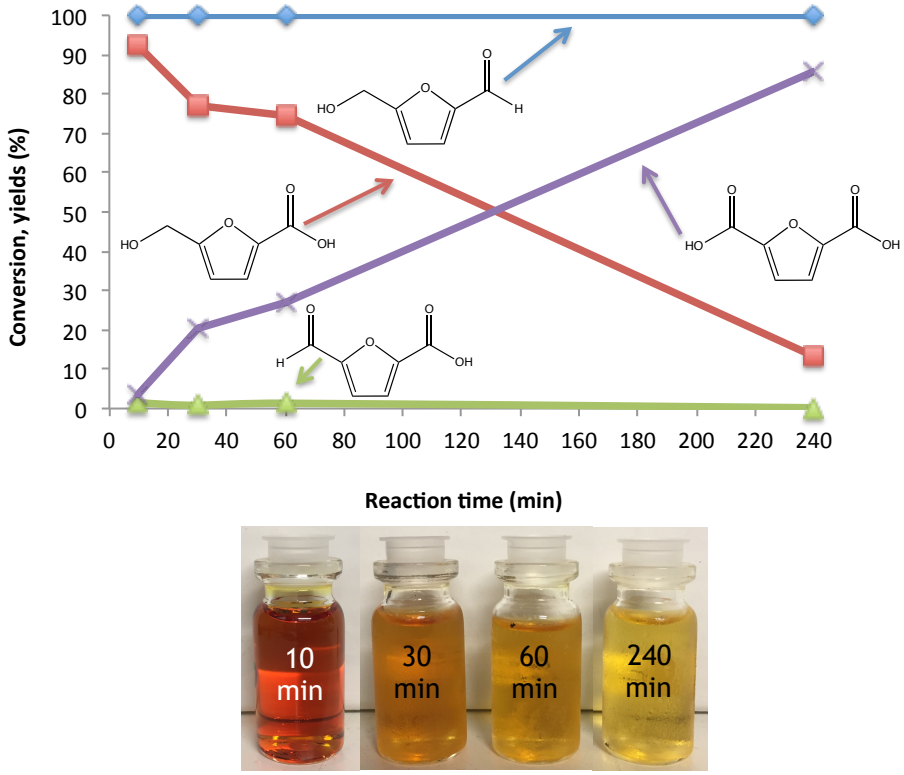

Figure 6.21. Conversion and product yields over AuAl catalysts as function of the reaction time (samples imaged at 0, 30, 60 and 240 min.)
Reaction conditions: HMF:Au:NaOH molar ratio 1:0.01:2, 10 bar O_2, 70 ºC, 400 rpm.

At this point, it is interesting to evaluate the possible contribution of the bare support to the reaction. Table 6.7. compares the HMF conversion

and product selectivity over AuAl, bare Al and in absence of support at the same reaction conditions. The comparison between AuAl and Al (Table 6.7. entries 1 and 2) shows clearly that without gold the oxidation reaction is virtually inexistent, leading to very low HMFCA selectivity (8%) and high byproducts selectivity (92 %) for 57% of HMF conversion. These results are very similar to those obtained without catalyst for the blank experiment in the same reaction conditions (Table 6.7. entry 3). Therefore, it is possible to affirm that the support is not contributing to the overall oxidation process in a separate manner in absence of gold.

Table 6.7. Comparison of the selectivity to different products over AuAl, bare Al and in absence of catalyst

Entry	Catalyst	HMF conversion (%)	HMFCA selectivity (%)	FFCA selectivity (%)	FDCA selectivity (%)	Byproducts selectivity (%)
1	AuAl	100	29	1	70	0
2	Al	57	8	0	0	92
3	None	67	8	0	0	92

Reaction conditions: HMF:NaOH 1:2, 70 ºC, 10 bar O_2, 240 min, 400 rpm

On the other hand, it is also important to take into account that some gold leaching could occur like for the glucose oxidation reaction. In such a case, lixiviated gold could catalyze HMF (or intermediates) transformation. In order to check this possibility, a leaching test was carried out in the standard reaction conditions used above (Figure 6.22.). In this experiment, the reaction was cooled down after 1 hour of reaction, the mixture was centrifuged and then microfiltered to ensure that no catalyst remains in the liquid. The first sample was measured by HPLC at this moment. After that, the reactor was charged again and the oxygen was re-introduced following the same protocol. The mixture reacted the

remaining 3 hours to reach a total reaction time of 4 hours. As deduced from Fig. 6.22., no conversion and product yields changes were observed, both remain constant and confirm the absence of activity of gold possibly dissolved in the solution. XRF analyses of the post reaction mixtures indicates absence of gold loss and only a traces of Al_2O_3 were observed in the mixture, accounting for slight support dissolution.

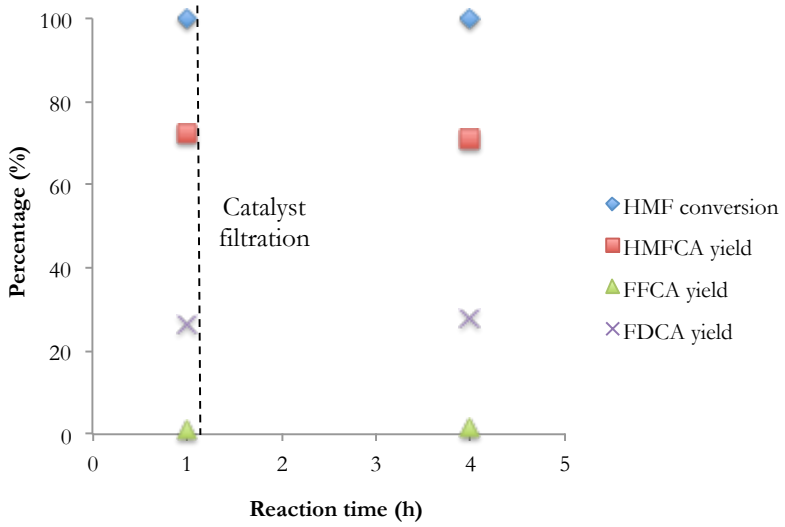

Figure 6.22. Leaching test. Reaction conditions: HMF:Au:NaOH molar ratio 1:0.01:2, 10 bar O_2, 70 ºC, 400 rpm. After 1 h, the catalyst is removed, O_2 re-introduced and the mixture re-reacted.

The influence of the support on catalyst' performance was investigated over AuCeAl, AuCe, AuCe50Zr and AuCe25Zr catalysts (Figure 6.23.). The HMF conversion is complete in all cases suggesting that the support nature does not influence the HMF conversion. On the contrary, clear influence of the support on products yield and distribution appears. On the basis of supports' chemical composition and specific surface area the samples are separated in two groups. AuAl and AuCeAl fit in the first group whereas AuCe, AuCe50Zr and AuCe25Zr, integrate the second.

Within the first group, the presence of ceria seems to promote the FDCA formation, leading to 75 % yield instead of 70 % for AuAl sample. This result is logical since it has been reported that CeO_2 support is particularly effective for the oxidation of alcohols to corresponding aldehyde [74]. In fact, the role of CeO_2 support in gas phase reactions correlates normally oxide' capacity to facilitate oxygen transfer to the metal and to activate molecular oxygen [75].

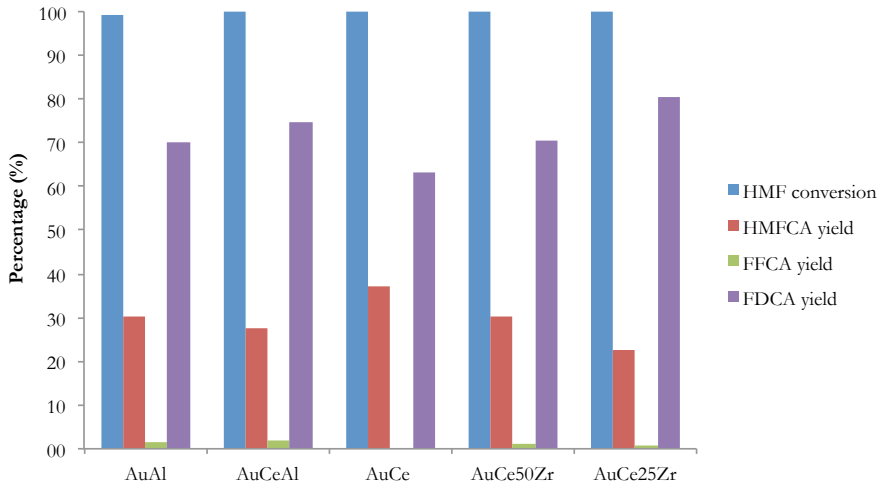

Figure 6.23. Influence of support in the HMF oxidation reaction. Reaction conditions: HMF:Au:NaOH molar ratio 1:0.01:2, 10 bar O_2, 70 ºC, 400 rpm.

A more proper comparison between AuAl and AuCeAl could be done by TOF and reaction rate calculations. However, the calculations with respect to HMF conversion (or converted HMF moles) are meaningless due to the fast and complete conversion. For this reason, a TOF based on FDCA yield is defined, according to Eq. 6.5. In the same way, the reaction rate is taken as the rate of FDCA formation instead of HMF conversion (Eq. 6.6.)

$$TOF\ (s^{-1}) = \frac{moles\ of\ FDCA\ formed}{moles\ Au{*}s{*}dispersion} \qquad \text{Eq. 6.5.}$$

$$r(s^{-1}) = \frac{moles\ of\ FDCA\ formed}{moles\ Au{*}s} \qquad \text{Eq. 6.6.}$$

Table 6.8. summarizes the obtained results. In terms of TOF, the AuAl seems to work better than AuCeAl. However, this comparison is only correct when the particle size of the samples is similar. Therefore, when the difference is significant, the reaction rate should be used. In this case, the velocity of FDCA formation is higher for AuCeAl catalyst, suggesting an collaborative effect between CeO_2 and Au.

Table 6.8. Summary of particles sizes, dispersions and BET specific surfaces of the tested catalysts. Turn over frequencies (see Eq. 6.5.) and reaction rates (see Eq. 6.6.) in the HMF oxidation reaction.

Sample	Average particle size, nm	Dispersion, %	S_{BET} (m^2/g)	TOF, $s^{-1} * 10^2$	Rate, $s^{-1} * 10^3$
AuAl	5.1±1.5	26	187	1.88	4.36
AuCeAl	3.4±0.8	38	158	1.36	5.19
AuCe	3.9±1.5	33	57	0.65	2.19
AuCe50Zr	3.3±1.4	39	55	0.89	4.88
AuCe25Zr	3.9±1.2	33	57	1.6	5.36

As for the second group of samples FDCA yield increases with increasing ZrO_2% in the support. Since the particle sizes of these three catalysts are comparable, TOF value could be used to compare their activity. The AuCe25Zr is the most efficient catalyst, producing 80% of FDCA, followed by AuCe50Zr (70%) and AuCe (63%). This result is also corroborated by the reaction rate calculations, following the same trend.

From the results is clear that the support plays a role in the oxidation reaction and this role is related to the presence of ceria, for the first group, and to the presence of zirconia, in the second group, i.e. depends on the support nature. Within the first group and due to the irreducible character of Al_2O_3, the collaborative CeO_2-Au effect may be tentatively attributed to support' oxygen mobility, as a consequence of Ce^{4+}/ Ce^{3+} fast redox cycles, and oxygen vacancies formation. However, in the second group, this possible effect should couple with other effect, as the observed tendency is the opposite, higher the ceria content lower the selectivity.

The CeO_2 ability to facilitate the oxygen transfer to metal site could indeed influence the activity. This oxygen storage ability is quantified by means of oxygen storage capacity (OSC) and oxygen storage complete capacity (OSCC) measurements. The OSCC offers information about the total oxygen species available within the sample and is estimated from the formed CO_2 during ten consecutive CO pulses. On the other hand OSC corresponds to the most accessible species and is calculated from the average of CO_2 species formed under sample' exposure to consecutive CO – O_2 pulse sequences. The redox processes involved in oxygen storage are:

$$CeO_2 + xCO \rightarrow CeO_{2-x} + xCO_2 \text{ (reduction)}$$
$$2CeO_{2-x} + O_2 \rightarrow 2CeO_2 \text{ (oxidation)}$$

$$Ce_xZr_{1-x}O_2 + \delta CO \rightarrow Ce_xZr_{1-x}O_{2-\delta} + \delta CO_2 \text{ (reduction)}$$
$$Ce_xZr_{1-x}O_{2-\delta} + O_2 \rightarrow Ce_xZr_{1-x}O_2 \text{ (oxidation)}$$

The OSCC measurements expressed in μmol formed CO_2 are presented in Figure 6.24. For the bare supports, the measured temperatures are 200 and 250 ºC, whereas for the catalysts are 70 ºC (the reaction temperature) and 200 ºC (a temperature that allows support/catalyst comparison). As a

general trend, the increase of the temperature increases the OSCC value. The bare support follows the O_2 mobility trend Ce > Ce50Zr > Ce25Zr at 200 ºC and Ce ~ Ce50Zr >> Ce25Zr at 250 ºC. Zirconia presence improves ceria' oxygen mobility and an optimal value for ceria mobility promotion is observed for the Ce50Zr.

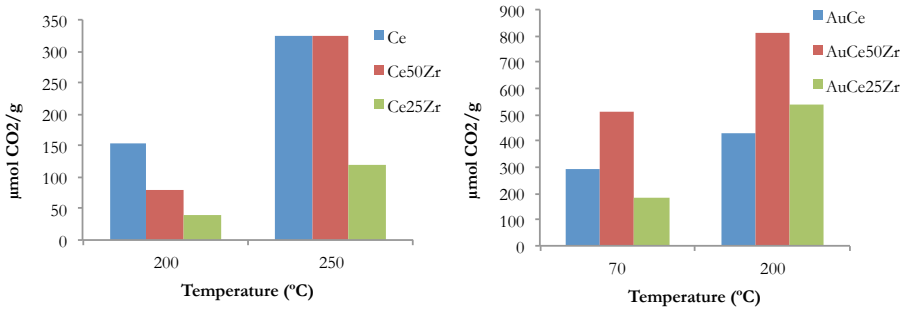

Figure 6.24. OSCC for the supports (200 and 250 ºC) and for the catalysts (70 ºC and 200 ºC)

The oxygen mobility is promoted even more in the presence of gold, being noticeable even at 70 ºC (reaction temperature). Here the tendency differs from that of supports, being AuCe50Zr > AuCe > AuCe25Zr the one at low temperatures and AuCe50Zr > AuCe25Zr > AuCe at high temperatures. The later is consistent with previous studies, in which it was demonstrated that the oxygen storage capacity depends on zirconia content and a maximal value is obtained between 25-50 mol% of Zr [76]. Considering only the OSCC at the reaction temperature (70ºC), the oxygen mobility does not correspond to the observed activity. Although a clear benefit of the ceria presence is deduced for the first group of supports, the opposite is found for the second group. If we consider the information received by the OSC measurements, the number of the

atomic oxygen layers (NL) directly involved in the process can be calculated, according to Eq. 6.7.

$$NL = \frac{OSC_{experimental}}{OSC_{surface}} \quad \text{Eq. 6.7.}$$

where $OSC_{experimental}$ is the that obtained experimentally and $OSC_{surface}$ accounts for the theoretically reducible oxygen on the surface. The $OSC_{surface}$ is calculated by equation 6.8.

$$OSC_{surface}\ \mu molCO_2 g^{-1} = N_0\ x\ S_{BET}\ x\ \frac{1}{N_A}\ x \frac{1}{a^2}\ x\ 10^6 \quad \text{Eq. 6.8.}$$

where S_{BET} is the specific surface area of the sample, N_A is Avogadro's number, a is the ceria lattice parameter (5.413 Å) and N_0 is the number of oxygen atoms of the ceria lattice that participate in the process. This number depends on the exposed CeO_2 lattice planes. In this study an average of the exposed oxygen from the (001), (110) and (111) faces has been assumed for the calculations resulting in a N_0 value of 1. Indeed, only one oxygen is participating in both redox process exposed above. It is worth to clarify that NL < 1 means that only oxygen from the surface is playing a role in the reduction process while NL > 1 indicates the participation of bulk oxygen.

The calculations of OSC are based on the methodology proposed by Duprez *et al.* [77]. More precisely, it is considered that i) only oxygen atoms bonded to cerium participate in the storage process; ii) the surface is homogeneous iii) only one of four oxygen atoms is involved in the storage (CeO_2 → Ce_2O_3 + "O"); and iv) null gold metal contribution to the reduction, e.g. the gold metal cannot re-oxidize. For the OSC

theoretical calculations, the number of surface oxygen atoms and BET area of each sample are considered.

For the supports (Table 6.9.), similar to the OSCC higher the temperature higher the fraction of layer (and therefore the OSC) involved in the reduction. Similarly to OSCC, the OSC decreases in order Ce > Ce50Zr > Ce25Zr at 200 and 250 ºC. The addition of gold changes dramatically the oxygen mobility at 200 ºC (Table 6.10.) as well as the OSC tendency. At reaction temperature, the oxygen dynamics is 16 times higher for AuCe50Zr that for the support at 200 ºC. The trend AuCe50Zr > AuCe > AuCe25Zr, differs from the activity relation. Therefore, although the ability of the support to transfer oxygen could influence the activity, is neither the only one involved factor nor the most important one. It is logical to consider that the catalytic activity is affected by a combination of different factors.

Table 6.9. Oxygen storage capacity (OSC), expressed as (**μ**mol CO_2/g), and number of oxygen layers (NL) for the supports as a function of the temperature.

Sample	OSC 200ºC	OSC 250ºC	NL 200ºC	NL 250ºC
Ce	16.40	67.97	0.05	0.21
Ce50Zr	6.39	28.96	0.02	0.09
Ce25Zr	3.57	14.89	0.01	0.01

Table 6.10. Oxygen storage capacity (OSC), expressed as (μmol CO_2/g), and number of oxygen layers (NL) for the catalysts as a function of the temperature.

Sample	OSC 70ºC	OSC 200ºC	NL 70ºC	NL 200ºC
AuCe	68.57	103.03	0.21	0.32
AuCe50Zr	99.23	332.68	0.32	1.07
AuCe25Zr	58.20	124.88	0.19	0.40

Another determining factor should be the chemical composition and, concretely, the Lewis acid character of the support. Gutiérrez-Ortiz *et al.* [78] demonstrated that the oxidation activity of C_2 chlorohydrocarbons over ceria-zirconia catalysts is function of the Ce/Zr ratio. The results were explained on the base of Lewis acidic sites increase and support' oxygen mobility. In fact, the incorporation of higher amounts of zirconium into ceria lattice shows a complex influence on the acidity of the pure parent oxide. Pure ceria presents the lowest acidity, markedly increased upon zirconia addition and the sample with maximally incorporated zirconia presents the strongest Lewis acidity. On the other hand, Corma *et al.* demonstrated that the collaborative gold-support effect promotes the selective oxidation of alcohols [74]. The proposed mechanism over Au/CeO_2 (nanometric ceria) based on their studies is presented in Scheme 6.7. The interaction between gold and ceria gives rise to an important population of positively charged gold and Ce^{3+}species (step 1). The alcohol or the corresponding alkoxide then react with the Lewis acid sites of Au/CeO_2 to give a metal alkoxide (step 2), which subsequently undergoes a rapid hydride transfer from C-H to Ce^{3+} and Au^{+} to give the ketone and Ce-H (indicated as LA-H in Scheme 6.7.) and Au-H. Upon admission of oxygen into the system and coordination to the

oxygen-deficient sites of ceria, formation of cerium-coordinated superoxide (Ce-OO·) species occurs (step 4) [79]. These superoxide species evolve into cerium hydroperoxide by hydrogen abstraction from Au-H (step 5). The reoxidation of Ce^{3+} to Ce^{4+} and the release of water close the catalytic cycle.

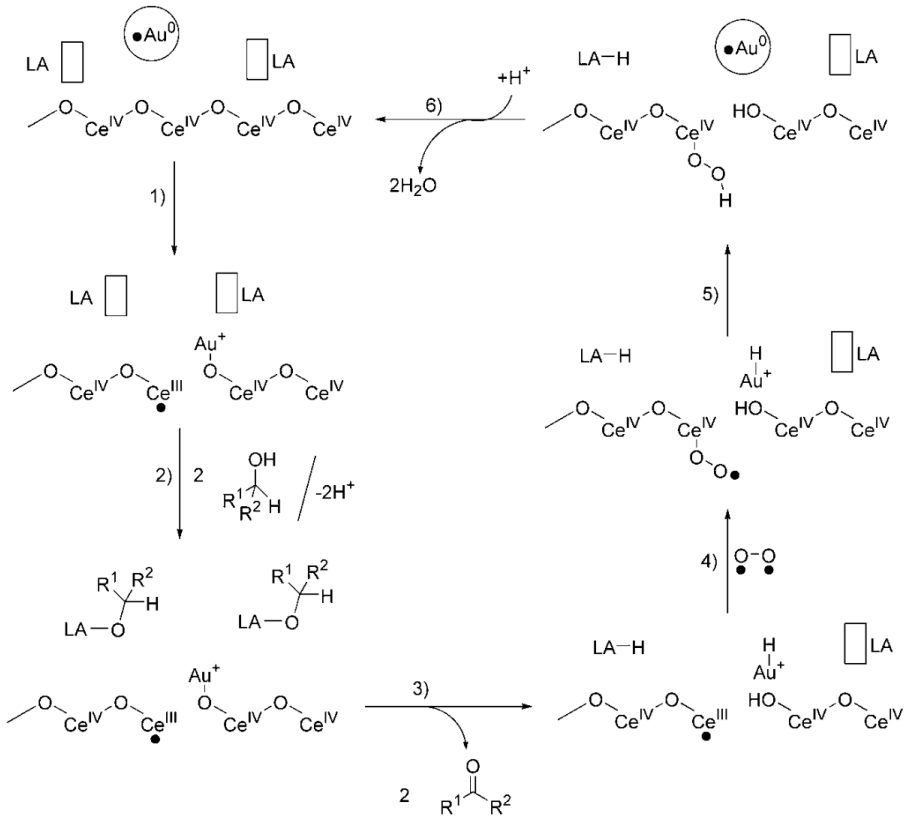

Scheme 6.7. Proposed mechanism for the oxidation of alcohols in the presence of Au/CeO_2 as the catalyst. LA = Lewis acid. Reprinted from [74]

Taking into account all studies, one can consider that both, oxygen mobility and Lewis acidity influence the HMF oxidation activity of the catalysts. Actually, the activity increases with the zirconia content, accounting for the importance of the Lewis acidity in the process. Although a deeper study is necessary, we can affirm that both, oxygen

mobility and Lewis acidity appear as factors influencing the activity, being the later the most important.

Numerous studies reported a rapid loss of activity for the gold-based catalysts during HMF oxidation, due to Au leaching and/or active phase blocking by competitive absorption. The stability of two representative samples (with and without ceria in its composition) was studied reusing the catalysts under repeating operation conditions. Figure 6.25. shows the obtained results after 5 cycles over AuAl. The conversion is complete in all cases (not plotted) and only the product yields are considered. The FDCA yield decreases after 5 runs from 70 to 58% in favor to HMFCA accounting for the catalyst deactivation. As the carbon balances, close to 100%, do not reflect important carbon loss, the activity decrease may be attributed to catalyst changes.

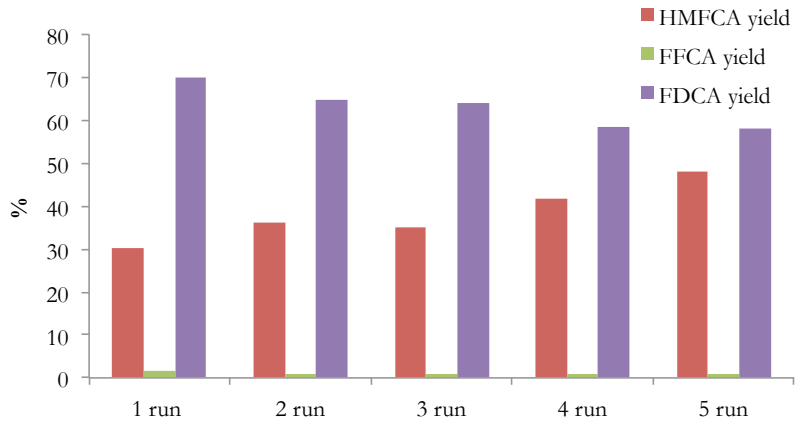

Figure 6.25. Reusability study over AuAl catalyst. Reaction conditions: HMF:Au:NaOH molar ratio 1:0.01:2, 10 bar O_2, 70 ºC, 400 rpm.

XRF analysis of the post reaction mixtures and solid confirms the absence of gold leaching. The post reaction gold loading is the same as the initial one.

As for the gold sintering, spent sample' particle size was analyzed by TEM. The particle size distributions of fresh and spent catalysts are

compared in Fig. 6.26. Although the size increment is not alarming, it appears to be the reason for FDCA yield drop. The mean particle size increases from 5.1 to 7.4 nm, accompanied by wider size distribution.

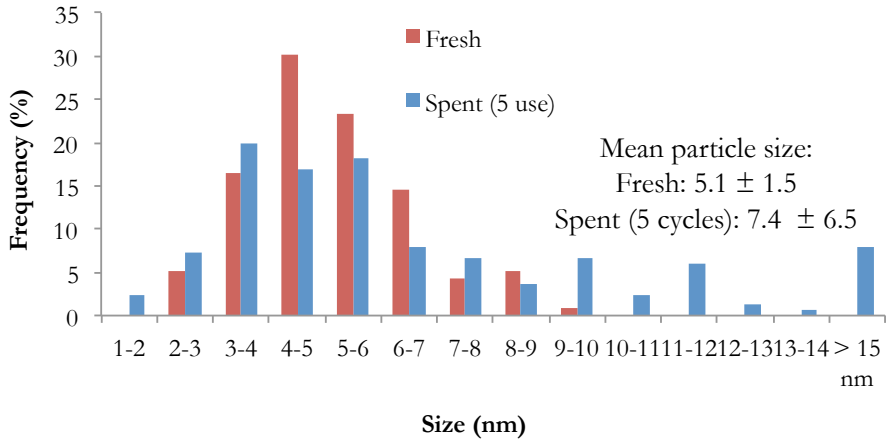

Figure 6.26. Particle size distributions of spent (after 5 cycles) and fresh AuAl

Considering only particle size change, one could suspect that smaller particles help to decrease the energy barrier of the limiting step - hydroxyl group oxidation and accelerate the oxidation to FDCA. On the contrary, when Au particle size increases the HMFCA oxidation could not proceed on bigger particles and its yield increases.

Analogously, the reusability tests over AuCe25Zr are presented in Fig. 6.27. In the same way, HMF conversion is complete in all runs and the HMFCA yield increases continuously in detriment to FDCA yield. The deactivation seems to be stronger than the Au/Al system. While for Au/Al the FDCA yield decreases 12% between the 1st and the 5th cycle, over AuCe25Zr decreases 30% (from 80 to 50 %). No gold leaching was detected, for both post reaction mixture and spent catalysts. On the other hand, TEM analysis shows gold size increase from 3.9 to 5.9 after 5 cycles (Fig. 6.28.), probably the reason for catalyst deactivation similarly to

Au/Al catalyst. The later suggests that HMFCA oxidation is strictly size sensitive, and lower the gold particle size higher the FDCA yield.

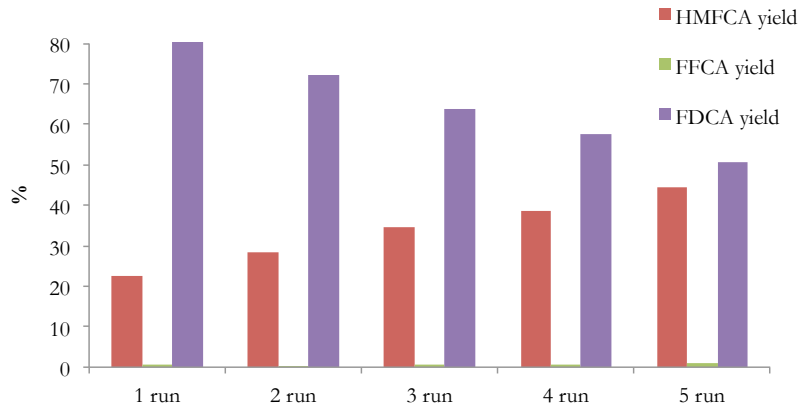

Figure 6.27. Reusability study for the oxidation of HMF using AuCe25Zr catalyst. Reaction conditions: HMF:Au:NaOH molar ratio 1:0.01:2, 10 bar O_2, 70 ºC, 400 rpm.

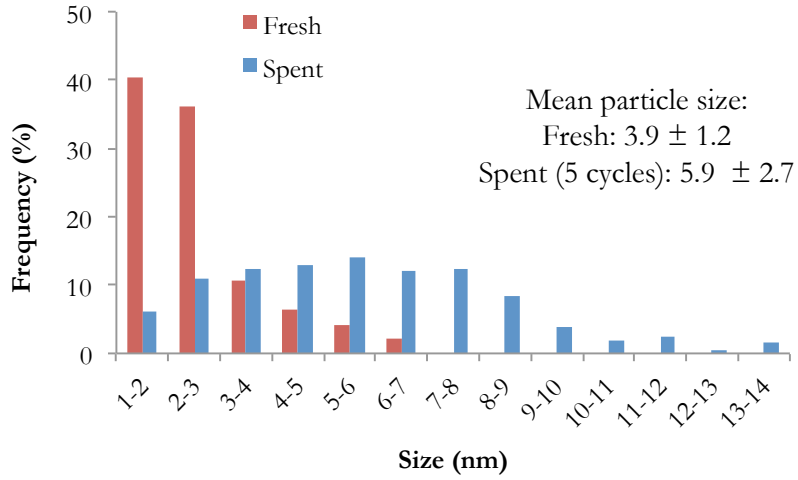

Figure 6.28. Particle size distributions of spent (after 5 cycles) and fresh AuCe25Zr

It is clear that metal sintering is the main problem to solve, and the future efforts have to be focused on avoiding it.

In addition to the commercially available supports, a series of similar oxide supports was prepared to complete the study and to include in it the bare ZrO_2.

6.2.3.2. Synthesis and characterization of homemade supports

- Synthesis

A complete series of CeO_2, CeO_2(50wt%)/ZrO_2, CeO_2(25wt%)/ZrO_2 and ZrO_2 were prepared by using the co-precipitation (precipitation) method. The used precursors were $Ce(NO_3)$ x $6H_2O$ and $ZrO(NO_3)_2$ (both from Sigma Aldrich).

The synthesis of CeO_2 and ZrO_2 was carried out as follows: appropriate amount of precursor was dissolved in 100 mL of H_2O and heated to 60 ºC, under vigorous stirring. Upon total dissolution, the necessary amount of NH_3 (30%) was added to reach a final pH of 9. The resulted precipitate was aged overnight and then filtered and washed to neutral pH of the waste water. The pure oxides were dried at 110 ºC for 5 hours in a conventional oven and grinded in an agate mortar before calcination at 500 ºC during one hour with a temperature ramp of 10 ºC/min.

As for the mixed oxides, the amount of metal precursors were calculated to obtain final solids with concrete proportions (50 wt% CeO_2 - 50 wt% ZrO_2 and 25 wt% CeO_2 - 75 wt% ZrO_2). Taking CeO_2(25wt%)/ZrO_2 as representative mixed oxide, the synthesis was carried out as follows:

Zirconia precursor (7.76 g) was dissolved in 100 mL of water and heated to 60 ºC till total dissolution. Separately, ceria precursor (3.16 g) was dissolved in 100 mL of H_2O and added to the first solution. The mixed oxide precipitates after addition of NH_3 (30%) until reaching pH of 9. The resulted precipitate was aged overnight, filtrated, dryed and calcined in the same manner as the pure oxides.

The gold deposition (2% nominal value) was carried out according to the DAE method explained elsewhere [80] by using chloroauric acid as metal precursor, as described in details in Chapter 5.

- Characterization

- *XRD*

The X-ray diffraction patterns of both homemade (H) supports and catalysts are shown in Fig. 6.29. The binary systems presented typical diffraction patterns of $Ce_xZr_{1-x}O_2$ solid solutions [78,81]. The CeO_2 solid shows well-defined peaks corresponding to the cubic fluorite structure (ICSD #00-034-0394). For the mixed oxides, the formation of homogeneous solid solutions and absence of segregate phases are envisaged on the basis of the diffraction patterns. Neither Ce50Zr nor Ce25Zr show diffractions peaks corresponding to pure CeO_2 and ZrO_2. Upon 50% Zr addition the diffractions shift to significantly higher diffraction angles, attributed to ceria lattice shrinkage due to the replacement of Ce^{4+} (ionic radius 0.098 nm) with smaller Zr^{4+}cations (0.084 nm), and a solid solution formation. However, the 75% Zr addition seems to be attributed to the zirconia lattice expansion due, in this case, to the replacement of Zr^{4+}cations with bigger Ce^{4+} cations. According to Vegard's Law, the diminution of the lattice parameter due to the introduction of smaller cations should be proportional to the % of dopant agent, Zr^{4+}in our case, which is roughly perceptible on the basis of the shift. Ce50Zr sample has a cubic structure (ICSD #00-028-0271) whereas Ce25Zr sample has a tetragonal one (ICSD #01-080-0785). This is consistent with the reported literature [78]. A mixture of cubic (ICSD

#00-003-0640) and monoclinic (ICSD #00-007-0343) structures is observed in the case of pure ZrO_2.

The addition of Zr to ceria implies a secondary effect, oxides particle size diminution, confirmed by the broadening of the diffractions for both mixed oxide samples.

As for the catalysts, gold diffractions are hardly observed, suggesting particle size below 4 nm, the detection limit of the technique.

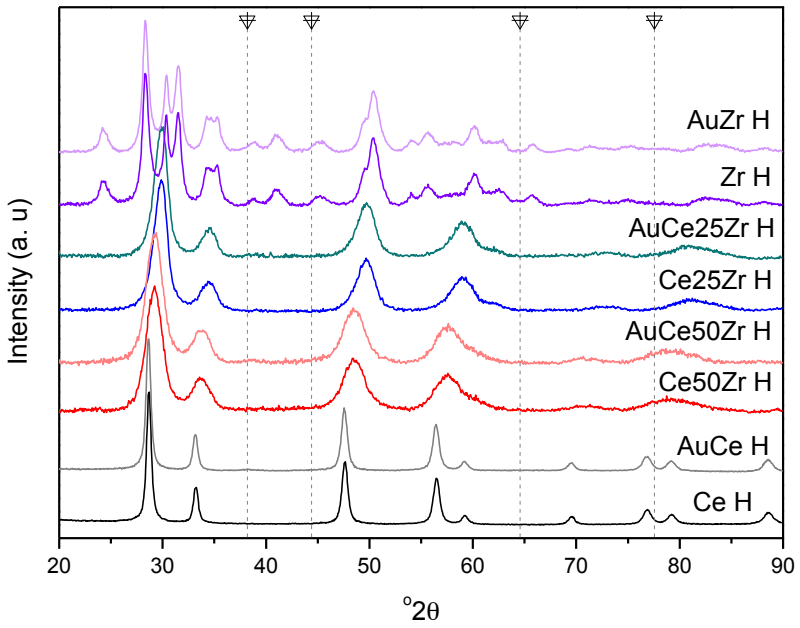

Figure 6.29. X-ray diffraction patterns of $Ce_xZr_{1-x}O_2$ supports and its corresponding gold catalysts.

- *TEM microscopy*

High-resolution transmission electron microscopy (HR-TEM) and high-angle annular dark-field scanning transmission electron microscopy (HAADF-STEM) were used to evaluate the average gold particle size of all samples. Due to the similar atomic weight of gold and cerium, their individual identification often becomes a difficult task. For this reason,

both techniques were combined to get the best possible contrast. Representative micrographs and particle size distributions are presented in Figure 6.30.

Similarly, to the commercial samples, the mean gold particle size ranges 2.1-3.7 nm, with a typical Gaussian particle size distribution. Table 6.11. compares the gold particles sizes observed for both commercial and homemade series. In both series, gold sizes are similar, which allows directly the catalytic comparison of the samples.

Table 6.11. Comparison of gold particle sizes (estimated from both XRD and TEM) of homemade and commercial samples.

	Commercial		**Homemade**	
Sample	**Scherrer, nm**	**TEM, nm**	**Scherrer, nm**	**TEM, nm**
AuCe	4.4	3.9 ± 1.5	4.9	3.7 ± 1.3
AuCe50Zr	3.0	2.2 ± 0.9	4.0	2.9 ± 0.8
AuCe25Zr	4.8	3.9 ± 1.2	2.7	2.1 ± 0.4
AuZr	-	-	★	3.1 ± 1.5

★ Au and ZrO_2 diffractions overlap

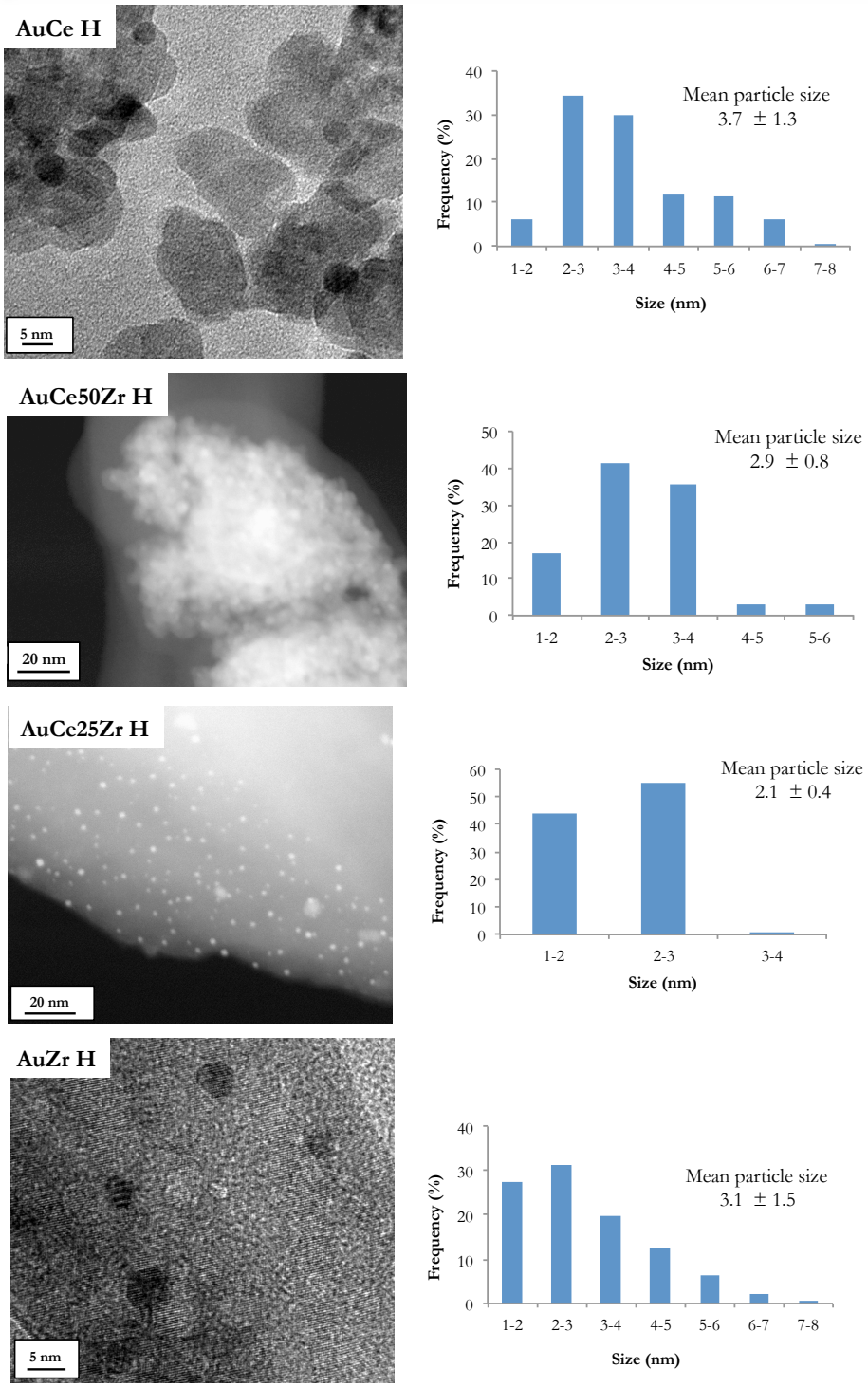

Figure 6.30. TEM images and particle size distribution of the homemade catalysts

- *Chemical composition and textural properties*

The chemical composition of the samples was estimated through X-Ray Fluorescence (XRF) and the obtained results are listed in Table 6.12. The CeO_2 and ZrO_2 weight percentages of the mixed oxides are very close to the targeted ones: 44.7 wt.% CeO_2 is registered for the Ce50Zr H support and 24.2 wt.% for Ce25Zr H. Regarding the gold contents, AuCe H sample contains an unexpectedly high amount of gold unlike the rest of samples. These results are very similar to those obtained with commercial samples, in which also the AuCe sample has the higher gold content, very close to 4%. Since the gold deposition was carried out in the same manner for all the samples, the doubled Au loading indicates rather analysis problem and probable matrix effect.

Table 6.12. Chemical composition of the homemade samples

Sample	wt.% Au	wt.% CeO_2	wt.% ZrO_2
Ce H	-	100	-
AuCe H	4	96	-
Ce50Zr H	-	44.7	55.2
AuCe50Zr H	2.5	45.1	52.4
Ce25Zr H	-	24.2	75.8
AuCe25Zr H	2.5	19.4	78.1
Zr H	-	-	100
AuZr H	2.3	-	97.7

The textural properties were estimated by means of N_2 adsorption measurements. Table 6.13. compares the specific surface area, average pore size and pore volume of both commercial and homemade samples. The BET surface area is very similar for all solids, being that of the homemade mixed oxides higher. In fact, the mixed oxide samples have 30

m^2/g more area than the commercial ones. This increment is due to the diminution of the registered average pore size in comparison with the commercial samples. The pore size of the homemade samples is around 3 nm except for the AuCe sample, whereas the commercial ones present pore sizes between 9 and 13 nm, approximately. These differences are also noticeable on the pore volumes.

Table 6.13. Textural properties of commercial and homemade catalysts

Sample	S_{BET} (m^2/g)	Average pore size (nm)	Pore volume (cm^3/g)
AuCe	57	13.45	0.1989
AuCe50Zr	55	8.95	0.1608
AuCe25Zr	57	11.78	0.2011
AuCe H	49	9.95	0.1433
AuCe50Zr H	82	3.13	0.0720
AuCe25Zr H	81	3.60	0.0950
AuZr H	56	3.65	0.0759

- *TPR-H_2*

The redox properties of the catalysts were investigated by means of temperature-programmed reduction (TPR). H_2 TPR profiles of the prepared samples are presented in Figure 6.31. The ceria sample shows a reduction peak at 749 ºC, assigned to the reduction of the ceria surface. Hence, the typical profile of ceria samples is characterized by two reduction zones, for both surface ceria (at lower temperatures) and bulk ceria (at higher temperatures) reduction [78], the appearance of only one peak suggests that the reduction of bulk ceria happens probably at temperatures higher than 900 ºC and cannot be registered by our equipment. The later is consistent with some reports [76].

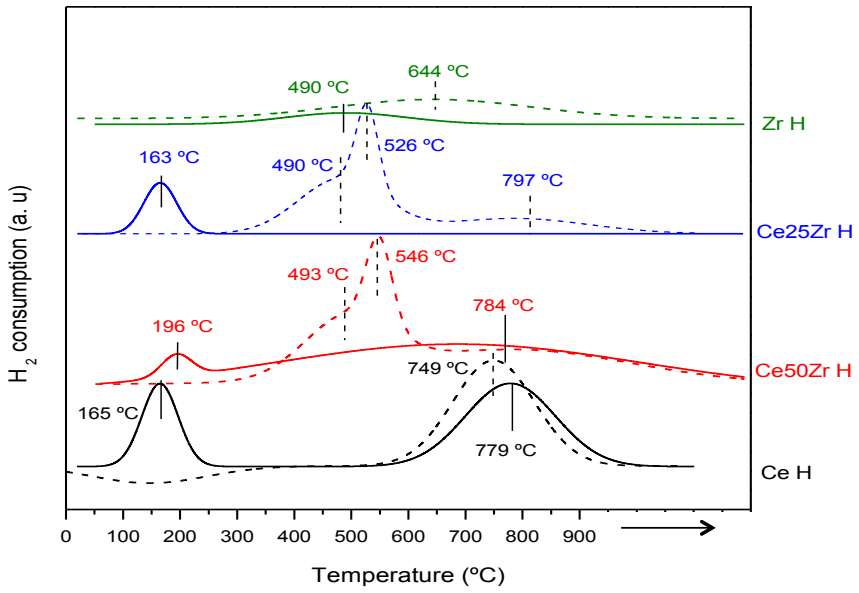

Figure 6.31. TPR-H_2 profiles of the supports (dashed lines) and their corresponding gold catalysts (full lines)

In contrast, the TPR profiles of the mixed oxides show a broad reduction zone. Actually, the introduction of ZrO_2 in the ceria lattice leads to certain deformation in the lattice, as revealed by XRD. As a consequence, the reduction process is not limited to the surface and extends to the bulk [78]. On the other hand, the reduction (understood as loss of oxygen atoms) is strongly influenced by the mobility of oxygen, boosted by the presence of zirconia, as demonstrated during the OSC/OSCC measurements. Therefore, the reduction zones observed for the mixed oxides are shifted to lower temperatures, in comparison with the ceria profile. It is possible to distinguish three reduction zones for the mixed oxides, attributed to the mobility of oxygen from different layers between surface and bulk. As showed in OSC measurements, the O_2 mobility is improved with the temperature, being higher the number of oxygen layers

involved. ZrO_2 profile is very different to those containing ceria. In this case, no clear reduction is observed, in agreement with the literature [76], although very low hydrogen consumption is detected, most probably due to some hydrogen adsorption on the surface.

As for the catalysts, for all studied samples, pure zirconia as exception, the gold addition helps the oxide reduction by facilitating the mobility of the H_2 molecule on the surface. It was reported earlier [82] a shift in the reduction peaks related to the surface ceria oxygen in the presence of gold to much lower temperatures. Within the profiles, the low temperature reduction zone is assigned to the noble metal promoted ceria surface reduction and the high temperature reduction process to the ceria bulk reduction. Only one reduction event centered at 163 ºC is observed for the AuCe25Zr sample and on the contrary, the AuCe50Zr, looks more like pure ceria reduction. It could be concluded that the redox behavior of the solids depends strongly on the zirconia content.

The reducibility percentages (RP) are calculated according Eq. 5.5. (see in Chapter 5) and used to compare the solids under the consideration that only the Ce^{4+} can be reduced to Ce^{3+}in presence of H_2 for all the samples. The results are presented in Fig. 6.32.

The samples of pure ceria show only a 50 % of reduction in the temperature range considered in this study. However, the mixed oxide samples present higher RP due to the higher oxygen mobility confirmed by the OSCC measurement. Similarly to the OSCC trend for the catalysts the reduction degree decreases following the trend AuCe50Zr H> AuCe25Zr H> AuCe H.

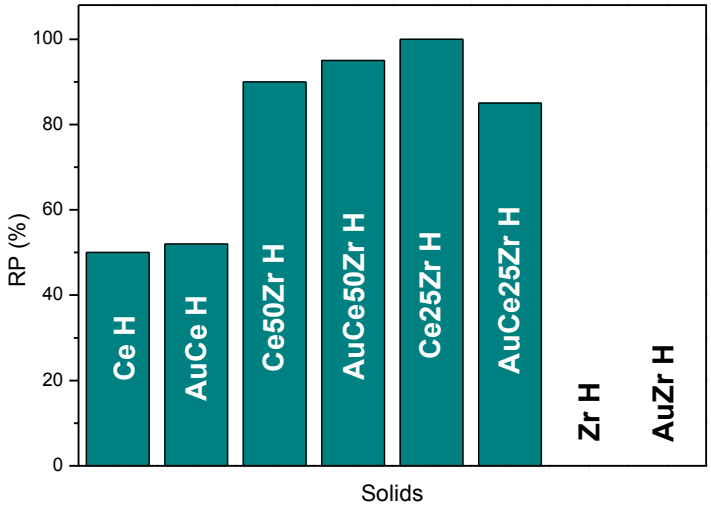

Figure 6.32. Reducibility percentage (RP) of the prepared solids

6.2.3.3. Catalytic activity of homemade series: results and discussion

The influence of the support nature in the catalytic performance of the homemade series is presented in Fig. 6.33. Similarly, to the commercial samples, the HMF conversion is complete for all samples. However, the product yields are completely different, showing the tendency: AuCe H > AuZr H > AuCe50Zr H > AuCe25Zr H. Moreover, independently to the observed tendency, the FDCA yields are significantly lower than those obtained over the commercial homologues.

These differences cannot be related to the metal nature, since the gold contents and particle sizes are practically the same for both series. Therefore, they should be related to the support. As the chemical composition is very similar, one can consider that the textural properties could play a role in the oxidation process. The porosity is then an additional factor to be taken into account.

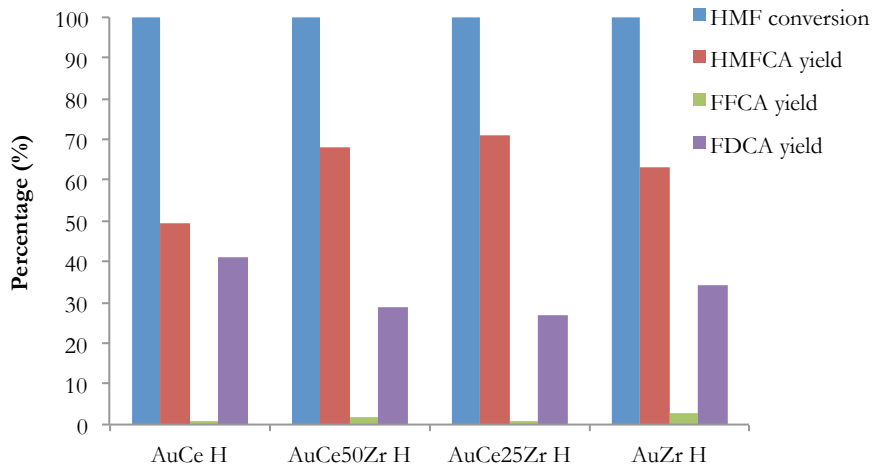

Figure 6.33. Influence of support in the HMF oxidation over homemade samples. Reaction conditions: HMF:Au:NaOH molar ratio 1:0.01:2, 10 bar O_2, 70 ºC, 400 rpm.

In order to study the influence of the porosity, FDCA yield is plotted as function of the pore diameter of both homemade and commercial samples in Fig.6.34. As could be deduced, the samples can be separated in two groups, the commercial ones having a higher pore diameter and leading to higher FDCA yields, and the homemade samples, with lower pores diameter and lower FDCA yield.

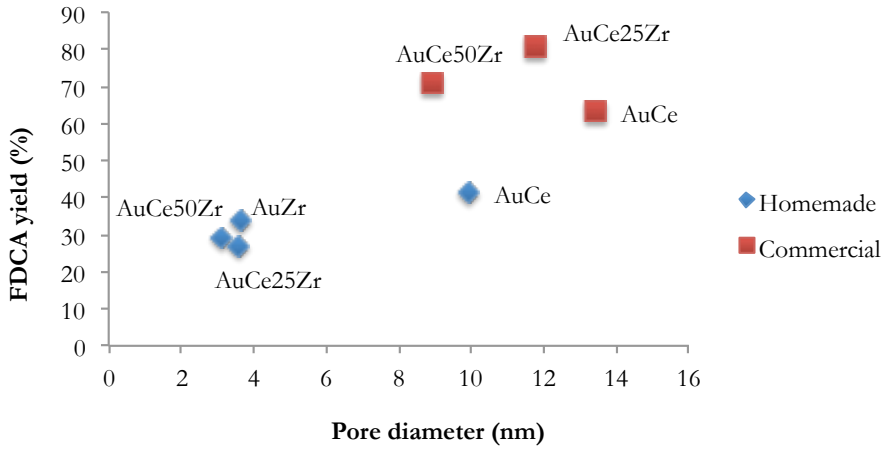

Figure 6.34. FDCA yield (%) dependence on supports pore diameter. Reaction conditions: HMF:Au:NaOH molar ratio 1:0.01:2, 10 bar O_2, 70 ºC, 400 rpm.

The obtained relation suggests that i) gold nanoparticles may be located in the pores ii) the FDCA production occurs in the pores. Both suggestions imply that in small pores some diffusional limitations could appear. In order to check that, different experiments were carried out at different stirring rates, at 200 and 600 rpm over both AuCe50Zr H and AuCe25Zr H (Fig. 6.35.)

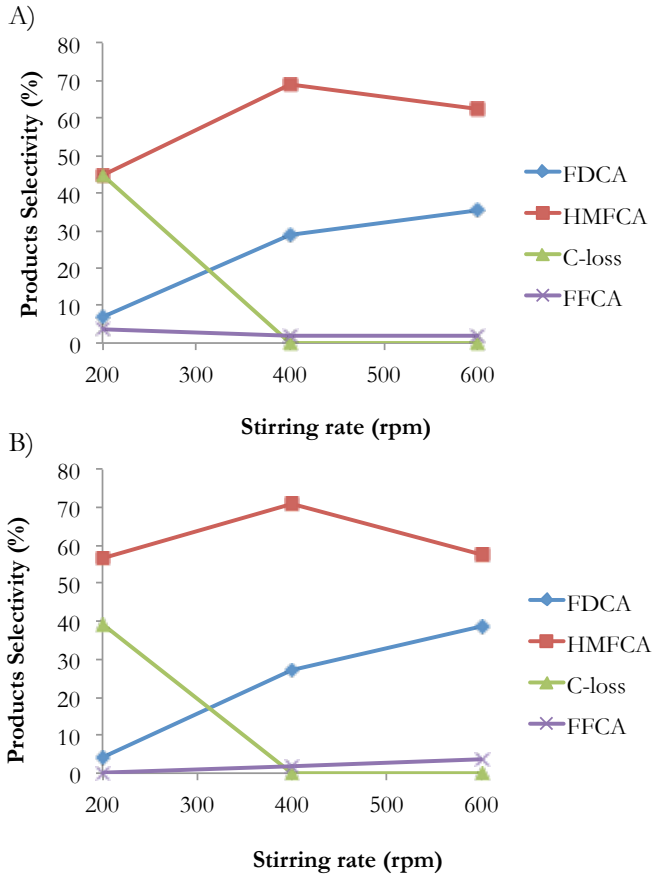

Figure 6.35. Stirring rate dependence of FDCA yield. A) AuCe50Zr H and B) AuCe25Zr H. Reaction conditions: HMF:Au:NaOH molar ratio 1:0.01:2, 10 bar O_2, 70º C.

In both cases the FDCA yield decreases at 200 rpm (5%), resulting also in important carbon loss of 40-45%. It seems that the low stirring rate prevents the proper diffusion of the HMF molecule to the active sites,

being promoted the HMF degradation (via Cannizzaro reaction), resulting in byproducts formation and low carbon balance. On the other hand, a FDCA yield increases at 600 rpm, as consequence of better diffusion.

However, deducing which diffusion step is the limiting one is very difficult, due to the multiple mass-transfer processes involved, such as i) the oxygen dissolution in the HMF solution (gas-liquid transfer); ii) the oxygen and reactants diffusion from the liquid bulk towards the outer surface of the catalyst grain (external diffusion); iii) the transfer of the substrates from the outer surface inside the catalyst pores towards active sites of the reaction (internal diffusion) and iv) the transport of the reaction product from the pores to the outer surface of the catalyst grain (internal diffusion).

Unfortunately, the catalytic activity of the homemade series does not give additional insights on the support dependency on catalytic behavior due to the encountered mass transfer problems. However, it demonstrates that the porosity of the used support is a key parameter to ensure a proper catalytic performance and it must be taken into account together with the catalyst' acidity and redox properties. All parameters require additional studies in order to conclude without any doubt about the support-activity relationship.

6.2.3.4. Partial conclusions

A series of gold catalysts supported on metal oxides have been prepared and tested in the HMF oxidation reaction. All catalysts prepared by DAE, exhibit high catalytic activity and selectivity to the desired product. The bare supports do not participate in the reaction; only byproducts via Cannizzaro reaction are formed. However, when gold is the HMF

conversion reaches 100% without byproducts formation. Within the first group of catalysts, AuAl and AuCeAl, the presence of ceria promotes de oxidation to FCDA through Ce^{4+}/ Ce^{3+} redox cycles, by increasing the oxygen mobility. The behavior of the second group (AuCe, AuCe50Zr and AuCe25Zr) ceria based supports changes in presence of zirconia. Indeed, the catalytic performance improves with the increase of the Zr content, attributed to both the increment of the oxygen mobility in presence of zirconia, as demonstrated by OSCC/OSC measurements, and the increment of the Lewis acid sites on the support (stronger Lewis acid character of Zr^{4+} than those Ce^{4+}). The acid sites play a significant role in the adsorption and reaction of alcohols.

The stability of two representative samples was studied by recycling tests. The HMF conversion results complete in every cycle but the FDCA yield decreases due to particle growth, confirmed by TEM. No metal leaching was detected by XRF.

The synthesis and characterization of a series of homemade ceria and zirconia based catalysts, pure oxides and mixed combinations, have been carried out to gain more information about the support influence. Unfortunately, diffusional problems over homemade samples have prevented the proper evaluation of the catalytic activity, nevertheless the study demonstrates the importance of the controlled porosity for high FDCA yields.

6.2.4. Gold supported on carbon: influence of particle size

6.2.4.1. Catalytic activity: results and discussion

The influence of the gold particle size in the HMF oxidation has been studied over four AuC samples with different particle sizes and similar gold loading. Before starting the experiments, a blank test with active

carbon was carried out in order to get information about the contribution of the bare support as well as the possible adsorption of the reactants. Indeed, 85% of carbon balance was obtained in the blank test, accounting for a 15% of HMF adsorption in absence of NaOH and catalyst.

The influence of the gold particle size in the HMF oxidation is presented in figure 6.36. where, in addition to the conversion and product yields, the carbon balance is plotted. The reaction conditions are those selected in the previous section.

As for the other supports the conversion is 100% in all cases. The influence of the particle size is very clear in terms of product yields and carbon balances. When the gold size is 5.2 nm the FDCA yield reached 92%, an excellent result in presence of only 2 NaOH equivalents per mole of HMF. The carbon balance is 96%, which means that the oxidation reaction occurs so fast that no HMF adsorption takes place, The 4% of deviation may be due only to experimental and analytical errors. Anyway, if there is adsorption on the carbon surface, is negligible. Both FDCA yield and carbon balance irreparably decreases when the particles size increases from 5.2 nm to 8.5, 15.6 and 34.9 nm. For the FDCA yield, the values decrease from 92% to 89, 86 and 25%, which suggest that AuC catalysts are significantly actives even at 15.6 nm, although the loss of activity is important when the size overtakes this value.

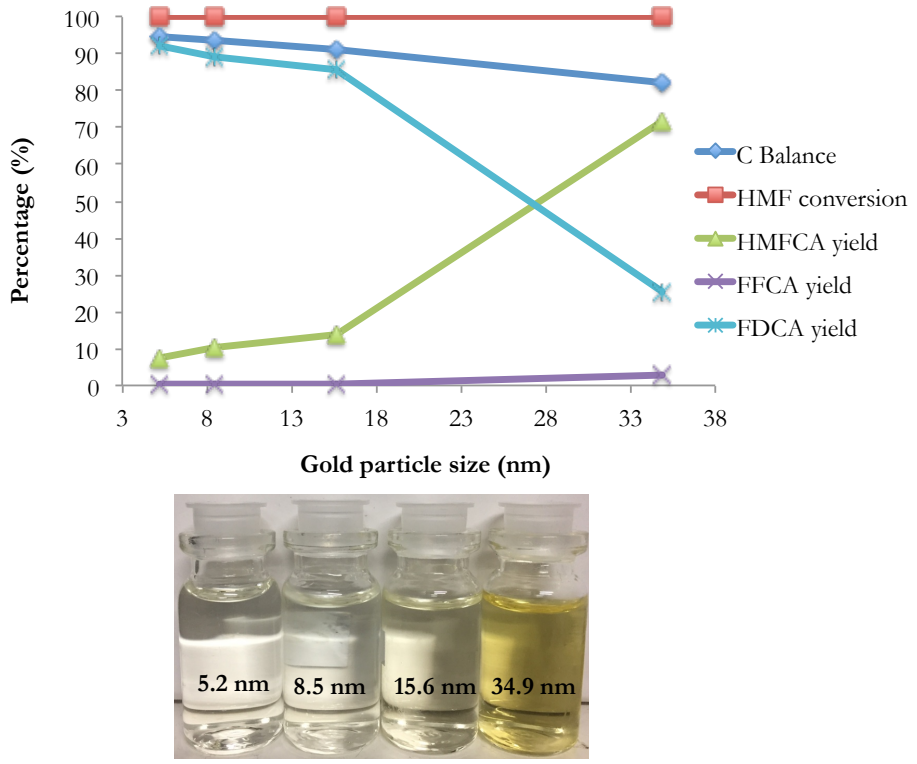

Figure 6.36. Influence of gold particle size in the HMF oxidation reaction. Reaction conditions: HMF:Au:NaOH molar ratio 1:0.01:2, 10 bar O_2, 70 ºC, 400 rpm

As for the carbon balance, it suggests that the higher the particle size the lower the rate of HMF oxidation and higher the reactant adsorption. In fact, the carbon balance registered at 5.2 nm suggests that the products are not adsorbed on the carbon. The adsorption problems in this case if any should be assigned only to the reactant. On the other hand, a possible formation of byproducts can be ruled out on the basis of the post reaction mixture color (Fig. 6.36.). Indeed, the gradual variation from colorless to yellow contrasts the obtained results, since FDCA is the only colorless product in solution. Anyway, the resulted solution after using the 34.5 nm catalyst has the normal color of a HMFCA solution. The presence of byproducts could not be confirmed as it would turn to dark yellow-orange solution or even darker if the Canizzaro reaction occurs.

The superiority of carbon facing the metal oxides supported catalyst is evident in the HMF oxidation reaction. At the same reaction conditions and comparable gold particle sizes the FDCA yield overtakes 90% for the best obtained result over AuCe25Zr of 80%. As explained in Chapter 5, the real relevance of carbon in aqueous-phase oxidation reactions derived from its hydrophobicity, which usually difficult the active metal phase leaching, thus improving the catalyst inherent activity. Taking into account that leaching does not occurs in basic conditions the difference in activity between mineral oxide and carbon supported gold catalyst can be tentatively assigned to the stronger adhesion between the hydrophobic catalyst grains and the oxygen bubbles presented in the feed. The later leads to an increase of the catalyst grains number at the gas-liquid interface and, therefore, to an increase of the gas transfer rate towards the catalysts [23]. The later in combination with its excellent stability (demonstrated in the base-free glucose oxidation reaction) makes gold on carbon an excellent candidate for highly efficient HMF oxidation to FDCA.

6.2.4.2. Partial conclusions

A series of four AuC samples with different gold particle sizes were tested in HMF oxidation. The gold size variation does not influence the HMF conversion; it is 100% in all cases. However, the product yields are strongly affected in a way that higher the gold particle size lower the yield of the final product. Though, HMF adsorption on the carbon surface could be a problem for these systems, 85% of carbon balance registered in the blank test, the presence of gold in an optimal size could suppress the adsorption and result in 92% of FDCA yield.

6.2.3. General conclusion in the HMF oxidation to FDCA

Gold nanoparticles are highly active in the oxidation of HMF to FDCA at low NaOH/HMF molar ratio. Both support and particle size influence the overall process, as concluded in each section, respectively. The problem of gold leaching is solved in basic media, being the catalyst deactivation much less pronounced, and mainly attributed to a particles sintering. Therefore, the next studies have to be focused to avoid it. The obtained results are very competitive and promising, especially taking into account that companies like Avantium started to produce and commercialize polyethylene furandicarboxylate (PEF), the polymer based on FDCA.

References

[1] M.J. Climent, A. Corma, S. Iborra, Converting carbohydrates to bulk chemicals and fine chemicals over heterogeneous catalysts, Green Chem. 13 (2011) 520.

[2] E.S. H. Hustede, H.J. Haberstroh, Ullmann's Encyclopedia of Industrial Chemistry, 1989.

[3] M. Bellardita, E.I. García-López, G. Marcì, B. Megna, F.R. Pomilla, L. Palmisano, Photocatalytic conversion of glucose in aqueous suspensions of heteropolyacid–TiO 2 composites, RSC Adv. 5 (2015) 59037–59047.

[4] J.-Z. Liu, L.-P. Weng, Q.-L. Zhang, H. Xu, L.-N. Ji, A mathematical model for gluconic acid fermentation by Aspergillus niger, Biochem. Eng. J. 14 (2003) 137–141.

[5] J.M.H. Dirkx, J.M.H. Dirkx, H.S. van Der Baan, H.S. van Der Baan, The oxidation of glucose with platinum on carbon as catalyst, J. Catal. 67 (1981) 1–13.

[6] M. Besson, F. Lahmer, P. Gallezot, P. Fuertes, G. Fléche, Catalytic Oxidation of Glucose on Bismuth-Promoted Palladium catalysts, J. Catal. 152 (1995) 116–121.

[7] I. Nikov, K. Paev, Palladium on alumina catalyst for glucose oxidation: reaction kinetics and catalyst deactivation, Catal. Today. 24 (1995) 41–47.

[8] M. Besson, P. Gallezot, Selective oxidation of alcohols and aldehydes on metal catalysts, Catal. Today. 57 (2000) 127–141.

[9] P. Gallezot, Selective oxidation with air on metal catalysts, Catal. Today. 37 (1997) 405–418.

[10] C. Della Pina, E. Falletta, Gold-catalyzed oxidation in organic synthesis: a promise kept, Catal. Sci. Technol. 1 (2011) 1564.

[11] C. Della Pina, E. Falletta, M. Rossi, Update on selective oxidation using gold, Chem. Soc. Rev. 41 (2012) 350–369.

[12] Y. Önal, S. Schimpf, P. Claus, Structure sensitivity and kinetics of D-glucose oxidation to D-gluconic acid over carbon-supported gold catalysts, J. Catal. 223 (2004) 122–133.

[13] H. Yin, C. Zhou, C. Xu, P. Liu, X. Xu, Y. Ding, Aerobic Oxidation of D - Glucose on Support-Free Nanoporous Gold, J. Phys. Chem. C. 112 (2008) 9673–9678.

[14] S. Biella, L. Prati, M. Rossi, Selective Oxidation of D-Glucose on Gold Catalyst, J. Catal. 206 (2002) 242–247.

[15] P. Qi, S. Chen, J. Chen, J. Zheng, X. Zheng, Y. Yuan, Catalysis and Reactivation of Ordered Mesoporous Carbon-Supported Gold Nanoparticles for the Base-Free Oxidation of Glucose to Gluconic Acid, ACS Catal. 5 (2015) 2659–2670.

[16] Y. Wang, S. Van de Vyver, K.K. Sharma, Y. Román-Leshkov, Insights into the stability of gold nanoparticles supported on metal oxides for the base-free oxidation of glucose to gluconic acid, Green Chem. 16 (2014) 719–726.

[17] E.C. Koch, Acid-Base Interactions in Energetic Materials: I. The Hard and Soft Acids and Bases (HSAB) Principle-Insights to Reactivity and Sensitivity of Energetic Materials, Prop.,Expl.,Pyrotech. 30 (2005) 5.

[18] R.G. Pearson, Hard and Soft Acids and Bases, J. Am. Chem. Soc. 85 (1963) 3533–3539.

[19] Y. Román-Leshkov, M. Moliner, J. a. Labinger, M.E. Davis, Mechanism of glucose isomerization using a solid lewis acid catalyst in water, Angew. Chemie - Int. Ed. 49 (2010) 8954–8957.

[20] Y. Wang, W. Deng, B. Wang, Q. Zhang, X. Wan, Z. Tang, et al., Chemical synthesis of lactic acid from cellulose catalysed by lead(II) ions in water, Nat Commun. 4 (2013).

[21] Y. Guan, D.A.J.M. Ligthart, Ö. Pirgon-Galin, J.A.Z. Pieterse, R.A. van Santen, E.J.M. Hensen, Gold Stabilized by Nanostructured Ceria Supports: Nature of the Active Sites and Catalytic Performance, Top. Catal. 54 (2011) 424–438.

[22] R. Battino, T.R. Rettich, T. Tominaga, The Solubility of Oxygen and Ozone in Liquids, J. Phys. Chem. Ref. Data. 12 (1983) 163–178.

[23] I. V. Delidovich, B.L. Moroz, O.P. Taran, N. V. Gromov, P. a. Pyrjaev, I.P. Prosvirin, et al., Aerobic selective oxidation of glucose to gluconate catalyzed by Au/Al2O3 and Au/C: Impact of the mass-transfer processes on the overall kinetics, Chem. Eng. J. 223 (2013) 921–931.

[24] M. Comotti, C. Della Pina, R. Matarrese, M. Rossi, The catalytic activity of "naked" gold particles, Angew. Chemie - Int. Ed. 43 (2004) 5812–5815.

[25] M. Haruta, Gold as a novel catalyst in the 21st century: Preparation, working mechanism and applications, Gold Bull. 37 (2004) 27–36.

[26] L. Prati, A. Villa, A.R. Lupini, G.M. Veith, Gold on carbon: one billion catalysts under a single label, Phys. Chem. Chem. Phys. 14 (2012) 2969.

[27] S. Ivanova, V. Pitchon, C. Petit, Application of the direct exchange method in the preparation of gold catalysts supported on different oxide materials, J. Mol. Catal. A Chem. 256 (2006) 278–283.

[28] T. Ishimoto, Y. Hamatake, H. Kazuno, T. Kishida, M. Koyama, Theoretical study of support effect of Au catalyst for glucose oxidation of alkaline fuel cell anode, Appl. Surf. Sci. 324 (2015) 76–81.

[29] T. Mallat, A. Baiker, No TitleOxidation of alcohols with molecular oxygen on platinum metal catalysts in aqueous solutions, Catal. Today. 19 (1994) 247–284.

[30] T. Ishimoto, H. Kazuno, T, Kishida, M. Koyama, No Title, Solid State Ionics. 262 (2014) 328–331.

[31] A. Franceschetti, S.J. Pennycook, S.T. Pantelides, Oxygen chemisorption on Au nanoparticles, Chem. Phys. Lett. 374 (2003) 471–475.

[32] M. Comotti, C. Della Pina, E. Falletta, M. Rossi, Aerobic oxidation of glucose with gold catalyst: Hydrogen peroxide as intermediate and reagent, Adv. Synth. Catal. 348 (2006) 313–316.

[33] J. Weiss, The catalytic decomposition of hydrogen peroxide on different metals, Trans. Faraday Soc. 31 (1935) 1547–1557.

[34] T. Ishida, N. Kinoshita, H. Okatsu, T. Akita, T. Takei, M. Haruta, Influence of the Support and the Size of Gold Clusters on Catalytic Activity for Glucose Oxidation, Angew. Chemie Int. Ed. 47 (2008) 9265–9268.

[35] H. Okatsu, N. Kinoshita, T. Akita, T. Ishida, M. Haruta, Deposition of gold nanoparticles on carbons for aerobic glucose oxidation, Appl. Catal. A Gen. 369 (2009) 8–14.

[36] B.N. Zope, R.J. Davis, Inhibition of gold and platinum catalysts by reactive intermediates produced in the selective oxidation of alcohols in liquid water, Green Chem. 13 (2011) 3484–3491.

[37] B.J. Meldrum., C.H. Rochester, Infrared spectra of carbonaceous chars under carbonization and oxidation conditions, Fuel. 70 (1991) 57–63.

[38] B.J. Meldrum, C.H. Rochester, In situ infrared study of the surface oxidation of activated carbon in oxygen and carbon dioxide, J. Chem. Soc., Faraday Trans. 86 (1990) 861–865.

[39] G. Socrates, Infrared and Raman Characteristic Group Frequencies: Tables and Charts, 3rd Edition, 2004.

[40] J.. Figueiredo, M.F.. Pereira, M.M.. Freitas, J.J.. Órfão, Modification of the surface chemistry of activated carbons, Carbon N. Y. 37 (1999) 1379–1389.

[41] B.J. Meldrum, C.H. Rochester, In situ infrared study of the modification of the surface of activated carbon by ammonia, water and hydrogen, J. Chem. Soc., Faraday Trans. 86 (1990) 1881–1884.

[42] Abdel-Nasser A., El-Hendawy, No Title, J Anal Appl Pyrolisis. 75 (2006) 159–166.

[43] D.B. Mawhinney, J.T.Y. Jr., FTIR study of the oxidation of amorphous carbon by ozone at 300 K — Direct COOH formation, Carbon N. Y. 39 (2001) 1167–1173.

[44] M.J. Climent, A. Corma, S. Iborra, fuel additives and liquid hydrocarbon fuels, (2014) 516–547.

[45] B.R. Caes, R.E. Teixeira, K.G. Knapp, R.T. Raines, Biomass to Furanics : Renewable Routes to Chemicals and Fuels, ACS Sustain. Chem. Eng. 3 (2015) 2591–2605.

[46] S.P. Teong, G. Yi, Y. Zhang, Hydroxymethylfurfural production from bioresources : past , present and future, Green Chem. 16 (2014) 2015–2026.

[47] R.J. Van Putten, J.C. Van Der Waal, E. De Jong, C.B. Rasrendra, H.J. Heeres, J.G. De Vries, Hydroxymethylfurfural, a versatile platform chemical made from renewable resources, Chem. Rev. 113 (2013) 1499–1597.

[48] H. Kimura, K. Yoshida, Y. Uosaki, M. Nakahara, Effect of water content on conversion of D-cellobiose into 5-hydroxymethyl-2-furaldehyde in a dimethyl sulfoxide-water mixture, J. Phys. Chem. A. 117 (2013) 10987–10996.

[49] T.D. Swift, H. Nguyen, A. Anderko, V. Nikolakis, D.G. Vlachos, Tandem Lewis/Brønsted homogeneous acid catalysis: conversion of glucose to 5-hydoxymethylfurfural in an aqueous chromium(III) chloride and hydrochloric acid solution, Green Chem. 17 (2015) 4725–4735.

[50] S. Dutta, S. De, B. Saha, Advances in biomass transformation to 5-hydroxymethylfurfural and mechanistic aspects, Biomass and Bioenergy. 55 (2013) 355–369.

[51] J.N. Chheda, Y. Roma, J.A. Dumesic, Production of 5-hydroxymethylfurfural and furfural by dehydration of biomass-derived mono- and poly-saccharides {, (2007) 342–350.

[52] A. Gandini, M.N. Belgacem, IN POLYMER CHEMISTRY, Prog. Polym. Sci. 22 (1997) 1203–1379.

[53] A. Gandini, Green Chemistry The irruption of polymers from renewable resources on the scene of macromolecular science and technology, Green Chem. 13 (2011) 1061–1083.

[54] T. Werpy, G. Peterson, Top Added chemicals from biomass, 2004.

[55] J.J. Bozell, G.R. Petersen, Cutting-edge research for a greener sustainable future

Technology development for the production of biobased products from biorefinery carbohydrates — the US Department of Energy ' s " Top 10 " revisited, Gre. 12 (2010) 539–554.

[56] A. Lolli, S. Albonetti, L. Utili, R. Amadori, F. Ospitali, C. Lucarelli, et al., Insights into the reaction mechanism for 5-hydroxymethylfurfural oxidation to FDCA on bimetallic Pd – Au nanoparticles, Appl. Catal. A, Gen. 504 (2015) 408–419.

[57] A. Gandini, A.J.D. Silvestre, C.P. Neto, A.F. Sousa, M. Gomes, The furan counterpart of poly(ethylene terephthalate): An alternative material based on renewable resources, J. Polym. Sci. A Polym. Chem. 47 (2008) 295–298.

[58] O. Casanova, S. Iborra, A. Corma, Biomass into Chemicals : Aerobic Oxidation of 5-Hydroxy- methyl-2-furfural into 2 , 5-Furandicarboxylic Acid with Gold Nanoparticle Catalysts, ChemSusChem. 2 (2009) 1138–1144.

[59] S.E. Davis, L.R. Houk, E.C. Tamargo, A.K. Datye, R.J. Davis, Oxidation of 5-hydroxymethylfurfural over supported Pt , Pd and Au catalysts, Catal. Today. 160 (2011) 55–60.

[60] W. Partenheimer, V. V. Grushin, Synthesis of 2,5-Diformylfuran and Furan-2,5-Dicarboxylic Acid by Catalytic Air-Oxidationof 5-Hydroxymethylfurfural. Unexpectedly SelectiveAerobic Oxidation of Benzyl Alcoholto Benzaldehyde with Metal/Bromide Catalysts, Adv. Synth. Catal. 343 (2001) 102–111.

[61] E. Article, L. Ardemani, G. Cibin, A.J. Dent, M.A. Isaacs, G. Kyriakou, et al., Solid base catalysed 5-HMF oxidation to 2,5-FDCA over Au/hydrotalcites: fact or fiction?, Chem. Sci. 6 (2015) 4940–4945.

[62] A.S. Amarasekara, D. Green, E. McMillan, Efficient oxidation of 5-hydroxymethylfurfural to 2,5-diformylfuran using Mn(III)-salen catalysts, Catal. Commun. 9 (2008) 286–288.

[63] Y.Y. Gorbanev, S.K. Klitgaard, J.M. Woodley, C.H. Christensen, A. Riisager, Gold-Catalyzed Aerobic Oxidation of 5-Hydroxymethyl- furfural in Water at Ambient Temperature, ChemSusChem. 2 (2009) 672–675.

[64] H. Ait Rass, N. Essayem, M. Besson, Selective Aerobic Oxidation of 5-HMF into 2 , 5- Furandicarboxylic Acid with Pt Catalysts Supported on TiO2- and ZrO2-Based ... Selective Aerobic Oxidation of 5-HMF into 2 , 5-Furandicarboxylic Acid with Pt Catalysts Supported on, ChemSusChem. 8 (2015) 1206–1217.

[65] N. Zheng, G.D. Stucky, Promoting gold nanocatalysts in solvent-free selective

aerobic oxidation of alcohols, Chem. Commun. 1 (2007) 3862–3864.

[66] C. Della Pina, E. Falletta, L. Prati, M. Rossi, Selective oxidation using gold, Chem. Soc. Rev. 37 (2008) 2077–2095.

[67] S. Albonetti, A. Lolli, V. Morandi, A. Migliori, C. Lucarelli, F. Cavani, Conversion of 5-hydroxymethylfurfural to 2 , 5-furandicarboxylic acid over Au-based catalysts : Optimization of active phase and metal – support interaction, Appl. Catal. B, Environ. 163 (2015) 520–530.

[68] S.K.R. Patil, C.R.F. Lund, Formation and Growth of Humins via Aldol Addition and Condensation during Acid-Catalyzed Conversion of 5-Hydroxymethylfurfural, Energy Fuels. 25 (2011) 4745–4755.

[69] S.E. Davis, B.N. Zope, R.J. Davis, Green Chemistry On the mechanism of selective oxidation of 5-hydroxymethylfurfural to 2 , 5-furandicarboxylic acid over supported Pt and Au catalysts, Green Chem. 14 (2012) 143–147.

[70] S. Albonetti, T. Pasini, A. Lolli, M. Blosi, M. Piccinini, N. Dimitratos, et al., Selective oxidation of 5-hydroxymethyl-2-furfural over TiO 2 -supported gold – copper catalysts prepared from preformed nanoparticles : Effect of Au / Cu ratio, 195 (2012) 120–126.

[71] X. Wan, C. Zhou, J. Chen, W. Deng, Q. Zhang, Y. Yang, et al., Base-Free Aerobic Oxidation of 5 - Hydroxymethyl-furfural to 2 , 5- Furandicarboxylic Acid in Water Catalyzed by Functionalized Carbon Nanotube-Supported Au − Pd Alloy Nanoparticles, ACS Catal. 4 (2014) 2175–2185.

[72] J. Artz, R. Palkovits, Base-Free Aqueous-Phase Oxidation of 5-Hydroxymethylfurfural over Ruthenium Catalysts Supported on Covalent Triazine Frameworks, ChemSusChem. 8 (2015) 3832–3838.

[73] G. Yi, S.P. Teong, Y. Zhang, Base-free conversion of 5-hydroxymethylfurfural to 2,5-furandicarboxylic acid over a Ru/C catalyst, Green Chem. 18 (2016) 979–983.

[74] A. Abad, P. Concepción, A. Corma, H. García, A Collaborative Effect between Gold and a Support Induces the Selective Oxidation of Alcohols, Angew. Chem., Int. Ed. 44 (2005) 4066–4069.

[75] M. Cargnello, P. Fornasiero, R.J. Gorte, Opportunities for Tailoring Catalytic Properties Through Metal-Support Interactions, Catal. Letters. 142 (2012) 1043–1048.

[76] J. Kaspar, P. Fornasiero, M. Graziani, Use of CeO 2 -based oxides in the three-

way catalysis, Catal. Today. 50 (1999) 285–298.

[77] Y. Madier, C. Descorme, A.M. Le Govic, D. Duprez, Oxygen Mobility in CeO2 and CexZr(1-x)O2 Compounds: Study by CO Transient Oxidation and 18O/16O Isotopic Exchange, J. Phys. Chem. B. 103 (1999) 10999–11006.

[78] J.I. Gutiérrez-ortiz, B. De Rivas, R. López-fonseca, J.R. González-velasco, Combustion of aliphatic C 2 chlorohydrocarbons over ceria – zirconia mixed oxides catalysts, Appl. Catal. A Gen. 269. 269 (2004) 147–155.

[79] V. V. Pushkarev, V.I. Kovalchuk, J.L. D'Itri, Probing Defect Sites on the CeO2 Surface with Dioxygen, J. Phys. Chem. B. 108 (2004) 5341–5348.

[80] S. Ivanova, C. Petit, V. Pitchon, A new preparation method for the formation of gold nanoparticles on an oxide support, Appl. Catal. A Gen. 267 (2004) 191–201.

[81] M. Thammachart, V. Meeyoo, T. Risksomboon, Somchai Osuwan, Catalytic activity of CeO2–ZrO2 mixed oxide catalysts prepared via sol–gel technique: CO oxidation, Catal. Today. 68 (2001) 53–61.

[82] G. Jacobs, E. Chenu, P.M. Patterson, L. Williams, D. Sparks, G. Thomas, et al., Water-gas shift: comparative screening of metal promoters for metal/ceria systems and role of the metal, Appl. Catal. A Gen. Gen. 258 (2004) 203–214.

General conclusions

The research work in this thesis exemplifies the application in practice of the multifunctional catalyst concept to possible cascade reactions for possible future chemical valorization of the lignocellulosic biomass. A new generation of polyoxometalate/ionic liquid hybrids is studied as catalysts in reactions covering an important part of glucose platform molecule transformation to valuable compounds. The viability of those multifunctional hybrids for the glucose epimerization, oxidation and dehydration was studied and the most relevant conclusions are as follows:

The formed hybrids are new-structured materials composed by inorganic anions and organic cations. A long-range order exists for these compounds and becomes more evident with the increase in length of the imidazolium ring alkyl chain substituents. Unlike Keggin frameworks, the hybrids structures do not include water molecules and their space arrangement takes place only through electrostatic interactions between the organic cation and the terminal and bridging Keggin oxygen atoms. In all cases, the imidazolium based and Keggin structures remain preserved in the hybrid. Crystallographic data reveal three-dimensional $[Cxmim]_3PMo_{12}O_{40}$ framework, in which channels and cavities are formed due to the alternate organization of cations and anions. The structure is directly related with the number of carbon atoms in the alkyl chain of the imidazolium ring substitute, shorter chains results in open channels and cavities and less compact structure.

Three different catalytic processes involving glucose transformation are studied leading to the following conclusions:

❖ Molybdenum-based hybrids are highly active and selective for the epimerization of glucose. The organic cations do not participate in the carbon shift mechanism; however, their presence influences the overall

process indirectly by the organization of the hybrid structure and channel system. Smaller cations give rise to less compact structures with large cavities and channels with improved glucose diffusion and metal availability, whereas the longer chain cations exert a negative effect on metal-glucose complex formation and retards the glucose epimerization. The presence of different metal centers in the Keggin anion strongly influences the activity and selectivity of the systems. The substitution of Mo with W leads to important activity loss whereas the substitution of two atoms of Mo by V entails the formation of other products like glyceraldehyde, suggesting secondary reactions on the additional V centers.

❖ POM-ILs hybrids are active catalysts for mild glucose oxidation reaction with hydrogen peroxide. The different organic cations do not influence directly the catalytic performance, but most probably participates indirectly in the stabilization of the intermediates of the proposed mechanism. The later is proposed on the base of free radical organic molecule oxidation mechanism and the Haber-Weiss cycle of hydrogen peroxide decomposition/activation. The Keggin structure change produces higher impact on the activity/selectivity balance. The substitution of Mo by W results in higher catalytic performance, but with different catalyst loading/activity dependence. Higher conversions are also obtained upon 2 atoms Mo substitution by V. However, the selectivity to gluconic acid decreases and the formation of formic acid is observed.

❖ The viability of the hybrids structures in the glucose/fructose dehydration was considered in biphasic systems. The dual nature of the hybrids allows the accommodation of the catalyst at the solvents interface.

In a general manner the dehydration of fructose is easier than that of glucose. The HMF selectivity is higher when starting with fructose, but also a high quantity of byproducts is detected, accounting for secondary undesired reactions in aqueous phase.

The introduction of gold supported catalysts for the efficient oxidation of carbohydrates becomes necessary since the POM-ILs structures resulted scarcely efficient in the presence of molecular oxygen. In order to study both the influence of support and particle size two groups of solids were prepared: a series of similar particle sizes gold supported on different in nature mineral oxides and two series of gold on carbon, where the variation of the average gold particle sizes between 4 to 20 nm is obtained. The main conclusion on the use of gold catalyst for glucose oxidation in the presence of molecular oxygen are:

- Gold catalysts show high activity and important selectivity to gluconic acid in base-free reaction conditions. Both, selectivity and activity depend on the support nature, in a way, that the presence of ceria promotes the oxidation reaction at lower reaction times and the presence of zirconia promotes the secondary reactions to lactic acid formation.
- On the other hand, structure/size sensitivity correlation reveals the existence of an optimal size of 15-20 nm for maximum glucose conversion is found after a normalization on the exposed surface gold atoms (TOF).
- No matter the group of catalysts gold leaching remains the main problem to be solved. The choice of partially hydrophobic support, as is the case of active carbon, reduces the leaching significantly, with gold loss observed only in the first cycle of operation.

❖ For the HMF oxidation, gold catalysts exhibit high catalytic activity and selectivity to the desired final product, FDCA. No matter the support nature or particle size, always complete HMF conversion is obtained. However, the products distribution is affected by both parameters. With respect to the support influence we consider AuAl and AuCeAl catalysts, the presence of ceria promotes the oxidation to FCDA. The behavior of AuCe, AuCe50Zr and AuCe25Zr changes as a function of zirconia concentration. The FDCA yield improves with the increase in the Zr content; this is attributed to both, the increment in the oxygen mobility in the presence of zirconia, as demonstrated by OSCC/OSC measurements, and the increase of the Lewis acid sites on the support (stronger Lewis acid character of Zr^{4+} than those Ce^{4+}). The acid sites play a significant role in the adsorption and reaction of alcohols. As for the particle size effect, gold size variation does not influence the HMF conversion; it is 100% in all cases. However, the product yields are strongly affected in a way that the higher the gold particle size the lower the yield of the final product. But the HMF adsorption on the carbon surface could be a problem since 85% of carbon balance is registered in a blank test. However, the presence of gold in optimal size suppress this adsorption and result in 92% FDCA yield. This result is the best known in the scientific literature nowadays.

Contrary to glucose oxidation reaction the leaching is avoided in basic conditions and the slight catalysts deactivation for the HMF oxidation is attributed to particle growth.

Where the future points?

Although a centennial knowledge acquired over POMs properties and applications still new fields arise. Their use as combined hybrid organo-

inorganic materials should be studied in a systematic way outside of the purely fundamental crystallographic and theoretical manner. More application fields have to be explored. They are potentially interesting in biphasic systems, due to their capability to act as nanocatalyst at the interface. A lot of work have to be done to understand hybrids catalytic action, and especially their participation in the product transfer. Also a optimization of the reaction parameters are required in order to reveal their true potential especially in the glucose/fructose dehydration reaction taken as example in this manuscript. It is clear that these materials are very useful for epimerization reaction and the application to other reaction of interest represents a new potential field of application.

In all touched field in this thesis still much work is needed. The findings presented here establish only the main items to which a future investigation have to be addressed.

Conclusiones generales

El trabajo de investigación desempeñado durante esta tesis doctoral lleva a la práctica el concepto de catalizador multifuncional para su posible uso en reacciones en cascada que implican la valorización química de la biomasa lignocelulósica. Los resultados obtenidos constituyen el primer paso en la aplicación de una nueva generación de materiales híbridos basados en polioxometalatos y líquidos iónicos en reacciones que involucran la transformación de glucosa a compuestos de elevado valor. Aunque es evidente que se requiere más trabajo e investigación en este ámbito, los resultados que arroja el presente estudio establecen la base para futuras investigaciones. Las conclusiones más relevantes se presentan a continuación:

Los híbridos formados a través de la interacción de aniones inorgánicos y cationes orgánicos son materiales estructuralmente nuevos en los cuales se mantiene la estructura de Keggin. Se ha demostrado que existe un orden de largo alcance en estos compuestos, que se hace más evidente con el aumento en el número de carbonos de la cadena alquílica unida al anillo de imidazol. A diferencia de las estructuras de Keggin, las estructuras híbridas no incluyen moléculas de agua y su disposición en el espacio tiene lugar a través de interacciones electrostáticas entre el catión orgánico y los átomos de oxígeno terminales y de puente del anión. En todos los casos, el anillo de imidazolio conserva su estructura en el híbrido. Los datos cristalográficos ponen de manifiesto la existencia de una estructura tridimensional constituida por unidades con fórmula molecular $[C_xmim]_3PMo_{12}O_{40}$, en las que se evidencia la formación de canales y cavidades como consecuencia de una disposición alterna de cationes y aniones. Esta disposición está íntimamente relacionada con el número de carbonos del sustituyente del anillo: cadenas alquílicas más cortas dan

lugar a la aparición de canales y cavidades más abiertos y, por tanto, a la aparición de una estructura menos compacta.

La actividad catalítica de los híbridos ha sido evaluada en tres procesos distintos. Las conclusiones más destacadas son las siguientes:

❖ Los híbridos basados en molibdeno son muy activos y selectivos en la reacción de epimerización de glucosa. Aunque el catión orgánico no participa en el mecanismo descrito para esta reacción, tiene una influencia indirecta en el proceso, inducida por la propia organización estructural del híbrido. Los cationes más pequeños, con estructuras menos compactas y cavidades más amplias, mejoran la difusión de glucosa hacia el metal, mejorando también por tanto, la disponibilidad del metal. En cambio, la presencia de cationes más grandes dificulta la formación del complejo molibdeno-glucosa, afectando negativamente a la epimerización. Por otra parte, la sustitución de Mo por W en el anión de Keggin resulta en una pérdida importante de actividad mientras que la sustitución de dos átomos de Mo por V da lugar a la formación de otros productos como gliceraldehído, poniendo de manifiesto que ciertas reacciones secundarias pueden tener lugar en los nuevos centros metálicos.

❖ Las estructuras sintetizadas son activas en la reacción de oxidación de glucosa en presencia de peróxido de hidrógeno. En este caso, los resultados obtenidos son independientes del catión orgánico en la estructura aunque, probablemente, estén involucrados en la estabilización de algún intermedio de reacción. La sustitución de Mo por W en el anión de Keggin se traduce en una mejora en la actividad, aunque la dependencia de esta con la cantidad de catalizador añadido cambia, mientras que en el caso de molibdeno un aumento de catalizador se traduce en un aumento en la conversión, en el caso de wolframio la

conversión se mantiene. La sustitución de dos átomos de Mo por V da lugar a un incremento en la conversión, sin embargo, la selectividad se ve influenciada negativamente apareciendo, además de ácido glucónico, ácido fórmico.

❖ La viabilidad de los híbridos en la deshidratación de glucosa/fructosa ha sido evaluada en sistemas bifásicos. La naturaleza dual de estos compuestos influye en la disposición del catalizador en el sistema, acomodándose preferencialmente en la interfase. De forma general, la deshidratación de fructosa es más fácil que la de glucosa. La selectividad a HMF registrada cuando el azúcar de partida es fructosa es bastante más alta, sin embargo, la cantidad de subproductos detectados también es alta, elucidando el progreso de reacciones no deseadas en la fase acuosa.

La introducción de catalizadores soportados de oro resulta necesaria para reacciones que involucren la oxidación de carbohidratos, ya que los híbridos han resultado no ser eficientes en presencia de oxígeno molecular. Con objeto de estudiar tanto la influencia del soporte empleado como la del tamaño de partícula, se preparan dos grupos de catalizadores: en primer lugar, una serie de catalizadores de oro soportado sobre distintos óxidos metálicos con tamaños de partículas similares y, en segundo lugar, dos series de catalizadores de oro sobre carbón, en los cuales el tamaño de oro varía desde 4 a 20 nm.
Las principales conclusiones derivadas del uso de catalizadores de oro en la reacción de oxidación de glucosa con oxígeno molecular son las siguientes:

❖ Todos los catalizadores de oro han demostrado ser muy activos y selectivos en ausencia de base. Tanto actividad como selectividad están

influenciadas por la naturaleza del soporte de tal modo que la presencia de ceria promueve la reacción de oxidación mientras que la presencia de zircona impulsa la aparición de ácido láctico, producto derivado de reacciones secundarias.

- En cuanto a la influencia del tamaño, la normalización de la conversión obtenida por la superficie de átomos de oro expuesto (TOF) revela la existencia de un valor óptimo en el rango de 15-20 nm.
- En todos los casos, la lixiviación de oro en el seno de la disolución acuosa es el principal problema asociado a la pérdida de actividad tras diferentes ciclos de reutilización. Sin embargo, la elección de un soporte parcialmente hidrofóbico, como es el caso del carbón, reduce la pérdida de oro de forma significativa.

En cuanto a la reacción de oxidación de HMF:

- Los catalizadores propuestos demuestran ser altamente activos y selectivos hacia el producto deseado, FDCA. Las conversiones obtenidas en todos los casos son del 100%, independientemente del soporte y del tamaño de partícula. Contrariamente, la distribución de productos se ve fuertemente afectada por ambos parámetros. Atendiendo a los catalizadores soportados en óxidos metálicos y considerando AuAl y AuCeAl, la presencia de ceria promueve la reacción de oxidación hacia la formación de FDCA. Sin embargo, este comportamiento cambia en presencia de zircona. El rendimiento a FDCA aumenta con el contenido de zircona en el soporte, lo cual puede atribuirse a un incremento en la movilidad de oxígeno, demostrado a través de las medidas de OSCC/OSC, y al aumento en el carácter ácido de Lewis (Zr^{4+} es un ácido de Lewis más fuerte que Ce^{4+}). Por otra parte, la lixiviación de oro se inhibe totalmente en las condiciones básicas utilizadas durante la reacción

por lo que la leve desactivación registrada durante los ciclos de reutilización parece ser debida a un incremento en el tamaño de partícula.

❖ Del mismo modo, el tamaño no influye en la conversión obtenida, que es completa en todos los casos, pero influye de manera importante en la distribución de productos y en el balance de carbono. Mayores tamaños dan lugar a peores rendimientos del producto final y a balances de carbono bajos. Esto último se atribuye a la adsorción del reactivo (o productos) en la superficie del carbón. Sin embargo, la presencia de oro con un tamaño adecuado inhibe la adsorción y da lugar a excelentes rendimientos en el producto totalmente oxidado.

¿Cuáles son las perspectivas de futuro en este ámbito?

Aunque el descubrimiento de los POMs así como de sus propiedades data de 200 años de antigüedad, nuevos campos de aplicación siguen surgiendo a día de hoy. Su uso como materiales híbridos, orgánico-inorgánicos, debe estudiarse de forma sistemática y práctica, fuera de las disciplinas puramente cristalográficas y teóricas. Estos compuestos son potencialmente interesantes en sistemas bifásicos, debido a su capacidad para actuar como nanocatalizador en la interfaz, aunque se necesita mucho trabajo en este ámbito como para llegar a entender la función catalítica real de estos híbridos y, especialmente, su posible participación en la transferencia del producto. También se requiere una optimización exhaustiva de los parámetros de reacción de forma que se ponga de manifiesto su verdadero potencial, especialmente en la reacción de deshidratación de glucosa/fructosa. Es evidente que este tipo de materiales son muy útiles para la reacción de epimerización y, su posible

aplicación en otros sistemas de interés dentro del campo de valorización de biomasa, supone un campo de aplicación novedoso e importante.

Todos los procesos tratados durante la tesis deben estudiarse ampliamente y en profundidad. Los hallazgos aquí presentados sólo establecen los principales puntos que debe abordar una futura investigación.

Resumen

1. Introducción

El concepto de biorrefinería, aunque conocido desde finales del siglo pasado [1,2], ha sido objeto de numerosas definiciones durante la última década [3]. Según la Agencia Internacional de Energía (Bioenergía, apartado 42), biorrefinería hace referencia al procesado sostenible de biomasa con el fin de obtener un amplio abanico de bioproductos comercializables (compuestos químicos, materiales y comida apta para consumo humano y animal) y bioenergía (combustibles, energía y/o calor) [4]. Aunque son ya varias las empresas que procesan biomasa [5–7], principalmente de origen vegetal, el desarrollo de nuevos procesos orientados a la obtención eficiente de combustibles y compuestos plataforma ha llamado especialmente la atención en la última década, tanto dentro de la comunidad científica como industrial. Y es que, aunque en la actualidad no pretenden reemplazar a los combustibles fósiles, el agotamiento inminente de estas reservas está imponiendo la necesidad de desarrollar alternativas eficientes que permitan, en un plazo relativamente corto, disminuir el porcentaje de dependencia directa de la sociedad actual. Para este fin, sin embargo, los procesos deben ser económicamente viables y deben estar adaptados a la multifuncionalidad de las moléculas presentes en los residuos vegetales, de modo que la calidad y el precio de los productos bio, puedan ser competitivos a los obtenidos a partir del petróleo de forma tradicional [8–10]. En este ámbito, el desarrollo de catalizadores eficientes y fácilmente reciclables, que no se vean afectados por las impurezas presentes en la materia prima y permitan trabajar en continuo, es sumamente importante [11].

Una de las principales limitaciones es el desarrollo de catalizadores multifuncionales [12] que puedan aplicarse en reacciones "en cascada", es decir, en reacciones sucesivas, lo cual permitiría la intensificación de

procesos [13]. En cualquier caso, la combinación efectiva de catalizadores homogéneos y heterogéneos en reacciones que involucran muchos pasos también es una opción deseada y viable en la actualidad [14].

La biomasa lignocelulósica es la materia prima de origen vegetal más abundante y disponible de nuestro planeta [15]. Está constituida por un 60-70% de azúcares/carbohidratos, lo cuales se encuentran en diferentes proporciones en los tres polímeros que mayoritariamente la conforman: celulosa, hemicelulosa y lignina. La fracción mayoritaria, con un 35-50% del peso total es la celulosa, polímero de alto peso molecular formando únicamente por unidades de glucosa, cuyo grado de polimerización puede sobrepasar las 10,000 unidades [16]. Dado que la hemicelulosa está constituida por distintos monosacáridos y la lignina es la fracción más compleja, compuesta por la unión de compuestos aromáticos, en este estudio se toma la fracción de celulosa como modelo de materia prima de la cual solo se obtiene glucosa, azúcar que será utilizado como material de partida en todos los estudios catalíticos.

El número de compuestos de elevado valor (compuestos plataforma) que pueden obtenerse a partir de glucosa es considerable, por lo que resulta más interesante focalizar la presente introducción a los procesos estudiados.

- **Epimerización de glucosa a manosa**

La epimerización de glucosa en el carbono 2 implica la transformación del azúcar en su homólogo quiral, el epímero (Esquema de reacción 1). Aunque esta reacción ha suscitado menos interés que otros procesos dentro del campo de valorización química de biomasa, es un proceso

ampliamente utilizado para la producción de fármacos y azúcares denotados como "raros" [17–19], que encuentran su aplicación en medicina, cosmética y dentro de las industrias alimentaria y farmacéutica. En la actualidad, la producción de manosa está limitada a procesos enzimáticos, cuyas desventajas motivan la búsqueda de catalizadores, a ser posible heterogéneos, como alternativa viable que pueda llegar a reemplazar los procesos actuales.

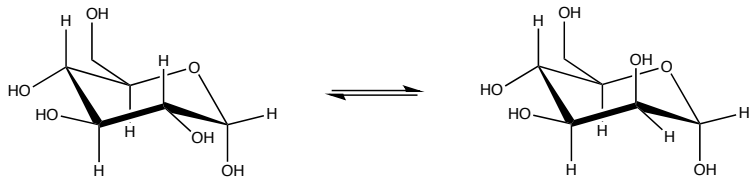

Esquema de reacción 1. Epimerización de glucosa a manosa.

Oxidación de glucosa a ácido glucónico.

Otro de los compuestos plataforma derivados de glucosa es el ácido glucónico, obtenido vía oxidación del grupo aldehído (Esquema de reacción 2). Este compuesto es muy útil en las industrias farmacéutica, química, alimentaria y textil, también como aditivo, y como agente quelante para la extracción de trazas metálicas en disolución [20]. Su producción enzimática industrial alcanza las 100,000 toneladas anuales [21–23], sin embargo, son muchos los problemas asociados a este tipo de procesos, como la gran cantidad de enzima que debe usarse, su elevado precio, la desactivación irreversible, los largos tiempos de reacción para obtener rendimientos aceptables, el control exhaustivo de parámetros de reacción como la temperatura y el pH, y la necesidad de varios pretratamientos de purificación para eliminar impurezas [24]. Todo ello estimula la búsqueda de nuevos procesos y catalizadores eficientes,

respetuosos con el medio ambiente, que mejoren la conversión de glucosa y, además, potencien la explotación de biomasa.

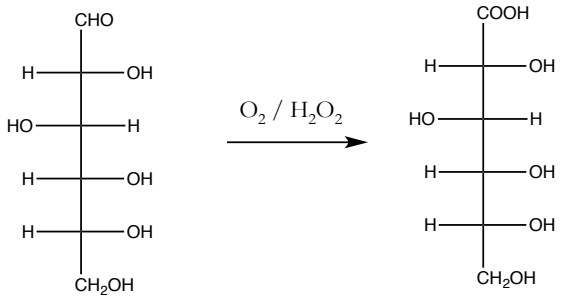

Glucosa (cadena abierta) Ácido glucónico

Esquema de reacción 2. Oxidación de glucosa a ácido glucónico

Deshidratación de glucosa/fructosa a 5-hidroximetil-2-furfural (HMF)

La producción de 5-hidroximetil-2-furfural (HMF) a partir de derivados de la fracción lignocelulósica de la biomasa es uno de los procesos más estudiados dentro del campo de valorización química. La mayoría de las investigaciones se centran en la conversión de fructosa a HMF [25–27], proceso menos costoso, desde el punto de vista energético, que está catalizado por ácidos de Brönsted, ya sean homogéneos o heterogéneos [28–30]. La deshidratación de glucosa, por su parte, es un proceso más costoso y complicado, la selectividad final obtenida a HMF suele ser muy baja, a menos que el catalizador usado transforme en primer lugar glucosa en fructosa [31]. La transformación de glucosa en fructosa tiene lugar vía isomerización, durante la cual hay un intercambio de un hidruro entre el C2 y C1, dando lugar a la formación de un grupo cetónico en el C2 y a la desaparición del grupo aldehído. La forma hemiacetálica (cíclica) de la molécula de fructosa es un anillo furánico de 5 miembros cuya estructura

general es muy parecida a la del HMF (ver Esquema de reacción 3), hecho que parece ser la clave en su subsecuente transformación a HMF, en comparación con la molécula de glucosa [32].

En cuanto a su interés, HMF es uno de los compuestos más versátiles e importantes dentro del campo de valorización de biomasa. Forma parte de la lista de los "Top 10", los 10 compuestos más importantes y de más alto valor, según el Departamento de Energía de los Estados Unidos [33], debido a la gran cantidad de productos químicos que pueden obtenerse a partir de su transformación, de gran interés en el desarrollo de combustibles y polímeros [34].

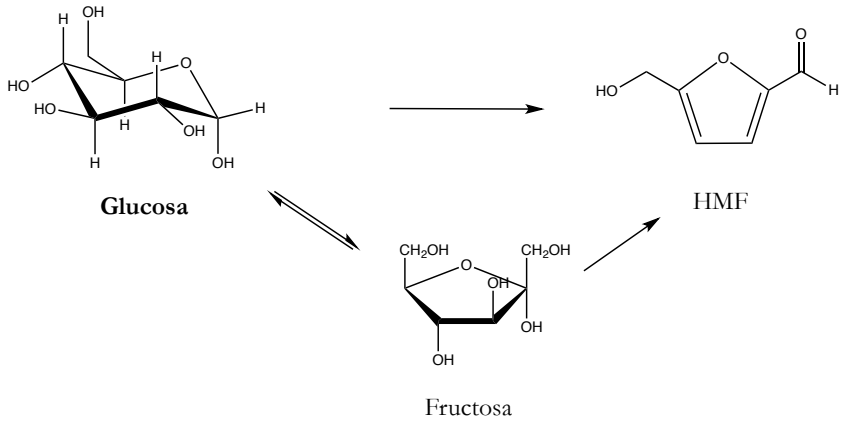

Esquema de reacción 3. Deshidratación de glucosa/fructosa a 5-hidroximetil-2-furfural (HMF)

Oxidación de 5-hidroximetil-2-furfural (HMF) a 2,5-furandicarboxílico (FDCA)

El más claro ejemplo de derivado de HMF con gran potencial es el ácido 2,5-furandicarboxílico (FDCA), obtenido vía oxidación de la molécula de HMF (Esquema de reacción 4). El proceso implica varias etapas de oxidación, en primer lugar: la oxidación del grupo aldehído, que da lugar a

la formación de ácido 5-hidroximetil-2-furancarboxílico (HMFCA) y, en segundo lugar, la oxidación sucesiva del grupo alcohol a aldehído dando lugar a ácido 5-formil-2-furancarboxílico (FFCA) y posteriormente del grupo aldehído ácido, teniendo lugar la formación de ácido 2,5-furandicarboxílico (FDCA).

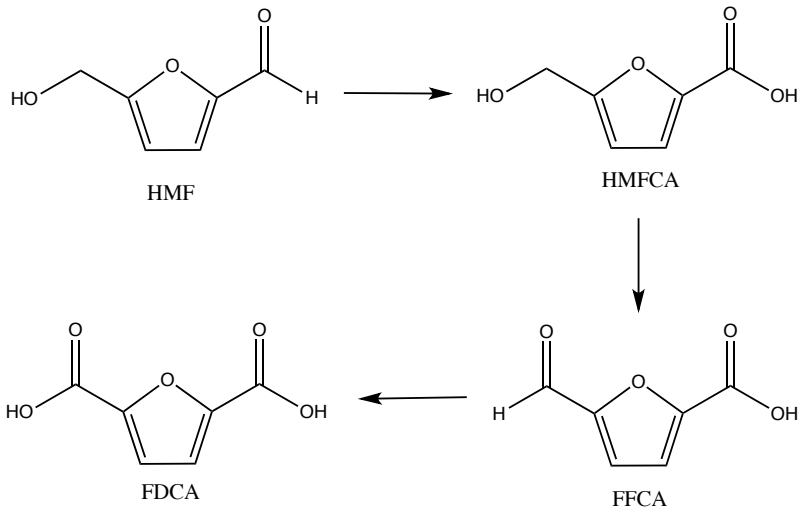

Esquema de reacción 4. Deshidratación de HMF a FDCA.

FDCA es uno de los compuestos que encabeza la lista de productos "Top 10", dada su alta aplicabilidad en la obtención de bioproductos. De hecho, actualmente es considerado un potencial monómero con posibilidad de reemplazar al ácido tereftálico, unidad monomérica utilizada en la producción de polietilentereftalato (PET). La tecnología para la producción de PEF (polietilenfuranoato) ya está siendo aplicada a nivel industrial, con la implantación de la primera planta comercial por parte de la empresa Avantium (Ámsterdam) en 2017.

2. Catalizadores propuestos

Los catalizadores propuestos para el estudio de los procesos mencionados anteriormente están basados en sales de polioxometalatos (POMs) preparadas a partir de la precipitación simple de una disolución del heteropoliácido correspondiente, con formula molecular $H_3PM_{12}O_{40}$ donde M es el metal (en nuestro caso molibdeno, tungsteno o molibdeno-vanadio), y una disolución del líquido iónico (ILs). Los líquidos iónicos utilizados están constituidos por cationes orgánicos e iones inorgánicos, por lo que, al reaccionar con aniones del tipo $[PM_{12}O_{40}]^{3-}$, dan lugar a la formación de la sal híbrida correspondiente, constituida por aniones inorgánicos y cationes orgánicos. Los tres ILs comerciales usados tienen en común el tipo de catión orgánico, un anillo sustituido de imidazol, los cuales difieren en el número de carbonos de uno de sus sustituyentes. Así, se tiene el 1-etil-3-metil imidazolio, 1-butil-3-metil imidazolio y 1-hexil-3-metil imidazolio, cationes que han sido denotados como [C2mim], [C4mim] y [C6mim], respectivamente, nomenclatura que hace alusión al número de carbonos del sustituyente. Por tanto, se obtienen compuestos con fórmula molecular $[Cxmim]_3[PM_{12}O_{40}]$, donde x = 2, 4 o 6 y M = Mo, W o Mo-V (Figura 1).

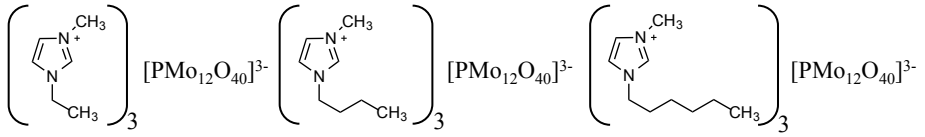

$[C2mim]_3[PMo_{12}O_{40}]$ $[C4mim]_3[PMo_{12}O_{40}]$ $[C6mim]_3[PMo_{12}O_{40}]$

Figura 1. Estructura de tres híbridos POM-IL representativos, basados en el ácido fosfomolíbdico

El número de catalizadores sintetizados asciende a 9 como resultado de la combinación de cada uno de los POM (tres en total) con cada uno de los tres ILs. La Tabla 1 recoge cada una de las estructuras obtenidas, así como la nomenclatura adoptada (simplificada) para los híbridos.

Tabla 1. Lista de todos los compuestos sintetizados y nomenclatura adoptada

Compuesto	Abreviatura
$H_3PW_{12}O_{40}$	PWA
$[C2mim]_3\,[PW_{12}O_{40}]$	[C2mim]PW
$[C4mim]_3\,[PW_{12}O_{40}]$	[C4mim]PW
$[C6mim]_3\,[PW_{12}O_{40}]$	[C6mim]PW
$H_3PMo_{12}O_{40}$	PMoA
$[C2mim]_3\,[PMo_{12}O_{40}]$	[C2mim]PMo
$[C4mim]_3\,[PMo_{12}O_{40}]$	[C4mim]PMo
$[C6mim]_3\,[PMo_{12}O_{40}]$	[C6mim]PMo
$H_5PMo_{10}V_2O_{40}$	PMoVA
$[C2mim]_5\,[PMo_{10}V_2O_{40}]$	[C2mim]PMoV
$[C4mim]_5\,[PMo_{10}V_2O_{40}]$	[C4mim]PMoV
$[C6mim]_5\,[PMo_{10}V_2O_{40}]$	[C6mim]PMoV

La elección de este tipo de compuestos, recientemente sintetizados por primera vez, se realiza en base a dos aspectos fundamentales:

- Potencial de las dos fracciones por separado en reacciones que implican la valorización química de biomasa

Ambas fracciones han demostrado tener un gran potencial en reacciones que implican de un modo u otro el procesado de la fracción lignocelulósica de la biomasa.

La gran aplicabilidad de los polioxometalatos deriva de su multifuncionalidad, la cual transforma este tipo de compuestos en catalizadores adecuados para reacciones que transcurren en varios pasos y, por tanto, pueden necesitar centros activos de distinta naturaleza. En general, estos compuestos son ácidos de Brönsted fuertes (rondando casi la superacidez), contienen cationes metálicos en sus estados de oxidación más altos (Mo^{VI}, W^{VI} y Mo^{VI}- V^{V}), los cuales pueden actuar como centros ácidos de Lewis y tienen un gran potencial de oxidación, lo cual los convierte en catalizadores ideales en reacciones de oxidación. Además de ello, son térmicamente estables y resistentes frente a hidrólisis, lo cual amplía la ventana de trabajo en reacciones en fase líquida.

Hasta ahora, la aplicación principal de estos compuestos en el procesado de biomasa ha sido la despolimerización de celulosa [35] en agua, dando lugar a glucosa, y la disolución y delignificación de lignocelulosa [36]. Por tanto, su uso en reacciones que impliquen la conversión de glucosa a distintos compuestos plataforma es altamente importante, dado que permitiría llevar a cabo procesos que constan de varios pasos en un solo paso.

En cuanto a los líquidos iónicos, han sido usados principalmente como disolventes, formando o no sistemas bifásicos, durante la deshidratación de glucosa/fructosa a HMF [34,37–39]. También durante la delignificación de lignocelulosa [36]. Sin embargo, el verdadero papel de los ILs en ambos procesos no está claro, ya que se ha demostrado que presentan un carácter dual: pueden actuar como disolventes y catalizadores o como co-catalizadores [40]. De hecho, se piensa que durante la deshidratación de fructosa, la formación de HMF está "mediada" por este tipo de compuestos [34].

Teniendo en cuenta el potencial de ambas fracciones por separado, su combinación parece ser el siguiente paso lógico, esperando que los efectos

positivos de ambas se mantengan en los híbridos POM-IL, buscando una mayor multifuncionalidad y, lo más importante, una mayor productividad.

- Centros activos necesarios en cada proceso

De forma general, la epimerización de glucosa a manosa tiene lugar sobre centros ácidos de Lewis, la oxidación de glucosa a ácido glucónico (y la oxidación de HMF a FDCA) necesita catalizadores con buenas propiedades redox y la deshidratación de glucosa tiene lugar sobre una combinación de centros ácidos de Lewis (que potencien la isomerización a fructosa) y ácidos de Brönsted (que lleven a cabo la deshidratación de fructosa a HMF).
Atendiendo a las propiedades y número de centros activos distintos, los catalizadores propuestos parecen ser una opción viable.

3. Objetivos y estructura de la tesis

Varios POMs y tres líquidos iónicos se han seleccionado con el fin de proporcionar el conjunto de sitios activos necesarios para las reacciones de transformación de glucosa que van a abordarse durante este proyecto de investigación. Así, por ejemplo, la epimerización de glucosa necesita centros ácidos de Lewis, la oxidación de glucosa/HMF catalizadores con buenas propiedades redox y la deshidratación de Glucosa/Fructosa la combinación de centros ácidos de Lewis y Brönsted. Con este propósito, se han seleccionado polioxometalatos basados en Mo (alto potencial de oxidación, carácter ácido de Lewis y acidez de Brönsted fuerte), en una combinación de Mo y V, para mejorar las propiedades redox y W, que posee una mayor fuerza ácida. Estas propiedades, combinadas con la de tres líquidos iónicos distintos, dan lugar a materiales multifuncionales

avanzados, cuya combinación de aniones y cationes, permite llevar a cabo un estudio exhaustivo en el que se evalúe tanto la influencia del tipo de anión como de catión.

Por todo lo descrito anteriormente, esta tesis doctoral está dedicada a la aplicación de materiales híbridos, basados en POMs y ILs, en reacciones de transformación de glucosa a distintos compuestos de elevado valor. El principal objetivo de esta tesis es, por tanto, elaborar sistemas catalíticos multifuncionales que sean capaces de participar en reacciones de tipo cascada, partiendo de glucosa como molécula plataforma.

La tesis está organizada en seis capítulos. En el capítulo uno se presenta una introducción general y se sientan las bases que motivan la realización de la investigación en este ámbito. El capítulo dos está dedicado a la descripción de las diferentes técnicas experimentales utilizadas tanto para caracterizar los materiales como para evaluar la actividad catalítica. En el capítulo tres, se expone la síntesis y caracterización estructural de los híbridos, incluyendo la estructura y parámetros cristalográficos de los tres híbridos basando en el ácido fosfomolíbdico. El capítulo cuatro recoge todos los resultados de actividad catalítica de los catalizadores mencionados en tres procesos distintos: la epimerización de glucosa a manosa, la oxidación de glucosa a ácido glucónico y la deshidratación de glucosa/fructosa a HMF. En todos los casos, la estructura sigue una introducción (en la que se explica detenidamente el proceso y se exponen los resultados y catalizadores más relevantes), una parte experimental, un apartado de resultados (donde se realiza la discusión extensa de los mismos), y finalmente una sección dedicada a las conclusiones más relevantes. Derivado de los resultados obtenidos en este capítulo, aparecen los capítulos cinco y seis. Ante la ineficiencia de los híbridos en

reacciones de oxidación, se propone la búsqueda de catalizadores de oxidación alternativos, que puedan aplicarse de forma eficiente tanto en la reacción de oxidación de glucosa como en la de HMF. En este contexto, se introducen catalizadores de oro soportado, cuya síntesis y caracterización se presenta en el capítulo cinco. En este último pueden diferenciarse dos partes: i) la primera, dedicada a la síntesis y caracterización de catalizadores de oro sobre distintos soportes oxídicos a través de un método optimizado, el cual permite obtener nanopartículas de tamaños similares, y ii) la segunda, dedicada a la síntesis y caracterización de catalizadores de oro soportado sobre carbón. En este caso, el método de preparación no está optimizado por lo que, a partir de la variación de ciertos parámetros de la síntesis, se obtiene una batería de 11 muestras con distintos tamaños de partícula. En el capítulo seis, los dos grupos de catalizadores son evaluados en dos reacciones, la oxidación de glucosa y la oxidación de HMF. En ambos casos, se presentan los resultados tras evaluar, entre otros parámetros de reacción, cuál es la influencia del soporte y del tamaño de partícula.

4. Resultados y discusión: breve exposición de algunos datos representativos.

En esta sección se muestran algunos datos representativos obtenidos durante los ensayos catalíticos en cada una de las reacciones citadas. Cabe mencionar que se han seleccionado datos concretos a modo de ejemplo, por lo que esta parte no expone un resumen de resultados riguroso y para su correcto entendimiento deben verse integrados dentro del conjunto de datos obtenidos para cada reacción, respectivamente.

- Epimerización de glucosa a manosa (incluido en capítulo cuatro)

En la Figura 1 se muestran los valores de conversión de glucosa para los tres híbridos basados en el ácido fosfomolíbdico en función de la temperatura de reacción. De forma general, la conversión de glucosa aumenta con la temperatura. Cuando se comparan los datos obtenidos experimentalmente con la literatura (Tabla 2, entradas 2, 3 y 4), es posible asegurar que las conversiones corresponden al equilibrio (o *quasi* equilibrio) a 80, 90 y 100 ºC tras 60 min de reacción.

Indudablemente, la conversión de glucosa depende fuertemente del tipo de catión presente en la estructura, de forma que, a medida que aumenta el número de carbonos del sustituyente en el imidazol, la conversión disminuye, siguiendo la tendencia [C2mim]PMo > [C4mim]PMo > [C6mim]PMo.

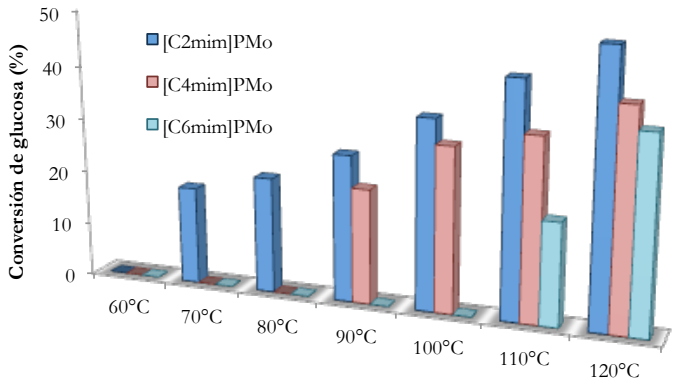

Figura 1. Conversión de glucosa (%) en función de la temperatura de reacción para los híbridos basados en PMoA

Tabla 2. Comparación de los valores de conversión obtenidos experimentalmente usando [C2mim]PMo frente a las conversiones en el equilibrio (literatura).

Entrada	Temperatura (ºC)	Conversión (%) sobre [C2mim]PMo [a]	Conversión en el equilibrio (literatura)
1	70	18	-
2	80	21	26 [41]
3	90	27	30 [42]
4	100	34	32 [43]
5	110	43	-
6	120	49	-

[a] Condiciones de reacción: 5 mL de una disolución 0.2M de glucosa, catalizador 0.4 % molar, referido a la cantidad de glucosa (1:0.05 Glucose:Metal ratio), 60 min y 600 rpm.

- Deshidratación de glucosa/fructosa a HMF (incluido en capítulo cuatro)

La reacción de deshidratación es un proceso complicado en el que deben tenerse en cuenta multitud de parámetros a la hora de optimizar el proceso con un sistema catalítico nuevo. Esta optimización debe incluir un estudio completo del efecto de la concentración inicial de azúcar en la conversión y en la distribución de productos, parámetro clave para controlar la cantidad de subproductos que pueden aparecer como consecuencia del gran número de reacciones secundarias que pueden darse en medio ácido [44,45]. Del mismo modo, debe estudiarse en detalle la influencia del tiempo de reacción, la cantidad de catalizador, el tipo de disolvente y la relación de volumen agua:disolvente orgánico (utilizado para extraer HMF y así evitar reacciones secundarias que conllevan su degradación). En esta tesis, solo una parte de todos los parámetros implicados ha sido estudiada, de manera superficial, con el fin de obtener conocimientos acerca del sistema, que puedan ser utilizados como punto

de partida para futuras investigaciones. A modo de ejemplo, en el presente resumen se exponen los resultados obtenidos tras evaluar la influencia de la relación de volúmenes de fase acuosa y orgánica. Como fase orgánica (disolvente extractor) se utiliza metilisobutilcetona (MIBK), disolvente ampliamente utilizado dado su bajo punto de ebullición (lo cual permitiría aislar el compuesto puro) y el buen coeficiente de reparto de HMF. En la Tabla 3 aparece la conversión de fructosa (%) así como la selectividad a HMF comparada con la selectividad a los subproductos (%) en función de la relación H_2O:MIBK, cuando se usa como catalizador [C2mim]PMo (las condiciones de reacción se encuentran detalladas en el pie de tabla).

Tabla 3. Selectividad a HMF y subproductos en función de la relación de volumen H_2O:MIBK

Entrada	H_2O:MIBK relación de volumen	Conversión (%)	Selectividad (%)	
			HMF	Subproductos (no analizados)
1	1:3	90	**27**	36
2	1:5	99	**21**	56
3	1:7	93	**30**	44
4	1:10	90	**34**	19

Condiciones de reacción: 1mmol de fructosa (0.1802 g), catalizador en un 0.25% molar referido a la cantidad de azúcar (0.006 g), 1 mL of H_2O y 3, 5, 7 y 10 mL of MIBK, respectivamente, tras 18 h a 120 ºC y 600 rpm

El incremento en el volumen de fase orgánica utilizado no influencia la conversión, sin embargo, la selectividad a HMF y, más importante, a los subproductos, depende fuertemente de la cantidad de MIBK utilizada. A medida que aumenta el volumen de fase orgánica, aumenta la selectividad a HMF y disminuye la cantidad de subproductos. Esto último es lógico teniendo en cuenta la migración de HMF de una fase a otra: un mayor volumen de fase orgánica implica una mayor concentración de HMF hasta

alcanzar el equilibrio de reparto, lo cual se traduce en un aumento en la selectividad.

- Oxidación de glucosa sobre catalizadores soportados de oro (incluido en capítulo seis)

La influencia del soporte en la reacción de oxidación de glucosa en presencia de O_2 ha sido estudiada a través de la evaluación catalítica de catalizadores de oro de tamaño de partícula similar. Los soportes usados para tal fin fueron Al_2O_3, CeO_2, CeO_2(20%wt)/Al_2O_3, CeO_2(25%wt)/ZrO_2 y CeO_2(50%wt)/ZrO_2. Con el fin de simplificar, se adoptó la nomenclatura Al, Ce, CeAl, Ce25Zr y Ce50Zr, respectivamente. En el caso de los catalizadores, el prefijo Au precede a las abreviaturas anteriores.

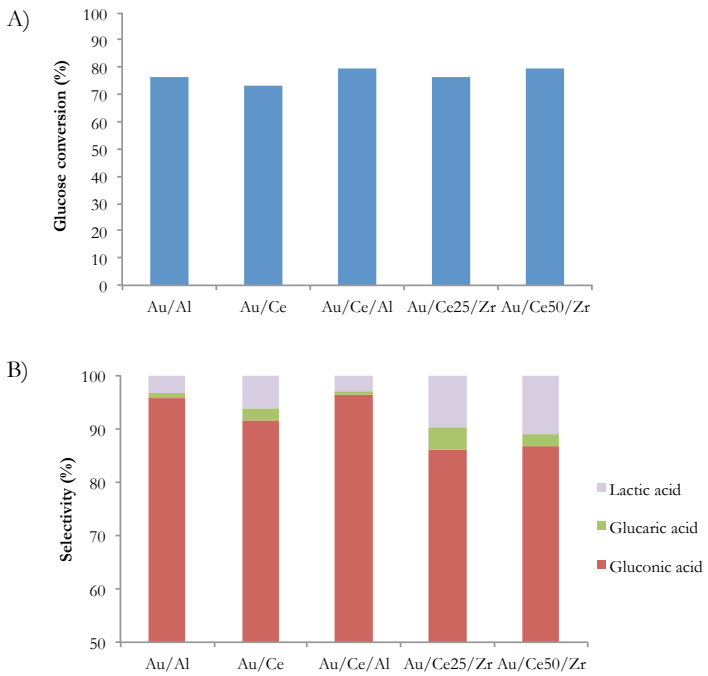

Figura 2. A) Conversión de glucosa (%) sobre diferentes catalizadores de oro soportado (18 h, 120ºC, 600 rpm), B) Selectividad (%)

La conversión de glucosa tras 18 h de reacción no parece estar influenciada por la naturaleza del soporte, estando por encima del 75% en todos los casos (Figura 2). Sin embargo, la distribución de productos se ve afectada enormemente, apareciendo productos como consecuencia de reacciones secundarias. Tal es el caso del ácido láctico, cuya selectividad aumenta en los sistemas que contienen zircona, siendo AuAl y AuCeAl los catalizadores más selectivos hacia la formación de ácido glucónico.

- Oxidación de HMF sobre catalizadores soportados de oro (incluido en capítulo seis)

Del mismo modo al apartado anterior, la influencia del soporte en la actividad catalítica fue evaluada en la reacción de oxidación de HMF a FDCA, con los mismos catalizadores (Figura 3, las condiciones de reacción aparecen en el pie de figura). La conversión alcanzada en todos los casos es del 100%, sin embargo, se observa una influencia clara del soporte en la distribución de productos (representados como rendimientos). Entre los soportes que incluyen alúmina, la adición de cerio parecer promover la oxidación al producto final, FDCA, mientras que, teniendo en cuenta AuCe, AuCe50Zr y AuCe25Zr, donde la cantidad de ceria en el soporte decrece desde 100 a 50 y a 25%, la presencia de zirconio parece impulsar la oxidación. La posible explicación y causas a este comportamiento se exponen en el correspondiente capítulo.

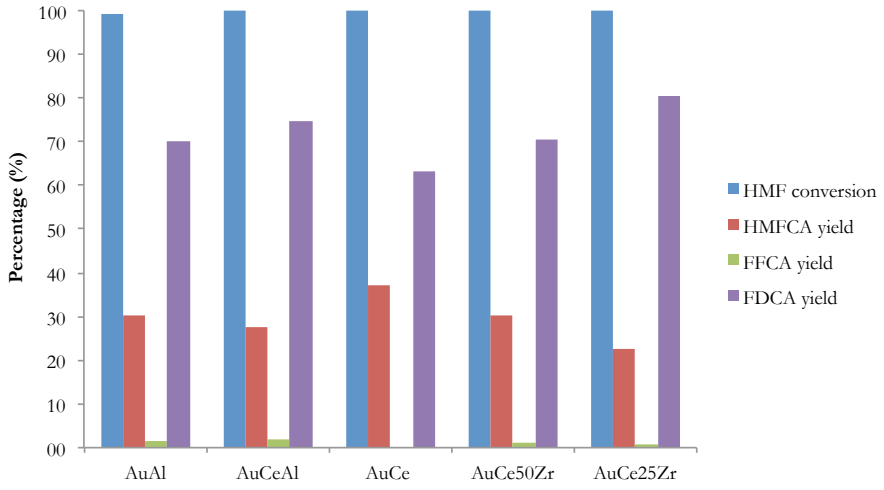

Figura 3. Influencia del soporte en la reacción de oxidación de HMF. Condiciones de reacción: relación molar HMF:Au:NaOH 1:0.01:2, 10 bar O_2, 70 ºC, 400 rpm

Referencias

[1] B. Kamm, M. Kamm, Principles of biorefineries, Appl. Microbiol. Biotechnol. 64 (2004) 137–145.

[2] P. Gallezot, Conversion of biomass to selected chemical products, Chem. Soc. Rev. 41 (2012) 1538–1558.

[3] F. Cherubini, The Biorefinery Concept: Using Biomass Instead of Oil for Producing Energy and Chemicals, Energy Convers. Manag. 51 (2010) 1412–1421.

[4] Biorefineries: adding value to the sustainable utilisation of biomass, IEA Bioenergy, (2009).

[5] http://www.roquette.com/documentation/roquette-group-communicationkit/swf_article=6790/;model_name:documentation_ request/, (n.d.).

[6] http://www.cognis.com, (n.d.).

[7] L.E. Manzer, Recent Developments in the Conversion of Biomass to Renewable Fuels and Chemicals, Top. Catal. 53 (2010) 1193–1196.

[8] J.-P. Lange, Sustainable chemical manufacturing: a matter of resources, wastes, hazards, and costs, ChemSusChem. 2 (2009) 587–592.

[9] V. Dornburg, B. Hermann, M. Patel, Scenario projections for future market potentials of biobased bulk chemicals, Env. Sci Technol. 42 (2008) 2261–2267.

[10] T. Willke, K. Vorlop, Industrial bioconversion of renewable resources as an alternative to conventional chemistry, Appl Microbiol Biotechnol. 66 (2004) 131–142.

[11] P. Gallezot, Direct routes from biomass to end-products, Catal. Today. 167 (2011) 31–36.

[12] R. Rinaldi, F. Schüth, Design of solid catalysts for the conversion of biomass, Energy Environ. Sci. 2 (2009) 610–626.

[13] M.J. Climent, A. Corma, S. Iborra, M. Mifsud, A. Velty, New one-pot multistep process with multifunctional catalysts: decreasing the E factor in the synthesis of fine chemicals, Green Chem. 12 (2010) 99–107.

[14] H. Mehdi, V. Fábos, R. Tuba, A. Bodor, L.T. Mika, I.T. Horváth, Integration of Homogeneous and Heterogeneous Catalytic Processes for a Multi-step Conversion of Biomass: From Sucrose to Levulinic Acid, γ-Valerolactone, 1,4-Pentanediol, 2-Methyl-tetrahydrofuran, and Alkanes, Top. Catal. 48 (2008) 49–

54.

[15] A. Brandt, J. Gräsvik, J.P. Halletta, T. Welton, Deconstruction of lignocellulosic biomass with ionic liquids, Green Chem. 15 (2013) 550–583.

[16] H. Jørgensen, J.B. Kristensen, C. Felby, Enzymatic conversion of lignocellulose into fermentable sugars: challenges and opportunities, Biofuels, Bioprod. Bioref. 1 (2007) 119–134.

[17] T. Granström, G. Takata, M. Tokuda, I. K., Izumoring: a novel and complete strategy for bioproduction of rare sugars., J. Biosci. Bioeng. 97 (2004) 89–94.

[18] G. Gumina, G.-Y. Song, C.K. Chu, l-Nucleosides as chemotherapeutic agents, Microbiol. Lett. 202 (2001) 9–15.

[19] B. Kamm, Production of Platform Chemicals and Synthesis Gas from Biomass, Angew. Chemie Int. Ed. 46 (2007) 5056–5058. doi:10.1002/anie.200604514.

[20] S. Ramachandran, P. Fontanille, A. Pandey, C. Larroche, Gluconic Acid : Properties , Applications and Microbial Production, Food Technol. Biotechnol. 44 (2006) 185–195.

[21] M.J. Climent, A. Corma, S. Iborra, Converting carbohydrates to bulk chemicals and fine chemicals over heterogeneous catalysts, Green Chem. 13 (2011) 520.

[22] E.S. H. Hustede, H.J. Haberstroh, Ullmann's Encyclopedia of Industrial Chemistry, 1989.

[23] M. Bellardita, E.I. García-López, G. Marcì, B. Megna, F.R. Pomilla, L. Palmisano, Photocatalytic conversion of glucose in aqueous suspensions of heteropolyacid–TiO_2 composites, RSC Adv. 5 (2015) 59037–59047.

[24] K. Buchholz, J. Seibel, Industrial carbohydrate biotransformations, Carbohydr. Res. 343 (2008) 1966–1979.

[25] Y. Xiao, Y.-F. Song, Efficient catalytic conversion of the fructose into 5-hydroxymethylfurfural by heteropolyacids in the ionic liquid of 1-butyl-3-methyl imidazolium chloride, Appl. Catal. A Gen. 484 (2014) 74–78.

[26] Y. Qu, C. Huang, J. Zhang, B. Chen, Efficient dehydration of fructose to 5-hydroxymethylfurfural catalyzed by a recyclable sulfonated organic heteropolyacid salt, Bioresour. Technol. 106 (2012) 170–172.

[27] Y. Liu, L. Zhu, J. Tang, M. Liu, R. Cheng, C. Hu, One-pot, One-step Synthesis of 2,5-Diformylfuran from Carbohydrates over Mo-Containing Keggin Heteropolyacids, ChemSusChem. 7 (2014) 3541–3547.

[28] J.S. Kruger, V. Nikolakis, D.G. Vlachos, Carbohydrate dehydration using porous catalysts, Curr. Opin. Chem. Eng. 1 (2012) 312–320.

[29] J.S. Kruger, V. Nikolakis, D.G. Vlachos, Aqueous-phase fructose dehydration using Brønsted acid zeolites: Catalytic activity of dissolved aluminosilicate species, Appl. Catal. A Gen. 469 (2014) 116–123.

[30] J.C. Serrano-Ruiz, R.M. West, J.A. Dumesic, Catalytic Conversion of Renewable Biomass Resources to Fuels and Chemicals, Annu. Rev. Chem. Biomol. Eng. 1 (2010) 79–100.

[31] E. Nikolla, Y. Román-Leshkov, M. Moliner, M.E. Davis, "One-Pot" Synthesis of 5-(Hydroxymethyl)furfural from Carbohydrates using Tin-Beta Zeolite, ACS Catal. 1 (2011) 408–410.

[32] E. Sairanen, R. Karinen, J. Lehtonen, Comparison of Solid Acid-Catalyzed and Autocatalyzed C5 and C6 Sugar Dehydration Reactions with Water as a Solvent, Catal. Letters. 144 (2014) 1839–1850.

[33] J.J. Bozell, G.R. Petersenb, Technology development for the production of biobased products from biorefinery carbohydrates—the US Department of Energy's "Top 10" revisited, Green Chem. 12 (2010) 539–554.

[34] M.E. Zakrzewska, E. Bogel-łukasik, R. Bogel-łukasik, Ionic Liquid-Mediated Formation of 5-Hydroxymethylfurfural s A Promising Biomass-Derived Building Block, Chem. Rev. 111 (2011) 397–417.

[35] W. Deng, Q. Zhang, Y. Wang, Polyoxometalates as efficient catalysts for transformations of cellulose into platform chemicals, Dalt. Trans. 41 (2012) 9817.

[36] F. Cheng, H. Wang, R.D. Rogers, Oxygen Enhances Polyoxometalate-based Catalytic Dissolution and Deligni fi cation of Woody Biomass in Ionic Liquids, ACS Sustain. Chem. Eng. 2 (2014) 2859–2865.

[37] F.D. Anna, S. Marullo, P. Vitale, C. Rizzo, P. Lo Meo, R. Noto, Applied Catalysis A : General Ionic liquid binary mixtures : Promising reaction media for carbohydrate conversion into 5-hydroxymethylfurfural, Appl. Catal. A Gen. 482 (2014) 287–293.

[38] J. Song, H. Fan, J. Ma, B. Han, Conversion of glucose and cellulose into value-added products in water and ionic liquids, Green Chem. 15 (2013) 2619–2635.

[39] S. Hu, Z. Zhang, J. Song, Y. Zhou, B. Han, Efficient conversion of glucose into 5-hydroxymethylfurfural catalyzed by a common Lewis acid SnCl4 in an ionic liquid, Green Chem. 11 (2009) 1746. doi:10.1039/b914601f.

[40] H. Olivier-Bourbigou, L. Magna, D. Morvan, Ionic liquids and catalysis: recent progress from knowledge to applications, Appl. Catal. A. 373 (2010) 1–56.

[41] S.J. Angyal, The composition and conformation of sugars in solution, Angew. Chemie - Int. Ed. 8 (1969) 157–166.

[42] A. Cybulski, B.F.M. Kuster, G.B. Marin, The kinetics of the molybdate-catalysed epimerization of D-glucose and D-mannose in aqueous solutions, J. Mol. Catal. 68 (1991) 87–103.

[43] F. Ju, D. Vandervelde, E. Nikolla, Molybdenum-Based Polyoxometalates as Highly Active and Selective Catalysts for the Epimerization of Aldoses, ACS Catal. 4 (2014) 1358–1364.

[44] Q. Zhao, L. Wang, S. Zhao, X. Wang, S. Wang, High selective production of 5-hydroymethylfurfural from fructose by a solid heteropolyacid catalyst, Fuel. 90 (2011) 2289–2293.

[45] M.B. Fusaro, V. Chagnault, D. Postel, Reactivity of D-fructose and D-xylose in acidic media in homogeneous phases, Carbohydr. Res. 409 (2015) 9–19.

Anexos

Durante el desarrollo de la presente tesis, se han publicado los siguientes trabajos, que se incluyen a continuación:

- C. Megías-Sayago, C.J. Carrasco, S. Ivanova, F.J. Montilla, A. Galindo, J.A. Odriozola, "Influence of the ionic liquid presence on the selective oxidation of glucose over molybdenum based catalysts" Catalysis Today 278 (2016) 82-90

- C. Megías-Sayago, S. Ivanova, C. López-Cartes, M.A. Centeno, J.A. Odriozola, "Gold catalysts screening in base-free aerobic oxidation of glucose to gluconic acid" Catalysis Today 279 (2017) 148-154

- C. Megías-Sayago, J.L. Santos, F. Ammari, M. Chenouf, S. Ivanova, M.A. Centeno, J.A. Odriozola, "Influence of gold particle size in Au/C catalysts for base-free oxidation of glucose" Catalysis Today (2017) *In press* http://dx.doi.org/10.1016/j.cattod.2017.01.007

- C. Megías-Sayago, L.F. Bobadilla, S. Ivanova, A. Penkova, M.A. Centeno, J.A. Odriozola, "Gold catalyst recycling study in base-free glucose oxidation reaction" " Catalysis Today (2017) *In press* http://dx.doi.org/10.1016/j.cattod.2017.03.022

Asimismo, han sido aceptadas las siguientes comunicaciones a congresos:

- "Oxidación selectiva de glucosa en presencia de O_2 sobre catalizadores de oro soportado", C. Megías-Sayago, S. Ivanova, M. A. Centeno, J. A. Odriozola. Reunión Bienal de la Sociedad Española de Catálisis (SECAT 15), Barcelona (España) 13-15 Julio 2015. Comunicación oral.

- "Influence of the ionic liquid presence on the selective oxidation of glucose over molybdenum based catalysts", C. Megías-Sayago, C.J. Carrasco, S. Ivanova, F.J. Montilla, A. Galindo, J.A. Odriozola. XII European Congress on Catalysis (EUROPACAT XII), Kazán (Rusia), 30 de Agosto – 4 de Septiembre 2015. Comunicación oral

- "Polyoxometalate/ionic liquids hybrids as a catalyst for the isomerization of glucose to fructose in water", C. Megías-Sayago, S. Ivanova, M. A. Centeno, J. A. Odriozola. 11th International Symposium on Heterogeneous Catalysis, Varna (Bulgaria) 6-9 Septiembre 2017. Comunicación oral.

- "Gold catalysts screening in the selective aerobic oxidation of glucose", C. Megías-Sayago, S. Ivanova, M. A. Centeno, J. A. Odriozola. 3nd International Congress on Catalysis for Biorefineries, Rio de Janeiro (Brasil), 28-30 Septiembre 2017. Comunicación oral.

- "Direct catalytic conversion of glucose to lactic acid", C. Megías-Sayago, S. Ivanova, M. A. Centeno, J. A. Odriozola. French Conference on Catalysis (FCCat 2016) Frejus (Francia) 23-27 Mayo 2016. Póster.

- "Gold on carbon for biomass conversion: the case of selective base-free glucose oxidation", C. Megías-Sayago, J. L. Santos, M. Chenouf, F. Ammari, S. Ivanova, M. A. Centeno, J. A. Odriozola. 7th International Symposium on Carbon for Catalysis (CarboCat VII), Estrasburgo (Francia), 12-16 Junio 2016. Comunicación oral.

- "Crystal structure of new polyoxometalate/ionic liquid hybrids and their application in catalysis", C. Megías-Sayago, E. Álvarez, S. Ivanova, J. A. Odriozola. Challenges and Prospects for Solid State Chemistry (CPSSC 16), Sevilla (España) 9-10 Septiembre 2016. Póster.

- "Influence of support to gold catalyst activity for the production of 2,5-furandicarboxilic acid", C. Megías-Sayago, A. Lolli, S. Ivanova, S. Albonetti, F. Cavani, J. A. Odriozola. Reunión Bienal de la Sociedad Española de Catálisis (SECAT 17), Oviedo (España) 26-26 Junio 2017. Comunicación oral.

- "Which is the support contribution to gold catalyst activity for FDCA production?", C. Megías-Sayago, A. Lolli, S. Ivanova, S. Albonetti, F. Cavani, J. A. Odriozola. 8th World Congress on Oxidation Catalysis (WCOC 2017), Cracovia (Polonia), 3-8 Septiembre 2017. Comunicación oral.

- "Catalizadores de oro, platino y paladio sobre carbón para la producción de ácido 2,5-furandicarboxílico" C. Megías-Sayago, J. L. Santos, A. Lolli, S. Ivanova, S. Albonetti, M. A. Centeno, F. Cavani, J. A. Odriozola. Reunión del Grupo Español del Carbón (GEC 17), Málaga (España), 22-25 Octubre 2017. Comunicación oral.

Catalysis Today 278 (2016) 82–90

Contents lists available at ScienceDirect

Catalysis Today

journal homepage: www.elsevier.com/locate/cattod

Influence of the ionic liquid presence on the selective oxidation of glucose over molybdenum based catalysts

C. Megías-Sayago[a,b,*], C.J. Carrasco[a], S. Ivanova[a,b], F.J. Montilla[a], A. Galindo[a], J.A. Odriozola[a,b]

[a] Departamento de Química Inorgánica, Universidad de Sevilla, C/Profesor García González, S/N, 41012, Sevilla, Spain
[b] Instituto de Ciencia de Materiales de Sevilla, Centro mixto CSIC-US, Avda. Américo Vespucio 49, 41092, Sevilla, Spain

ARTICLE INFO

Article history:
Received 14 December 2015
Received in revised form 14 June 2016
Accepted 15 June 2016
Available online 22 June 2016

Keywords:
Glucose oxidation
Ionic liquids
Molybdenum catalysts
Polioxometalates

ABSTRACT

Two different approaches are proposed in this work in order to study the influence of the ionic liquid presence in the reaction of glucose oxidation by H_2O_2 in mild conditions. The ionic liquids are applied either as a solvent by using homogeneous Mo based catalyst, $[Mo(O)(O_2)_2(H_2O)_n]$ complex, or by using it as an integral part of a heterogeneous catalyst, organic inorganic hybrids based on Mo Keggin structure. Both catalytic strategies resulted in acceptable glucose transformation degrees but lead to different oxidation products depending on the role of the ionic liquid. The hybrid approach restrains the number of the received products being the most selective one. A detailed study of the effect of the hybrid nature and reaction conditions is proposed in the second part of this study.

1. Introduction

The efficient transformations of polysaccharides into valuable compounds, such as fuels and important intermediate chemicals is a relevant topic nowadays and has attracted the attention of the scientific community [1–4]. The glucose, the monomer of cellulose, constitutes the most abundant and available monosaccharide and its transformations into furan derivatives like HMF (hydroxymethyl furfural) [5], FDCA (Furan dicarboxylic acid) [6], DFF (2,5 diformylfuran) [7] or sugar acids (aldonic and aldaric acids) is being widely investigated in the last years [8–10]. Within added-value chemicals issued from glucose, the gluconic acid, obtained via oxidation of the glucose aldehyde group is in versatile use in pharmaceutical, chemical, food, beverage and textile industries, either as additive, as chelating agent for cleaning purposes or for the extraction of metal traces in solutions [11]. Its current production is carried out via enzymatic process, in presence of glucose oxidase. However, this methods presents several drawbacks such as need of high amounts of expensive enzyme, its irreversible deactivation, the exhaustive control of process parameters (such as pH and temperature), the need of several pre-reaction purification processes in order to remove impurities and the long reaction times to obtain acceptable yields [12]. All this disadvantages stimulates the pursuit for new efficient, environmental friendly catalysts and processes to improve carbohydrate conversion and, therefore, biomass exploitation.

The production of gluconic acid has been studied over catalysts of different nature, including enzymatic [13] and heterogeneous, based on platinum [14,15] and, more recently, on gold [16,17]. Recently, a group of compounds, the as called ionic liquids (ILs), showed great potential in carbohydrate chemistry either as catalyst or as a solvent. The ILs are compounds consisting in ions with melting points below 100 °C whose principal advantages could be resumed in high ionic mobility, good electric conductivity, low vapor pressure and good thermal and chemical stability [18,19]. Most commonly used ILs are composed by quaternary ammonium salts or cyclic amine salts [20]. They have already found its application in catalysis as a solvents [21–24] in electrochemistry [25] and organic synthesis, however, the use of the ionic liquid as a part of hybrid catalyst is barely studied [20,26–30].

On the other hand the polyoxometalates, well-known catalytically active compounds were also considered as a potential glucose transformation catalysts [20]. In particular, the Keggin-type polyoxometalates, classified as anionic metal-oxygen clusters of the early transition metals, appear as a good candidates for carbohydrate conversion [31–33]. Properties like strong Brönsted acidity, fast multi-electron transfer, high proton mobility, high solubility in various solvents and resistance to hydrolytic and oxidative degradations in solutions converts these compounds in versatile

* Corresponding author at: Instituto de Ciencia de Materiales de Sevilla, Centro mixto CSIC-US, Avda. Américo Vespucio 49, 41092, Sevilla, Spain.
E-mail address: cristina.megias@icmse.csic.es (C. Megías-Sayago).

http://dx.doi.org/10.1016/j.cattod.2016.06.040
0920-5861/

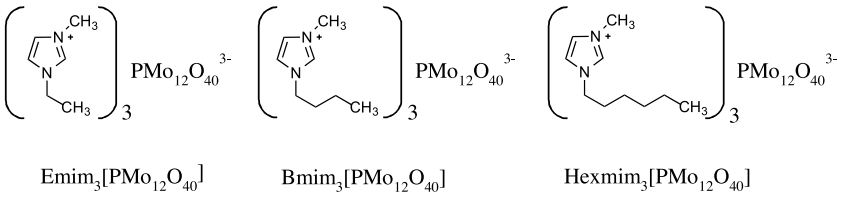

Fig. 1. Structure of IL/$PMo_{12}O_{40}$ hybrids used as catalytic *System 2*.

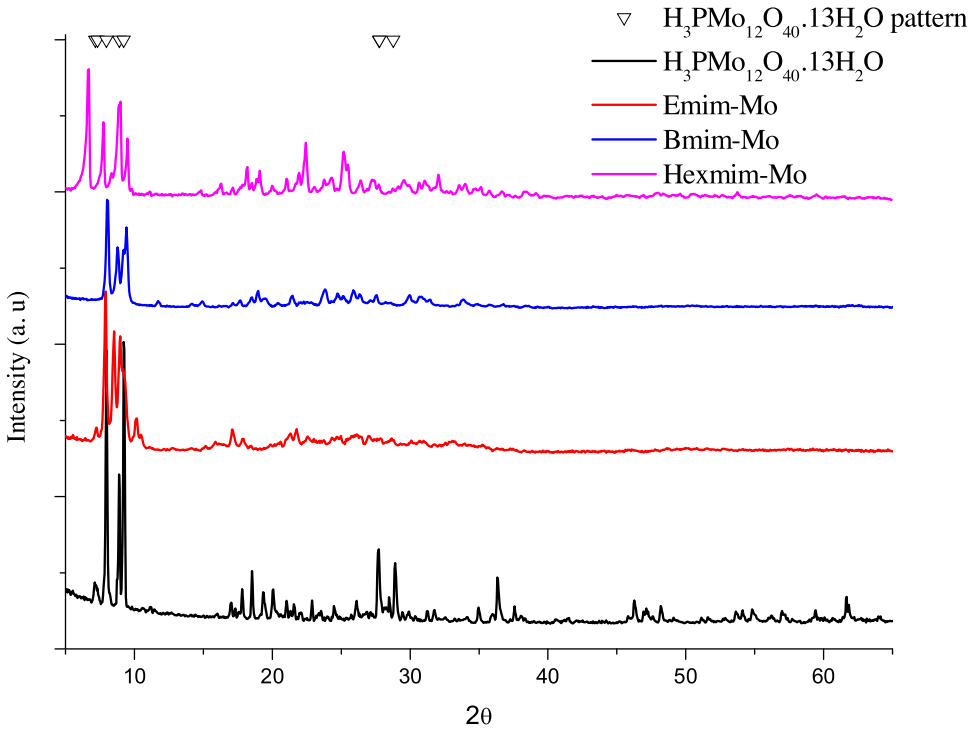

Fig. 2. XRDiffractograms of $H_3PMo_{12}O_{40}{\cdot}13H_2O$ (JCPDS #01-075-1588) and its hybrids.

materials for using in catalysis [34]. Furthermore, their properties can be tuned by varying the composition and the counter cations [31,35,36]. The proton compensated polyoxometalates, known as heteropoly acids (HPA) however cannot be used in liquid-phase reactions with polar solvents due to their solubility and impossibility for recuperation. However, the substitution of protons with another organic or inorganic cations results in insoluble materials and, therefore, useful in heterogeneously catalyzed liquid-phase reactions [31]. Additionally, the substitution of all the protons with organic cations could results in a new class of organic-inorganic hybrid materials which takes advantages on both inorganic (strength, thermal stability and chemical resistance) and organic part (lightness, flexibility and versatility) features. Perfect example of organic cations which could be applied in the hybrid are those of ionic liquids (ILs) [20,37–39].

In this context, the main goal of this work is to study the influence of the IL on the catalytic performance of Mo based compounds. The ionic liquids are evaluated either as a solvent (*System 1*) or as integral part of the catalyst (*System 2*) in the liquid-phase oxidation of glucose with hydrogen peroxide as oxidant. In *system 1*, 1-butyl-3-methylimidazolium hexafluorophosphate (Bmim)PF_6 ionic liquid is used as solvent and $[Mo(O)(O_2)_2(H_2O)_n]$ complex as catalyst. In *system 2*, three different hybrids based on phosphomolybdic acid ($PMo_{12}O_{40}^{3-}$) and three IL cations, 1-ethyl-3-methylimidazolium (Emim), 1-buthyl-3-methylimidazolium (Bmim) and 1-hexyl-3-methylimidazolium (Hexmim), are used as catalysts in aqueous solution.

2. Experimental

2.1. Synthesis

2.1.1. Synthesis of oxodiperoxomolybdenum complex (System 1)

Solution of the aqua complex of oxodiperoxomolybdenum, $[Mo(O)(O_2)_2(H_2O)_n]$ (henceforth $[MoO_5]$) was prepared as follows. A suspension of MoO_3 (Sigma Aldrich, 3.617 g, 25 mmol) in 40 mL 30% aqueous hydrogen peroxide (VWR) was heated at 50 °C with continuous stirring overnight after which complete dissolution of the molybdenum resulting in a clear yellow solution was observed. At this point the solution was cooled to 0 °C and several drops of hydrogen peroxide were added and the solution was then made up to 100 mL and stored in a sealed volumetric flask at 4 °C. Occasional venting of this solution is advised upon prolonged storage due to the accumulation of pressure following catalytic decomposition of hydrogen peroxide. A solution of $[MoO_5]$ with concentration 0.25 M is thus obtained.

2.1.2. Synthesis of heteropolyacid and hybrids (System 2)

Phosphomolybdic acid was prepared as reported in the literature [40] by using $Na_2MoO_4{\cdot}2H_2O$ (Sigma Aldrich), H_3PO_4 (85%) (Panreac), HCl (37%) (VWR), diethyl ether (Panreac), HNO_3 (65%) (VWR) and distilled water.

For the $Emim_3[PMo_{12}O_{40}]$ (from this point forward Emim-Mo) synthesis [30], appropriate quantities of prepared $H_3PMo_{12}O_{40}$ (0.9 g) and 1-ethyl-3-methylimidazolium methanesulfonate (Alfa

Table 1
Identified crystal phases at different temperatures.

Temperature, °C	Phases ($H_3PMo_{12}O_{40}\cdot13H_2O$)	Phases ($Emim_3[PMo_{12}O_{40}]$)	Phases ($Bmim_3[PMo_{12}O_{40}]$)	Phases ($Hexmim_3[PMo_{12}O_{40}]$)
RT	$H_3PMo_{12}O_{40}\cdot13H_2O$	$Emim_3[PMo_{12}O_{40}]$	$Bmim_3[PMo_{12}O_{40}]$	$Hexmim_3[PMo_{12}O_{40}]$
50	$H_3PMo_{12}O_{40}\cdot13H_2O$	$Emim_3[PMo_{12}O_{40}]$	$Bmim_3[PMo_{12}O_{40}]$	$Hexmim_3[PMo_{12}O_{40}]$
100	$H_3PMo_{12}O_{40}\cdot6H_2O$	$Emim_3[PMo_{12}O_{40}]$	$Bmim_3[PMo_{12}O_{40}]$	$Hexmim_3[PMo_{12}O_{40}]$
150	$H_3PMo_{12}O_{40}\cdot1.5H_2O$	$Emim_3[PMo_{12}O_{40}]$	$Bmim_3[PMo_{12}O_{40}]$	$Hexmim_3[PMo_{12}O_{40}]$
200	$H_3PMo_{12}O_{40}\cdot1.5H_2O$	$Emim_3[PMo_{12}O_{40}]$	$Bmim_3[PMo_{12}O_{40}]$	$Hexmim_3[PMo_{12}O_{40}]$
250	$H_3PMo_{12}O_{40}\cdot1.5H_2O$	$Emim_3[PMo_{12}O_{40}]$	$H_3PMo_{12}O_{40}\cdot13H_2O$ + $10MoO_3\cdot H_3PO_4\cdot24H_2O$	Amorphous
300	$H_3PMo_{12}O_{40}\cdot1.5H_2O$	$Emim_3[PMo_{12}O_{40}]$	$H_3PMo_{12}O_{40}\cdot13H_2O$ + $10MoO_3\cdot H_3PO_4\cdot24H_2O$	Amorphous
350	$H_3PMo_{12}O_{40}\cdot1.5H_2O$	$H_3PMo_{12}O_{40}\cdot13H_2O$ + $10MoO_3\cdot H_3PO_4\cdot24H_2O$	$H_3PMo_{12}O_{40}\cdot13H_2O$ + $10MoO_3\cdot H_3PO_4\cdot24H_2O$	Amorphous
400	$H_3PMo_{12}O_{40}\cdot1.5H_2O$	$H_3PMo_{12}O_{40}\cdot13H_2O$ + $10MoO_3\cdot H_3PO_4\cdot24H_2O + MoP_2O_7$	$H_3PMo_{12}O_{40}\cdot13H_2O$ + $10MoO_3\cdot H_3PO_4\cdot24H_2O + MoP_2O_7$	Amorphous
450	$MoP_2O_7 + MoO_3$	$H_3PMo_{12}O_{40} + MoP_2O_7 + MoO_3$	$10MoO_3\cdot H_3PO_4\cdot24H_2O + MoP_2O_7$	Amorphous
500	$MoP_2O_7 + MoO_3$	MoO_3	MoO_3	Amorphous + MoO_3
550	MoO_3	MoO_3	MoO_3	MoO_3
600	MoO_3	MoO_3	MoO_3	MoO_3
650	MoO_3	MoO_3	MoO_3	MoO_3
700	MoO_3	MoO_3	MoO_3	MoO_3
750	MoO_3	MoO_3	MoO_3	MoO_3

Aesar) were dissolved in distilled water (20 mL) separately. When mixed, a precipitate was formed, then filtered and dried at room temperature. Another two hybrids were analogously prepared by using 1-butyl-3-methylimidazolium methanesulfonate (Sigma Aldrich) to produce the $Bmim_3[PMo_{12}O_{40}]$ (Bmim-Mo) and 1-hexyl-3-methylimidazolium chloride (Alfa Aesar) for $Hexmim_3[PMo_{12}O_{40}]$ (Hexmim-Mo). All the hybrids were used as prepared and their structures are presented in Fig. 1.

2.2. Characterization

X-ray diffraction (XRD) analysis were registered on a Panalitycal X'Pert Pro diffractometer, equipped with Cu anode with 0,05° step size and time acquisition of 80 s at room temperature in the 5 65°2θ range.

Temperature dependent X-ray diffraction (TDRX) analysis was performed in a high temperature camera Anton Paar HTK 1200 coupled with an X'Pert Pro Philips diffractometer equipped with Cu anode. The diffractograms were taken every 50 °C in the range of 30–750 °C, from 5° to 65° 2θ (step size 0,05° and step time 50 s) in air. The heating ramp was fixed to 10 °C/min.

Raman spectroscopy analysis were performed in a LabRAM Horiba Jobin Yvon microscope equipped with confocal microscopy and green laser (λ = 532 nm). Samples were studied with 50× lens and intensity filter (D2).

2.3. Catalytic reaction

2.3.1. General procedure for System 1

The reactor (a 50 mL vial equipped with a Young valve and containing a stirrer flea) was charged with 0.25 M aqueous $[MoO_5]$ (100 μL, 2.5 mol% of glucose), the solvent [41] ($BmimPF_6$, 2 mL), the oxidant (30% aqueous H_2O_2, 340 μL, 3 mmol) and α-D-Glucose (Sigma Aldrich, 182 mg, 1 mmol), in the aforementioned order. The reactor was sealed and the solution reacted with constant stirring (600 rpm) in a thermostated oil bath (60 °C) during 18 h. Upon completion, the reactor was immediately cooled to 0 °C and the mixture was extracted with H_2O (3 × 2 mL) and filtered with 0.45 μm nylon syringe filter. The resulting solution was diluted in ultra-pure water (500 μL of sample + 500 μL of H_2O) and analyzed by HPLC by using a Hi-Plex H column (300 × 7.7 mm), a refractive index detector (Varian 360-LC) and MilliQ water as mobile phase. Conversion, selectivity and C balance were obtained from HPLC measurements.

2.3.2. General procedure for System 2

α-D-Glucose (1 mmol) and 30% hydrogen peroxide (3 mmol) were added to the reactor using water (2 mL) as solvent and each hybrid (0.25 or 2.5 mol% of glucose) as catalyst, respectively, at the above mentioned reaction conditions. In this case, no extraction process was necessary. Samples were analyzed in the same manner by HPLC.

3. Results and discussion

3.1. Hybrids characterization

3.1.1. Ray diffraction study

XRD patterns of the phosphomolybdic acid and its corresponding hybrids are presented in Fig. 2. The hybrid patterns are very similar to that of the parent acid. Nevertheless, a shift and some new diffractions are detected accounting for the presence of organic cation around the Keggin anion and the formation of a new structure. The changes of the XRD profiles appear to be related to the type of cation being the XRD profile of Emim-Mo more similar to the parent acid than Bmim-Mo and Hexmim-Mo, in a way that shorter the aliphatic chain, smaller the modification of the parent acid diffractogram. For the Hexmim-Mo hybrid even new diffraction lines appear at low 2θ angles indicating most probably the formation of an ordered structure.

3.1.2. X-ray diffraction study as a function of temperature

The phase transformations of the samples as a function of temperature are studied and presented. The XRD measurements are performed in flowing air from 30 °C to 750 °C with isotherms at every 50 °C. However, Fig. 3 presents only the temperatures for which significant changes are detected. The parent acid $H_3PMo_{12}O_{40}\cdot13H_2O$ (JCPDS #01-075-1588) loses hydration water and transforms to $H_3PMo_{12}O_{40}\cdot6H_2O$ (JCPDS#01-070-1705) and $H_3PMo_{12}O_{40}\cdot1.5H_2O$ (JCPDS#00-046-0482) at 100 and 150 °C, respectively. This phase remains intact till 450 °C where transforms into MoP_2O_7 (JCPDS#00-039-0026) and MoO_3 (JCPDS #00-001–0706 + #00-047-1081). From 550 °C till the last measured temperature only MoO_3 is detected.

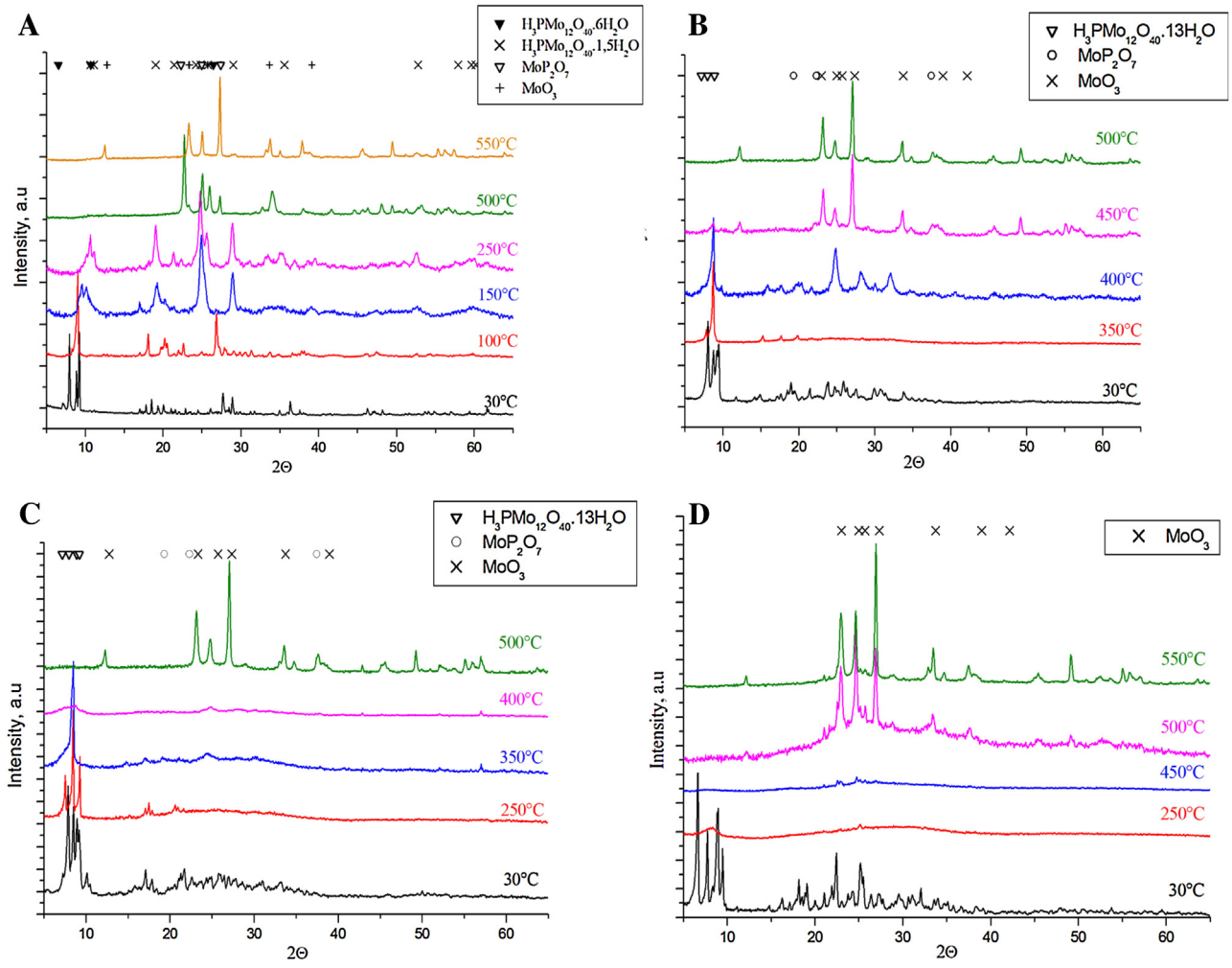

Fig. 3. XRDiffractograms as a function of temperature: A) $H_3PMo_{12}O_{40}{\cdot}13H_2O$, B) Emim-Mo, C) Bmim-Mo and D) Hexmim-Mo.

The phase transformations of the hybrids seem to depend on the cation nature. Longer the substituted aliphatic chains of the imidazolium ring (ethyl through butyl to hexyl) lower the temperature of the first transformation. In addition, the transition of the hybrid structure to the decomposition products of the parent acid is always accompanied by samples amorphization. Emim-Mo is no longer available at temperatures higher than 300 °C and converts into MoO_3 at 500 °C. Bmim-Mo is not observed at temperatures higher than 200 °C, and instead, products issued from the decomposition of phosphomolybdic acid are detected with increasing of the temperature: $H_3PMo_{12}O_{40}{\cdot}13H_2O$ (JCPDS #01-075-1588), $10MoO_3{\cdot}H_3PO_4{\cdot}24H_2O$ (JCPDS #00-001-0032), MoP_2O_7 (JCPDS #00-039-0020) and MoO_3 (JCPDS #00-001-0706, #00-047-1081). Similar to Emim-Mo, at 500 °C only MoO_3 is detected. Hexmim-Mo is observed till 200 °C then an amorphization occurs and directly the MoO_3 appears at 550 °C. In all the cases a MoO_3 crystallizes as a monocrystal, indicating a probable structure directing role of the imidazolium cations.

All identified phases for the three hybrids and parent phosphomolybdic acid at every studied temperature are summarized in Table 1. The dependence of the hybrid's stability on the organic counter cation could be easily observed. Emim-Mo hybrid is the most stable followed by Bmim-Mo and Hexmim-Mo hybrids. A possible relationship could be envisaged, less perturbation of the Keggin-structure higher phase transformation stability.

3.1.3. *Raman spectroscopy*

The XRD studies demonstrate the structural similarity of the hybrids to the parent acid and the changes induced by the aliphatic chain of the substituted imidazolium ring. These changes are also studied by Raman spectroscopy (Fig. 4). The Keggin structural units present four types of oxygen [42]: terminal oxygen, Ot (Mo=O), two types of bridging oxygen atoms (Mo—O—Mo), edge sharing oxygen Oe and corner sharing oxygen Ob, as well as corner sharing oxygen atoms between the central heteroatom and surrounding metal atoms Oa (P—O—Mo(x3)). Therefore, four oxygen bonds can be distinguished. The Raman spectra of the hybrids can be separated in two vibrational zones: the first one, within 100–1100 cm^{-1} metal-oxygen bonds range, (Fig. 4A) and the second one corresponding to organic fraction vibrations, in the 2700–3200 cm^{-1} range (Fig. 4B). The bands attribution and its comparison with literature data are presented in Table 2.

In general, the vibrational bands assigned to the metal-oxygen bonds do not change significantly in the presence of different imidazolium derivatives, the Keggin unit seems preserved, as confirmed by XRD. The Mo—Ob—Mo and Mo—Oe—Mo bands are slightly shifted for the hybrids: indicating that the organic cations situates near the bridging oxygens thus affecting their electronic density and causing the blue shift.

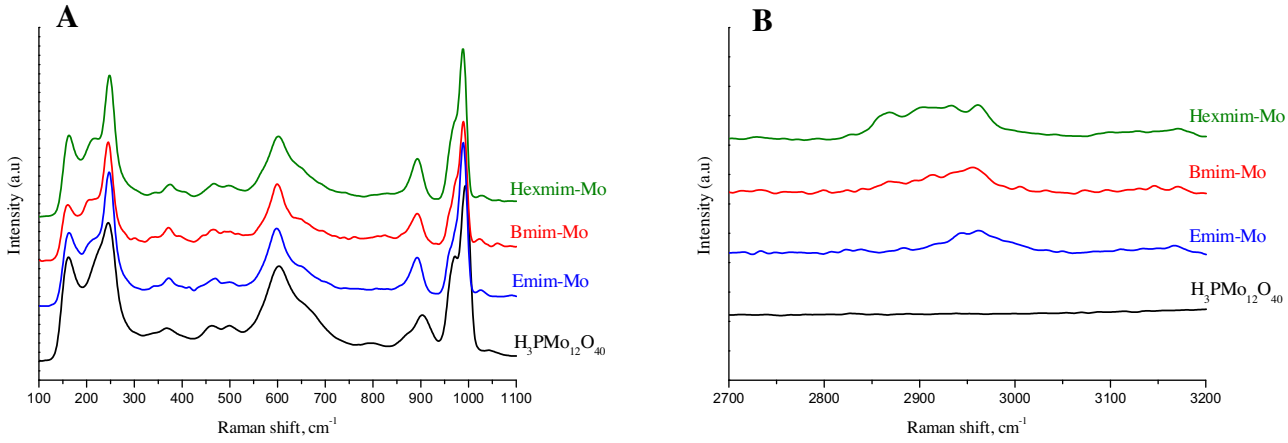

Fig. 4. Raman spectra of $H_3PMo_{12}O_{40}{\cdot}13H_2O$ and hybrids.

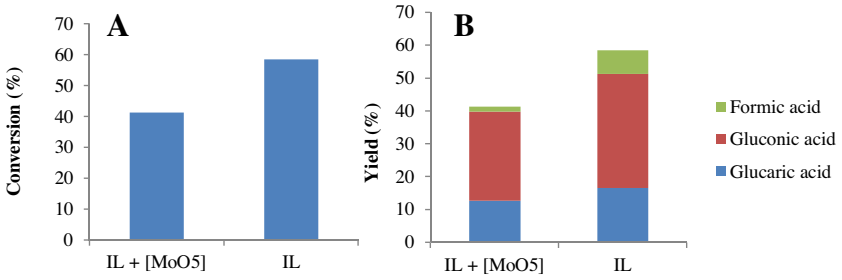

Fig. 5. Glucose conversion (%) A) and product yield (%) B) with IL as a solvent reaction conditions: 1 mmol of glucose, 3 mmol of H_2O_2, [MoO_5] (2.5 mol% of glucose), 2 mL of $BmimPF_6$, 600 rpm, 60 °C, 18 h.

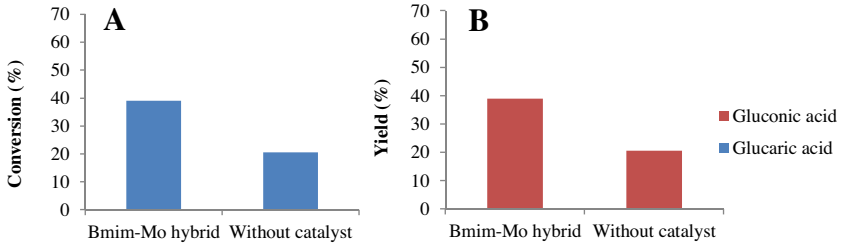

Fig. 6. Glucose conversion (%) A) and product yield (%) B) for $Bmim_3[PMo_{12}O_{40}]$ catalyst. Reaction conditions: 1 mmol of glucose, 3 mmol of H_2O_2, catalyst (2.5 mol% of glucose), 2 mL of H_2O, 600 rpm, 60 °C, 18 h.

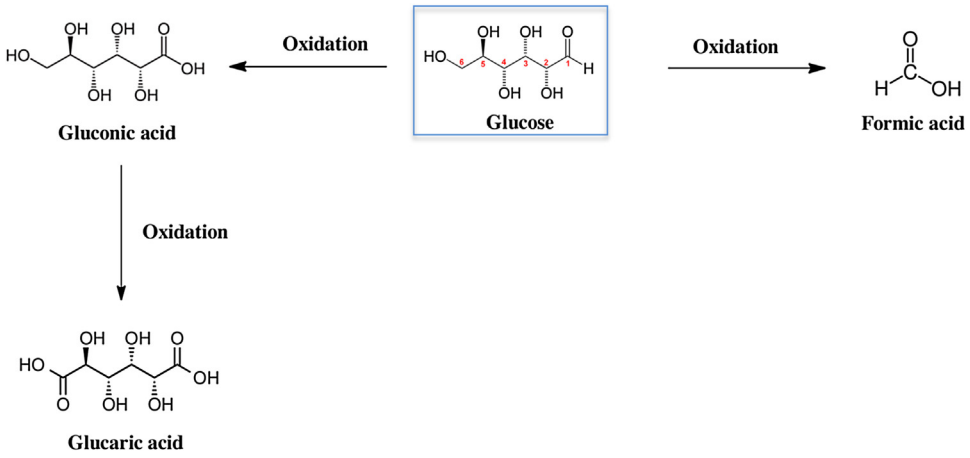

Fig. 7. Oxidation products in *System 1* and *System 2*.

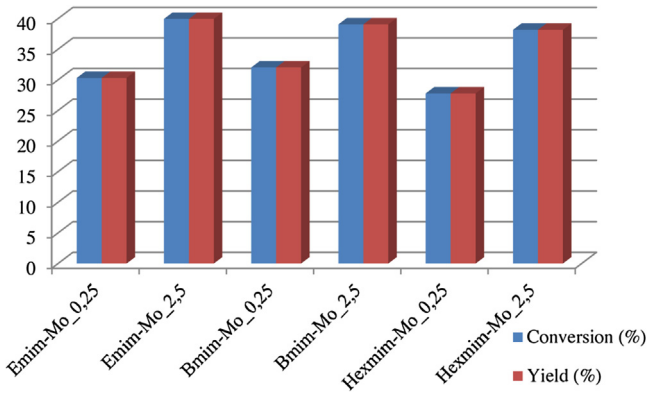

Fig. 8. Glucose conversion (%) and product yield (%) as a function of the catalyst's amount and the ILs nature.

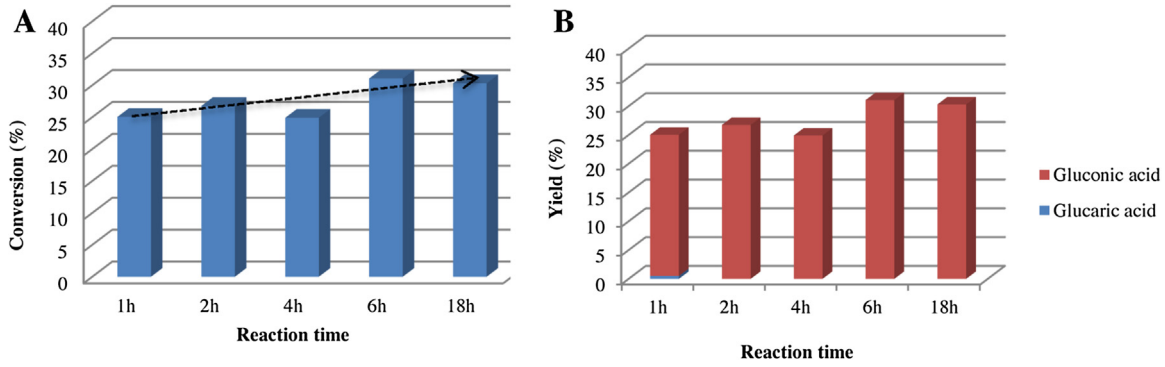

Fig. 9. Glucose conversion (%) A) and yield (%) B) over Emim-Mo_0.25mol% catalyst as a function of reaction time.

Table 2
Vibrational assignments for inorganic and organic fractions.

Experimental Raman shift, cm^{-1}	Raman shift, cm^{-1} [43,44]	Assignment	Experimental Raman shift, cm^{-1} [45–48]	Assignment[a]
993	995[43]	ν_s (Mo = Ot)	2835	ν_s CH-CH $_{(imidazolium)}$
969	981[43]	ν_{as} (Mo = Ot)	2876	ν_s CH R_2
904,878	909–876 [44]	ν_{as} (Mo-Ob-Mo)	2919	ν_s CH R_1
602	603[44]	ν_s (Mo-Oe-Mo)	2940	CH_3NHCH
245, 222	251[44]	ν_s (Mo-Oa)	2968	ν_{as} CH R_1
			3018	ν_{as} CH R_2
			3107	NC(H)N
			3170	ν_{as} CH-CH $_{(imidazolium)}$

[a] R_1 (ethyl, butyl or hexyl), R_2 (methyl).

For all the hybrids the CH vibration are present confirming the formation of the hybrids together with the preservation of the Keggin structural unit.

3.2. Catalytic performance

The oxidation of glucose was carried out following the procedure described above for the two systems. The obtained results for *System 1* are shown in Fig. 5, as glucose conversion and yield in presence or absence of $[MoO_5]$. As could be expected, $BmimPF_6$ plays an important role when used as reaction media, a glucose conversion of 60% is observed (Fig. 5A) in absence of catalyst, which suggests the participation of the ionic liquid not only as a solvent but also as a catalyst. The conversion surprisingly drops in presence of the catalyst $[MoO_5]$ to 41% of conversion. As for the products (Fig. 5B), both reactions result in the same oxidation products, being gluconic acid the main product. Thus, higher yields are observed in absence of catalyst (35% of yield vs. 27% in presence of $[MoO_5]$) in the same way for glucaric acid (17% of yield vs. 13% in presence of $[MoO_5]$) and formic acid (7% in absence of $[MoO_5]$ vs. 1.6%). A C balance of 100% is obtained in presence of $[MoO_5]$ and only 89% balanced when IL is used. These results suggest that, although a lower conversion obtained in presence of $[MoO_5]$ the oxidation reactions to glucaric and gluconic acids are promoted and the total degradation of glucose to formic acid suppressed. On the other hand the deficiency of the C balance in the case of the IL catalyzed reaction suggests additional products formation, either probably resulting from polymerization reactions or not extracted in the aqueous phase, and not detected by our HPLC method.

The obtained results for *System 2* are presented in Fig. 6, in presence or absence of the hybrid Bmim-Mo catalyst. Approximately a 21% of conversion is obtained in absence of catalyst, and corresponds to the formation of gluconic acid (glucaric acid traces are also observed). This result changes in presence of Bmim-Mo, where the conversion of glucose doubles to 40% with 100% selectivity to gluconic acid. The presence of Bmim-Mo catalyst inhibits the glucose oxidation to glucaric acid. However, in the same way that for *System 1*, a C balance of 78% is reached which suggests the formation of polymerization products, as the most probable cause for C lost.

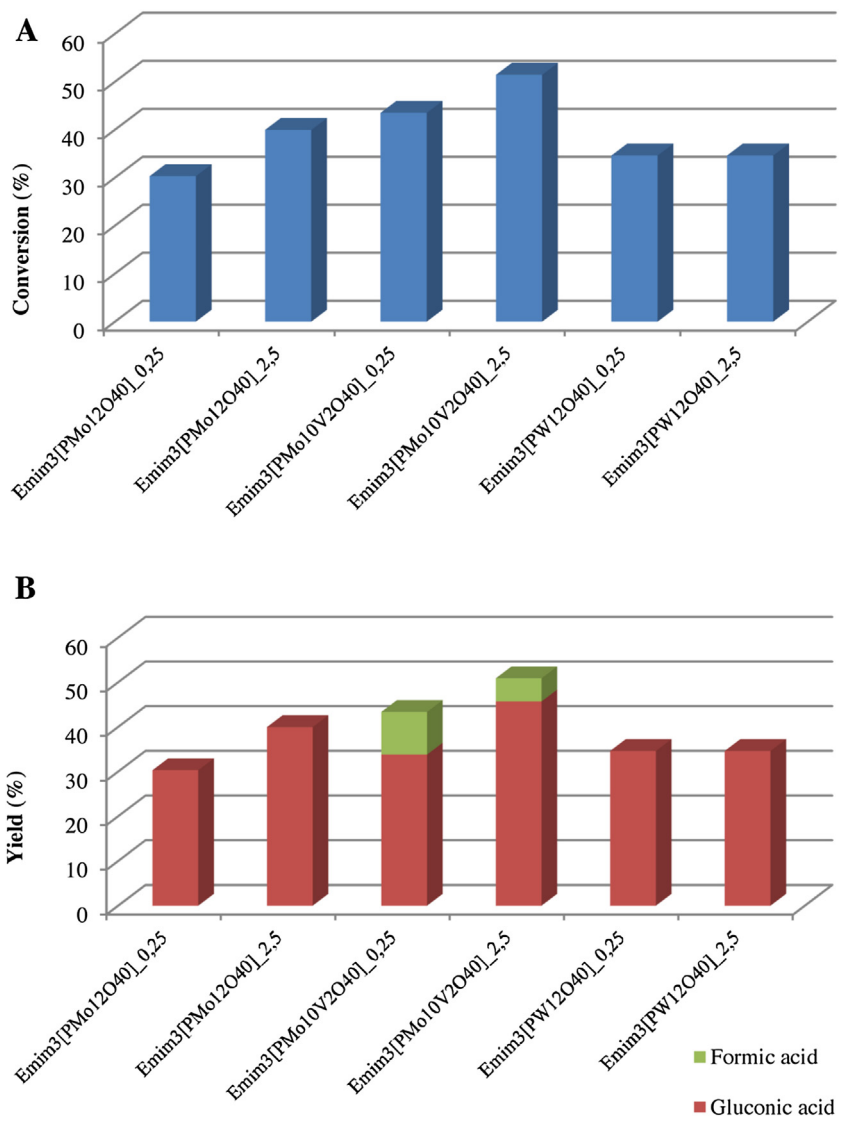

Fig. 10. Glucose conversion (%) A) and products yield (%) B) as a function of the catalyst's amount and the Keggin anions nature.

When comparing both systems (*System 1* vs. *2*) higher selectivity and yield to gluconic acid are observed when the IL hybrid is used as catalyst, suppressing the degradation of glucose to formic acid and the formation of glucaric acid as secondary oxidation product. The higher conversion observed for the *System 1* could be attributed only to higher IL/Glucose ratio, when IL is used as solvent/co-catalyst. At this point the *System 1* was abandoned due to the lowest selectivity in terms of number of formed products and only the hybrid materials are used for more detailed study. All oxidation products obtained in both systems are summarized in Fig. 7.

The influence of the amount of catalyst was studied by reducing ten times the quantity of catalyst (0.25 mol%), with the same reaction conditions described above. In addition, to find out how the ILs nature affects the reaction parameters, the Emim-Mo, Bmim-Mo and Hexmim-Mo hybrids are prepared and reacted. The obtained results are presented in Fig. 8.

It seems that the organic cation nature is hardly important in terms of glucose conversion. Nevertheless the conversion slightly increases with the amount of catalyst, as we could expect, obtaining a 100% of selectivity to gluconic acid in all cases. Regarding the C balance, a 100% is obtained when the used catalyst is 0.25 mol% of glucose while about only 80% when the amount of catalyst is ten times higher.

In order to evaluate the influence of the reaction time, the conversion and product distribution were also studied as a function of the time over Emim-Mo_0,25 mol% ($Emim_3[PMo_{12}O_{40}]$; 0.25 mol% of glucose amount) catalyst (Fig. 9).

The glucose conversion remains practically unaltered with the reaction time obtaining a 25% of conversion after 1 h of reaction and only 30% after 18 h. However, 100% of gluconic acid is reached at every point.

The results described above suggest that the IL/Keggin hybrid appears as a very selective catalyst for glucose oxidation. As the different organic fractions seem not to influence the conversion, an increase of that could be reached by the change of the Keggin part hybrid nature. Three different anions were used to obtain the hybrids with the following molecular formula $Emim_3[PMo_{12}O_{40}]$, $Emim_3[PMo_{10}V_2O_{40}]$ [49] and $Emim_3[PW_{12}O_{40}]$ [30,40], respectively. In the same way, catalysts were used in a 0.25mol% and 2.5mol% of glucose. The results are presented in Fig. 10.

The glucose conversion is slightly higher for the Mo-V containing Keggin anion hybrid while no significant differences between the two monoatomic (Mo, W) compounds are detected. The conversion increases with the amount of used catalyst except for

$Emim_3[PW_{12}O_{40}]$ which is the less active one. Regarding the product selectivity, 100% of gluconic acid is obtained for the two monoatomic hybrids whereas formic acid is also detected in the case of $Emim_3[PMo_{10}V_2O_{40}]$. It seems that the introduction of heteroatoms, like V, in the Keggin organization promotes the oxidation and total degradation of glucose although the main product is still the desired gluconic acid. In fact, higher amount of catalyst leads to more gluconic acid yield in detriment to formic acid (10% of yield vs. 5% when 2.5 mol% is used).

All the studied hybrids present ability to catalyze the oxidation of glucose. However the products diversity should be controlled by the change of the Keggin heteroatoms or by the adjustment of the reaction parameters in order to increase the selectivity towards the gluconic acid formation.

4. Conclusions

Two different glucose conversion routes are proposed in this study: the direct transformation giving formic acid as a product and the oxidation reaction with gluconic and glucaric acid as products. The bare ionic liquid used as a solvent in *System 1* appears to catalyze both the glucose transformation into formic acid and the oxidation of the two terminal carbons, respectively. When combined with $[Mo(O)(O_2)_2(H_2O)_n]$ catalyst, the direct transformation route is suppressed to some degree promoting the oxidation to aldonic and aldaric acids. The second approach using the ionic liquid/Keggin structure hybrids as catalytic *System 2* results in total selectivity to gluconic acid and the disappearing of the direct transformation route. Conversion can be increased at higher catalyst charge without modifications in the selectivity. The changes in the ionic liquid nature result in a little variation of conversion, being the long chain hybrid the less active. On the other hand the changes of the Keggin structure affects the number of the obtained products suggesting that this change together with the reaction parameters readjustment could result in interesting modifications of the selectivity.

Acknowledgements

C.J. Carrasco, F. Montilla and A. Galindo acknowledge financial support from the Junta de Andalucía (Proyecto de Excelencia FQM-7079). C. Megías-Sayago, S. Ivanova and J. A. Odriozola acknowledge Junta de Andalucía (TEP 106 group) and Ministerio de Economía y Competitividad (ENE201347880-C3-2-R).

References

[1] M.J. Climent, A. Corma, S. Iborra, Converting carbohydrates to bulk chemicals and fine chemicals over heterogeneous catalysts, Green Chem. 13 (2011) 520, http://dx.doi.org/10.1039/c0gc00639d.
[2] J. Song, H. Fan, J. Ma, B. Han, Conversion of glucose and cellulose into value-added products in water and ionic liquids, Green Chem. 15 (2013) 2619–2635, http://dx.doi.org/10.1039/C3GC41141A.
[3] D.M. Alonso, J.Q. Bond, J.A. Dumesic, Catalytic conversion of biomass to biofuels, Green Chem. 12 (2010) 1493, http://dx.doi.org/10.1039/c004654j.
[4] J.P.M. Sanders, J.H. Clark, G.J. Harmsen, H.J. Heeres, J.J. Heijnen, S.R. a Kersten, et al., Process intensification in the future production of base chemicals from biomass, Chem. Eng. Process. Process Intensif. 51 (2012) 117–136, http://dx.doi.org/10.1016/j.cep.2011.08.007.
[5] S. Hu, Z. Zhang, J. Song, Y. Zhou, B. Han, Efficient conversion of glucose into 5-hydroxymethylfurfural catalyzed by a common Lewis acid SnCl4 in an ionic liquid, Green Chem. 11 (2009) 1746, http://dx.doi.org/10.1039/b914601f.
[6] A. Jain, S.C. Jonnalagadda, K.V. Ramanujachary, A. Mugweru, Selective oxidation of 5-hydroxymethyl-2-furfural to furan-2 5-dicarboxylic acid over spinel mixed metal oxide catalyst, Catal. Commun. 58 (2015) 179–182, http://dx.doi.org/10.1016/j.catcom.2014.09.017.
[7] A.S. Amarasekara, D. Green, E. McMillan, Efficient oxidation of 5-hydroxymethylfurfural to 2 5-diformylfuran using Mn(III)-salen catalysts, Catal. Commun. 9 (2008) 286–288, http://dx.doi.org/10.1016/j.catcom.2007.06.021.
[8] S. Jia, Z. Xu, Z.C. Zhang, Catalytic conversion of glucose in dimethylsulfoxide/water binary mix with chromium trichloride: role of water on the product distribution, Chem. Eng. J. 254 (2014) 333–339, http://dx.doi.org/10.1016/j.cej.2014.05.121.
[9] X. Tong, Y. Ma, Y. Li, Biomass into chemicals: conversion of sugars to furan derivatives by catalytic processes, Appl. Catal. A Gen. 385 (2010) 1–13, http://dx.doi.org/10.1016/j.apcata.2010.06.049.
[10] D. Bin, H. Wang, J. Li, H. Wang, Z. Yin, J. Kang, et al., Controllable oxidation of glucose to gluconic acid and glucaric acid using an electrocatalytic reactor, Electrochim. Acta 130 (2014) 170–178, http://dx.doi.org/10.1016/j.electacta.2014.02.128.
[11] S. Ramachandran, P. Fontanille, A. Pandey, C. Larroche, Gluconic acid: properties, applications and microbial production, Food Technol. Biotechnol. 44 (2006) 185–195.
[12] K. Buchholz, J. Seibel, Industrial carbohydrate biotransformations, Carbohydr. Res. 343 (2008) 1966–1979, http://dx.doi.org/10.1016/j.carres.2008.02.007.
[13] S. Anastassiadis, H.J. Rehm, Continuous gluconic acid production by the yeast-like Aureobasidium pullulans in a cascading operation of two bioreactors, Appl. Microbiol. Biotechnol. 73 (2006) 541–548, http://dx.doi.org/10.1007/s00253-006-0499-y.
[14] M. Besson, F. Lahmer, P. Gallezot, P. Fuertes, G. Fléche, Catalytic oxidation of glucose on bismuth-promoted palladium catalysts, J.Catal. 152 (1995) 116–121.
[15] I. Nikov, K. Paev, Palladium on alumina catalyst for glucose oxidation: reaction kinetics and catalyst deactivation, Catal. Today 24 (1995) 41–47, http://dx.doi.org/10.1016/0920-5861(95)00011-4.
[16] P. Beltrame, M. Comotti, C. Della Pina, M. Rossi, Aerobic oxidation of glucose, Appl. Catal. A Gen. 297 (2006) 1–7, http://dx.doi.org/10.1016/j.apcata.2005.08.029.
[17] U. Prüße, M. Herrmann, C. Baatz, N. Decker, Gold-catalyzed selective glucose oxidation at high glucose concentrations and oxygen partial pressures, Appl. Catal. A Gen. 406 (2011) 89–93, http://dx.doi.org/10.1016/j.apcata.2011.08.013.
[18] J.P. Hallett, T. Welton, Room-temperature ionic liquids: solvents for synthesis and catalysis. 2, Chem. Rev. 111 (2011) 3508–3576, http://dx.doi.org/10.1021/cr1003248.
[19] P. Wasserscheid, T. Welton, Ionic Liquids in Synthesis, Wiley-VCH, 2003.
[20] S. Ivanova, Hybrid organic-inorganic materials based on polyoxometalates, ISRN Chem. Eng. (2014), http://dx.doi.org/10.1155/2014/963792, Article ID 963792, 13 pages.
[21] C. DeCastro, Immobilised ionic liquids as lewis acid catalysts for the alkylation of aromatic compounds with dodecene, J. Catal. 196 (2000) 86–94, http://dx.doi.org/10.1006/jcat.2000.3004.
[22] R.S. Avellaneda, S. Ivanova, O. Sanz, F. Romero-Sarria, M.A. Centeno, J.A. Odriozola, Ionic liquid templated TiO2 nanoparticles as a support in gold environmental catalysis, Appl. Catal. B Environ. 93 (2009) 140–148, http://dx.doi.org/10.1016/j.apcatb.2009.09.023.
[23] M. Herbert, F. Montilla, A. Galindo, R. Moyano, A. Pastor, E. Álvarez, Influence of N-donor bases and the solvent in oxodiperoxomolybdenum catalysed olefin epoxidation with hydrogen peroxide in ionic liquids, Dalton Trans. 40 (2011) 5210–5219, http://dx.doi.org/10.1039/c1dt10065c.
[24] M. Herbert, A. Galindo, F. Montilla, Catalytic epoxidation of cyclooctene using molybdenum(VI) compounds and urea-hydrogen peroxide in the ionic liquid [bmim]PF6, Catal. Commun. 8 (2007) 987–990, http://dx.doi.org/10.1016/j.catcom.2006.10.008.
[25] L. Zhang, Q. Zhang, J. Li, Electrochemical behaviors and spectral studies of ionic liquid (1-butyl-3-methylimidazolium tetrafluoroborate) based sol-gel electrode, J. Electroanal. Chem. 603 (2007) 243–248, http://dx.doi.org/10.1016/j.jelechem.2007.02.021.
[26] S. Ivanova, X. Nitsch, F. Romero-Sarria, B. Louis, M.A. Centeno, A.C. Roger, et al., Ionic liquid protected heteropoly acids for methanol dehydration, Catal. Today 171 (2011) 236–241, http://dx.doi.org/10.1016/j.cattod.2011.03.077.
[27] Y. Leng, J. Wang, D. Zhu, X. Ren, H. Ge, L. Shen, Heteropolyanion-based ionic liquids: reaction-induced self-separation catalysts for esterification, Angew. Chem. Int. Ed. 48 (2009) 168–171, http://dx.doi.org/10.1002/anie.200803567.
[28] H. Li, Y. Qiao, L. Hua, Z. Hou, B. Feng, Z. Pan, et al., Imidazolium polyoxometalate: an ionic liquid catalyst for esterification and oxidative esterification, ChemCatChem 2 (2010) 1165–1170, http://dx.doi.org/10.1002/cctc.201000021.
[29] T. Rajkumar, G. Ranga Rao, Characterization of hybrid molecular material prepared by 1-butyl 3-methyl imidazolium bromide and phosphotungstic acid, Mater. Lett. 62 (2008) 4134–4136, http://dx.doi.org/10.1016/j.matlet.2008.06.029.
[30] G. Ranga Rao, T. Rajkumar, B. Varghese, Synthesis and characterization of 1-butyl 3-methyl imidazolium phosphomolybdate molecular salt, Solid State Sci. 11 (2009) 36–42, http://dx.doi.org/10.1016/j.solidstatesciences.2008.05.017.
[31] W. Deng, Q. Zhang, Y. Wang, Polyoxometalates as efficient catalysts for transformations of cellulose into platform chemicals, Dalton Trans. 41 (2012) 9817, http://dx.doi.org/10.1039/c2dt30637a.
[32] D. An, A. Ye, W. Deng, Q. Zhang, Y. Wang, Selective conversion of cellobiose and cellulose into gluconic acid in water in the presence of oxygen, catalyzed by polyoxometalate-supported gold nanoparticles, Chem. A Eur. J. 18 (2012) 2938–2947, http://dx.doi.org/10.1002/chem.201103262.
[33] Y. Liu, L. Zhu, J. Tang, M. Liu, R. Cheng, C. Hu, One-pot, one-step synthesis of 2,5-diformylfuran from carbohydrates over Mo-containing keggin

heteropolyacids, ChemSusChem 7 (2014) 3541–3547, http://dx.doi.org/10.1002/cssc.201402468.
[34] F. Cavani, Heteropolycompound-based catalysts: a blend of acid and oxidizing properties, Catal. Today 41 (1998) 73–86, http://dx.doi.org/10.1016/S0920-5861(98)00039-X.
[35] N. Mizuno, M. Misono, Heterogeneous catalysis, Chem. Rev. 98 (1998) 199–218, http://dx.doi.org/10.1002/anie.201410738.
[36] I.V. Kozhevnikov, Catalysis by heteropoly acids and multicomponent polyoxometalates in liquid-phase reactions, Chem. Rev. 98 (1998) 171–198, http://dx.doi.org/10.1021/cr960400y.
[37] X.X. Han, Y.F. He, C. Te Hung, L.L. Liu, S.J. Huang, S. Bin Liu, Efficient and reusable polyoxometalate-based sulfonated ionic liquid catalysts for palmitic acid esterification to biodiesel, Chem. Eng. Sci. 104 (2013) 64–72, http://dx.doi.org/10.1016/j.ces.2013.08.059.
[38] E. Rafiee, F. Mirnezami, Keggin-structured polyoxometalate-based ionic liquid salts: thermoregulated catalysts for rapid oxidation of sulfur-based compounds using H2O2 and extractive oxidation desulfurization of sulfur-containing model oil, J. Mol. Liq. 199 (2014) 156–161, http://dx.doi.org/10.1016/j.molliq.2014.08.036.
[39] X. Han, W. Yan, K. Chen, C.-T. Hung, L.-L. Liu, P.-H. Wu, et al., Heteropolyacid-based ionic liquids as effective catalysts for the synthesis of benzaldehyde glycol acetal, Appl. Catal. A Gen. 485 (2014) 149–156, http://dx.doi.org/10.1016/j.apcata.2014.08.001.
[40] H. Wu, Contribution to the chemistry of phosphomolybdic acids phosphotungstic acids, and allied substances, J. Biol. Chem. 43 (1920) 189–220.
[41] S. Carda-Broch, A. Berthod, D.W. Armstrong, Solvent properties of the 1-butyl-3-methylimidazolium hexafluorophosphate ionic liquid, Anal. Bioanal. Chem. 375 (2003) 191–199.
[42] S. Ganapathy, M. Fournier, J.F. Paul, L. Delevoye, M. Guelton, J.P. Amoureux, Location of protons in anhydrous keggin heteropolyacids H3PMo12O40 and H3PW12O40 by 1H{31P}/31P{1H} REDOR NMR and DFT quantum chemical calculations, J. Am. Chem. Soc. 124 (2002) 7821–7828, http://dx.doi.org/10.1021/ja017848n.
[43] J. Tatibou, A two-Step transformation of the magnesium salt of phosphomolybdic acid HMgPMo12O40 supported on silica, J. Catal. 32 (1997) 22–32.
[44] C. Rocchiccioli-Deltcheff, A. Aouissi, M.M. Bettahar, S. Launay, M. Fournier, Catalysis by 12-Molybdophosphates, J.Catal. 164 (1996) 16–27.
[45] N.E. Heimer, R.E. Del Sesto, Z. Meng, J.S. Wilkes, W.R. Carper, Vibrational spectra of imidazolium tetrafluoroborate ionic liquids, J. Mol. Liq. 124 (2006) 84–95, http://dx.doi.org/10.1016/j.molliq.2005.08.004.
[46] K.M. Dieter, C.J. Dymek, N.E. Heimer, J.W. Rovang, J.S. Wilkes, Ionic structure and interactions in 1-methyl-3-ethylimidazolium chloride-alcl3 molten-salts, J. Am. Chem. Soc. 110 (1988) 2722–2726, http://dx.doi.org/10.1021/ja00217a004.
[47] E.R. Talaty, S. Raja, V.J. Storhaug, A. Dölle, W.R. Carper, Raman and infrared spectra and ab initio calculations of C 2–4 MIM imidazolium hexafluorophosphate ionic liquids, J. Phys. Chem. B 108 (2004) 13177–13184, http://dx.doi.org/10.1021/jp040199s.
[48] S.A. Katsyuba, E.E. Zvereva, A. Vidis, P.J. Dyson, Application of density functional theory and vibrational spectroscopy toward the rational design of ionic liquids, J. Phys. Chem. A 111 (2007) 352–370, http://dx.doi.org/10.1021/jp064610i.
[49] Y. Leng, J. Wang, D. Zhu, L. Shen, P. Zhao, M. Zhang, Heteropolyanion-based ionic hybrid solid: a green bulk-type catalyst for hydroxylation of benzene with hydrogen peroxide, Chem. Eng. J. 173 (2011) 620–626, http://dx.doi.org/10.1016/j.cej.2011.08.013.

Catalysis Today 279 (2017) 148–154

Contents lists available at ScienceDirect

Catalysis Today

journal homepage: www.elsevier.com/locate/cattod

Gold catalysts screening in base-free aerobic oxidation of glucose to gluconic acid

C. Megías-Sayago*, S. Ivanova, C. López-Cartes, M.A. Centeno, J.A. Odriozola

Departamento de Química Inorgánica, Universidad de Sevilla e Instituto de Ciencias de Materiales de Sevilla, Centro mixto CSIC-US, Avda. Américo Vespucio 49, 41092, Sevilla, Spain

ARTICLE INFO

Article history:
Received 30 November 2015
Received in revised form 9 June 2016
Accepted 22 June 2016
Available online 28 June 2016

Keywords:
Glucose oxidation
Gold catalysts
Screening
Gluconic acid
Base free oxidation

ABSTRACT

Base-free aerobic oxidation of glucose in presence of Au/Al_2O_3, Au/CeO_2, Au/CeO_2(20 wt%)/Al_2O_3, Au/CeO_2(25 wt%)/ZrO_2 and Au/CeO_2(50 wt%)/ZrO_2 catalysts using molecular oxygen at atmospheric pressure is studied. Within the whole series high conversion and selectivity to gluconic acid are observed after 18 h of reaction at 120 °C. The activity and especially the selectivity changes are related to the support nature in a way that the higher the Lewis acidity of the support the lower the selectivity to gluconic acid and the higher the production of lactic acid. The highest yield to gluconic acid is obtained over Au/Al_2O_3 for which the influence of the reaction time, temperature and stirring rate are further evaluated and discussed.

1. Introduction

Biomass is the most abundant and sustainable carbon source nowadays. Carbohydrates constitute 75% of the annual renewable biomass with glucose as monomer of cellulose the most abundant monosaccharide [1]. Efficient conversion of cellulose and glucose to valuable compounds, so called platform chemicals, is of great importance and it is current topic of interest in Chemistry [2,3]. Within the glucose platform chemicals, D-Gluconic acid obtained by aerobic oxidation of glucose is an important compound. It is widely used as environmentally friendly chelating agent and water soluble cleansing agent in food and pharmaceutical industries with an annual market of about 100,000 tons per year [2,4,5]. It is usually produced by fermentation of glucose with microbial species such as *Aspergillus niger*, *Penicillium* sp., *Zymomonas mobilis*, *G. oxydans* and *Gluconobacter* sp. [6–8]. However in the fermentation medium, the accumulation of gluconic acid inhibits the microbes function leading to lower yields and slow overall reaction rate [5,6]. In recent years, due to the complexity of fermentation process, increased research efforts are devoted to find environmentally friendly alternative, such as technology based on heterogeneous catalysis [9]. Several studies have been reported on gluconic acid production over platinum group metals (PGM) catalysts [10–12]. being main drawback of these systems their deactivation due to oxygen poisoning of the metal surface [13]. In order to improve PGM catalysts activities, bimetallic Bi-Pt and trimetallic Bi-Pd-Pt catalysts were reported with higher activity and selectivity [11,14]. However, Bi is prone to leaching which converts these catalysts in inadequate candidates for the production of chemicals for food and pharmaceutical industries.

As an alternative, gold has been successfully used in aerobic oxidation of carbohydrates [15,16]. Specifically, aerobic oxidation of glucose carried out over different unsupported and supported gold catalysts, showed important activity and very good resistance to oxygen poisoning. However, an important drawback of these processes is the strong dependence of gold activity on the reaction pH value which entails the use of base, usually sodium hydroxide [17,18]. Biella et al. [19] have demonstrated that the use of alkaline conditions improves the activity and increases the catalyst stability during recycling tests. Additionally, basic conditions (pH at 9.5) seems to avoid gold nanoparticles leaching and sintering, and therefore, prevents catalyst deactivation. Besides gold leaching, another cause of deactivation is the strong interaction between gold nanoparticles and carboxylic compounds, also suppressed in presence of base due to salt formation. Despite all the advantages of using base in glucose oxidation reaction, base-free process is highly desired in order to simplify the treatment of the post-reaction mixture and to obtain pure acid instead of gluconate salt. In addition, glucose isomerization to fructose occurs catalyzed by the presence of base and lowers the selectivity to gluconic acid.

* Corresponding author.
E-mail address: cristina.megias@icmse.csic.es (C. Megías-Sayago).

http://dx.doi.org/10.1016/j.cattod.2016.06.046
0920-5861/

Some recent studies report the base-free oxidation of glucose over gold supported catalysts under mild conditions. Qi et al. [20] studied glucose oxidation over gold supported on structured carbon and ZrO_2 at 110 °C and 0.3 MPa $P(O_2)$ and reported high initial glucose conversion over Au/C (92.4%) in comparison to zirconia based catalyst (12.7%), with conversion decrease of approx. 20% after 4 runs. Wang et al. [21] investigated base-free oxidation of glucose over different CeO_2 and ZrO_2 supported gold catalysts at 65 °C and 0.23 MPa $P(O_2)$ and reported activity dependence on gold loading, being the catalysts with lower gold content the most active. Approximately 30% to 60% decrease of glucose conversion over Au/CeO_2 catalysts after 5 runs were observed. To palliate this effect the authors proposed a catalyst treatment, calcination and/or base washing before the reuse cycles, in order to improve the activity and to avoid fast deactivation. Those treatments suggest that any change of the support state, such as particle size or acid-base properties could influence in a great manner the activity towards gluconic acid formation.

In this context, we report herein the base-free aerobic glucose oxidation study under mild conditions over different gold supported catalyst as a function of the support nature. Various gold supported systems are screened, using γ-Al_2O_3, CeO_2 as simple oxides and CeO_2(20%wt)/Al_2O_3, CeO_2(25%wt)/ZrO_2, and CeO_2(50%wt)/ZrO_2 as mixed oxides combinations. The effect of support nature, reaction time, temperature and stirring rate on the catalytic activity and product distribution are evaluated and the catalyst reusability discussed.

2. Experimental

2.1. Materials and methods

D-(+)-Glucose (anhydrous, 99%) was purchased from Alfa Aesar and used as received. $HAuCl_4$ (Johnson Matthey) was used as gold precursor. All supports are commercially available solids and were used in this study without any previous treatment: γ-Al_2O_3 (Sasol, hereinafter Al), CeO_2(20%wt)/Al_2O_3 (Sasol, Ce/Al), CeO_2 (Ce), CeO_2(25%wt)/ZrO_2 (Ce25/Zr) and CeO_2(50%wt)/ZrO_2 (Ce50/Zr) (last three solids available from Daiichi Kigenso Kagaku Kogio Co., Ltd.).

XRD measurements were carried out at room temperature on Panalitycal X'Pert Pro diffractometer, equipped with Cu anode. All diffractograms were recorded in the 10–90° 2θ range, with 0,05° step size and 240 s acquisition time.

Gold loadings were determined by X Ray Fluorescence (XRF) using Panalitycal AXIOS spectrometer with Rh tube of radiation.

Transmission electron microscopy (TEM) observations were carried out on PHILIPS CM-200.

The products of glucose oxidation were identified and quantified by HPLC using a Hi-Plex H column (300 × 7.7 mm) and refractive index detector (Varian 360-LC) and MilliQ water as mobile phase.

2.2. Catalytic test conditions

The catalytic tests were performed in a glass batch reactor (50 mL) saturated with oxygen at atmospheric pressure (approximate $P(O_2)$ of 0.1 MPa) with 5 mL 0.2 M glucose solution and Glucose/Au molar ratio of 100. In a typical experiment, a 20 mL/min pure oxygen flux was introduced in the reactor in order to supply an oxygen rich atmosphere. Then, the reactor was closed and the mixture stirred at 600 rpm at various times and temperatures (0 °C–120 °C temperature range) without base addition. After reaction, 500 μLof sample was taken from the final mixture, diluted in 500 μL of MilliQ water and immediately analyzed by HPLC. The conversion, selectivity, yield and C balance calculations were based on the HPLC measurements. The reported conversions were obtained after comparing the glucose concentration before and after the reaction, Eq. (1). Owing to the wide variety of products that could be obtained, selectivity was calculated on the base of the carbon moles, as described in Eq. (2). Finally, yields were calculated by Eq. (3). Carbon balance deviation from 100% was always less than 5%.

Table 1
Gold contents (%) for the fresh catalysts.

Au(%)	Au/Al	Au/Ce	Au/Ce/Al	Au/Ce25/Zr	Au/Ce50/Zr
	1.64	3.94	2.36	2.31	2.39

$$Conversion\,(\%) = \frac{[Glucose]_I - [Glucose]_F}{[Glucose]_I} \times 100 \quad (1)$$

$$Selectivity\,(\%) = \frac{Carbon\ mol\ of\ specific\ product}{Carbon\ mol\ of\ total\ products} \times 100 \quad (2)$$

$$Yield\,(\%) = \frac{Conversion\,(\%)}{100} \times Selectivity\,(\%) \quad (3)$$

For the reuse of catalyst, higher amount of glucose (0.2 M, 15 mL) and gold catalyst were used in order to maintain the same glucose-to-catalyst ratio during the recycle runs. Between runs the catalyst was recovered by filtration, and reused under the same reaction conditions without any further pretreatment.

3. Results and discussion

Gold was deposited (2 wt.% nominal value) by direct anionic exchange (DAE) method assisted by ammonia as proposed previously by Ivanova et al. [22]. Gold precursor solution (around 10^{-4} M) was heated to 70 °C, and then contacted with the support and 20 min later with NH_3. The final solid was filtered, dried at 100 °C overnight and calcined at 300 °C during 4 h.

Table 1 presents the actual gold loading of the fresh catalysts.

For Au/Al_2O_3 catalyst, a metal loss of around 18% from the nominal value was detected, due to incomplete gold deposition. On the other hand, all ceria-containing solids, present experimental values close or even higher to the expected ones. The later suggests that, although a complete metal deposition occurs some support loss is also possible. In the case of the bare ceria support, almost the double of gold loading is detected suggesting that the use of strongly basic media during gold deposition could provoke support dissolution. In addition, the support loss increases with the ceria content increase within support composition. In the preparation process the amount of gold precursor is always slightly higher than required to account for the metal losses; nevertheless, the greater values observed may be due to incident blends, or also to the fact that the commercial support could contain other components, which are removed after calcination.

The diffraction patterns of the prepared catalysts compared to their corresponding supports are presented in Fig. 1.

The diffraction peaks corresponding to the gold metal phase are, in general, not observed for the ceria containing catalysts, suggesting an average size of the gold crystallites under the detection limit of the technique (4 nm). Nevertheless, and despite the lower crystallinity of bare alumina support, weak diffraction, which could be attributed to gold at 77° 2θ, is observed for Au/Al sample. The later suggests an average gold particles size slightly superior to 4 nm, which cannot be properly quantified by using Scherrer equation because of its low intensity.

It is worth to mention the CeO_2 - ZrO_2 solid solution formation (Fig. 1B), independently to the Ce/Zr molar ratio, confirmed by the diffraction shifts toward higher 2θ with the increase of Zr content.

Transmission electron microscopy (TEM) was used to evaluate the average gold particle size for Au/Al, Au/Ce/Al and Au/Ce

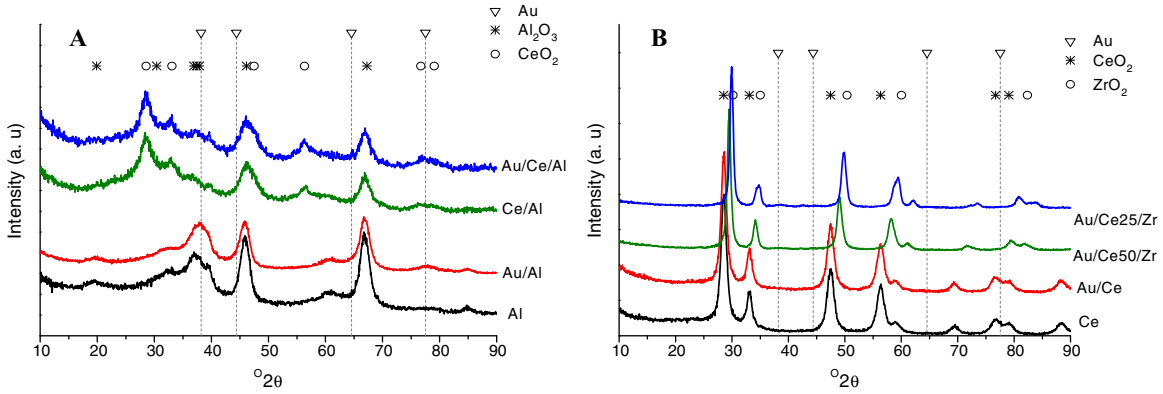

Fig. 1. XRD of the supported systems: A) Al_2O_3 containing supports, B) CeO_2 containing supports.

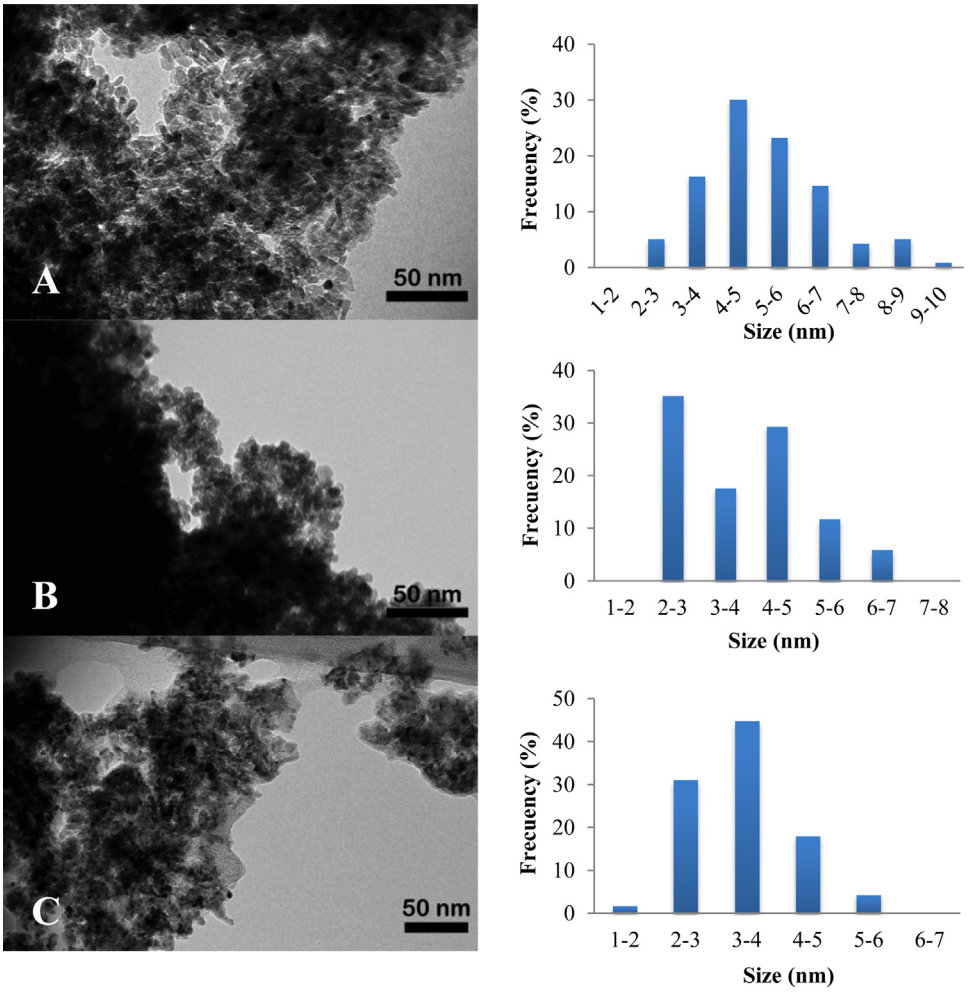

Fig. 2. TEM images and particle size distribution of fresh catalysts: A) Au/Al, B) Au/Ce, C) Au/Ce/Al.

samples. The former is chosen as the only one for which a diffraction peak attributed to gold is detected and the other two samples as representative for the rest of the samples. The corresponding micrographs and particle size distribution are presented in Fig. 2. As detected by XRD, the Au/Al catalyst present an average particle size slightly superior to 4 nm unlike the rest of the samples (Table 2). The particle size distribution follows a typical Gaussian curve except for Au/Ce sample, a possible cause being the low TEM contrast between gold and cerium, which complicates the detection of gold.

Table 2
Estimated particle size, dispersion and TOF for the samples.

Sample	Average particle size, nm	Dispersion, %	TOF, $s^{-1}*10^3$
Au/Al	5.1 ± 1.5 (5.6 ± 1.9)[a]	26	5.44
Au/Ce/Al	3.4 ± 0.8 (3.5 ± 0.8)[a]	38	2.64
Au/Ce	3.9 ± 1.5 (4.3 ± 1.2)[a]	33	1.66
Au/Ce25/Zr	3.4 ± 0.8[b]	38[a]	2.52
Au/Ce50/Zr	3.4 ± 0.8[b]	38[a]	1.58

[b]Assuming the same particle size and dispersion as Au/Ce/Al.
[a] Particle size of the spent catalyst in parenthesis.

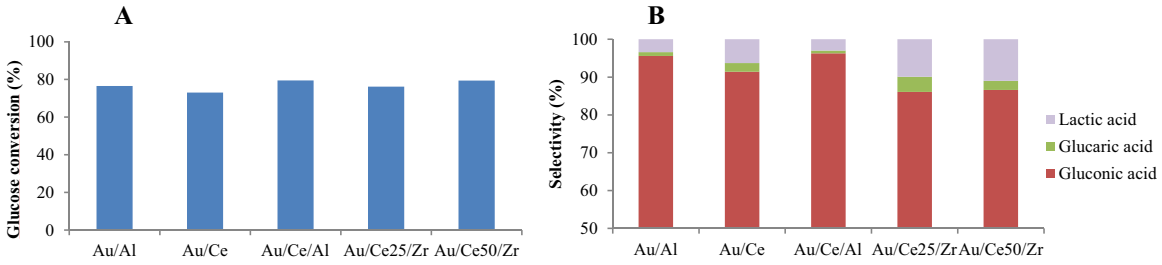

Fig. 3. A) Glucose conversion (%) over different gold supported catalysts (18 h, 120 °C, 600 rpm), B) Selectivity (%).

Based on the calculated average particle size for the fresh catalysts and using the hemispherical ball model, the Au dispersion can be evaluated [23] (Table 2). The calculated dispersion for all samples varies within the 25–40% range with all alumina-containing samples positioned in the lower limit.

Several effects on catalytic activity are studied. Firstly, the influence of support nature is evaluated and on the base of the obtained results, few samples chosen for subsequent reaction parameters study.

3.1. Effect of the support

The conversion of glucose after 18 h of reaction does not seem to be influenced by the nature of support being over 75% in all cases (Fig. 3A). As all the catalysts present different gold loadings, a normalization of the activity to the surface available gold atoms is needed to properly compare the samples. The TOF is calculated on the basis of Au dispersion and presented in Table 2. Due to low mass contrast, gold particles are difficult to measure with adequate accuracy for CeZr supported samples. That is why, their particle size and dispersion are considered equal to those of Au/Ce/Al sample because of sample's similar gold loading, and absence of visible XRDiffractions.

The Au/Al sample doubles the activity of almost all ceria-containing samples, which within its series obey the following order:

$$Au/Ce/Al > Au/Ce25/Zr > Au/Ce50/Zr \sim Au/Ce$$

It looks like the activity is inversely proportional to the ceria loading, the higher the ceria loading the lower the TOF. Nevertheless, above 50% of ceria, the activity maintains the same order, suggesting that the activity is related to the support nature and more particularly to its Lewis acidity. Using the Pearson concept for hard and soft Lewis acids and bases, the relative Lewis acids hardness can be calculated by considering all ions in its real proportions. The acidity hardness decreases almost in the same order as the activity Au/Al > Au/Ce/Al > Au/Ce25/Zr > Au/Ce50/Zr > Au/Ce indicating that the change of the support nature plays some role during the reaction [24,25].

The products distribution (Fig. 3B) is also influenced by the support nature. The alumina supported sample presents the highest selectivity to gluconic acid (95%) followed by the Au/Ce/Al sample and Au/Ce. The zirconia containing samples show the lowest selectivity to gluconic acid, favoring some lactic acid formation (10%) in comparison to Au/Al (3%) and Au/Ce (6%) based catalysts. The formation of glucaric acid seems to follow the same trend. In general, the formation of lactic acid involves several reactions such as isomerization [26] retro-aldol reaction [27], and secondary isomerization reaction, which normally occurs in the presence of Lewis acid sites. However, it looks like the lactic acid formation is not guided by acid strength of sites as the opposite tendency is observed. The presence of some specific acid sites and more probably their density on the support changes the product distribution and leads to lactic acid formation. For the zirconia-containing solids, the glucose conversion and the product distribution follows the same trend, the lowest selectivity and activity in terms of TOF are registered. It is obvious that the support plays an important role in the process and further research about support acidity, type and strength are required.

Based on the results only three samples are selected for further study of the reaction time effect, Au/Al, Au/Ce and Au/Ce/Al.

3.2. Effect of the reaction time

As expected, the conversion increases with the reaction time (Fig. 4), and insignificant differences between the catalysts are observed. No matter the reaction time the selectivity is clearly governed by the support.

Gluconic acid yield (Fig. 4B) for the Au/Al catalyst increases linearly with the reaction time unlike for Au/Ce and Au/Ce/Al (Fig. 4C, D) catalysts where the yield attains a constant value in the first 4 h of reaction. The presence of ceria in both samples suggests that the oxidation of the glucose might involve labile surface oxygen of this oxide. Therefore the oxidation process is improved, especially at short reaction times probably by the participation of its lattice oxygen and oxygen vacancies [28].

3.3. Effect of reaction temperature

All the other experiments are carried out over Au/Al catalyst. The temperature effect is studied in the 0–120 °C range with 2 h of reaction at every temperature and the results are shown in Fig. 5A.

The glucose conversion rises with the temperature till a constant value at around 55% at 60 °C. This result is expected as the oxygen solubility in water decreases with the temperature [29]. The solubility of oxygen reaches the lowest point at 60 °C and does not change significantly when the temperature increases [29]. To achieve then a higher activity the oxygen pressure has to be risen. It is interesting to underline that relatively high glucose conversion is achieved at 0 °C (35%) which indicates that Au/Al could work successfully at atmospheric pressure, low temperatures and in absence of base. The product distribution also changes with temperature (Fig. 5B), favoring lactic acid formation at low temperatures. Thus low temperatures imply low reaction rates for the glucose oxidation and higher selectivity to lactic acid formation.

3.4. Stirring rate dependence

It is well known for the liquid-phase reactions, that the diffusional processes of either reactants arrival to the active sites or products desorption from the catalyst' surface depend on mixing degree. For this reason, some experiments are carried out over Au/Al sample at 120 °C (2 h reaction time) by varying the stirring rate from 300 to 900 rpm. As expected, the higher the stirring rate, the higher the conversion of glucose (Fig. 6) and the higher the gluconic acid yield (47% vs. 59%).

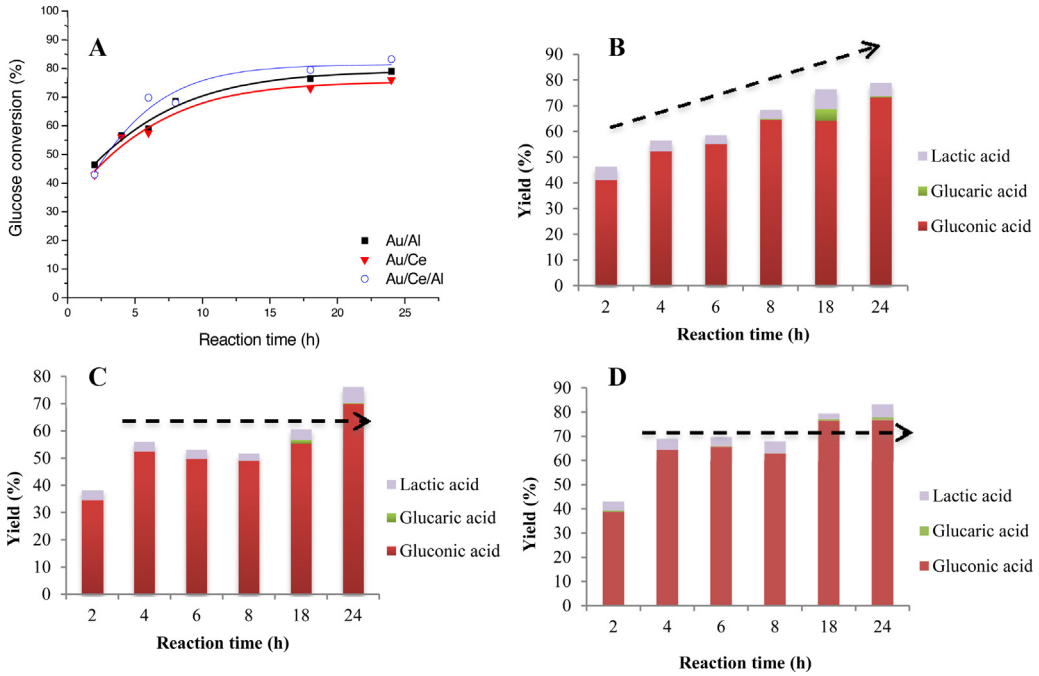

Fig. 4. A) Glucose conversion (%) vs. reaction time (120 °C, 600 rpm), B) Yield over Au/Al, C) Yield over Au/Ce, D) Yield over Au/Ce/Al.

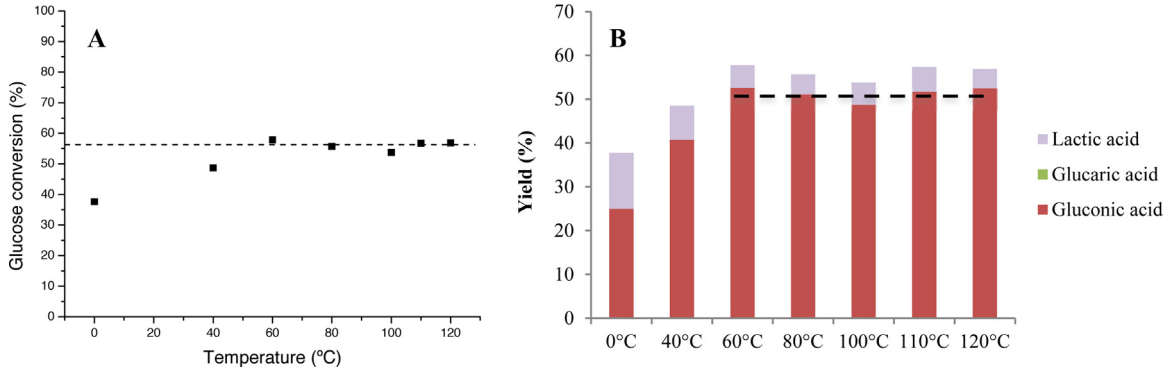

Fig. 5. A) Glucose conversion (%) as a function of the temperature over Au/Al (600 rpm, 2 h) B) Yield (%).

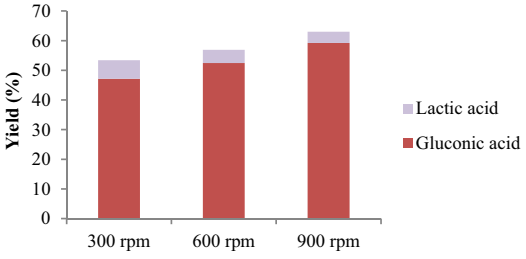

Fig. 6. Yield (%) as a function of the stirring rate over Au/Al (120 °C, 2 h).

Besides glucose conversion, the lactic acid yield is also related to the mixing degree, being higher at low stirring rates (6% of yield at 300 rpm vs. 3% at 900 rpm). This result could be tentatively explained by the higher residence time of the reactants on the surface of the catalyst at lower mixing and/or by lower oxygen concentration in solution, both allowing the secondary reaction to lactic acid formation. As observed above in reaction temperature effect, the lower the reaction rate of oxidation reaction the higher the selectivity towards lactic acid. The formation of lactic acid at low conversions and low mixing rate suggests that great glucose coverage on the catalyst surface is one of the key factors for a proper product distribution.

On the other hand, the limited conversions above 60 °C and the fact that higher conversions can be reached by increasing the stirring rate might also suggest some limitation due to the mass-transfer process. However, as reported by Delidovich et al. [30] the diffusional processes limiting the glucose oxidation reaction rate on Au/Al_2O_3 strongly depend on the Glucose:Au molar ratio. It was reported in this study that for low Glucose:Au molar ratios (below 750:1) the apparent reaction rate is only limited by the rate of oxygen dissolution. Therefore, we can consider that in our study (Glucose:Au 100:1) the limitations due to the mass-transfer process although existing are not so important as those caused by oxygen dissolution process.

3.5. Catalyst reusability

The reuse experiments are carried out over Au/Al catalyst in 4 successive runs. A clear drop of the glucose conversion is observed (Fig. 7).

The initial conversion of 53% achieved in the first run (120 °C, 2 h) drops to 44% in the second and 39% and 37% in the third and

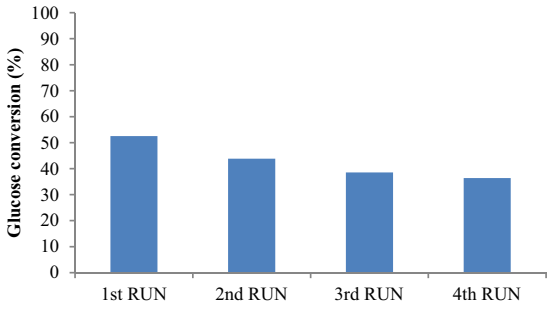

Fig. 7. Catalyst reuse, conversion of glucose (%) over Au/Al (120 °C, 2 h, 600 rpm).

fourth runs, respectively. The slope of activity loss becomes smaller with the number of runs, and appears to stabilize after the 3^{d} one. On the other hand, the change of the reaction solution color occurs, turning to mauve and pointing to gold leaching process. Indeed, the X ray fluorescence (XRF) analysis of the spent sample shows that after 18 h of reaction at 120 °C, the metal loading drops to 1.14% instead 1.64% for the initial catalyst. Generally, in the literature, the gold particle size growth during the reaction is reported as the main reason for gold catalysts deactivation. Comotti et al. [31] observed that the rate of glucose oxidation is inversely proportional to the gold particles diameter, being especially detrimental the size increase above 10 nm. In our case very slight increase of the gold particle size is detected. TEM images and particle size distribution of Au/Al, Au/Ce and Au/Ce/Al spent catalysts after 18 h reaction time are shown in Fig. 8.

Upon reaction the average gold particle size hardly changes, however, a broader particle size distribution is always obtained. The estimated particle size of the spent catalysts is presented in parenthesis in Table 2. Although, the increase of the average gold particle size observed, the difference in size is insignificant and might not be the cause of the observed activity loss, suggesting that leaching of gold should be the problem to solve in order to avoid catalyst deactivation.

In order to verify this assumption, Au/Al was tested again at the same reaction conditions (120 °C, 600 rpm) during 4 h and at this time, the catalyst was microfiltered, oxygen re-introduced the reaction continued to reach a total reaction time of 18 h but this time without solid catalyst. In this way the change of the activity in the last 14 h are caused by the leached gold particles. The obtained results (in red) compared with those of typical experience at 4 and 18 h (in blue) are shown in Fig. 9.

In a typical experiment after 4 h run, the obtained conversion is 57% which increases to 77% after 18 h, being the difference in the conversion directly attributed to the presence of supported catalyst and increase of the reaction time. On the other hand in the blank test, 59% of conversion is reached after 4 h with catalysts while 69% is measured after 18 h over the leached gold solution. Hence, this 10% can be ascribed to both leached gold and reaction time increase. As the change of the reaction time is the same, we can consider that the difference is due to the different gold present, in one case supported and leached in the other leached gold only. These results confirm that the leached gold is also participating in the reaction although lower conversion obtained. However, the color of the leached gold solution changes dramatically from purple

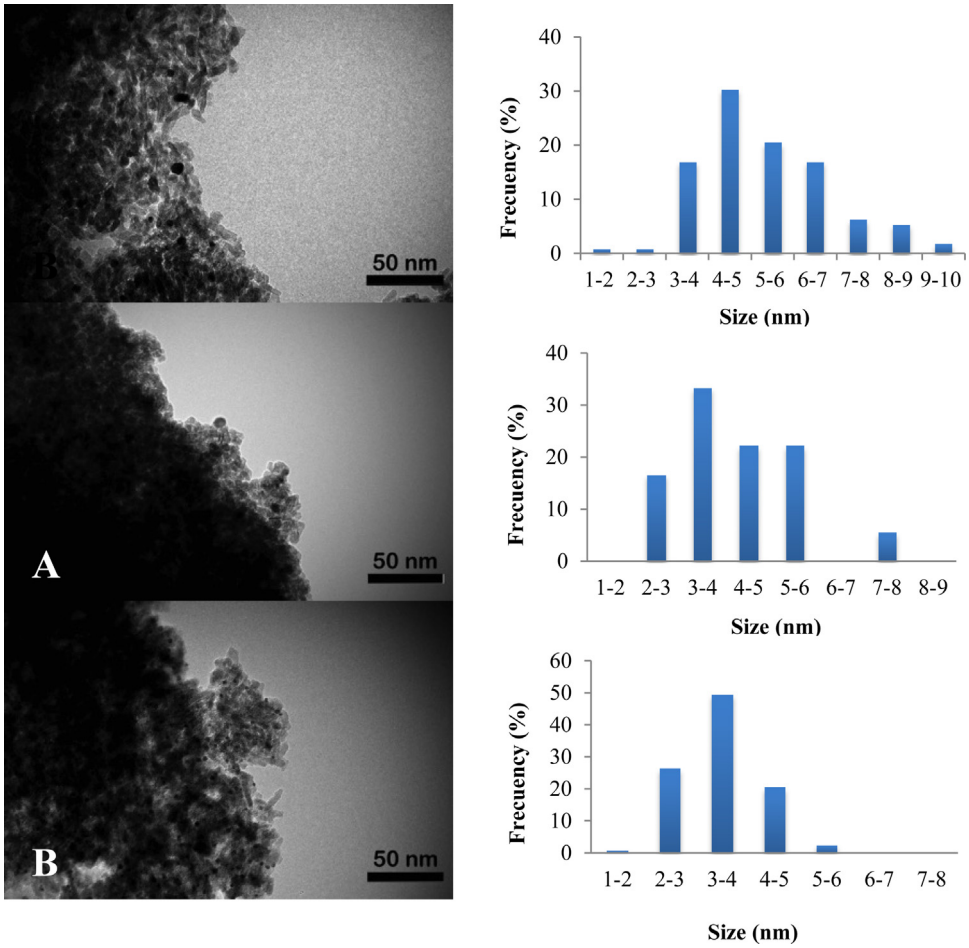

Fig. 8. TEM images and particle size distribution of spent catalysts: A) Au/Al, B) Au/Ce, C) Au/Ce/Al.

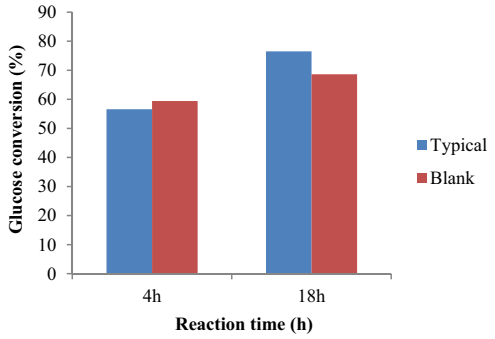

Fig. 9. Typical vs. Blank experiment over Au/Al at different reaction time. (For interpretation of the references to colour in the text, the reader is referred to the web version of this article.)

to black after 18 h, indicating detrimental particles agglomeration in absence of support. Color change was not observed for any typical experiment including supported gold.

Even though leached gold can participate in the oxidation process, higher activity is observed for the supported catalysts. With the later experiments we can affirm that the loss of activity during reuses runs is due mainly to the gold metal leaching and active sites lost during the catalysts recuperation and also that the presence of support is necessary for particles stabilization against agglomeration.

4. Conclusions

A series of gold supported on different metal oxides are synthesized, obtaining uniform gold nanoparticles size in the 3.5–5.5 nm range. All screened catalysts show high glucose conversion and important selectivity to gluconic acid in base- free conditions. Both, selectivity and activity depend on the support nature, in a way, that the presence of ceria promotes the oxidation reaction at lower reaction times and the presence of zirconia promotes the secondary reactions to lactic acid formation. The higher the zirconia concentration, the lower the glucose conversion and the higher the selectivity to lactic acid. The secondary reaction is also promoted at low reaction temperatures and stirring rates.

When exposed to various catalytic cycles the Au/Al catalyst fails to maintain constant conversion, with the reason for this activity decrease being the gold metal leaching.

References

[1] A. Corma, S. Iborra, A. Velty, Chemical routes for the transformation of biomass into chemicals, Chem. Rev. 107 (2007) 2411–2502, http://dx.doi.org/10.1021/cr050989d.
[2] M.J. Climent, A. Corma, S. Iborra, Converting carbohydrates to bulk chemicals and fine chemicals over heterogeneous catalysts, Green Chem. 13 (2011) 520, http://dx.doi.org/10.1039/c0gc00639d.
[3] J. Song, H. Fan, J. Ma, B. Han, Conversion of glucose and cellulose into value-added products in water and ionic liquids, Green Chem. 15 (2013) 2619–2635, http://dx.doi.org/10.1039/C3GC41141A.
[4] E.S.H. Hustede, H.J. Haberstroh, Ullmann's Encyclopedia of Industrial Chemistry, vol. A 12, Weinheim, 1989, p. 449–456.
[5] M. Bellardita, E.I. García-López, G. Marcì, B. Megna, F.R. Pomilla, L. Palmisano, Photocatalytic conversion of glucose in aqueous suspensions of heteropolyacid–TiO_2 composites, RSC Adv. 5 (2015) 59037–59047, http://dx.doi.org/10.1039/C5RA09894G.
[6] J.-Z. Liu, L.-P. Weng, Q.-L. Zhang, H. Xu, L.-N. Ji, A mathematical model for gluconic acid fermentation by Aspergillus niger, Biochem. Eng. J. 14 (2003) 137–141, http://dx.doi.org/10.1016/S1369-703X(02)00169-9.
[7] H. Znad, J. Markoš, V. Baleš, Production of gluconic acid from glucose by Aspergillus niger: growth and non-growth conditions, Process Biochem. 39 (2004) 1341–1345, http://dx.doi.org/10.1016/S0032-9592(03)00270-X.
[8] N.V. Sankpal, B.D. Kulkarni, Optimization of fermentation conditions for gluconic acid production using Aspergillus niger immobilized on cellulose microfibrils, Process Biochem. 37 (2002) 1343–1350, http://dx.doi.org/10.1016/S0032-9592(01)00335-1.
[9] P. Beltrame, M. Comotti, C. Della Pina, M. Rossi, Aerobic oxidation of glucose, Appl. Catal. A Gen. 297 (2006) 1–7, http://dx.doi.org/10.1016/j.apcata.2005.08.029.
[10] J.M.H. Dirkx, J.M.H. Dirkx, H.S. van Der Baan, H.S. van Der Baan, The oxidation of glucose with platinum on carbon as catalyst, J. Catal. 67 (1981) 1–13, http://dx.doi.org/10.1016/0021-9517(81)90256-6.
[11] M. Besson, F. Lahmer, P. Gallezot, P. Fuertes, G. Fléche, Catalytic oxidation of glucose on bismuth-promoted palladium catalysts, J. Catal. 152 (1995) 116–121.
[12] I. Nikov, K. Paev, Palladium on alumina catalyst for glucose oxidation: reaction kinetics and catalyst deactivation, Catal. Today 24 (1995) 41–47, http://dx.doi.org/10.1016/0920-5861(95)00011-4.
[13] M. Besson, P. Gallezot, Selective oxidation of alcohols and aldehydes on metal catalysts, Catal. Today 57 (2000) 127–141, http://dx.doi.org/10.1016/S0920-5861(99)00315-6.
[14] P. Gallezot, Selective oxidation with air on metal catalysts, Catal. Today 37 (1997) 405–418, http://dx.doi.org/10.1016/S0920-5861(97)00024-2.
[15] C. Della Pina, E. Falletta, Gold-catalyzed oxidation in organic synthesis: a promise kept, Catal. Sci. Technol. 1 (2011) 1564, http://dx.doi.org/10.1039/c1cy00283j.
[16] C. Della Pina, E. Falletta, M. Rossi, Update on selective oxidation using gold, Chem. Soc. Rev. 41 (2012) 350–369, http://dx.doi.org/10.1039/C1CS15089H.
[17] Y. Önal, S. Schimpf, P. Claus, Structure sensitivity and kinetics of D-glucose oxidation to D-gluconic acid over carbon-supported gold catalysts, J. Catal. 223 (2004) 122–133, http://dx.doi.org/10.1016/j.jcat.2004.01.010.
[18] H. Yin, C. Zhou, C. Xu, P. Liu, X. Xu, Y. Ding, Aerobic oxidation of D-glucose on support-free nanoporous gold, J. Phys. Chem. C 112 (2008) 9673–9678, http://dx.doi.org/10.1021/jp8019864.
[19] S. Biella, L. Prati, M. Rossi, Selective oxidation of D-glucose on gold catalyst, J. Catal. 206 (2002) 242–247, http://dx.doi.org/10.1006/jcat.2001.3497.
[20] P. Qi, S. Chen, J. Chen, J. Zheng, X. Zheng, Y. Yuan, Catalysis and reactivation of ordered mesoporous carbon-supported gold nanoparticles for the base-free oxidation of glucose to gluconic acid, ACS Catal. 5 (2015) 2659–2670, http://dx.doi.org/10.1021/cs502093b.
[21] Y. Wang, S. Van de Vyver, K.K. Sharma, Y. Román-Leshkov, Insights into the stability of gold nanoparticles supported on metal oxides for the base-free oxidation of glucose to gluconic acid, Green Chem. 16 (2014) 719–726, http://dx.doi.org/10.1039/C3GC41362D.
[22] S. Ivanova, C. Petit, V. Pitchon, A new preparation method for the formation of gold nanoparticles on an oxide support, Appl. Catal. A Gen. 267 (2004) 191–201, http://dx.doi.org/10.1016/j.apcata.2004.03.004.
[23] S. Ivanova, V. Pitchon, Y. Zimmermann, C. Petit, Preparation of alumina supported gold catalysts: influence of washing procedures, mechanism of particles size growth, Appl. Catal. A Gen. 298 (2006) 57–64, http://dx.doi.org/10.1016/j.apcata.2005.09.020.
[24] E.C. Koch, Acid-base interactions in energetic materials: I. The hard and soft acids and bases (HSAB) principle-insights to reactivity and sensitivity of energetic materials, Prop. Expl. Pyrotech. 30 (2005) 5.
[25] R.G. Pearson, Hard and soft acids and bases, J. Am. Chem. Soc. 85 (1963) 3533–3539.
[26] Y. Román-Leshkov, M. Moliner, J.a. Labinger, M.E. Davis, Mechanism of glucose isomerization using a solid lewis acid catalyst in water, Angew. Chem. Int. Ed. 49 (2010) 8954–8957, http://dx.doi.org/10.1002/anie.201004689.
[27] Y. Wang, W. Deng, B. Wang, Q. Zhang, X. Wan, Z. Tang, et al., Chemical synthesis of lactic acid from cellulose catalysed by lead(II) ions in water, Nat. Commun. 4 (2013), http://dx.doi.org/10.1038/ncomms3141.
[28] Y. Guan, D.A.J.M. Ligthart, J.A.Z. Pirgon-Galin, E.J.M. van Santen, Gold stabilized by nanostructured ceria supports: nature of the active sites and catalytic performance, Top. Catal. 54 (2011) 424–438, http://dx.doi.org/10.1007/s11244-011-9673-2.
[29] R. Battino, T.R. Rettich, T. Tominaga, The solubility of oxygen and ozone in liquids, J. Phys. Chem. Ref. Data 12 (1983) 163–178.
[30] I.V. Delidovich, B.L. Moroz, O.P. Taran, N.V. Gromov, P. a. Pyrjaev, I.P. Prosvirin, et al., Aerobic selective oxidation of glucose to gluconate catalyzed by Au/Al2O3 and Au/C: impact of the mass-transfer processes on the overall kinetics, Chem. Eng. J. 223 (2013) 921–931, http://dx.doi.org/10.1016/j.cej.2012.11.073.
[31] M. Comotti, C. Della Pina, R. Matarrese, M. Rossi, The catalytic activity of naked gold particles, Angew. Chem. Int. Ed. 43 (2004) 5812–5815, http://dx.doi.org/10.1002/anie.200460446.

Catalysis Today xxx (2016) xxx–xxx

Contents lists available at ScienceDirect

Catalysis Today

journal homepage: www.elsevier.com/locate/cattod

Influence of gold particle size in Au/C catalysts for base-free oxidation of glucose

C. Megías-Sayago[a,*], J.L. Santos[a], F. Ammari[b], M. Chenouf[a,b], S. Ivanova[a], M.A. Centeno[a], J.A. Odriozola[a]

[a] Instituto de Ciencia de Materiales de Sevilla, Departamento de Química Inorgánica, Universidad de Sevilla-CSIC, Américo Vespucio 49, 41092, Sevilla, Spain
[b] LGPC, Department of Chemical Process Engineering, Farhat-Abbas Sétif-1 University, Setif, Algeria

ARTICLE INFO

Article history:
Received 30 September 2016
Received in revised form 5 December 2016
Accepted 3 January 2017
Available online xxx

Keywords:
Gold catalysts
Carbon-supported catalysts
Glucose oxidation
Liquid-phase oxidation
Biomass conversion

ABSTRACT

A series of gold colloids were prepared and immobilized on commercial activated carbon. The influence of the colloid preparation and stability were studied and related to the gold particle size in the final catalyst. The catalysts show an important activity in the glucose to gluconic acid oxidation reaction, leading to gluconic acid yield close to 90% in base free mild conditions (0.1 MPa O_2 and 40 °C). The size-activity correlation and probable mechanism were also discussed. Finally, the viability of the catalyst was tested by recycling it up to four times.

1. Introduction

Biorefinery, defined as the efficient transformation of renewable materials to fuels and intermediate chemicals, and associated to environmental and economic benefits, has driven the research in this area to notable increase in the last decades [1–4]. Within the renewable materials the vegetal biomass, mostly constituted by carbohydrates, represents around 75% of the total renewable biomass [5]. Among the carbohydrates represented in this biomass the cellulose remains the most attractive fuel precursor, mainly due to its low price, chemical purity and because it is formed only by one monomer – glucose [6]. After cellulose depolimerazion the subsequent transformation of glucose to valuable compounds involves a variety of processes such as hydrogenation [7], isomerization [8], dehydration [9] and oxidation [10]. Every single mentioned process or a combination of them lead to the formation of different 'platform chemicals'. As an example, the D-Gluconic acid, derived from the oxidation of glucose at anomeric position, results to be an useful food additive and raw material for drugs and biodegradable polymers manufacturing [11,12]. Industrially D-Gluconic acid is produced by enzymatic fermentation process [13,14] for which the principal inconvenient for sustainable large-scale production is the necessity of a neutralization step in order to avoid enzymes deactivation by the produced acid [15]. This problem could be solved either by using a base or by the substitution of the enzymes with a heterogeneous catalyst able to oxidize glucose under mild base-free conditions by using either O_2 or H_2O_2 as oxidants [16–19].

Although the use of base (NaOH and a relatively high pH of around 9-9.5) results in increase of heterogeneous catalyst's activity due to particle size stabilization and metal leaching suppression [20–22], a decrease in the selectivity to gluconic acid is often observed caused by the glucose to fructose isomerization process [23]. In addition, the formation of gluconate salt instead of pure gluconic acid occurs and entails the need of cost effective post-reaction treatment to obtain the target acid. Therefore, a simple base-free heterogeneously catalyzed process able to produce selectively gluconic acid and avoiding the problems of particle size sintering and metal leaching is highly desirable.

Within the catalyst's candidates for such a process, the most promising alternative is nanometric gold. Glucose oxidation has been carried out over both unsupported [24,25] and supported [20,26] gold catalysts with good results in activity and selectivity; however, some issues must be addressed in order to improve the catalytic system. Various studies reported the base-free aero-

* Corresponding author.
E-mail address: cristina.megias@icmse.csic.es (C. Megías-Sayago).

http://dx.doi.org/10.1016/j.cattod.2017.01.007
0920-5861/

bic oxidation of glucose over gold supported catalysts with good results in activity and selectivity [22,27–29]. Most authors found a clear dependence of glucose oxidation activity on average gold particle size, suggesting that the oxidation proceeds directly on gold metal surface rather than on the contact perimeter between gold and support [26,28,30]. On the other side, it is still under debate the optimal gold particle size and if the nanoparticle shape plays any significant role in oxidation process. A serious inconvenient for the use of supported nanogold catalysts in the base-free glucose oxidation is related to the possible metal leaching and/or the gold sintering during the reuse cycles, driving to loss of activity [29]. The latter suggests the importance of adequate choice of support, able to stabilize the gold particles thus avoiding the leaching/sintering phenomena.

Most of the studied supports are simple or mixed metal oxides such as TiO_2 [27], MgO [31] Al_2O_3, CeO_2, CeO_2(25 wt%)/ZrO_2, CeO_2(50 wt%)/ZrO_2 and CeO_2(20 wt%)/Al_2O_3 [29]. The use of carbon supports has been also widely reported [32–36]. No matter the type of carbon supports i.e., activated carbon, carbon nanotubes or carbon nanofibers, Au/C systems showed high activity and selectivity in the oxidation of glucose [22,37,38].

In general, the substantial importance of active carbon as metal support in industrial catalysis is well recognized. Its stability in both acidic and basic media, its tunable pore structure and stability at high temperatures, the easiness of metal phase recovery by carbon burn away and its lower costs in comparison with conventional supports such as alumina and silica [39,40] convert it in a versatile material for heterogeneous catalysis. The real relevance of carbon in aqueous-phase oxidation reactions derived from its hydrophobicity, which usually difficults active metal phase leaching, thus improving catalyst's inherent activity. In fact, higher activity of hydrophobic catalysts in glucose oxidation compared to hydrophilic catalysts application has been reported [41,42]. This difference in activity was assigned to stronger adhesion between hydrophobic catalyst grains and oxygen bubbles leading to an increase of the catalyst grains number at the gas-liquid interface and, therefore, to an increase in the rate of the gas transfer towards the catalysts [38]. The only disadvantage of using hydrophobic support is that the conventional methods for gold nanoparticles preparation, such as deposition-precipitation or direct anionic exchange are less useful resulting in important gold loss and low reproducibility. Within the existing gold nanoparticles preparation methods, the gold colloidal route seems the most appropriated to obtain a homogeneous and reproducible gold nanoparticles size distribution which allows a more direct gold size/activity correlation. Nevertheless, the use of the colloidal route for preparing Au/C samples includes the utilization of particles stabilizing agents as citrates, polyvinyl alcohol (PVA) etc. which if not removed from the gold surface could influence the measured activity due to some shielding effects [30]. It is important therefore to remove any rests of stabilizing agents in order to observe the "real" size/activity effect on the reaction of glucose oxidation.

From all above, the aim of this work is to gain insights into the role of gold particle size and shape in the base free oxidation of glucose to gluconic acid. For that, a series of Au/C catalysts with different gold particle size were prepared and their catalytic performances evaluated in the oxidation reaction. The catalysts resulted from immobilization of gold colloids with different gold sizes on a commercial activated carbon, and were subjected to a calcination treatment at 300 °C in order to remove any precursor leftovers and to stabilize the gold nanoparticles onto the carbon surface in order to assure as much as possible the permanence of the gold size during the reaction course. The evaluation of the catalyst's reusability was also undertaken.

2. Experimental

2.1. Synthesis

Activated charcoal powder DARCO® (Sigma Aldrich, 100 mesh particle size) and $HAuCl_4$ (Johnson Matthey) gold precursor were used as received.

The deposition of gold (2 wt.% nominal value) on the carbon support was carried out according to the colloidal method assisted by polyvinyl alcohol (PVA) where $NaBH_4$ (Sigma Aldrich) was used as reducing agent [43]. The necessary amount of gold precursor was dissolved in water to a final concentration of 5.10^{-4} M and the corresponding quantity of PVA (1% wt. aqueous solution) was added and stirred during 20 min. After that, the appropriate amount of 0.1 M freshly prepared $NaBH_4$ solution was quickly added to reduce the gold precursor. After 20 min stirring, sample of 5 mL was taken to characterize the colloid and the rest of solution was put in contact to the adequate amount of the commercial activated carbon in order to have a nominal gold loading of 2%wt. 45 min later, the final mixture was centrifuged at 15000 rpm for 20 min in order to ensure the anchorage of the totality of gold nanoparticles on carbon. The resulted samples were filtered and dried at 100 °C for 2 h and finally calcined at 300 °C for 2 h in static air. Following this procedure, 11 samples, were prepared as a function of PVA:Au weight ratio (Series 1) and $NaBH_4$:Au molar ratio (Series 2). The Table 1 summarizes the synthesis parameters of both series of gold samples. Gold colloids and their corresponding catalysts were named as 'Col X' and 'AuC X' respectively, being X a distinctively roman number of order.

2.2. Characterization techniques

UV–vis measurements were carried out on UV–vis Avantes AvaLight-DH-S-BAL spectrometer equipped with optic fiber liquid sensor for wavelengths ranged from 100 to 1000 nm.

XRD measurements were performed at room temperature on Panalitycal X'Pert Pro diffractometer, equipped with Cu anode with 0.05° step size and acquisition time of 300 s in 10–90° 2θ range. The average gold crystallite size of the Au/C catalysts was calculated from the broadening of the (111) Au plane at 38.28° 2θ applying Scherrer's equation.

Transmission electron microscopy (TEM) micrographs were acquired on PHILIPS CM-200. The mean gold particle diameter was considered on the basis of its homogeneity, degree of dispersion and number of particles. The average gold particle size was estimated considering the surface distribution calculation, expressed in Eq. (1).

$$D[3,2] = \frac{\sum_{1}^{n} D_i^3 v_i}{\sum_{1}^{n} D_i^2 v_i} \quad (1)$$

where D_i is the geometric diameter of the i^{th} particle, and v_i the number of particles with this diameter. For every distribution the total number of measured particles overcomes 200 particles per sample (colloid or catalyst).

The gold loadings were estimated through ICP analysis by using Horiba Jobin Yvon spectrometer after fluorhydric acid digestion of the samples.

2.3. Catalytic tests

Aerobic oxidation of glucose (D-(+)-Glucose anhydrous, 99%, from Alfa Aesar) was carried out in a glass batch reactor (50 mL) equipped with Young valve, magnetic stirrer and saturated with

Please cite this article in press as: C. Megías-Sayago, et al., Influence of gold particle size in Au/C catalysts for base-free oxidation of glucose, Catal. Today (2016), http://dx.doi.org/10.1016/j.cattod.2017.01.007

Table 1
Code and Au/PVA/$NaBH_4$ ratios of the prepared gold samples.

	Sample	PVA:Au ratio[a]	$NaBH_4$:Au ratio[b]
Series 1	Col I/AuC I	0	5
	Col II/AuC II	0.5	5
	Col III/AuC III	**0.85**	**5**
	Col IV/AuC IV	3	5
	Col V/AuC V	5	5
	Col VI/AuC VI	10	5
Series 2	Col VII/AuC VII	0.85	0.5
	Col VIII/AuC VIII	0.85	1
	Col IX/AuC IX	0.85	2
	Col X/AuC X	0.85	3
	Col III/AuC III	**0.85**	**5**
	Col XII/AuC XII	0.85	10

[a] Weight ratio.
[b] molar ratio.

oxygen at atmospheric pressure (P_{O2} approximately 0.1 MPa). In a typical experiment, the reactor was charged with a 0.2 M aqueous glucose solution, catalyst in Glucose/Au molar ratio of 100 and oxygen, in the aforementioned order. The oxygen diffusion through solution was assured by 20 mL/min pure oxygen flux bubbling for few minutes. Afterwards, oxygen flow was stopped, the reactor was closed and the mixture stirred at 600 rpm, at 40 °C during 18 h in base-free conditions. Once the reaction finished, 500 μL of sample taken from the final reaction mixture and diluted in 500 μL of ultra-pure water was immediately analyzed by HPLC. The products of glucose oxidation were identified and quantified by using a Hi-Plex H column (300 × 7,7 mm), a refractive index detector (Varian 360-LC) and MilliQ water as mobile phase. Glucose conversion was calculated as described by Eq. (2).

$$Conversion \quad (\%) = \frac{[Glucose]_i - [Glucose]_f}{[Glucose]_i} \qquad (2)$$

3. Results and discussion

3.1. Colloids characterization

The influence of PVA:Au and $NaBH_4$:Au ratios on gold particle size and morphology was studied by both UV–vis spectroscopy and TEM microscopy. Fig. 1 presents the UV–vis absorption spectra of all synthesized colloids. All samples present an intense absorption with maxima in the 502–530 nm region. This absorption is characteristic of the surface plasmon resonance of Au metal fine particles and its position, intensity and width is strongly dependent on the size and shape of the Au particles, as well as of the dielectric properties of the surrounding environment [44].

For both colloidal series, a modification in the position, shape and width of the gold plasmon band is observed from one colloid to another, indicating differences in the average gold particle size and/or morphology. In good agreement, changes in the color of the colloidal solutions are also observed (see Fig. 1), all of them in the reddish mauve spectra. The color of gold colloids is also indicative for the resulted gold particles size and depends on support (if used), on gold concentration, morphology and size distribution [45]. In particular, colloidal gold is red when the corresponding particles are smaller than 20 nm. So far from the color we can deduce that our gold particles independently on the synthetic parameters present sizes always below/around 20 nm.

From Fig. 1A is obvious that increment in PVA:Au ratio during the preparation leads to blue shift of around 10 nm in the position of the gold plasm on which can be related with the formation of smaller nanoparticles. In the case of Col I, where no protective agent (PVA) was used, bigger gold particles is expected to be formed and possible partial sedimentation of the later, resulting in extremely high intense plasmon resonance band.

This size variation was also confirmed by TEM (Fig. 2) and the calculated average gold particle size decreases constantly from 3.6 nm (Col I) to 1.8 nm (Col VI) with the increase of the PVA concentration for series 1 (Table 2). In all cases, the obtained particle shape is similar, as deduced from the particle size distributions and TEM micrographs.

It is well known, that the final particles size is based on a fine balance between the velocity of nucleation and particle growth, which by themselves could be controlled by changing the nanoparticles' synthesis parameters. There exist many theories explaining the mechanisms of nucleation and growth of the metal nanoparticles. The velocity of gold nanoparticles nucleation and growth generally depends on the pH of the solution, on the reducing agent nature and concentration and on the presence of surfactants [46]. Ji et al. [47] reported that the pH dependence could be ascribed to the existence of differently hydrolyzed gold complexes and their reactivity towards reducing agent. When a very diluted gold precursor solutions (as in our case) are employed, the pH of the solution neighbors that of distilled water (6–6,5). At this pH, Ivanova et al. [48] reported that the 70% of Au could be found as $[Au(OH)_2Cl_2]^-$ and $[Au(OH)_3Cl]^-$ complexes. These complexes get reduced with slower nucleation time (60 s) than the less hydrolyzed ones and show lower growth velocity. The nature of the reducing agent is also very important, stronger the reductive potential of the agent lower the time of nucleation. The use of $NaBH_4$ indicates quasi-instantaneous nucleation within a few seconds to an average radius of 2 nm which then undergo coalescence up to 4 nm [49] in the first 20 min, the case of Col I when no stabilizing agent is used. The fast nucleation of gold could be then considered as separate processes from the particle size growth which will depends primarily on colloidal stability, i.e. on the increase of the aggregation barrier [46]. The later could be achieved by the use of stabilizing agent (PVA in our case). Indeed the stability of the colloidal solution as a function of time showed interesting differences between the samples. Whereas Col I and II samples agglomerate and precipitate after two days, the Col III to VI remain stable. The correlation between colloid stability and gold particle size suggests that stable gold colloids could be obtained at PVA/Au ratios superior to 0.85 with resulting particle size of 2.3 ± 0.5 nm. Because of this observation, the series 2 (Col VII to Col XII colloids) was prepared at a fixed PVA:Au ratio of 0.85 and varying the $NaBH_4$:Au proportion.

For this series, the increment of the $NaBH_4$:Au ratio also leads to a blue shift of the gold plasmon (see Fig. 1B), pointing out the formation of smaller nanoparticles at high concentration of the reductant agent (Table 2). However, the TEM analysis (Fig. 2) put in evidence that the variation $NaBH_4$:Au ratio affects also the shape and size heterogeneity of the produced gold nanoparticles. Thus, at low ratios (low concentration of reductant agent) a wide particle size distribution is obtained, generating gold particles from 7 to 25 nm and resulting in higher average particle size. Besides this, a change of particles morphology from spherical to triangular and/or irregular shapes is evidenced. Narrower particles size distribution and lower mean particle size were observed with the increase of the $NaBH_4$/Au ratio. For Col IX an important contribution of particles in the $1 - 5$ nm range is observed, with very few agglomerates. $NaBH_4$/Au ratio of 3 seems to be the limiting value above which stable colloids of gold particles of 2.3 nm are obtained.

3.2. Au/C catalysts

The pre-formed colloids were immobilized on activated carbon targeting Au loading of 2 wt.%. After the calcination treatment (300 °C, 2 h), no significant modification of the textural properties of the parent carbon support was observed. Diffuse Infrared Fourier

Please cite this article in press as: C. Megías-Sayago, et al., Influence of gold particle size in Au/C catalysts for base-free oxidation of glucose, Catal. Today (2016), http://dx.doi.org/10.1016/j.cattod.2017.01.007

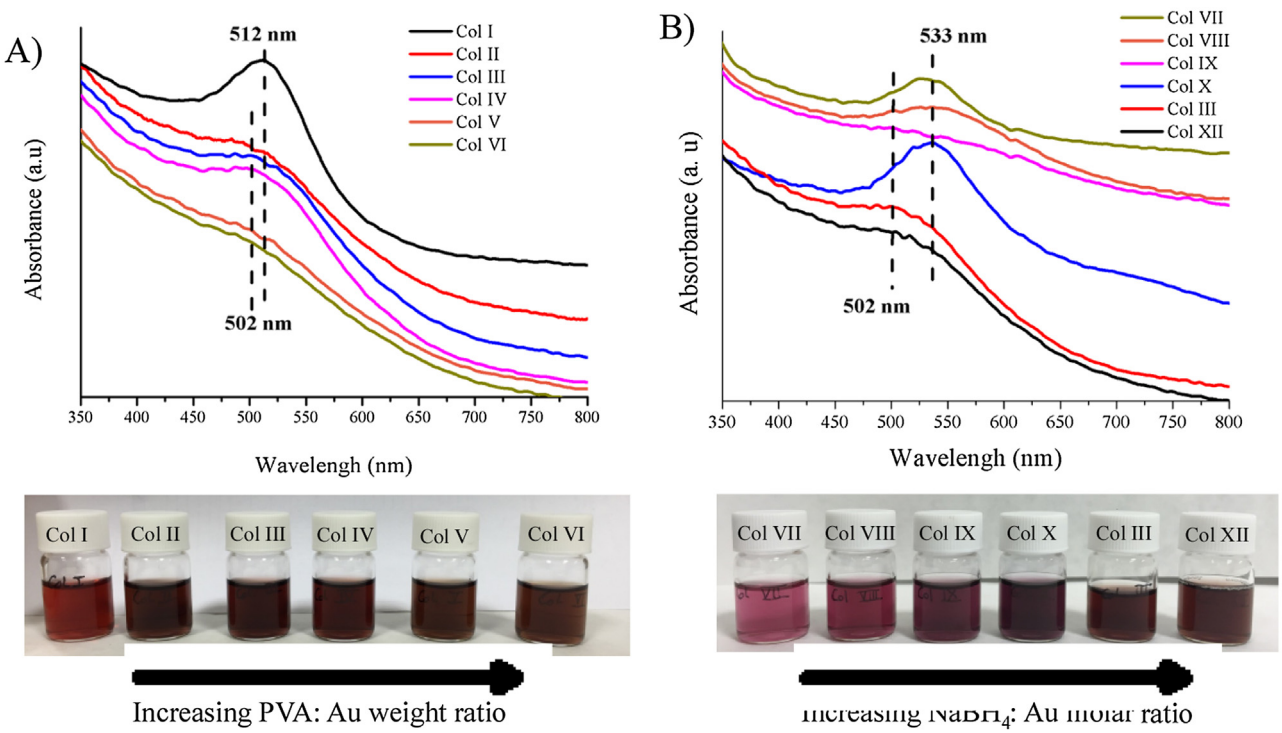

Fig. 1. UV–vis spectra of gold colloids. A) Series 1, B) Series 2.

Table 2
Mean Au particle size (colloids and catalysts), experimental gold loadings, dispersion and TOF of the supported gold catalysts.

	Sample	Average particle size of colloids (from TEM), nm	% Au [ICP]	Average particle size (from TEM), nm	Average particle size (from XRD), nm	Dispersion (%)	TOF, $s^{-1}*10^3$
Series 1	Col I/AuC I	3.6	2.0	15.4	14.9	10	11.24
	Col II/AuC II	3.3	2.3	9.3	9.3	15	7.08
	Col III/AuC III	**2.3**	2.4	8.7	10.4	16	6.19
	Col IV/AuC IV	2.8	2.3	10.1	11.1	14	5.60
	Col V/AuC V	2.3	1.1	6.8	6.6	20	7.58
	Col VI/AuC VI	1.8	0.5	4.1	4.4	32	8.59
Series 2	Col VII/AuC VII	18.9	2.1	22.8	28	7	9.40
	Col VIII/AuC VIII	3.7	2.3	20.1	25.4	7.5	12.04
	Col IX/AuC IX	7.6	2.3	22.2	22.5	7	14.5
	Col X/AuC X	4.9	2.2	20.4	16.1	7.4	14.7
	Col III/AuC III	**2.3**	2.4	8.7	10.4	16	6.19
	Col XII/AuC XII	2.2	2.3	4.8	5.2	27	3.77

Transform Spectroscopy (DRIFTS) study evidenced total removal of the PVA protective layer on the surface of the gold nanoparticles (figure not shown). The real gold loadings measured by ICP are summarized in Table 2.

The deposited amount of gold is slightly over 2 wt.% in majority of the samples indicating the successful immobilization of the colloid on carbon surface. However, for the samples prepared with the highest PVA/Au ratios (Au/C V and Au/C VI), a lower gold uptake is produced, in such a way that higher the PVA/Au ratio used for the colloid formation, lower the immobilized gold loading. Considering that, the stability of the colloids is proportional to the PVA concentration the anchoring of gold could become more difficult and responsible for the lower gold uptake. From here, and despite the low average gold particle size obtained for these colloids, PVA/Au ratios higher than 3 must be avoided in order to assure total immobilization of the gold nanoparticles.

The average gold particle sizes of the supported gold samples were calculated from both TEM and XRD measurements (Table 2) and present similar trends to those of the parent colloids. Fig. 3 shows representative TEM micrographs and gold particle size distribution for the Au/C samples.

For all samples, an 3–4 fold increase of the gold particles size was observed, which can be assigned to particles agglomeration occurred after the thermal treatment carried out in the supported catalysts (calcination at 300 °C for 2 h). An almost linear correlation was found between the metal particle size in the colloids and in the corresponding supported solid (Fig. 4), being only the sample corresponding to the Col VII pulled apart of the tendency due to the already aggregated state obtained in the initial colloid.

On the other hand, a good linear relationship was also achieved between the average gold particle size determined by TEM and XRD (Fig. 5).

In summary, the immobilization of the pre-formed colloids resulted in a series of Au/C catalysts with average gold particle sizes ranging from 4 to 20 nm. Most of the samples presented a similar gold contents (close to 2% wt) and gold particle shape (spherical), with a narrow gold size distribution, and thus, can be used to determine the influence of the gold particle size on the catalytic oxidation of glucose. Only samples prepared at high PVA/Au ratios (>3) or very

Please cite this article in press as: C. Megías-Sayago, et al., Influence of gold particle size in Au/C catalysts for base-free oxidation of glucose, Catal. Today (2016), http://dx.doi.org/10.1016/j.cattod.2017.01.007

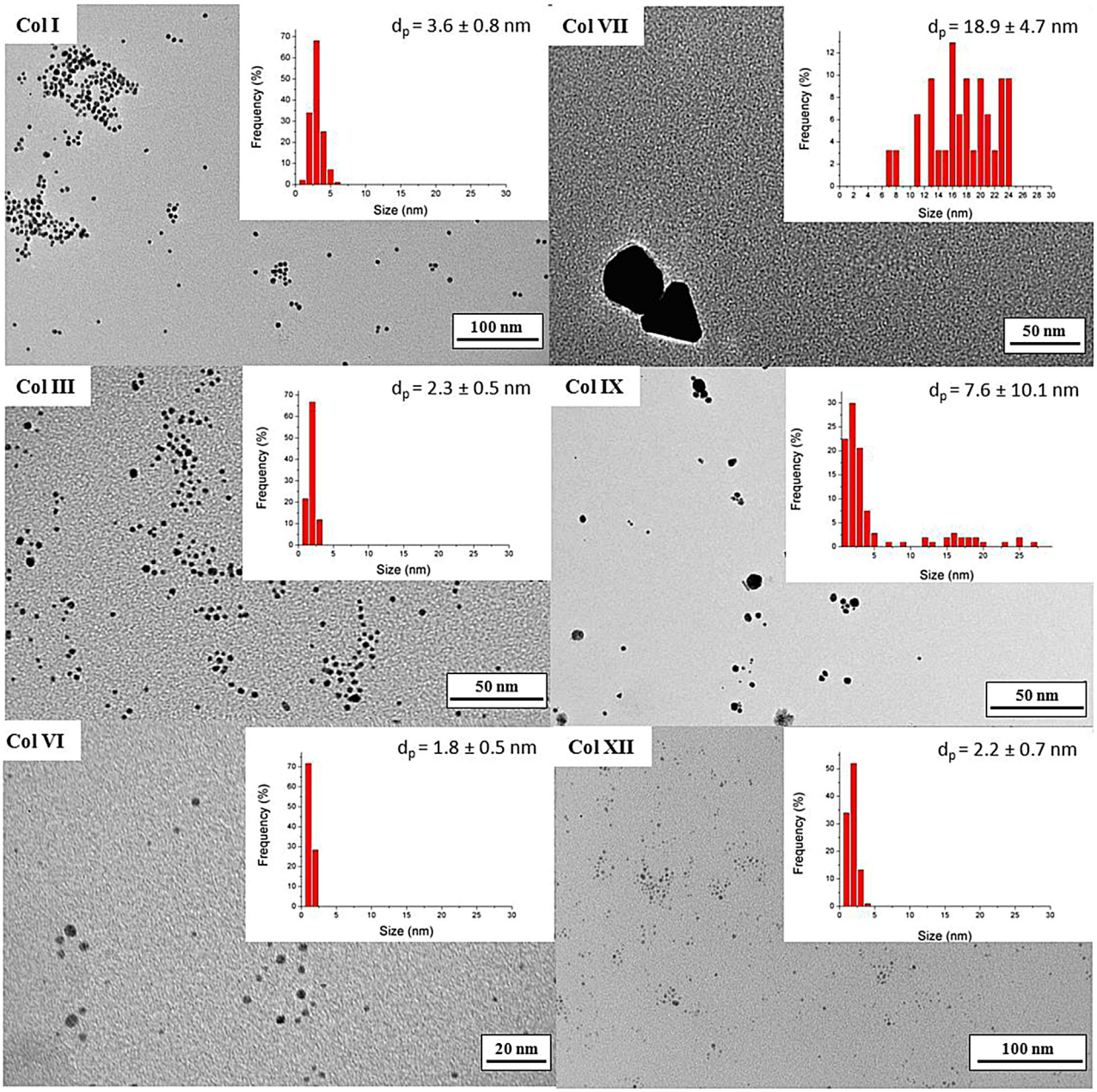

Fig. 2. Representative TEM micrographs and gold size distribution for selected prepared gold colloids.

low $NaBH_4$:Au ratio (<1) must be carefully analyzed, due to, respectively, their lower gold content or different gold particles shape and wide size distribution.

3.3. Catalytic screening

The catalytic activity in terms of glucose conversion of all synthesized Au/C catalysts as a function of the average gold particle size determined from TEM are shown in Fig. 6.

All samples showed 100% of selectivity to gluconic acid without formation of other products. Excluding the samples with a significant lower gold content and different gold particle shape and wide size distribution (in red), a linear trend, almost constant, is observed. The trend is a bit in decline, which could indicate that small gold particles are more active than big ones, which is a general conclusion for gold catalysis [50]. In fact, a maximum in activity for particles around 9 nm is observed, in agreement with the findings of Prati et al. during the last decade and resumed in a recent publication [30]. They found 7 nm as optimal gold nanoparticle size for the highest activity and assigned it to the exercised embedding effect of carbon on smaller nanoparticles.

Nevertheless if the activity is normalized to the exposed gold surface by using turn-over-frequency (TOF) values ($TOF = \frac{moles\ Glucose\ converted}{moles\ \ Au{*}s{*}dispersion}$) calculated taking into account the gold dispersion estimated from the average gold particle size deduced from TEM and mathematically modeled for cuboctahedral particles [51] and the real Au contents measured from ICP (see Table 2), the observed size/activity relationship is somehow different, Fig. 7.

Now, the samples could be organized in two groups, samples up to 10 nm showing similar TOF values below $8{\cdot}10^{-3}\ s^{-1}$ and samples with particle size around 15–20 showing superior TOF value of ($>10{\cdot}10^{-3}\ s^{-1}$). This result appears somehow contradictory as we consider that higher the particle size lower the gold atoms sur-

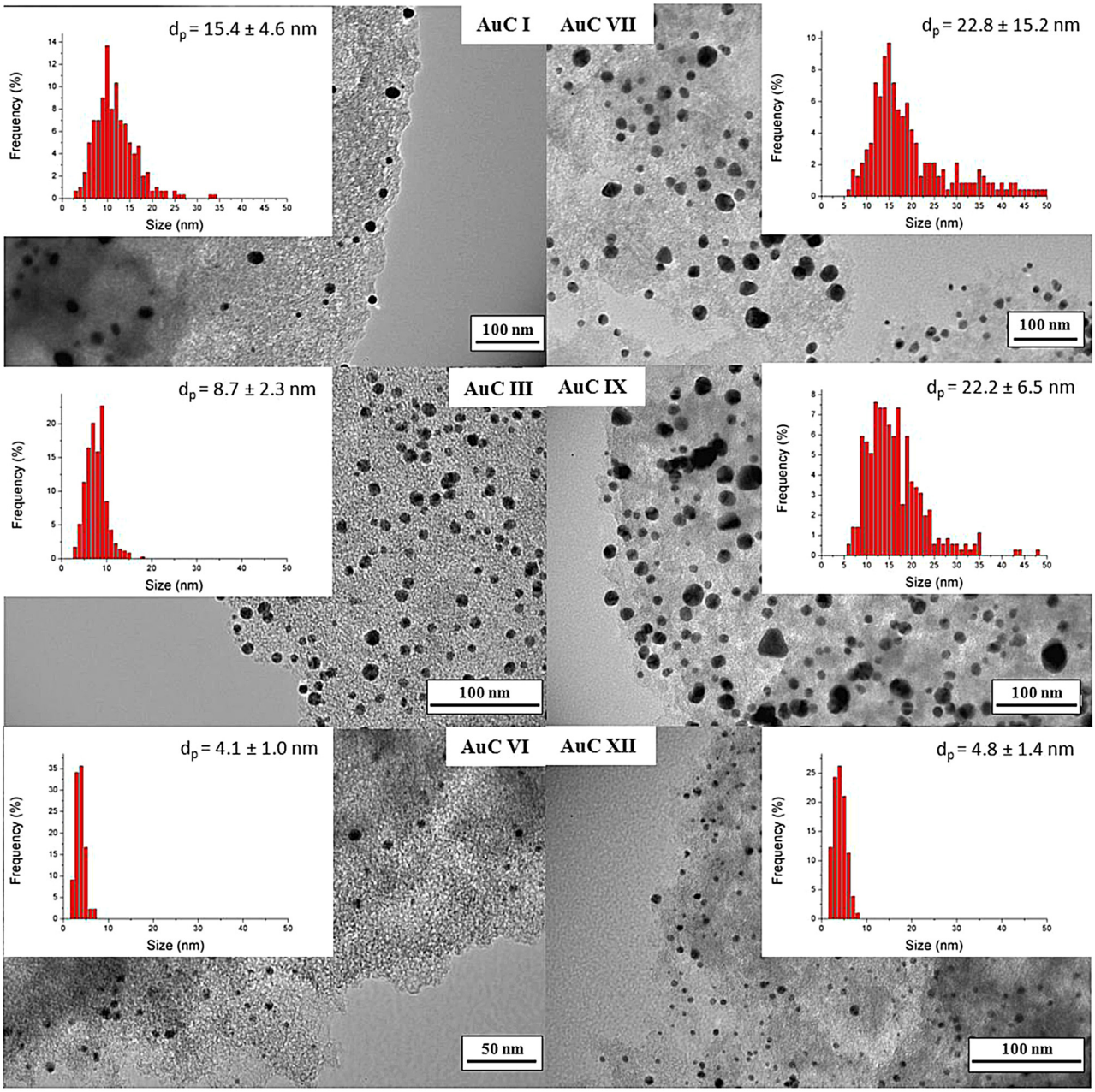

Fig. 3. Representative TEM micrographs and gold size distribution for selected Au/C catalysts.

face exposure. Anyway, this result suggests that glucose adsorption step should play an important role in the reaction mechanism. And that the adsorption strength and activation mechanism are probably different on small and big size gold particles. In this sense, there is lack of studies considering the reaction mechanism in base-free glucose oxidation conditions. In alkaline conditions, Ishimoto et al. [52] proposed 4 steps theoretical mechanism, where i) glucose is adsorbed on OH adsorbed on Au, ii) OH^- from the solution react with the CHO group of glucose to iii) form and release water by proton transfer and finally iv) gluconic acid is formed by OH transfer from the Au surface. However in base-free conditions the mechanism should occur in a different way. Normally is considered that the liquid phase oxidation of alcohols and aldehydes adopts the commonly known oxidative dehydrogenation mechanism [53] where the reactives are deprotonated on the metal surface with metal hydrate formation, which subsequently reacts with dissociatively adsorbed oxygen to form water. However, for this mechanism the structure/size dependency is the opposite of that observed in our study, i.e. lower the particle size higher the adsorption/hydrogenation of the CHO group and higher the activity toward acid formation. Taking into account both mechanisms one can consider the adsorption of glucose over metal as the important first step of reaction. Indeed, the energy of adsorption of glucose directly on Au was calculated stronger than that of OH on the same metal [54]. On the other hand, the interaction between activated carbon and Au proceeds through electron transfer from carbon to the metal, inferring slightly negative charge on gold. It was reported, that negatively charged gold clusters easily dissociate oxygen [55]. Taking into account the later the formation of secondary active sites AuO^- could be envisaged as the sites able to deprotonate CHO glucose group forming Au-OH, which finally react to form gluconic acid

It is also the place to consider the role of carbon in the reaction. The activated carbon possess a diversity of oxygen containing

Please cite this article in press as: C. Megías-Sayago, et al., Influence of gold particle size in Au/C catalysts for base-free oxidation of glucose, Catal. Today (2016), http://dx.doi.org/10.1016/j.cattod.2017.01.007

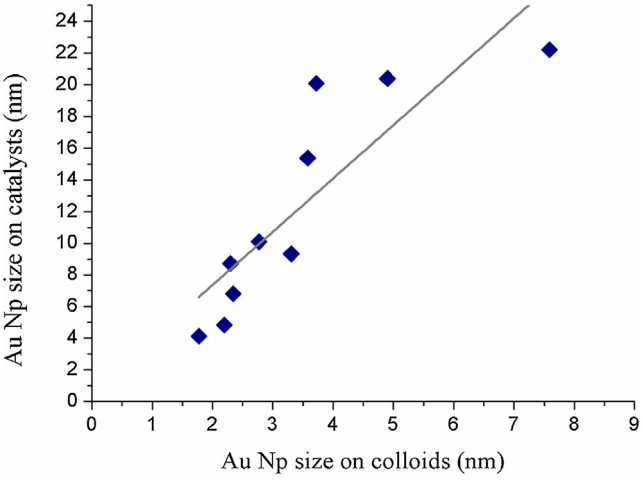

Fig. 4. Correlation between the average gold particle size in the colloids and in the corresponding prepared Au/C catalysts.

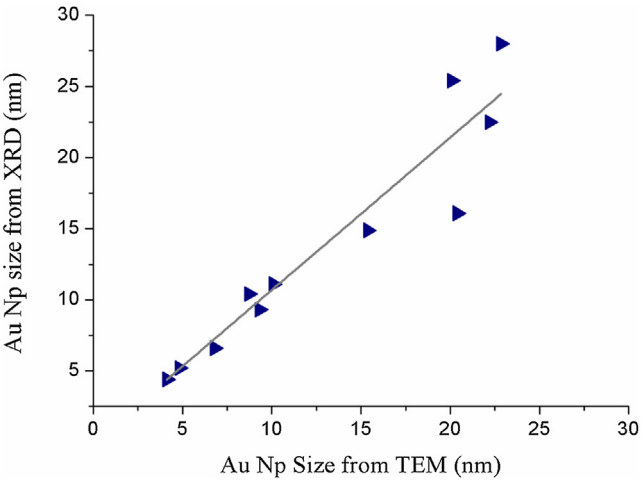

Fig. 5. Correlation between the average gold particle size determined by TEM and XRD.

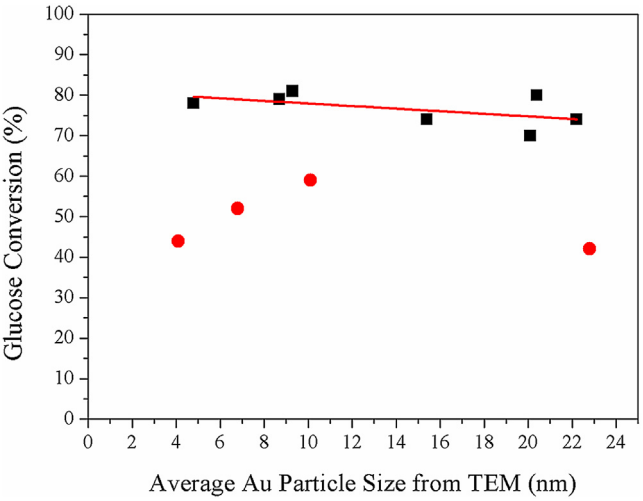

Fig. 6. Glucose conversion as a function of the average gold particle size determined by TEM (0.1 MPa O_2, 40 °C, 18 h). (Samples with a significant lower gold content and different gold particle shape and wide size distribution are shown in red). (For interpretation of the references to colour in this figure legend, the reader is referred to the web version of this article.)

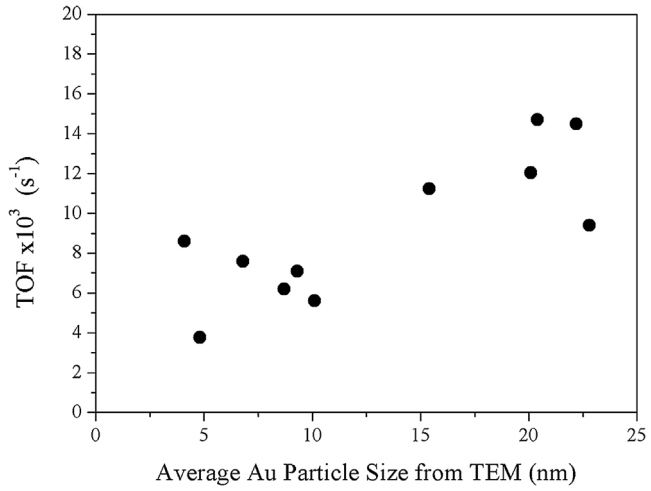

Fig. 7. Glucose oxidation turn-over-frequency (TOF) values as a function of the average gold particle size determined from TEM (0.1 MPa O_2, 40 °C, 18 h).

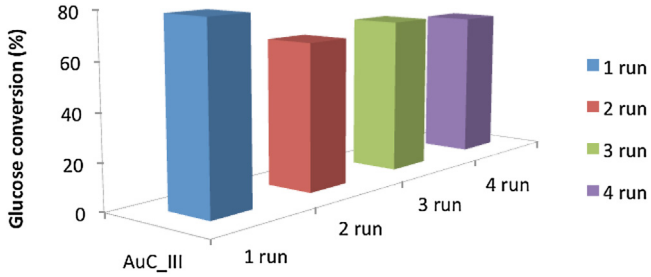

Fig. 8. Glucose conversion under recycle runs.

group being the more important the phenolic groups which could influence by itself or when situated in vicinity of gold particle the apparent reaction rate. Our blank test (using only activated carbon in the same reaction conditions) show 8% of glucose disappearing but without any detectable product formation, suggesting only glucose adsorption on the carbon surface at this temperature.

The reference sample AuC III, with an average gold size of 8.7 nm was selected for the recycling study. Four successive runs were carried out, with Glucose to catalyst ratio kept constant (Fig. 8).

The 2nd run presents of around 15% of activity loss which is half recuperated in the 3rd cycle and stabilized in the 4th one. The variation within the last 3 cycles and especially the loss of activity in the 2nd cycle could be due either to difference in the glucose adsorption coverage, to its adsorption/desorption equilibrium at this temperature or to gold metal sintering/leaching process. Nonetheless, more detailed study is needed to clarify the real causes of catalyst deactivation.

4. Conclusions

Gold colloids particle size is influenced by the stabilizing agent and reducing agent/Au ratio. Two limiting values were found in order to achieve stable colloid and homogeneous particles size distribution, the PVA/Au ratio should be superior to 0.85 and $NaBH_4$/Au superior to 3.

The immobilization of the colloids on the carbon support surface was effective. After the calcination treatment, an increment in the average gold particle size was observed, although a good correlation between colloids and supported gold particle sizes was maintained.

With that strategy, we have successfully prepared a series of Au/C samples with similar gold contents (close to 2% wt), gold par-

Please cite this article in press as: C. Megías-Sayago, et al., Influence of gold particle size in Au/C catalysts for base-free oxidation of glucose, Catal. Today (2016), http://dx.doi.org/10.1016/j.cattod.2017.01.007

ticle shape (spherical) and narrow gold size distribution, in which the influence of the gold particle size in the catalytic oxidation of glucose could be evaluated.

All catalysts show very good activity in the oxidation of glucose under base free mild conditions with a 100% selectivity to the desired product gluconic acid. The structure/size sensitivity shows optimal size for maximum conversion for particles of around 9 nm, although the normalization to exposed surface gold atoms (TOF) moves this optimum to gold particles in the 15–20 nm range, pointing to a possible influence of the glucose adsorption step in the reaction mechanism.

The catalysts show a very good recyclability with the loss of activity of only 10% after the 4th cycle.

Acknowledgements

Financial support for this work has been obtained from the Spanish Ministerio de Economía y Competitividad (MINECO) (ENE2013-47880-C3-2-R) co-financed by FEDER funds from the European Union. J.L. Santos also acknowledges the same Spanish Ministerio de Economía y Competitividad for his predoctoral fellowship (BES-2014-068244).

References

[1] D. Carpenter, T.L. Westover, S. Czernik, W. Jablonski, Green Chem. 16 (2014) 384.
[2] M. Yabushita, H. Kobayashi, A. Fukuoka, Appl. Catal. B Environ. 145 (2014) 1.
[3] M.J. Climent, A. Corma, S. Iborra, Green Chem. 13 (2011) 520.
[4] A. Corma, S. Iborra, A. Velty, Chem. Rev. 107 (2007) 2411.
[5] J. Song, H. Fan, J. Ma, B. Han, Green Chem. 15 (2013) 2619.
[6] S. Hu, Z. Zhang, J. Song, Y. Zhou, B. Han, Green Chem. 11 (2009) 1746.
[7] B. Kusserow, S. Schimpf, Claus. Adv. Synth. Catal. 345 (2003) 289.
[8] Y. Román-Leshkov, M. Moliner, J. a. Labinger, M.E. Davis, Angew. Chem. Int. Ed. 49 (2010) 8954.
[9] R. Karinen, K. Vilonen, M. Niemelä, ChemSusChem 4 (2011) 1002.
[10] U. Prüße, M. Herrmann, C. Baatz, N. Decker, Appl. Catal. A Gen. 406 (2011) 89.
[11] E.S.H. Hustede, H.J. Haberstroh, Ullmann's Encyclopedia of Industrial Chemistry, 1989.
[12] K. Marcincinova-benabdillah, M. Boustta, J. Coudane, M. Vert, Biomacromolecules 76 (2001) 1279.
[13] S. Ramachandran, P. Fontanille, A. Pandey, C. Larroche, Food Technol. Biotechnol. 44 (2006) 185.
[14] K. Buchholz, J. Seibel, Carbohydr. Res. 343 (2008) 1966.
[15] Y. Cao, X. Liu, S. Iqbal, P.J. Miedziak, J.K. Edwards, R.D. Armstrong, et al., Catal. Sci. Technol. 6 (2015) 107.
[16] C. Megías-Sayago, C.J. Carrasco, S. Ivanova, F.J. Montilla, A. Galindo, J.A. Odriozola, Catal. Today 278 (2016) 82.
[17] R. Saliger, N. Decker, U. Prüße, Appl. Catal. B Environ. 102 (2011) 584.
[18] I. Witońska, M. Frajtak, S. Karski, Appl. Catal. A Gen. 401 (2011) 73.
[19] a. M. Velarde, P. Bartl, T.E.W. Nießen, W.F. Hoelderich, J. Mol. Catal. A Chem. 157 (2000) 225.
[20] S. Biella, L. Prati, M. Rossi, J. Catal. 206 (2002) 242.
[21] Y. Önal, S. Schimpf, P. Claus, J. Catal. 223 (2004) 122.
[22] P. Qi, S. Chen, J. Chen, J. Zheng, X. Zheng, Y. Yuan, ACS Catal. 5 (2015) 2659.
[23] C. Kooyman, K. Vellenga, H.G.J.D.E. Wilt, Carbohydr. Res. 54 (1977) 33.
[24] M. Comotti, C. Della Pina, R. Matarrese, M. Rossi, Angew. Chem. Int. Ed. 43 (2004) 5812.
[25] P. Beltrame, M. Comotti, C. Della Pina, M. Rossi, Appl. Catal. A Gen. 297 (2006) 1.
[26] T. Ishida, N. Kinoshita, H. Okatsu, T. Akita, T. Takei, M. Haruta, Angew. Chem. Int. Ed. 47 (2008) 9265.
[27] X. Cao, X. Peng, S. Sun, L. Zhong, W. Chen, S. Wang, et al., Carbohydr. Polym. 118 (2015) 44.
[28] Y. Wang, S. Van de Vyver, K.K. Sharma, Y. Román-Leshkov, Green Chem. 16 (2014) 719.
[29] C. Megías-Sayago, S. Ivanova, M.A. Centeno, J.A. Odriozola, Catal. Today. 279 (2017) 148.
[30] L. Prati, A. Villa, A.R. Lupini, G.M. Veith, Phys. Chem. Chem. Phys. 14 (2012) 2969.
[31] P.J. Miedziak, H. Alshammari, S. a. Kondrat, T.J. Clarke, T.E. Davies, M. Morad, et al., Green Chem. 16 (2014) 3132.
[32] H. Okatsu, N. Kinoshita, T. Akita, T. Ishida, M. Haruta, Appl. Catal. A Gen. 369 (2009) 8.
[33] Y. Önal, S. Schimpf, P. Claus, J. Catal. 223 (2004) 122.
[34] H.F. Cui, J.S. Ye, X. Liu, W.D. Zhang, F.S. Sheu, Nanotechnology 17 (2006) 2334.
[35] L. Prati, M. Rossi, J. Catal. 176 (1998) 552.
[36] S. Gil, L. Muñoz, L. Sánchez-Silva, A. Romero, J.L. Valverde, Chem. Eng. J. 172 (2011) 418.
[37] C. Della Pina, E. Falletta, Catal. Sci. Technol. 1 (2011) 1564.
[38] I.V. Delidovich, B.L. Moroz, O.P. Taran, N.V. Gromov, P. a. Pyrjaev, I.P. Prosvirin, Chem. Eng. J. 223 (2013) 921.
[39] C. Bianchi, S. Biella, A. Gervasini, L. Prati, M. Rossi, Catal. Lett. 85 (2003) 91.
[40] F. Rodriguez-Reinoso, Carbon N. Y. 36 (1998) 159.
[41] J.H. Vleeming, B.F.M. Kuster, G.B. Marin, Catal. Lett. 46 (1997) 187.
[42] K.C. Ruthiya, J. van der Schaaf, B.F.M. Kuster, J.C. Schouten, Chem. Eng. Sci. 59 (2004) 5551.
[43] J. Luo, W. Chu, S. Sall, C. Petit, Colloids Surf. A Physicochem. Eng. Asp. 425 (2013) 83.
[44] P. Bera, M.S. Hedge, No Title Catal. Lett. 79 (2002) 107.
[45] G.C. Bond, D.T. Thompson, Catal. Rev. Sci. Eng. 41 (1999) 319.
[46] J. Polte, CrystEngComm 17 (2015) 6809.
[47] X. Ji, X. Song, J. Li, Y. Bai, W. Yang, X. Peng, J. Am. Chem. Soc. 129 (45) (2007) 13939.
[48] S. Ivanova, V. Pitchon, C. Petit, H. Herschbach, A. Van Dorsselaer, E. Leize, Appl. Catal. A Gen. 298 (2006) 203.
[49] N.T.K. Thanh, N. Maclean, S. Mahiddine, Chem. Rev. 114 (2014) 7610.
[50] M. Haruta, Gold Bull. 37 (2004) 27.
[51] S. Ivanova, V. Pitchon, C. Petit, J. Mol. Catal. A Chem. 256 (2006) 278.
[52] T. Ishimoto, Y. Hamatake, H. Kazuno, T. Kishida, M. Koyama, Appl. Surf. Sci. 324 (2015) 76.
[53] T. Mallat, A. Baiker, Catal. Today. 19 (1994) 247.
[54] T. Ishimoto, H. Kazuno, T. Kishida, M. Koyama, Solid State Ionics 262 (2014) 328.
[55] A. Franceschetti, S.J. Pennycook, S.T. Pantelides, Chem. Phys. Lett. 374 (2003) 471.

Please cite this article in press as: C. Megías-Sayago, et al., Influence of gold particle size in Au/C catalysts for base-free oxidation of glucose, Catal. Today (2016), http://dx.doi.org/10.1016/j.cattod.2017.01.007

Catalysis Today xxx (2017) xxx–xxx

Contents lists available at ScienceDirect

Catalysis Today

journal homepage: www.elsevier.com/locate/cattod

Gold catalyst recycling study in base-free glucose oxidation reaction

C. Megías-Sayago*, L.F. Bobadilla, S. Ivanova, A. Penkova, M.A. Centeno, J.A. Odriozola

Departamento de Química Inorgánica, Universidad de Sevilla e Instituto de Ciencia de Materiales de Sevilla, US-CSIC, Américo Vespucio 49, 41092, Sevilla, Spain

ARTICLE INFO

Article history:
Received 25 November 2016
Received in revised form 13 March 2017
Accepted 16 March 2017
Available online xxx

Keywords:
Base-free glucose oxidation
Gold
Activated carbon
Deactivation
Recycling

ABSTRACT

This work is devoted to the study of viability of immobilized gold colloids on carbon as catalysts for the base-free glucose oxidation reaction with a special emphasis made on catalysts' recycling, operational life and possible routes for deactivation/reactivation under batch conditions. The observed catalytic behavior is related to all possible manners of deactivation, like gold metal state changes (particle size agglomeration or leaching), support modifications or active sites blocking by intermediates. In an attempt to recover the initial catalytic activity, the samples are subjected to different treatments such as H_2O and NaOH washings and calcination. The failure of the regeneration procedures to recover the initial activity and after detailed catalyst' characterization allows us to find out the main cause of deactivation.

1. Introduction

In the last decades, an increasing necessity of readdressing the interest from fossil raw materials to renewable feedstocks arises due to the continuous depletion of the formers. A reorientation of the scientific interest towards carbohydrates as feedstock for fine chemistry is currently of actuality [1]. The "green catalysis" approach including orientation toward aqueous media low temperature catalytic transformations and carbohydrates highly functionalized type molecules increases by far its potential as fine chemical feedstock [2,3]. It is then of crucial importance to explore this potential toward efficient, environmentally friendly and economically viable technologies for large-scale conversion of carbohydrates into industrially viable bulk or intermediate compounds for chemical, pharmaceutical or polymeric use [4]. Among the existing reactions for carbohydrates conversion, the selective oxidation of plant-biomass monomers (hexoses or pentoses) to corresponding carboxylic acids presents a possibility to easy integration in already existing technologies and therefore an important economic interest. The heterogeneously catalyzed transformation of glucose to gluconic acid received important attention [5–8]. Nevertheless, the proposed processes must show an important activity/selectivity balance and especially long term stability in order to be competitive to the existing biotechnological process for gluconic acid production. The slow to severe catalyst deactivation and side reactions products are considered as the main challenges to undertake for future industrialization of heterogeneous process [9].

Among the metal catalysts discussed for selective oxidation of glucose to gluconic acid, the noble metal based ones are the most frequently reported. Important productivity was reported for Pt and Pd based catalysts [10–12]. Especially improved activities and product selectivity of the Pt based catalysts were obtained after doping with Bi [12,13]. However, during the reaction, bismuth leaching was observed which converts this catalytic system inadequate for pure chemicals production and may cause deactivation. In addition, alkaline conditions are required to increase the reaction rate and to avoid deactivation by reaction intermediates. Although beneficial for the reaction rate, the use of base conditions affects negatively the economics of the process as gluconate salt instead of pure gluconic acid is obtained at the end of reaction. Often, a decrease of selectivity due to the favored glucose to fructose isomerization reaction at high pH is observed [6,14]. Considering that the catalysts operate continuously under oxygen rich atmospheres Pt and Pd based catalyst could suffer also deactivation by "over-oxidation" responsible for active sites lost by oxidation. The majority of these inconvenients could be resolved by using gold based catalysts instead of platinum and palladium based ones. High selectivity and activity were reported for supported gold catalysts and convert them in the most promising candidates for future industrial implantation [8,15–19]. Gold catalysts successfully operate under oxygen. The inert nature of the metal avoids loss of activity by oxidation and present an important activity for aldehyde group oxidation and inertness towards secondary alco-

* Corresponding author.
E-mail address: cristina.megias@icmse.csic.es (C. Megías-Sayago).

http://dx.doi.org/10.1016/j.cattod.2017.03.022
0920-5861/

Table 1
Synthesis parameters of the prepared samples.

Sample	$NaBH_4$:Aumolar ratio
AuC_I	3
AuC_II	5
AuC_III	10

holic group oxidation [6]. Probably the most important findings concerning gold based systems is that they could operate under a wide range of pH with the same activity, which allows avoiding the glucose to fructose isomerization under base conditions.

Recently, the great potential of gold catalysts for direct glucose oxidation in base free conditions was demonstrated [20–23]. It was confirmed that catalyst productivity is barely influenced by the pH of the reaction and that the proper choice of support is very important for catalyst performance. Mineral oxides, as pure ceria or mixed cerium oxides, are not suitable as supports, since the catalysts suffer slow deactivation by metal leaching [21,23]. On the other hand, basic supports are reported to be most suitable in acidic conditions [20], although their stability towards hydroxylation has to be improved. Pointing industrial application, the catalysts should withstand continuous operation and repeated recycling for a long time, which implies low deactivation rate and/or easy activity recovery. Carbon based catalysts present excellent stability in acidic media and low active metal leaching which converts them in potential candidates to study their operation under base free glucose oxidation reaction.

In this context, the aim of this work is to study the catalytic performance of a series of Au/C catalysts prepared by gold colloids immobilization and their recyclability under repeated operation. All possible deactivation causes as gold leaching, sintering and chemical poisoning (active sites blocking by reaction intermediates) are contemplated and related to the variation of the initial gold particle size. The viability of some catalyst' treatments between the operation cycles aiming to recover the initial deactivation was also investigated.

2. Experimental

2.1. Catalyst preparation

Gold was deposited from pre-formed colloids prepared by reducing of the PVA stabilized gold precursor with $NaBH_4$. 5.10^{-4} M aqueous solution of $HAuCl_4$ (2 wt% nominal value) was mixed with the corresponding quantity of PVA (1 wt.% aqueous solution) and stirred for 20 min. After, appropriate amount of 0.1 M freshly prepared $NaBH_4$ solution was quickly added for other 20 min and the solution was put in contact with commercially available activated carbon powder DARCO® (Sigma Aldrich, 100 mesh particle size). After aging, the final mixture was centrifuged at 15000 rpm for 20 min and resulted solids separated by filtration. Samples were finally calcined in static air at 300 °C for 2 h.

Following this procedure, four samples were prepared keeping constant PVA:Au weight ratio of 0.85 and varying the $NaBH_4$:Au molar ratio from 3 to 10. The later was chosen in order to get different final gold particle size, as reported in previous studies [24]. Table 1 summarizes the synthesis parameters and labelling of the catalysts.

2.2. Characterization

The gold contents were estimated through ICP analysis by using Horiba Jobin Yvon spectrometer.

Transmission electron microscopy (TEM) study on particle size and dispersion of the catalysts was performed on PHILIPS CM-200. The average gold particle size was estimated based on surface distribution calculations as shown in Eq. (1)

$$D[3,2] = \frac{\Sigma_1^n D_i^3 v_i}{\Sigma_1^n D_i^2 v_i} \quad \text{Eq. (1)}$$

where D_i is the geometric diameter of the i^{th} particle, and v_i the number of particles with this diameter. For particle size distribution, the total number of measured particles overcomes 200 for every sample.

The DRIFTS spectra were recorded at room temperature without sample dilution using a Thermo Nicolet Nexus FT-IR spectrometer equipped with a liquid nitrogen cooled MCT detector at 4 cm^{-1} resolution and average of 128 scans. The whole optical path was purged with CO_2- and H_2O-free nitrogen. About 50 mg of fresh or used catalyst finely grounded was loaded in the Praying Mantis™ cell for each measurement.

XPS measurements were carried out on Leybold-Hereus LHS-1020 instrument coupled with EA200 detector and using non chromatic Mg Kα (220W, 11 kV, 1253,6 eV). Prior to use the sample were pressed into a thin disk. The XPS spectra of all sample were recorded at room temperature and the binding energy was calibrated on C1 s at 284,6 eV with an uncertainty ±0.2 eV. The spectra were recorded with constant pass energy of 44 eV and 0.1 eV resolution for the studied zones.

2.3. Base free aerobic oxidation of glucose

The oxidation of glucose was performed in a glass batch reactor (50 mL) at constant temperature and stirring rate at saturated oxygen atmosphere (approximate P_{O2} of 0.1 MPa). In a typical experiment, the reactor was charged with 0.2 M glucose aqueous solution, catalyst in Glucose/Au molar ratio of 100 and oxygen saturated by bubbling 20 mL/min of pure oxygen flow for few minutes. The reactor was then closed and reaction mixture stirred at 600 rpm, at 40 °C during 18 h in base-free conditions.

The recycling study was carried out in a similar manner separating the catalyst from the products by filtration between the runs and re-using it maintaining Glucose/Au molar ratio of 100 at every run. In some cases reactivation treatments were performed. The samples after filtration were treated either with distilled water, 0.1 M NaOH solution or thermally treated at 300 °C for 2 h before every run.

The reaction products were identified and quantified by HPLC equipped with refractive index detector (Varian 360-LC) and Hi-Plex H column (300 × 7,7 mm) set to 40 °C using MilliQ water as mobile phase.

Glucose conversion and product selectivity to gluconic acid (GA) were calculated as described by Eqs. (2) and (3).

$$Conversion\,(\%) = \frac{[Glucose]_{in} - [Glucose]_{out}}{[Glucose]_{in}} \times 100 \quad \text{Eq. (2)}$$

$$Selectivity\ GA\,(\%) = \frac{moleGA}{totalmolesofproducts} \times 100 \quad \text{Eq. (3)}$$

3. Results and discussion

The real gold loading measured by ICP and the mean particle size deduced from TEM is presented in Table 2.

All fresh samples present similar gold loadings close to the targeted value. The average gold particle size varies within the series attributed to the modification of the synthesis parameters, chosen in a way to have a real disparity of the initial particle size. Higher the $NaBH_4$:Au ratio at a constant PVA:Au ratio, lower the average gold particles size. The synthesis parameters influence strongly the average particle size but not the actual metal loadings. The

Please cite this article in press as: C. Megías-Sayago, et al., Gold catalyst recycling study in base-free glucose oxidation reaction, Catal. Today (2017), http://dx.doi.org/10.1016/j.cattod.2017.03.022

Table 2
Gold metal loadings and particle size for fresh and spent catalysts.

Sample	Au wt.% (fresh)	Au, wt.% (spent 4th cycle)	Au particle size, nm (fresh)	Au particle size, nm (spent 1st cycle)	Au particle size, nm (spent 4th cycle)
AuC_I	2.2	1.9	16.1	n.m.	20.4
AuC_II	2.4	1.9	8	17	16.6
AuC_III	2.3	1.9	4.8	8.9	7.7

n.m. not measured.

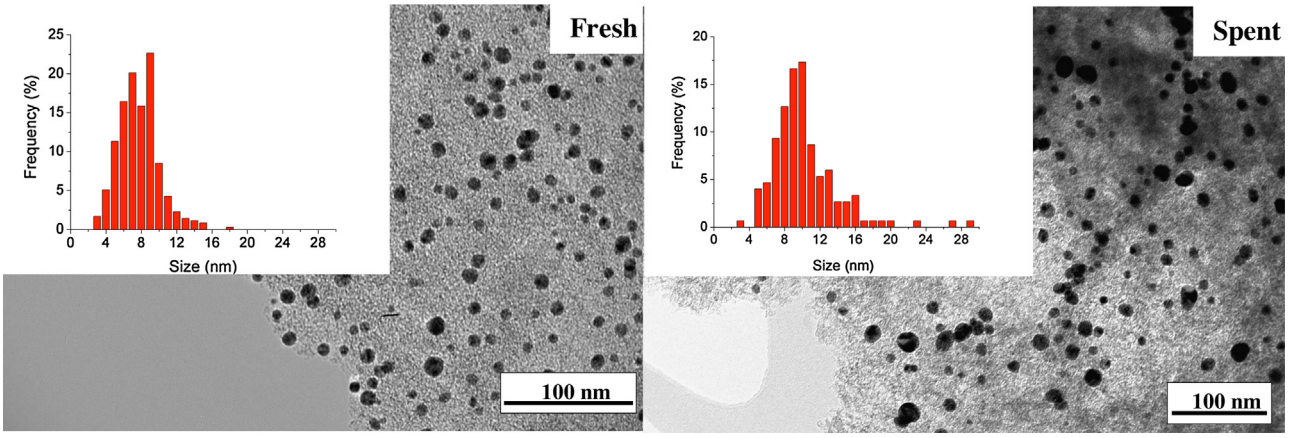

Fig. 1. Representative TEM micrographs and gold size distributions for fresh and spent (4th cycle) AuC_II samples.

representative micrographs of AuC_II sample and its particle size distribution are presented in Fig. 1.

3.1. Catalytic activity and recycling study

The catalyst activity of all samples and in every cycle, expressed as glucose conversion, is shown in Fig. 2a. The calculated carbon balance ranges from 86 to 95% (first vs. last cycle) indicating possible adsorption of reactive or intermediates after the first cycle but not after all successive ones. The gluconic acid selectivity on the base of liquid non-adsorbed products was found 100% and will not be discussed from now on.

No matter the gold particles size similar glucose conversions are obtained in the first cycles neighboring 80%. Systematically the second cycle gives always less conversion than the first one being the difference in the range of 20–25%. The performed blank test with activated carbon shows that at this temperature only 8% of glucose could be adsorbed on the carbon surface and false the initially calculated glucose conversion. Anyway the deactivation of the catalyst between the 1st and the 2nd cycle occurs unequivocally. It is also observed very similar 2nd and 3rd cycles and slightly different 4th cycle. The sample AuC_III shows continuous decrease of glucose conversion, while the AuC_I and AuC_II stabilized after the initial loss of activity. Nevertheless, from statistical point of view, within the series of samples only AuC_II behave differently (Fig. 2a).

As reported above the reasons for deactivation could be assembled in two groups, those altering directly the active sites, as sintering or metal loss, and those responsible for catalyst' blocking or support modifications. The leaching of gold was checked by ICP analysis of the remaining gold on catalyst after accomplished recycling study (Table 2) and in the filtration water before every cycle. No matter the starting catalyst and/or particle size, the same gold loss is detected averaging 15% of the initial gold loading and always the gold loss between the 1st and the 2nd cycle represents almost 80% of the total leaching.

On the other hand, gold particle size is also influenced (Table 2). The sample AuC_I does not change practically its initial particle size, only a slight increase is observed. AuC_II and AuC_III practically doubles their size after the 1st run after which the size remain constant in the last two runs. The increase of the average particle size is caused by the identification of some agglomerates that reflect on wider particles distribution, as presented in Fig. 1 b for AuC_II as representative sample. The specific activity could be then recalculated for the 1st and 4th cycle for all catalysts, considering gold quantity and dispersion. The dispersion was calculated using cubooctahedral particles mathematical model for the theoretically available gold surface atoms and this model was compared with the experimentally observed particle size by TEM. The estimations of the gold dispersion and specific activity in the 1st and the 4th cycle are presented in Table 3.

It is clear that the gold particle size increase during the 1st cycle of operation resulting in lower dispersion almost for all samples. Although negative influence on glucose oxidation activity for a samples with gold particle size superior to 10 nm is reported [8,25] the specific activity in our case shows a maximum placed between 15 and 20 nm average gold particle size (Fig. 2b). As long as the gold particles neighbor the optimum average size maximum specific activity could be achieved. Prati et al. [26] found 7 nm as optimal gold nanoparticle size for uncalcined catalyst, slightly inferior to the size of our best fresh catalyst. This result shows that the observed decrease of glucose conversion does not reflect in decrease of specific activity indicating that the particles sintering is not of primordial importance as activity inhibitor as the gold loading is for this reaction. But the gold metal particles size must be controlled in a range appropriate for the reaction. Wang et al. [21] found that gold particle size alteration and leaching is more pronounced in acidic conditions and that a reasonable stability and activity could be achieved by proper choice of support. However, the use of mineral supports as Al_2O_3 or CeO_2 based materials [23] results in even more severe gold leaching converting the carbon based supports in the most appropriate materials for this reaction conditions. The solution of the leaching problem still have to be found either by appropriate changes in the support (porosity and/or surface composition modifications) or by establishing an appro-

Please cite this article in press as: C. Megías-Sayago, et al., Gold catalyst recycling study in base-free glucose oxidation reaction, Catal. Today (2017), http://dx.doi.org/10.1016/j.cattod.2017.03.022

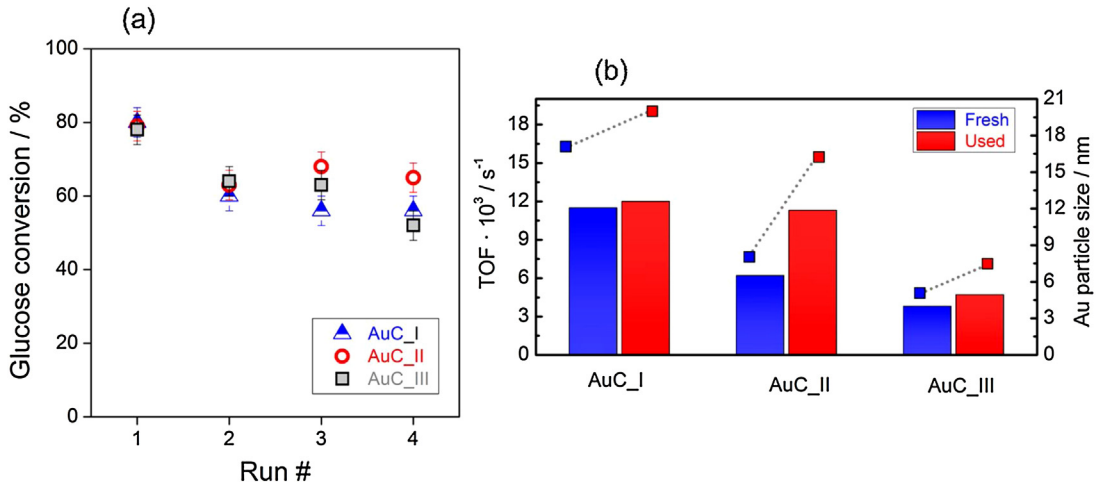

Fig. 2. (a) Glucose conversion on fresh and spent catalysts under 4 reaction cycles (b) TOF (bars) and particle size (points) comparison in 1st and 4th cycles on fresh and spent catalysts.

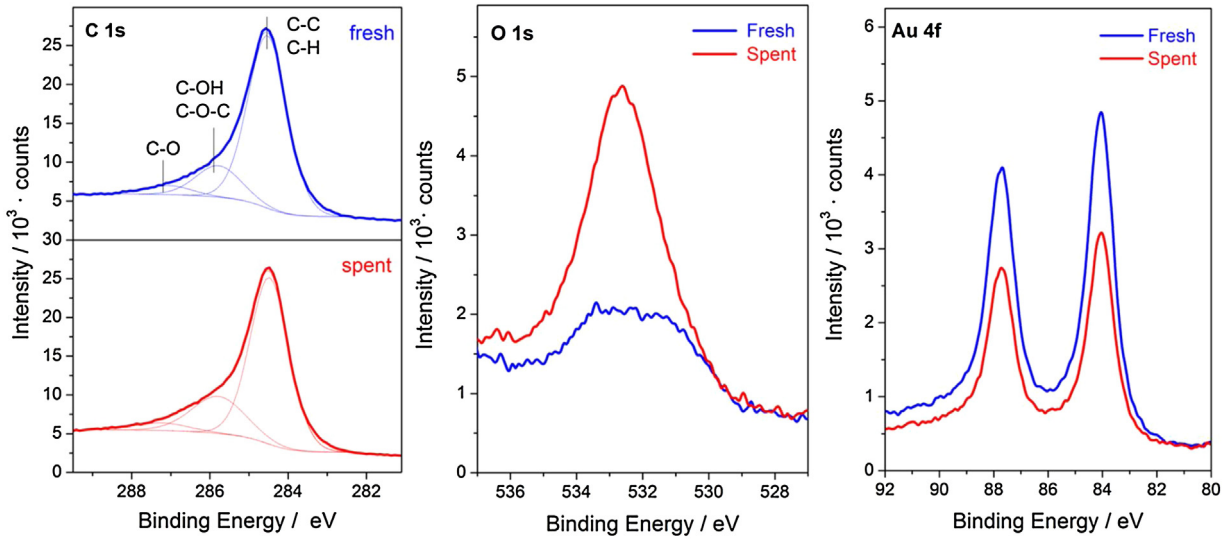

Fig. 3. XPS spectra of fresh (1st cycle) and spent (4th cycle) AuC_II catalyst.

Table 3
Gold particles dispersion and TOF for the fresh and spent samples (1st and 4th cycle of operation).

Sample	Au dispersion fresh, %	Au dispersion spent, %	TOF × 10³ (fresh), s^{-1}	TOF × 10³ (spent 4th cycle), s^{-1}
AuC_I	9	7	11.5	12.0
AuC_II	16	9	6.2	11.3
AuC_III	27	18	3.8	4.7

priate gold loading for high specific activity combined with low leaching rate.

Outward gold metal state (loadings and size) possible active sites blocking during the reaction was also reported as a reason for deactivation [21,27]. The surface properties of our fresh and spent catalysts were studied by XPS and DRIFT analysis. At this point as representative sample the AuC_II was selected owed to the highest changes in specific activity observed for this sample between the cycles (Fig. 2 B).

The XPS spectra of fresh and spent (after 4th cycle) AuC_II sample are presented in Fig. 3.

The C*1s* spectra of the fresh sample can be resolved into three peaks; one corresponding to graphitic carbon C—C sp^2 bond located at 284.5 eV, one of C—O single bond of phenols and esters at 285.8 eV and the C=O double bounded oxygen in ketones and quinones contribution at 287.0 eV. The three types of carbon are presented in the original activated carbon sample. After the 4th cycle the observed carbon contributions could be assigned to the same groups, with the major difference observed on the second group. The relative contribution of the organic carbon issued from phenols and esters increases together with the O/C ratio (0.045 vs. 0.13 for fresh and spent sample respectively). This increase could be related either to the oxidation of the activated carbon surface or to the adsorption of the reaction products. The O*1s* of the fresh sample indicates the presence of only one type of oxygen—"organic oxygen" C—O at 532.6 eV found in phenols or esters and this contribution increases dramatically after catalyst recycling. Zope and Davis [27] reported as a possible cause for gold deactivation, low

Please cite this article in press as: C. Megías-Sayago, et al., Gold catalyst recycling study in base-free glucose oxidation reaction, Catal. Today (2017), http://dx.doi.org/10.1016/j.cattod.2017.03.022

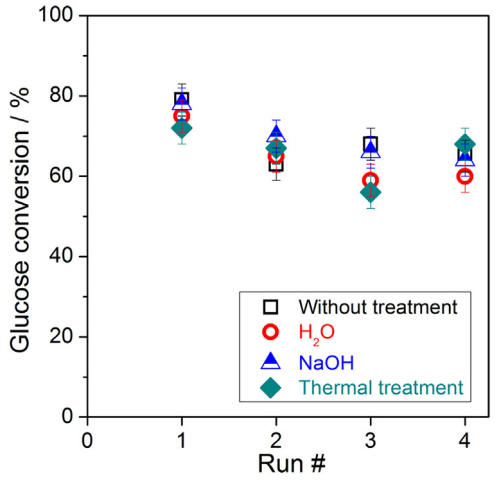

Fig. 4. Activity of the AuC_II sample after various regeneration treatments.

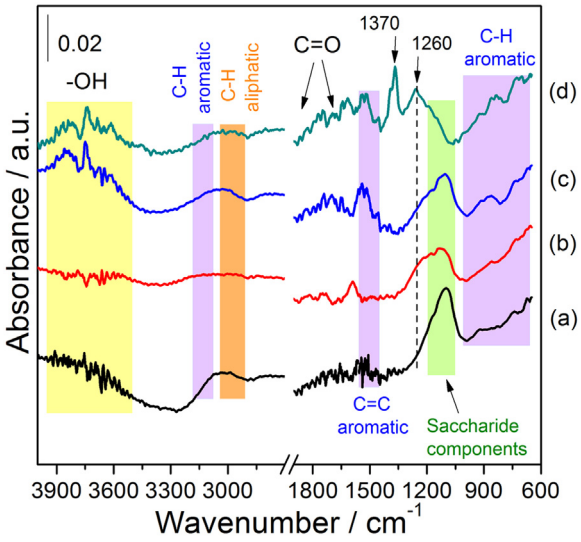

Fig. 5. Difference DRIFT spectra (spent vs. fresh) under different regeneration treatments: (a) without treament, (b) H_2O, (c) NaOH and (d) thermal treatment.

catalyst' tolerance to strongly adsorbed ketones, enones or compounds with β-dicarbonyl structure issued from highly oxygenated biomass derivatives with OH groups bounded to the secondary C atoms. Those intermediate species intereact eventually and adsorb strongly on the catalyst surface, producing active sites blocking. However, no oxygen contributions assigned to the C=O groups were observed in our XPS spectra indicating at this step, the absence of ketones on the surface and only richer in oxygen activated carbon surface at the end of the reaction.

On the other hand, the gold surface distribution, in both beginning and end of the reaction, shows the presence of metallic gold confirmed by the corresponding $4f_{5/2}$ and $4f_{7/2}$ transitions situated at 87.8 and 84.0 eV, respectively. The Au/C and Au/O atomic surface ratio decreases from fresh to spent catalyst (0.016–0.009 and 0.35–0.07) indicating in the first case gold particles size agglomeration (confirmed by TEM) and in the second one that the oxygen surface distribution originates more probably from intermediates and not from oxidized gold metal centers.

In order to estimate the role of the intermediates poisoning on the reaction and possible catalysts regeneration, different treatments (H_2O, 0.1 M NaOH, calcination in static air at 300 °C or no treatment) were carried out over representative sample, AuC_II. The results expressed in glucose conversion are presented in Fig. 4.

The analysis of the results leads to the conclusion that the treatments between the cycles do not influence excessively the catalyst performance. With or without treatments, the 2nd cycle is always affected negatively and no recuperation of initial activity is observed. Fig. 5 present the DRIFT spectra recorded to estimate the changes induced on the catalyst surface during the first cycle of operation and during the regeneration treatments. In order to clearly discern all formed or adsorbed species, the difference DRIFT spectra taking as a reference the fresh sample are considered.

As can be observed, the DRIFT spectra of the spent untreated catalysts clearly show the presence of adsorbed species or modification of the carbon support resulting after glucose oxidation. According to the literature data, all spectral features in the 900–650 cm^{-1} region could be attributed to the C—H out of the plane aromatic compounds vibrations, the bands in the 3100–3000 cm^{-1} region to the C—H ring stretching vibration, the bands in the 3000–2800 cm^{-1} region to the C—H aliphatic species stretching vibration and the bands in the 1600–1450 cm^{-1} region to the ring carbon–carbon stretching vibration, all caused by the presence of activated carbon [28,29]. In addition, the broad band with several contributions observed in the 1150–1050 cm^{-1} region could be assigned to the presence of polysaccharide (highly oxygenated) compounds [30]. Also bands in the 1600–1850 cm^{-1} range are observed and attributed to the C=O stretching vibration of carbonyl groups in aldehydes, ketones, carboxylic acids, esters or acid anhydrides [31–33]. Both regions (1150–1050 cm^{-1} and 1600–1850 cm^{-1}) indicate the presence of intermediates and/or products adsorbed on the catalyst surface. Also pronounced broad band in the 3900–3500 cm^{-1} indicates the presence of hydrogen bonds involved —OH groups. The assignment in this region, however, is of complex nature, since it includes contributions from various groups.

After regeneration, the samples treated with water and NaOH present similar bands to the untreated spent catalyst. Only a slight modification in the —OH stretching region seems to occur upon NaOH treatment. The saccharide like compounds remain adsorbed on the surface upon water and NaOH treatment. By contrast, the thermal treatment lead to polysaccharide bands disappearance and the appearance of two new bands. The first broad band centered at 1260 cm^{-1} could be assigned to the C—O stretching modes typical for ester/ether bridging groups, phenols and lactones [29] and the second at 1370 cm^{-1} to δ O—H vibrations and ν C=O vibrations [34]. The thermal treatment transformed the adsorbed polysaccharide species into new oxygen-containing compounds. Those compounds could result either from the subsequent oxidation of the initially adsorbed species or from the modification of the support and from its oxidation during the calcination treatment in static air. Therefore, it could be concluded that the adsorbed species during the reaction, strongly adsorbed on the catalyst surface, could not be removed without thermal treatment. Nevertheless nor soft chemical treatments (H_2O and NaOH) nor harder calcination treatment can regenerate the initial state of the catalyst. The adsorbed and remaining species on the surface formed after the 1st run (H_2O, NaOH or thermal treatments) do not change the catalyst activity (similar 2nd, 3rd and 4th cycle) indicating that nor the adsorbed intermediates nor the modification of the support play important role in catalyst deactivation. The similar 2nd, 3rd and 4th cycles demonstrate also that the presence of adsorbed intermediates or modifications of the support does not inhibit the reaction. It seems that gold metal state, i.e. gold particle size variation and metal leaching, is the most important parameter inducing loss of activity. On one hand the particles agglomeration could result in a beneficial optimal particle size and increase in the specific activity (AuC_II). And on the other, in our previous study [23] it was reported that the leached gold could participate in the reaction with around 10% conversion increase between the 4th and the 18th hour of reaction

Please cite this article in press as: C. Megías-Sayago, et al., Gold catalyst recycling study in base-free glucose oxidation reaction, Catal. Today (2017), http://dx.doi.org/10.1016/j.cattod.2017.03.022

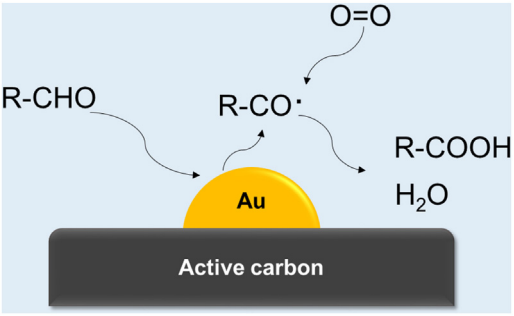

Fig. 6. Representation of possible mechanism of glucose oxidation in base free conditions.

which together with the 8% of glucose adsorption on activated carbon accounts for the 20% of glucose conversion decrease between the 1st and the 2nd cycle. All this leads to the conclusion that the most important problem to solve is gold metal leaching.

This statement leads to the assumption that the carbon support is not a key parameter in this reaction and that the glucose oxidation is occurring only on the low defect surface gold particles with preferable average size of 15–20 nm. Ishida et al. [8] also suggested that the glucose oxidation reaction occurs preferably on gold particles surface and not on the gold/support interface or support. Our observations also support this idea, as the most important deactivation is produced by the gold state change.

The mechanism of glucose oxidation in alkaline conditions is already known and includes preferable glucose adsorption on hydroxylated Au surface on which the glucose CHO group is firstly activated. After water is released by formyl group H removal and gluconic acid is formed by OH transfer from the Au surface [35]. However, in base free conditions the glucose oxidation should proceed through carbonyl conjugated radical [36] and probably will include oxidation through hydrogen peroxide formation, as the activation of molecular oxygen is improbable on gold. Comotti et al. [37] proposed as a key reaction step the presence of electron-rich gold species, formed by hydrated glucose anions on gold surface atoms, which activate the molecular oxygen by nucleophilic attack and lead to the formation of hydroxyperoxides, represented schematically in Fig. 6.

This step could be considered as one of the of Baeyer–Villiger reaction steps, including addition of peroxide to formyl group with hydroxyperoxide formation and its rearranging with cleavage of the C—C bond and products formation [38]. The proposed reaction steps are only a tentative for predicting the reaction mechanism in base free conditions. However a detailed study is needed to confirm the viability of the proposed reaction pathway.

4. Conclusions

Several sample with varying gold particle size are prepared and tested in base free oxidation of glucose. The samples show similar behavior around 80% of glucose conversion toward 100% selective gluconic acid production in the first cycle of reaction. The recycling of the samples reveals that deactivation occurs after the 1st cycle independently on the initial gold particle size. Gold leaching is confirmed to be the primary reasons for catalyst deactivation. Also a gold agglomeration occurs and results beneficial for the specific activity improvement when optimal gold average size is achieved. On the other hand, the support nature, its chemical state or adsorbed species do not seem to be very important. All reactivation treatments result in the same activity trend indicating that the catalyst operation is not affected by intermediates adsorption, removal or support modification. Therefore, every loss of activity is due to gold metal leaching after the 1st cycle and when the leaching stops the activity remains constant (2nd, 3rd, 4th cycle).

Acknowledgements

Financial support for this work has been obtained from the Spanish Ministerio de Economía y Competitividad (MINECO) (ENE2013-47880-C3-2-R) co-financed by FEDER funds from the European Union.

References

[1] C. Chatterjee, F. Pong, A. Sen, Green Chem. 17 (2015) 40–71.
[2] J.C. Serrano-Ruiz, R. Luque, A. Sepúlveda-Escribano, Chem. Soc. Rev. 40 (2011) 5266–5281.
[3] J. Chedda, G.W. Huber, J.A. Dumesic, Angew. Chem. Int. Ed. 46 (2007) 7164–7183.
[4] Frieder W. Lichtenthaler, C.R. Siegfried Peters, Chimie 7 (2004) 65–90.
[5] M. Besson, P. Callezot, Catal. Today 57 (2000) 127–144.
[6] S. Biella, L. Prati, M. Rossi, J. Catal 206 (2002) 242–247.
[7] P. Beltrame, M. Comotti, C. Della Pina, M. Rossi, Appl. Catal. A 297 (2006) 1–7.
[8] T. Ishida, N. Kinoshita, H. Okatsu, T. Akita, T. Takei, M. Haruta, Angew. Chem. Int. Ed. 47 (2008) 9265–9268.
[9] M.J. Climent, A. Corma, S. Iborra, Green Chem. 13 (2011) 520–540.
[10] D.J. Verraest, J.A. Peters, H. van Bekkum, Carbohydr. Res. 306 (1998) 197–203.
[11] J.M.H. Dirkx, H.S. van Der Baan, J. Catal. 67 (1981) 1–13.
[12] M. Besson, F. Lahmer, P. Gallezot, P. Fuertes, G. Fléche, J. Catal. 152 (1995) 116–121.
[13] P. Gallezot, Catal. Today 37 (1997) 405–418.
[14] C. Kooyman, K. Vellenga, H.G.J.D.E. Wilt, Carbohydr. Res. 54 (1977) 33–44.
[15] C. Baatz, U. Prüβe, J. Catal. 249 (2007) 34–40.
[16] N. Thielecke, K.D. Vorlop, U. Prüβe, Catal. Today 122 (2007) 266–269.
[17] U. Prüβe, M. Herrmann, C. Baatz, N. Decker, Appl. Catal. A 406 (2011) 89–93.
[18] A. Mirescu, H. Berndt, A. Martin, U. Prüβe, Appl. Catal. A 317 (2007) 204–209.
[19] C. Baatz, N. Thielecke, U. Prüβe, Appl. Catal. B 70 (2007) 653–660.
[20] P.J. Miedziak, H. Alshammari, S.A. Kondrat, T.J. Clarke, T.E. Davies, M. Morad, D.J. Morgan, D.J. Willock, D.W. Knight, S.H. Taylora, G.J. Hutchings, Green Chem. 16 (2014) 3132–3141.
[21] Y. Wang, S. Van de Vyver, K.K. Sharma, Y. Román-Leshkov, Green Chem. 16 (2014) 719–726.
[22] P. Qi, S. Chen, J. Chen, J. Zheng, X. Zheng, Y. Yuan, ACS Catal. 5 (2015) 2659–2670.
[23] C. Megías-Sayago, S. Ivanova, C. López-Cartes, M.A. Centeno, J.A. Odriozola, Catal. Today 279 (2017) 148–154.
[24] J. Luoa, W. Chu, S. Sall, C. Petit, Colloids Surf. A 425 (2013) 83–91.
[25] H. Okatsu, N. Kinoshita, T. Akita, T. Ishida, M. Haruta, Appl. Catal. A 369 (2009) 8–14.
[26] L. Prati, A. Villa, A. Lupini, G. Veith, Phys. Chem. Chem. Phys. 14 (2012) 2969–2978.
[27] B. Zope, R. Davis, Green Chem. 13 (2011) 3484–3491.
[28] B.J. Meldrum, C.H. Rochester, Fuel 70 (1991) 57–63.
[29] Brian J. Meldrum, Colin H. Rochester, J. Chem. Soc. Faraday Trans. 86 (1990) 861–865.
[30] Sócrates, Infrarred and Raman characteristic group frequencies, 3rd edition, Wiley.
[31] J.L. Figueiredo, M.F.R. Pereira, M.M.A. Freitas, J.J.M. Órfão, Carbon 37 (1999) 1379–1389.
[32] Brian J. Meldrum, Colin H. Rochester, J. Chem. Soc. Faraday Trans. 86 (1990) 1881–1884.
[33] Abdel-Nasser A. El-Hendawy, J. Anal. Appl. Pyrolisis 75 (2006) 159–166.
[34] Douglas B. Mawhinney, John T. Yates Jr., Carbon 39 (2001) 1167–1173.
[35] T. Ishimoto, Y. Hamatake, H. Kazuno, T. Kishida, M. Koyama, Appl. Surf. Sci. 324 (2015) 76–81.
[36] S: J. H. F. Arts, E.J.M. Mombang, H. van Bekkum, R. Sheldon, Synthesis 6 (1997) 597–613.
[37] M. Comotti, C. Della Pina, E. Falletta, M. Rossi, Adv. Synth. Catal. 348 (2006) 313–316.
[38] C.H. Hassall, The Baeyer-Villiger oxidation of aldehydes and ketones, Org. React. 9 (3) (2011) 73–106.